Maria Fátima Loureiro da Silva

VISUAL PROCESSING MECHANISMS WITHIN MAGNO, KONIO AND PARVOCELLULAR SYSTEMS: IMPLICATIONS FOR BASIC AND CLINICAL SCIENCES

2011

Cover image designed by Manuel Vitor

Dissertação de Doutoramento apresentada à Faculdade de Medicina da Universidade de Coimbra, para prestação de provas de Doutoramento em Ciências Biomédicas.

Este trabalho foi realizado no Centro de Oftalmologia e Ciências da Visão, no Instituto Biomédico de Investigação da luz e Imagem (IBILI) da Faculdade de Medicina da Universidade de Coimbra, sob a orientação do Prof. Doutor Miguel Castelo-Branco e ao abrigo de uma bolsa de doutoramento atribuída pela Fundação para a Ciência e a Tecnologia (SFRH/BD/18777/2004).

To my parents
To my children João Filipe and Pedro Filipe

ACKNOWLEDGMENTS

The completion of this thesis wouldn't have been possible without the support and encouragement of my family, friends and colleagues. I am immensely grateful to Professor Custódio Loureiro, from the Physics Department of the University of Coimbra, for his friendship and for introducing me to the Visual Neuroscience Laboratory of Professor Miguel Castelo-Branco.

To my supervisor Professor Miguel Castelo-Branco I wish to express my gratitude for all the opportunities given and confidence. He introduced me to basic visual science making it possible the interaction of clinical ophthalmology with basic vision research. It was a great pleasure to work with him in this scientific journey, where I could share his enthusiasm.

I thank my co-supervisor Professor Miguel Morgado for his scientific and strategic advices at all stages of this work, as well as the constant support and motivation.

I would like to thank Dr Cristina Januário and Professor Antonio Freire Gonçalves from the department of Neurology of Coimbra University Hospital, for the selection of the PD patients, which made possible the realization of this work and their interest in vision research. I also thank the group of medical students Frederico Regateiro, João Massano and Gustavo Januário. I would like to thank the department of ophthalmology of Coimbra University Hospital, specially Dr. Pedro Faria and Dr. Pedro Fonseca, for their direct involvement, providing a full ophtalmological examination of our controls and PD patients and helping me with my basic doubts of ophthalmology. I am also indebted to all the patients with Parkinson´s disease and their families that participated in this study, for their time and efforts, making this project possible. It is hoped that they have indeed contributed to a better understanding of their disease. Perhaps, in a not too distant future, this understanding can bring new resources to help them achieve the best of their daily activities and improve their quality of vision.

To our volunteers, from Coimbra University Hospital, clinical department of the Association for Innovation and Biomedical Research on Light and Image (AIBILI), colleagues and participants from the Centre of Ophthalmology and Visual Sciences of IBILI and Institute of Biophysics and Biomathematics for their indispensable cooperation.

I would like to thank all the staff at AIBILI, especially Dr Luísa Ribeiro (Director of Centre for Clinical Trials) for allowing me free access to the facility and to the most modern ophthalmological equipment, Ana Rita Soares, Mario Soares, Elisabete Almeida and Lilianne Duarte (both at the time in AIBILI) who were always available for me, performing the

ophthalmological exams, as well as to Sandra Pardal and Adozinda Simão which provided excellent secretarial support with the PD patients and controls. To the staff of the Centre of New Technologies for Medicine (CNTM) at AIBILI, especially Sandrina Nunes for the long scientific discussions we had together and the Director Rui Bernades for allowing me free access to equipment for my experiments.

Special thanks to Barbara Oliveiros (for advice concerning statistical analysis) and Francisco Caramelo from the Institute of Biophysics and Biomathematics. To my friends Monika Popper and Lajos Kozak (who spent three years at IBILI working in their PhD program), for the good times we spent together.

I would like to thank all my colleagues in the Visual Neuroscience Laboratory of IBILI for their support. There are, however, those who by their direct intervention played a leading role in implementing this project: Mafalda Mendes, Susana Maia-Lopes, Vasco Forjaz, Manuela Guerreiro, Catarina Mateus, Aldina Reis, Joana Sampaio, Inês Almeida and Inês Bernardino (my roommates, thank you for friendship), Maria Ribeiro and Otília d´Almeida that reviewd some chapters and gave valuable advice, Manuel Vitor for providing me the image for the cover, Alda Gonçalves (the secretary of IBILI) for all the assistance during this period, Dr Cristina Ramos for providing me some of the articles, which were not always easy to obtain and for reading this thesis and useful suggestions.

Finally, I express my gratitude to my family whose touch has not only shaped my vision but also taught me the good things that really matter in life, without the support of which this work would not have been possible and to whom I have dedicated this work. There are no words to express my gratitude for the love, encouragement and support of my mother and father. I am also thankful to my two sons, who were often deprived of my company and yet always supported me with their good mood.

PUBLICATION LIST

1. Silva MF, Guerreiro M, Castelo-Branco M. Disadvantage of the superotemporal fie field in normal subjects as revealed by techniques that study the function of the magnocellular pathway. Ophthalmic Res **2004**; 36 S1:60.

2. Mendes M, Silva MF, Simões L, Jorge M, Saraiva J, Castelo-Branco M. Visual magnocellular and structure from motion perceptual deficits in a neurodevelopmental model of dorsal stream function. Brain Res Cogn Brain Res. **2005** Dec;25(3):788-98. Epub 2005 Oct 26.

3. MF Silva, P Faria, FS Regateiro, V Forjaz, C Januário, A Freire, M Castelo-Branco. Independent patterns of damage within magno-, parvo- and koniocellular pathways in Parkinson's disease. Brain. **2005** Oct;128(Pt 10):2260-71. Epub 2005 Jul 6.

4. Castelo-Branco M, Mendes M, Silva MF, Januário C, Machado E, Pinto A, Figueiredo P, Freire A. Specific retinotopically based magnocellular impairment in a patient with medial visual dorsal stream damage. Neuropsychologia. **2006**;44(2):238-53. Epub 2005 Jul 7.

5. Castelo-Branco, M; Silva, MF; Januario, C; Freire, A. Reply to "Letter to the Editor: Independent patterns of damage within magno-, parvo- and koniocellular pathways in Parkinson's disease (Silva MF et al. Brain 2005; 128 : 2260-2271)". Concomitant impairment of multiple visual pathways in Parkinson's disease. BRAIN 129 Art No. E62 Part 12 **2006**.

6. Silva MF, Maia-Lopes S, Mateus C, Guerreiro M, Sampaio J, Faria P, Castelo-Branco M. Retinal and cortical patterns of spatial anisotropy in contrast sensitivity tasks. Vision Res. **2008** Jan;48(1):127-35. Epub 2007 Dec 11.

7. Maia-Lopes S, Silva ED, Silva MF, Reis A, Faria P, Castelo-Branco M. Evidence of widespread retinal dysfunction in patients with stargardt disease and morphologically unaffected carrier relatives. Invest Ophthalmol Vis Sci. **2008** Mar;49(3):1191-9.

8. Maia-Lopes S, Silva ED, Reis A, Silva MF, Mateus C, Castelo-Branco M. Retinal function in best macular dystrophy: relationship between electrophysiological, psychophysical, and structural measures of damage. Invest Ophthalmol Vis Sci. **2008** Dec;49(12):5553-60. Epub 2008 Sep 4.

9. Castelo-Branco M, Mendes M, Silva MF, Massano J, Januário G, Januário C, Freire A. Motion integration deficits are independent of magnocellular impairment in Parkinson's disease. Neuropsychologia. **2009** Jan;47(2):314-20. Epub 2008 Sep 7.

10. MF Silva, Mateus C, Reis A, Nunes S, , Fonseca P, Castelo-Branco M. Asymmetry of visual sensory mechanisms: electrophysiological, structural and psychophysical evidence. J Vis. **2010** June 28;10(6): 26; doi:10.1167/10.6.26.

11. Joaquim N Murta, Miguel Caixinha, Maria Fátima Silva, Sandrina Nunes, Robert van Velze, Susana Maia-Lopes, Miguel Castelo-Branco. Twelve months evaluation of quality of vision after Lasik (PLANOSCAN VS ZYOPTIX). Comparison of different new methodologies. (Under Revision) **2010**.

LIST OF CONTENTS

ACKNOWLEDGMENTS vii

PUBLICATION LIST ix

CONTENTS xi

LIST OF ABBREVIATIONS xix

RESUMO xxi

SUMMARY xxiii

AIMS xxv

PART I. THEORETICAL BACKGROUND 1

CHAPTER 1. PARALLEL PROCESSING IN VISION 3

1.1. GENERAL INTRODUCTION – CENTRAL VISUAL PATHWAYS 4

1.2. VISUAL PROCESSING STREAMS 5

1.3. SUBCORTICAL PATHWAYS FOR VISUAL PROCESSING 9

1.3.1. Physiological properties of the M, P and K pathways 9

1.3.2. The role of the M and P pathways in achromatic vision 11

1.4. CONTRAST SENSITIVITY 12

1.5. COLOUR VISION 15

1.5.1. Contrast and Opponent Spaces 17

1.6. THE VISUAL FIELD 19

1.6.1. The retinotopic representation of the visual field 19

1.7. VISUAL FIELD MEASURES 23

1.7.1. Perimetric techniques that try to isolate functional pathways 23

1.7.2. Non-Perimetric techniques that try to isolate functional pathways 26

CHAPTER 2. STUDY-SPECIFIC INTRODUCTION 27

2.1. EARLY RETINOCORTICAL CONTRIBUTIONS TO PERCEPTUAL ANISOTROPIES: EVIDENCE FROM ANATOMY, PSYCHOPHYSICS AND PHYSIOLOGY 27

2.1.1. Anatomical anisotropies within the primate retina 28

2.1.2. Evidence for left-right and dorso-ventral performance anisotropies - The “dual frequency filter” model of visual processing 29

2.1.3. Evidence for low-level retinal sources of asymmetry and cortical hemispheric asymmetry 31

2.2. NON-MOTOR MANIFESTATIONS IN PARKINSON´S DISEASE – FROM VISION TO MOTION PERCEPTION 31

2.2.1. Parkinson´s disease 32

2.2.2. Retinal dopaminergic decrease in PD patients 33

2.2.3. Evidence for deficits in sensory systems with a focus on vision 34

2.2.4. Damage across early visual pathways 35

2.2.5. Neurophysiological evidence of visual dysfunction in PD 36

2.2.5.1. Visual evoked potential (VEP) recordings 36

2.2.5.2. Flash and pattern electroretinograms (ERG) 36

2.2.6. Visual acuity 37

2.2.7. Contrast Sensitivity 38

2.2.8. Colour Vision 39

2.2.9. Visual hallucinations 40

2.2.10. Motion Perception 41

2.3. THE ROLE OF DOPAMINE 42

2.3.1. Medical treatment and its effects on visual function in PD 43

2.4. NEUROIMAGING IN PD 45

PART II. METHODS **47**

CHAPTER 3. METHODOLOGICAL OVERVIEW **49**

3.1. NOVEL PSYCHOPHYSICAL PERIMETRIC TECHNIQUES – CS APPARATUS 49

3.2. PSYCHOPHYSICS 50

3.3. VISUAL STIMULUS GENERATORS (VSG) 2/5 CARD 51

3.3.1. Calibration - Gamma Correction by vsgDesktop 52

3.4. MONITORING EYE MOVEMENTS - VIDEO EYETRACKER TOOLBOX 54

3.5. ACROMATIC CS STIMULI 55

3.5.1. LSF Stimulus: Frequency-doubling illusion 56

3.5.2. ISF Stimulus 58

3.6. PSYCHOPHSICAL PARAMETERS 58

3.6.1. Staircase protocol 58

3.6.2. Limits for reliability 59

3.6.3. Data analysis 60

3.7. MOTION PERCEPTION 60

3.7.1. Psychophysical technique to address local motion - Local Speed Discrimination 60

3.7.2. Psychophysical technique to address global motion perception 62

3.8. DATA BASE OF CUSTOM PERIMETRIES 63

3.8.1. Demographic distribution of the Custom LSF task 63

3.8.2. Demographic distribution of Matrix N-30-F participants 65

3.8.3. Bland-Altman analysis 67

3.8.4. Demographic distribution of the Custom ISF task (ISF_photopic) 68

PART III. RESULTS **73**

CHAPTER 4. RETINAL AND CORTICAL PATTERNS OF SPATIAL ANISOTROPY IN CS **75**

4.1. SUMMARY 75

4.2. INTRODUCTION 76

4.2.1. Psychophysical separation of asymmetries within the parvocellular and magnocellular pathways 77

4.3. METHODS 78

4.3.1. Ophthalmological examination 78

4.3.2. Participants 78

4.3.2.1. Participants of the ISF task 79

4.3.2.2. Demographic distribution of the LSF task 79

4.3.3. Perimetic CS assessment 79

4.3.3.1. ISF contrast sensitivity test 79

4.3.3.2. LSF contrast sensitivity - FD test 80

4.3.4. Magnification (M – scaling) factor analysis 83

4.3.5. Statistical analysis 83

4.4. RESULTS 84

4.4.1. Results for ISF test 84

4.4.1.1. Retinal naso/temporal VF asymmetries in the ISF task under photopic and mesopic conditions 84

4.4.1.2. Cortical left/right VF asymmetries in the ISF task 86

4.4.2. Results for LSF standard tests 88

4.4.2.1. Naso/temporal and dorso/ventral VF asymmetries in the LSF task 88

4.4.3. Center-periphery CS differences across distinct sensory mechanisms 91

4.5. DISCUSSION 92

CHAPTER 5. ASYMMETRY OF VISUAL SENSORY MECHANISMS: Electrophysiological, structural and psychophysical evidences 95

5.1. SUMMARY 95

5.2. INTRODUCTION 96

5.3. MATERIAL AND METHODS 98

5.3.1. Participants 98

5.3.2. Optical Coherence Tomography 98

5.3.3. Electrophysiological Recordings 99

5.3.4. Intermediate Spatial Frequency (ISF) Contrast Sensitivity Test 101

5.3.5. Statistical Analysis 102

5.4. RESULTS 103

5.4.1. Analysis of size effects 107

5.4.2. Correlation Analysis 107

5.5. DISCUSSION 108

5.6. CONCLUSION 111

CHAPTER 6. Independent patterns of damage across retinocortical pathways in Parkinson's disease 113

6.1. SUMMARY 113

6.2. INTRODUCTION 114

6.3. METHODS 117

6.3.1. Patient selection and classification 117

6.3.2. Participants 117

6.3.3. Statistical analysis 118

6.3.4. Psychophysical techniques to address the function of parvo- and koniocellular pathways 118

6.3.5. Psychophysical technique to address the function of the M pathway 122

6.4. RESULTS 123

6.4.1. Retinal assessment of parvo- and koniocellular damage 123

6.4.2. Chromatic parameters vs. clinical parameters 126

6.4.3. Adaptation experiments under saturated blue background 126

6.4.4. Perimetric assessment of magnocellular function 129

6.4.5. Correlation between achromatic psychophysical performance and disease progression 131
6.4.6. Correlation between CS tests: Achromatic vs. chromatic parameters 132
6.5. DISCUSSION 132
6.5.1. Independent assessment of multiple visual pathways and implications for understanding disease pathophysiology 132
6.5.2. Patterns of damage across M, P and K pathways 133
6.5.3. Retinal dopaminergic effect in PD 134
6.5.4. Differentiation of disease related patterns of damage 135
6.6. FINAL CONCLUSIONS 137

CHAPTER 7. Hierarchical approach to the study of magnocellular and dorsal stream processing in Parkinson's disease: relation between visual and motor patterns of impairment 139

7.1. SUMMARY 139
7.2. INTRODUCTION 140
7.3. METHODS 141
7.3.1. Participants 141
7.3.2. Statistical analysis 142
7.3.3. Low-level M processing task - high temporal/low spatial frequency channel 142
7.3.4. Assessment of low-level (M) and high-level (integrative dorsal stream) motion performance 142
7.3.5. Simple and Complex Motor Temporal processing 143
7.4. RESULTS - PERFORMANCE PATTERNS IN LOW- AND HIGH-LEVEL MOTION DISCRIMINATION TASKS: 144
7.4.1. Preferential impairment in tasks that require perceptual integration of moving surfaces 144
7.4.2. Correlation analyses of between-task performance 145
7.4.3. Correlation of motion performance measures with M contrast sensitivity ... 146
7.4.4. Correlation of motion parameters with disease progression 147
7.4.5. Correlation with quantitative parameters of motor sequence execution 149
7.5. DISCUSSION 151

PART IV. FINAL REMARKS **155**

CHAPTER 8. CONCLUSION AND FINAL REMARKS **157**

8.1. THE RELATIVE VALUE OF NOVEL PSYCHOPHYSICAL METHODS 157

8.1.1. Applications 158

8.1.2. Implications of the findings of VF anisotropies in terms of segregation of parallel visual processing across pathways and space 159

8.1.3. Implications for early diagnosis of retinocortical diseases 160

8.2. PARKINSONS´S DISEASE 161

8.3. FUTURE WORK 161

APPENDIX A 163

APPENDIX B 171

APPENDIX C 177

REFERENCES 181

LIST OF ABBREVIATIONS

2-AFC 2-Alternative Forced Choice

AMD age-related macular degeneration

BOLD blood-oxygen-level dependent

CCT Cambridge Color Test™ (Cambridge Research Systems Ltd., Rochester, UK)

CIE Commission internationale de l'éclairage (International Commission on Illumination)

CMF Color matching function

cpd cycles per degree

CRS Cambridge Research Systems Ltd., Rochester, UK

CRT Cathode-Ray-Tube

CS contrast sensitivity

CSF contrast sensitivity function

DA Dopamine

DAC digital-to-analogue converter

ERG electroretinogram

FD frequency-doubling

FDT frequency-doubling technology™ (Carl Zeiss Meditec, Inc)

FM 100-test Farnsworth-Munsell color test

fMRI functional magnetic resonance imaging

FN false negative

FP false positive

GPi Globus pallidus pars internal

HM horizontal meridian

H&Y Hoehn & Yahr Parkinson's Disease Staging Scale

IPL Inner Plexiform Layer

IN inferonasal

ISI interstimulus interval

ISF intermediate spatial frequency

IT inferotemporal

K koniocellular

L-cone long wavelength sensitive or red cone (peak sensitivity at 560 nm)

L-dopa levodopa

LGN lateral geniculate nucleus

LSF low spatial frequency

M magnocellular

M-cell retinal parasol ganglion cell projecting to the magnocellular pathway

M-cone medium wavelength sensitive or green cone (peak sensitivity at 530 nm)

MD mean deviation

mfERG multifocal electroretinogram

MMSE Mini-Mental State Examination

MPTP 1-methyl-4-phenyl-1, 2, 3, 6-tetrahydropyridine

MRI magnetic resonance imaging

ns non-significant

NMDA N-metil-D-aspartate

P parvocellular

P-cell retinal midget ganglion cell projecting to the parvocellular pathway

PD Parkinson´s disease

OCT Optical coherence tomography (Stratus^{TM} OCT3, Carl Zeiss Meditec)

OD right eye

OS left eye

OPs oscillatory potentials

PERG pattern electroretinogram

PET positron emission tomography

RDKs random kinematograms dots

RNFL retinal nerve fiber layer

RT retinal thickness

SAP standard automated perimetry Humphrey^{TM} Visual Field Analyzer (Carl Zeiss Meditec, Inc)

S-cone short wavelength sensitive or blue cone (peak sensitivity at 400 nm)

SD standard deviation

SEM standard error of the mean

SE standard error

SN superonasal

ST superotemporal

SPECT single photon emission computed tomography

V1 primary visual cortex

V2, V3, V4, V5 higher order visual areas

VA visual acuity

VEP Visual evoked potential

VET Video Eyetracker Toolbox

VF visual field

VH visual hallucinations

VM vertical meridian

VSG 2/5 Visual Stimulus Generator 2/5^{TM} (Cambridge Research Systems Ltd., Rochester, UK)

Resumo

Pretendemos compreender novos aspectos da biofísica das vias de processamento da informação visual no Homem, na saúde e na doença. Introduzimos uma abordagem inovadora de biologia quantitativa baseada no desenvolvimento de métodos biofísicos de estudo da função neurosensorial que permitem isolar o funcionamento de vias paralelas de processamento de forma psicofísica. A questão de fundo é compreender de que forma os sensores biológicos codificam a informação relativa aos contrastes cromático/acromático em diferentes níveis do sistema visual humano, e como essa informação se mantém segregada em diferentes vias na retina e no córtex. Este trabalho inseriu-se assim num projecto de desenvolvimento de novos métodos de biofísica neurosensorial, em particular a sensibilidade ao contraste em vários canais de processamento, com aplicação às ciências da visão básicas e clínicas. Para tal desenvolveu-se uma metodologia psicofísica de análise do processamento da informação visual nos sistemas magno/conio/parvocelulares numa população de controlos e em indivíduos com a doença de Parkinson (DP). A quantificação biofísica dos défices das funções das vias conio/parvocelular realizou-se através da manipulação dos espaços de cor, de forma a medir limiares de discriminação cromática, permitindo medir independentemente a função dos cones (L, M e S). A função parvocelular foi ainda avaliada através de técnica perimétrica de sensibilidade ao contraste acromática. A função magnocelular foi isolada com a perimetria baseada em estímulos com duplicação ilusória de frequência (*frequency doubling*, FD) e através de uma bateria de testes de percepção visual de movimento (local e global). Este projecto de natureza interdisciplinar, que combina conceitos e ferramentas da física e da biologia, procurou ajudar a preencher uma lacuna ainda frequente na neurobiologia de sistemas, no que diz respeito à respeita a abordagem quantitativa da função do sistema visual na saúde e na doença. As novas metodologias estabelecidas, permitem o desenvolvimento de modelos funcionais de processamento da informação biológica, e sobretudo levam à reconsideração das relações genótipo-fenótipo e estrutura-função, que são de enorme relevância nas ciências da visão. Indivíduos de uma população normal de vários grupos etários foram estudados para a criação de uma base de dados normativa para cada método e foram adicionalmente validados em estudos isolados (em modelos clínicos de lesão das células ganglionares da retina, tais como, glaucoma e hipertensão ocular ou ainda num modelo genético do neurodesenvolvimento, o Síndrome de Williams).

As assimetrias da função visuoespacial têm sido documentadas em termos electrofisiológicos e anatómicos, mas as suas consequências no desempenho visual encontram-se ainda pouco exploradas.

Procurámos assim estudar estas assimetrias numa população normal através das técnicas psicofísicas de medição da sensibilidade ao contraste acromático que isolam as vias magno/parvocelulares. Foi comparada a performance entre os diversos quadrantes e hemicampos visuais. Este trabalho revelou pela primeira vez a presença de dois tipos de assimetria funcional nas vias visuais magno/parvocelulares, a primeira de origem provável na retina, e a segunda reflectindo também uma assimetria cortical inter-hemisférica. Neste estudo, centrámo-nos também na análise de assimetrias objectivas funcionais e estruturais ao nível da retina, e analisámos a sua correlação com as assimetrias no desempenho visual. Concluímos que os padrões de assimetria estrutural/funcional surgem a diferentes níveis da retina, conforme sugerido pelo padrão de correlação parcial observado.

O presente trabalho teve também por objectivo aprofundar a avaliação de funções visuais em sujeitos com a DP, utilizando para tal testes psicofísicos mais precisos e sensíveis que os métodos anteriormente empregues. Estudámos de forma independente as vias magno/parvo/coniocelulares e encontrámos envolvimento significativo de todas estas vias neuronais nesta doença. Os resultados deste trabalho vêm revelar que a avaliação da via parvocelular (cones L e M) parece ser pelo menos tão promissora como a estratégia tradicional de estudo da via coniocelular (cones S). Verificou-se existir uma correlação da performance com a idade e com o estadio da doença, apenas para a via magnocelular. O estudo da percepção visual do movimento na DP permitiu comparar a disfunção em vias visuais de baixo nível (retinocortical magnocelular), de nível intermédio e superior (via dorsal), e análise das suas interdependências. Esta estratégia inovadora de análise a vários níveis hierárquicos do sistema visual permitiu demonstrar pela primeira vez, a dissociação entre baixo e alto nível de processamento visual na DP. Verificou-se alteração na percepção do movimento (de origem cortical), e curiosamente, os danos da via periférica magnocelular não se correlacionaram com a percepção de alto nível de movimento, sugerindo assim que a deficiência visual de baixo nível não prevê comprometimento da via dorsal. O que implica que, tais perturbações não podem ser explicadas totalmente por défices precoces na retina bem como ao nível da via precoce retinocortical magnocelular.

Este trabalho permitiu assim estudar, de forma independente, as funções visuais de baixo e alto nível na saúde e na doença.

Summary

We want to understand the biophysical aspects of parallel processing of visual information in humans, in health and disease. We introduced a novel approach to quantitative biology based on the development of new biophysical methods by isolating visual parallel processing in terms of psychophysics. The main question is to understand how the biological sensors encode the information on achromatic/chromatic contrast at different levels of the human visual system, and how that information is kept segregated in different pathways from the retina to the cortex. For this purpose, new methods were developed, in particular, contrast sensitivity multi-channel processing tasks, with application to basic science and clinical vision. The biophysical quantification of deficits in conio/parvocellular processing was held by manipulating the colour spaces in order to measure chromatic discrimination thresholds, allowing independent functional measures of the cones (L, M and S). Parvocellular function was further assessed by a custom perimetry technique of achromatic contrast sensitivity. The magnocellular function was isolated by custom perimetry based on frequency doubling (FD) stimuli and through a battery of visual motion perception tests (local and global motion tasks). This project of interdisciplinary nature, combining concepts and tools of physics and biology, has helped to fill a gap still widespread in neurobiology of systems, in terms, of a quantitative approach of visual function in health and disease. The new methodologies established allowed the development of functional processing models of biological information, and especially lead to the reconsideration of genotype-phenotype and structure-function relationships, which are of major importance in vision science. Individuals of a normal population of various age groups were studied to establish normative databases for each method and were further validated in isolated models (such as clinical models of injury to retinal ganglion cells, as in glaucoma and ocular hypertension or in genetic models of neurodevelopment, the Williams Syndrome).

Asymmetries of spatial vision processing have been documented in electrophysiological and anatomical terms, but their impact on visual performance are still poorly explored. We tried to study these asymmetries in a normal population through psychophysical measurements of achromatic contrast sensitivity by isolating magno/parvocellular pathways. We compared the functional visual performance between different visual field quadrants and hemifields. This study showed for the first time the presence of two types of functional asymmetry in magno/parvocellular pathways, the first one with a likely source on the retina, and the second reflecting also a cortical interhemispheric asymmetry. This suggests that both cortical and retinal visual maps are functionally heterogeneous.

We also focused on the analysis of structural and objective functional asymmetries at the level of the retina, and examined its correlation with asymmetries in terms of visual performance. We concluded that structural/functional patterns of asymmetry arise at different levels of the retina, as suggested by the observed pattern of partial correlation.

The present work also aimed to evaluate the visual function in subjects with PD, using more accurate and sensitive psychophysical tests than previous methods. We studied independently the magno/parvo/coniocellular pathways and found meaningful involvement of all of these neuronal pathways in PD disease. We found that the parvocellular (M and L cones) assessment seems to be at least as promising as the traditional approach of studying coniocellular stream (S cones). A correlation between visual performance with age and disease stage was found only for the magnocellular pathway.

The study of visual motion perception in PD involved the use of a range of hierarchical stimuli designed to bias responses from low-level (magnocellular), intermediate-level and higher-level (dorsal stream) visual pathways and study their interdependence. The novelty of this strategy lies in the analysis of various hierarchical levels of the visual system, showing for the first time, the dissociation between low- and high-level visual processing in PD. Impairment of motion perception in the cortex was found in PD, and interestingly, there was no correlation between low-level damage and motion integration impairment. Thus, suggesting that the visually impaired magnocellular stream does not predict impairment of the dorsal pathway, implying that such disturbances can not be explained entirely by early deficits in the retina as well as in the early magnocellular pathway (retina to sub-cortical, striate and extra-striate regions).

This study allowed to probe independently low- and high-level visual function in health and disease.

AIMS

The major focus of this thesis concerns the development of new biophysical methods to study neurosensory function in order to isolate the parallel channels of visual processing, using psychophysical methods. This need arose from the fact that most of the conventional clinical tests are semi-quantitative (providing limited quantification power), are less sensitive, have lower reproducibility than computerized methods, are prone to confounding factors that render demonstration of a pure sensory deficit problematic because they do not allow for extraction of subject reliability parameters. Aside from these methodological goals we took advantage of the functional isolation of particular visual pathways to understand normal visual perception and pathophysiology of diseases involving the visual system.

Disease-related changes in parallel processing were conducted in Parkinson´s disease (PD). In recent years, evidence has been accumulating regarding the existence of neurosensory deficits in PD, suggesting early changes of visual function at the retinal level. The involvement of visual cortical pathways is however not very clear in this disease. There is some evidence that a chromatic contrast sensitivity (CS) deficit in PD may be related to changes in dopamine neurotransmission in retinal pathways. Most of the published work has also documented motion perception deficits in PD. However these approaches have not considered the contribution of retinal effects that might contribute to a magnocellular deficit. In particular, it is important to separate processes that are related to local motion perception (at the level of the retina) and motion integration processes (at the level of the cortex). It is also important to document whether damage at a prior level of processing within subcortical pathways is causing visual impairment. In order to investigate these hypotheses we applied the developed methods to assess the contribution of each of these levels of processing in to visual impairment in PD.

The first part of this thesis starts with a theoretical background in Chapter 1, which covers some various topics in parallel processing in vision, fundamental concepts of colour vision, contrast sensitivity, visual field measures and previous perimetric and non-perimetric methods used to assess parallel functional pathways. Chapter 2 presents a specific introduction of the studies conducted, the first section presents a general review of anatomical and physiological anisotropies within distinct pathways in the human retina and in the second we present a literature review on visual deficits in Parkinson's Disease.

Chapter 3 describes the details of the methods used in the experimental work, i.e. covers the setup of the new custom CS measurement apparatus, the calibration procedures and experimental characterization by evaluating a population of controls, in order to validate these approaches and characterize the respective normative databases. The database created for these techniques allowed to explore perceptual asymmetries in a normal population. The results suggest the presence of two types of functional asymmetry in M and P visual pathways, the first likely routed in the retina, and the second reflecting cortical interhemispheric asymmetry (with right hemispheric dominance). These results are presented in Chapters 4 and 5.

Visual impairment concerning independent assessment of magno-, parvo- and koniocelular pathways in PD is reported in Chapter 6 and impairment of visual motion perception in Chapter 7. Chapter 8 presents the final conclusions of the thesis as well an indication of future work.

Part I

Theoretical background

Chapter 1

1. Parallel Processing in Vision

«Why are neural streams worth studying?

To our mind's eye, the world appears as a combination of colours, sizes, movements, locations, and other attributes of the visual world. It is tempting to assume that every one of these attributes is handled by a separate neural population, which constitutes an information channel or stream. The observation that the visual system comprises several neuronal populations or streams suggests the possibility that each stream performs a distinct function in vision. We believe that understanding the link between the properties of the neurons in each stream and those visual functions should illuminate the computations that are performed by the visual system as it analyses the visual world»

(Kaplan, 2004)

1.1. General Introduction – Central visual pathways

Information supplied by the retina initiates interactions between multiple subdivisions of the brain, leading to conscious perception of the visual scene, while stimulating more conventional reflexes such as adjusting the size of the pupil, directing the eyes to targets of interest, and regulating homeostatic behaviours that are tied to the day/night cycle. The pathways and structures that mediate these functions are necessarily diverse. The primary visual pathway (also called retinogeniculostriate projection) which includes the optic nerve, optic tract, lateral geniculate nucleus (LGN), optic radiation and striate cortex is the most important and certainly the most thoroughly studied component of the visual system. Different classes of neurons within this pathway encode a variety of visual information, such as luminance, spectral differences, orientation, colour and motion. The parallel processing of different categories of visual information continues in cortical pathways that extend beyond primary visual cortex (V1), supplying a variety of visual areas in the occipital, parietal and temporal lobes. Areas in the temporal lobe are primarily involved in object recognition, whereas those in the parietal lobe are concerned with motion. Normal vision depends on the integration of information in all these cortical areas. The study of the processes underlying visual perception still remains one of the major challenges of modern neuroscience, since they are not fully understood.

This chapter will give a general overview of the subcortical brain structures that are involved in visual processing and the way by which the perceived visual information can be roughly divided into streams and how these systems interact. Although the focus of this thesis is the retina, it must be borne in mind that the sensory visual system does not exist in isolation and many abnormalities of visual function can be attributed to retinal dysfunction, but also to other visual areas. In all of our experiments, we evaluated the way how visual information was processed from the retina to the visual cortex in the disease and in normal subjects. In the next sections, the three subcortical pathways called Magnocellular (M), Parvocellular (P) and Koniocellular (K) will be described and we will show that at this low-level stage, each pathway is dedicated to the processing of a specific class of information. Although the three pathways flow separately from the retina to the cortex, there is little doubt that their messages are intermingled in the cortex, as they blend to form a unified perception. Damage anywhere along the primary visual pathway results in a loss of vision confined to a predictable region of visual space. The difficulties in clear-cut assignment of functions to these pathways also impact the ability to design stimuli that affect one pathway without affecting the others. Compared to retinal ganglion cells, neurons at higher levels of the visual pathway become increasingly

selective in their stimulus properties/tuning. The distinction of the physiological properties of the neurons in both M and P pathways has stimulated the construction of psychophysical tests that can help in understanding the role of these pathways in vision. It has also allowed the comparisons between the visual performance of normal subjects and of individuals affected by diseases that impair the functioning of the visual system. The combination of psychophysics and other methods of investigation, such as electrophysiology and imaging techniques, have been extremely important for our understanding of how the visual system works. This is true for the visual system as a whole, as well as its subunits, which can be teased apart and isolated by particular psychophysical techniques. In this thesis, we will describe how psychophysics can be used to characterize the properties of the retino-geniculate (M, P and K) pathways.

1.2. Visual processing streams

The eye is a fluid-filled sphere enclosed by three layers of tissue: the fibrous layer which provides structure and protection, the vascular pigmented layer which provides blood supply, secretes aqueous humour and controls the amount of light entering the eye and the nervous layer or retina. The retina, at the back of the eye is the image plane on to which the optical system projects. The visual information is then processed by the retina before sending it to the brain. It is therefore here that incident photons are converted to neural impulses to be transmitted to the brain for analysis and interpretation. The outer surface of the sensory retina is apposed to the retinal pigment epithelium and the inner surface is next to the vitreous. The impulses are transmitted anteriorly through the retina layers (the ganglion cells, followed by the bipolar cells with the photoreceptors arranged posteriorly). The retina also contains other neurons; the horizontal and amacrine cells and supporting Muller cells. In sum, the light passes through the ganglion and bipolar cells and is detected by the photoreceptors (see **Figure 1.1**). So, vision begins in the photoreceptor layer where visual processing sets off with the transduction of light into chemical and electrical signals. The functional efference of the eye is the optic nerve head, here no visual stimulation can occur since there are no photoreceptors, and this small region of the retina is called the “blind spot”. The optic nerve is composed of about one million fibres, suggesting that, there is a great compression of data at this level before it is sent to the higher hierarchical levels of the visual system. It is important to emphasize that humans have on average 128 million photoceptor cells in the retina (Sekuler and Blake, 1994), 120 million of them being rods.

The other 8 million photoreceptors are three types of cones that are classified based on the wavelength sensitivity of the photopigment throughout the visible spectrum, namely, L-cones

(560 nm for red), M-cones (530 nm for green), and S-cones (400 nm for blue). At the lowest levels of light, only the rods are activated, this rod-mediated perception is called scotopic vision. The contribution of rods to vision drops out nearly entirely in the so called photopic vision because their response to light saturates. While mesopic vision occurs in levels of light at which both rods and cones contribute. The spatial arrangement of the photoreceptors is called *photoreceptor mosaic*, with the rods present at higher eccentricities, in the parafoveal and peripheral retina and designed for low-light vision and low spatial resolution. The cones are found predominantly in the macula corresponding to the central 13º of the visual field (VF) and are specialized in photopic colour vision and high spatial resolution.

The axons of the ganglion cells gather to form the optic nerve that project mainly to the dorsal Lateral Geniculate Nucleus (LGN) of the thalamus, the most important projection mediating vision and visual perception, but also to the pulvinar region of the thalamus and the superior colliculus, which lies on the roof of the midbrain and is important for the regulation of eye and head movements (Sommer and Wurtz, 2004). From the LGN, the visual signal is projected to V1, where it travels to more anterior sub-regions of the visual cortex (V2-V8) which are all extensively interconnected areas with specialized maps of the VF. The early part of the visual system in primates contains three parallel streams, the M, P and K systems. This division and the general topic of parallel processing in the visual system has been subject of numerous reviews (Shapley and Perry, 1986; Livingstone and Hubel, 1988; Shapley, 1990; Schiller and Logothetis, 1990; Irvin *et al*., 1993; Merigan and Maunsell, 1993; Van Essen and DeYoe, 1995; Hendry and Reid, 2000; Xu *et al*., 2001). In sum, the primary visual pathway is composed of separate functional streams that convey information from three different types of retinal ganglion cells to the initial stages of cortical processing: the M stream conveys information that is crucial for the detection of rapidly changing stimuli, the P stream mediates high acuity vision and shares involvement in colour vision with the K stream.

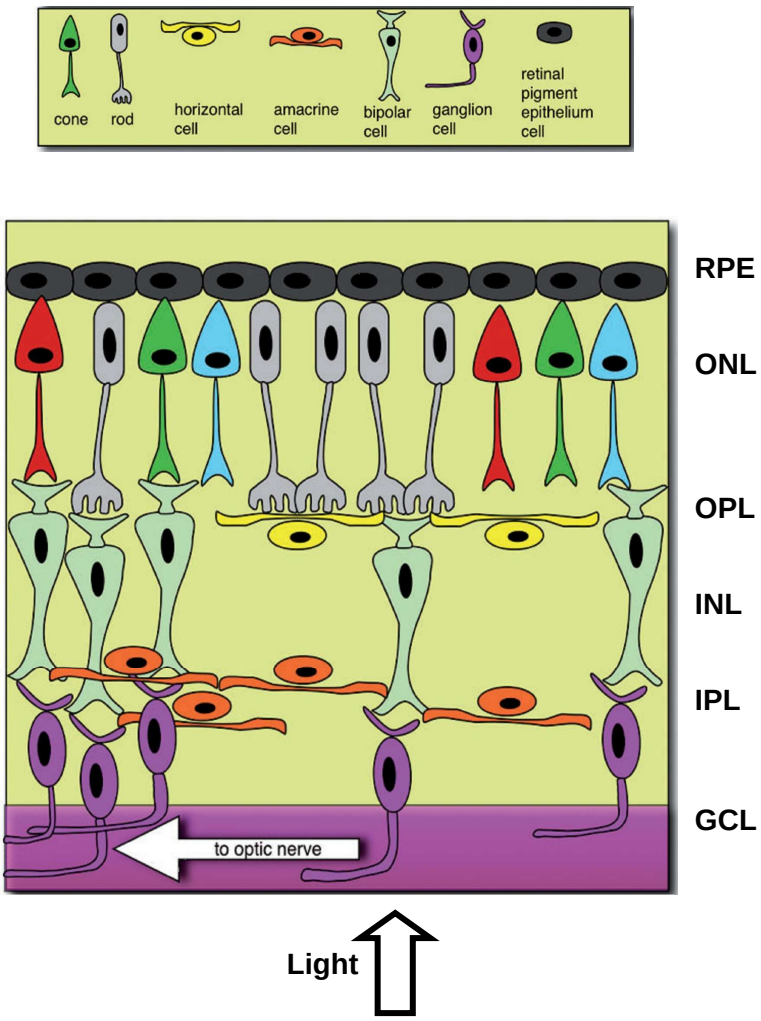

Figure 1.1. This figure illustrates the vertical cross-section of the retina and the principal wiring of different types of neurons. RPE - retinal pigment epithelium layer; ONL - outer nuclear layer; OPL - outer plexiform layer; INL - inner nuclear layer; IPL - inner plexiform layer; GCL - ganglion cell layer. (Adapted from Archibald *et al*., 2009).

Parcellation of function continues beyond the striate cortex (V1), in the ventral and dorsal steams that lead to the extrastriate and association areas in the temporal and parietal lobes, respectively (see **Figure 1.2**). The areas in the inferotemporal cortex (part of the so-called visual ventral stream), are especially important for object recognition, and their neurons respond to properties, such as shape, colour, etc. that result in recognition and identification of visual objects. Areas in the parietal lobe constitute the dorsal stream and are critical for understanding the spatial relations between objects in the VF and are in particular specialized in movement and spatial perception (Ungerleider and Haxby, 1994). This distinction is still being validated by recent studies (Shmuelof and Zohary, 2005). However, other investigators suggest the existence of separate circuits but substantially overlapped for the two types of

visual processing mechanisms (vision for action and vision for object identification) and that these do not necessarily correspond to a gross anatomical separation of dorsal and ventral processing streams (Braddick *et al*., 2000).

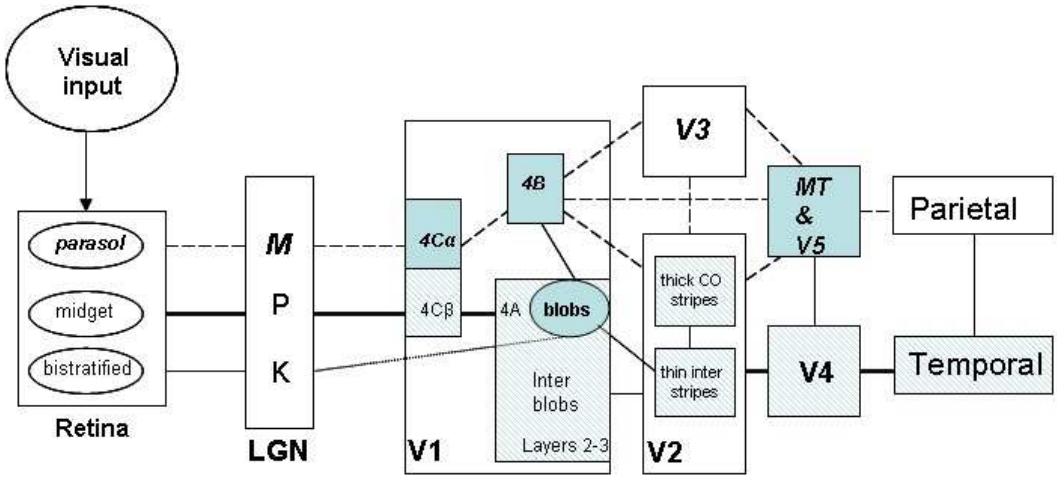

Figure 1.2. Schematic connectivity diagram of the main pathways involved in visual processing. Parallel processing is manifested already at subcortical levels by the distinction among parasol, midget and bistratified cells. Visual signals are sent from the retina to the LGN of the thalamus. From the LGN, signals are projected to area V1 of the visual cortex. The **Dorsal** ("where") pathway is indicated by dashed lines, bold italics and comprises of V2, V3, V5, medial temporal area (MT) of the superior temporal sulcus, and the parietal cortex; the **Ventral** ("what") stream is indicated by solid lines as faint stripes and consists of V2, V4 and the inferior temporal cortex. (Adapted from Kaplan, 2004).

In order to understand the division of labour between the M and P pathways other theories have emerged, such as: Goodale and Milner (1992) proposed the theory of mapping the M and P pathways in the cortical pathways for perception and action, although the dorsal, motion pathway appears to be M-dominated; more recently, Glover (2004) proposed separate visual representations in the planning and control of action.

1.3. Subcortical pathways for visual processing

Already at the stage of the retina, functional segregation of visual input takes place (**Figure 1.2**). In the human retina, the ganglion cells can be divided into 18 or more different morphological types. However the majority of the ganglion cells are parasol and midget cells (Kaplan, 2004). Approximately 80% of the ganglion cells are midget cells, the anatomical counterpart of the P-cells, feeding into the P LGN layers (Merigan, 1989; Dacey, 2000) and 10% are parasol ganglion cells, identified as the M-cells and terminate in the M layers (Perry et al., 1984). The Magno-/Parvo-/Koniocellular distinction is usually based on the anatomical organization of the LGN in primates, which has a multilayered structure with six different layers that are stacked upon one another. The six layers are arranged in two major divisions and are numbered from the bottom (1) to the top (6) and are distinguished on the basis of cell size: two ventral layers (1 and 2) are composed of large neurons and are referred to as the M layers, while the four more dorsal layers (3-6) are composed of small neurons and are referred to as the P layers. Apart from this division there is also one between input from the ipsilateral eye and the contralateral eye. Layers 2, 3 and 5 receive input from the ipsilateral eye, while layers 1, 4 and 6 are innervated by the contralateral eye. The output of LGN is similarly segregated as its input, the axons of relay cells in the M and P layers of the LGN terminate on distinct populations of neurons located in separate strata within layer 4 of striate cortex (V1) (see Figure 1.2). More recently, another distinct morphological cell type has been added to the P- and M-cells, the small bistratified ganglion cells that are thought to project to the regions between each layer of the LGN, which are also called as interlaminar layers, or the K layers (Kaplan, 2004).

1.3.1. Physiological properties of the M, P and K pathways

Neurons in both pathways are mostly different in their physiological characteristics. The major difference between them is the contrast gain (change in response for a unit change in contrast) for luminance patterns (Kaplan and Shapley, 1986). Indeed, M-cells of the retina and of the LGN are highly sensitive to luminance contrast and present a high contrast gain, being especially sensitive to low contrast stimuli and saturating at lower contrast level (10-15%) after which the gain of the M-cells is rather similar to that of P-cells (Derrington and Lennie, 1984; Purpura *et al*., 1988; Sclar *et al*., 1990) suggesting that the response of the M-cell is governed by two mechanisms one for low and the other for high contrasts. The M-cell exhibits high contrast sensitivity (CS) and single cells in the fovea show spatial resolution in a similar range to that observed for the P-cells. Their input originates from multiple cone bipolar cells that

receive synergistic input from L and M cones, consequently these cells respond strongly to achromatic stimuli. These cells have large cell bodies, extensive dendritic fields, large diameter axons and present lower density than P-cells. In addition, they apparently play an important role in transmitting information about the high temporal and low spatial frequencies in the stimuli (Derrington and Lennie, 1984). Therefore they are useful for the perception of high frequency flicker (Schiller and Colby, 1983; Lee *et al*., 1990; Benardete *et al*., 1992) and motion processing (Schiller *et al*., 1991).

In contrast, the P-cells of the retina and of the LGN are spectrally opponent and form the red-green pathway (by receiving antagonistic inputs from both L- and M-cones). Therefore, these cells are highly sensitive to chromatic contrast and saturate at a much higher contrast level. However, their contrast gain is relatively low for achromatic patterns (Derrington and Lennie, 1984; Purpura *et al*., 1988; Sclar *et al*., 1990). They detect high spatial but low temporal frequencies in the stimuli (Derrington and Lennie, 1984), which is mostly important for colour, texture and pattern discrimination and high visual acuity (VA) (Derrington *et al*., 1984; Merigan 1989; Schiller *et al*., 1991; Lynch *et al*., 1992). In short, the P-cells are sensitive to red-green opponency, and convey fine spatial detail, but whether the P pathway is specialized for both colour and achromatic spatial vision it is still controversial.

The small bistratified cells (K cells) represent a minority of the retinal ganglion cells (10%) feeding into the K pathway and in terms of their temporal and spatial sensitivities they form a physiologically heterogeneous group (Kaplan, 2004). Though overall, it is assumed that the response properties of these cells are more similar to those of P-cells than of M-cells (Solomon *et al*., 1999). This system (Dacey and Lee, 1994; Dacey, 2004) is indifferent to shape or depth, and primarily conveys information concerning blue-yellow opponency (*i.e*., S *vs*. L+M). They belong to the short wavelength system, which is more sensitive to lower spatial and temporal frequencies than the other two cone systems.

The study by Lee *et al*. (1989), which compares the results of electrophysiology in the monkey with psychophysical performance in humans, revealed that the M system is much more sensitive to luminance modulation while the P pathway is more sensitive to chromatic modulation. According to these results, the authors proposed that the physiological origin for the detection of luminance and chromatic modulations could be attributed to the systems M and P, respectively, ignoring the possible role of the P path in achromatic vision (see below). In this view, the M pathway mediates alone the processing of low contrast luminance patterns

(Shapley and Perry, 1986; Lee *et al*., 1993) while the P pathway is engaged principally in chromatic spatial tasks (Lee *et al*., 1993).

1.3.2. The role of the M and P pathways in achromatic vision

Anatomical variation of the M and P pathways can be verified both in nocturnal primates (monochromat), as in diurnal primates (trichomats and dichromats). The biggest difference found among primates (monochromats and dichromat species) is the absence of cells that respond to colour stimuli in the P pathway (review: Lee *et al*., 1996). According to Mollon (1989, 1991) and Boycott and Wassle (1991), there is evidence that the M and P pathways were ancestrally involved in achromatic vision. However, it is unknown why both are involved in achromatic vision and several studies have been done and are still being developed to address this issue. There has been a sustained interest in relating these early retinal pathways to psychophysical data. In the 1970´s (Breitmeyer and Ganz, 1977; Legge, 1978) some psychophysical studies indicated that detection of low spatial frequency stimuli was mediated by a part of the visual system that is highly sensitive to high temporal frequencies, has short temporal integration time (Breitmeyer and Ganz, 1977; Legge, 1978) and tends to respond to transient stimulus (Breitmeyer and Julesz, 1975; Tolhurst, 1975; Legge, 1978). This stream was initially referred to as the *transient system*. High spatial frequency stimuli, on the other hand, are detected by a part of the visual system with high sensitivity to low temporal frequencies, sustained presentations, and long temporal integration. This stream was called the *sustained system*. In fact, the spatial modulation of the CS function, shows evidence of both transient and sustained properties (Legge, 1978), suggesting involvement of both pathways. Lennie (1993) suggested that processing of luminance information is mediated at low spatial frequencies by the M pathway and at high spatial frequencies by the P pathway. The correspondence of the *transient* and *sustained systems* to M and P pathways, respectively, is now widely accepted (Skottun, 2000). This point of view implies that the P pathway participates not only in the processing of chromatic information but also of luminance patterns, while the M pathway mediates luminance information only (Mollon *et al*., 2003).

The most effective and reliable way to isolate M activity in psychophysical experiments is to measure CS (Skottun, 2000a). Studies in which lesions have been placed in various layers of monkey LGN have found that reductions in CS following lesions in the M layers are confined to cases in which the stimuli are of low spatial frequency and/or high temporal frequency (Merigan *et al*., 1991a; Merigan *et al*., 1991b; Merigan and Maunsell, 1990, 1993; Schiller *et al*., 1990a, 1990b). Psychophysical studies in humans are consistent with these findings (Legge, 1978; Tolhurst, 1975). Because the link between CS and M activity has been

established by both lesion studies in monkeys and human psychophysics, it represents the most reliable and direct psychophysical test of M sensitivity. It appears that the M system mediates sensitivity at spatial frequencies below about 1.5 cycles per degree (cpd) and that the P system (or a combination of the P and K systems) carries out detection above this frequency (Skottun, 2000b). One would therefore expect a magno deficit to manifest itself at spatial frequencies below the 1.5 cpd or, alternatively, to be most pronounced at low spatial frequencies. In the case of temporal CS, M deficits would be expected to show themselves at predominantly high temporal frequencies (Dacey and Petersen, 1992).

In this thesis, we have introduced a contrast discrimination technique that unravels P and M pathway function by taking advantage of their differences in achromatic contrast response. Our stimulus, as luminance gratings, allowed us to evaluate spatiotemporal processing of both pathways.

1.4. Contrast Sensitivity

The appearance of a natural scene or coloured stimulus, as is the case for grey level patterns, depends on its spatial and temporal frequency and on the sensitivity of the human eye. The characteristics of the human visual system from the temporal and spatial point of view are defined by the Contrast Sensitivity Functions (CSFs). Plotting contrast sensitivity against spatial frequency gives an inverted 'bell-shaped curve or inverted-U' called the CSF, allowing us to define the point of transition from the 'visible' to the 'invisible' world (see **Figure 1.3**). Therefore, if the detection of contrast were dictated solely by image contrast, the alternating bright and dark bars would appear to have equal height everywhere in the image. However the bars appear taller in the middle of the image than at the sides. The luminance CSF is band-pass in nature and the exact location of the peak depends on the viewing distance (because of the relation with viewing angle and effective spatial frequency of the same stimulus). At a viewing distance of 40 cm it should be possible to detect the bars nearer to the top (see grating in **Figure 1.3**) in the intermediate region of spatial frequencies (3-10 cpd), where the CS is higher. This function approaches zero at 0 cpd as well as around 60 cpd, the point at which details can no longer be resolved by the human eye (limiting optic factors or the photoreceptor mosaic). In fact responses to CS tests may be affected by many factors, such as optical (changes occurring between the image generated on the stimulation device and the image that is projected on the retina) and neural factors (corresponding to the processing and transmission of visual information that occur successively at the retina, the optic nerve, optical radiations and at the visual cortex). Refraction errors are also an important factor in CS. The decrease of VA resulting from a refractive error appears as a loss of the right

side of the limit curve in **Figure 1.3**, corresponding to the loss of the highest spatial frequencies. Loss of transparency of the ocular media (at the cornea and at the lens) results in optical phenomena such as absorption and diffusion. Depending on their relative importance, these phenomena produce a loss of intermediate and high spatial frequencies or even a loss over all frequencies.

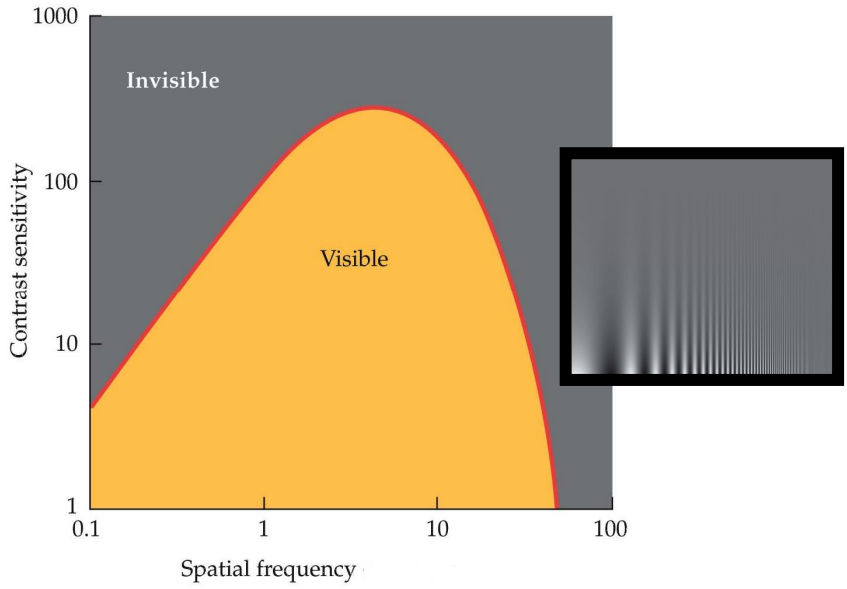

Figure 1.3. The contrast sensitivity (in dB) function (red line) and the Campbell–Robson grating which demonstrates our ability to discern gratings at intermediate frequency better than those of low- or high-spatial frequency (cpd): our window of visibility.

The band-pass CSF correlates with the concept of centre-surround antagonistic receptive fields that would be most sensitive to an intermediate range of spatial frequency. On the other hand, the chromatic mechanisms are of a low-pass nature and exhibit significantly lower cut-off frequencies, which indicates the reduced availability of chromatic information for fine details (high spatial frequencies). The blue-yellow CSF has a lower cut-off frequency then the red-green one, due to the small number of S cones in the retina. Note also that the luminance CSF is much higher than the chromatic CSFs. This denotes a greater sensitivity in the visual system to small changes in luminance contrast compared to chromatic contrast. Temporal CSFs for luminance and chromatic contrast, also share many characteristics with the spatial CSFs: luminance temporal CSF is still higher in both sensitivity and cut-off frequency than chromatic temporal CSFs; exhibits band-pass characteristics (suggesting the enhancement of temporal transients), while chromatic temporal CSFs have low-pass behaviour.

The retina is designed to process contrast, allowing the discrimination and identification of objects across a variety of illumination levels. This contrast detection of the retina is typically explored using visual stimuli such as gratings, although checkerboard patterns or simple letter optotypes can also be utilized. All tests of contrast are dependent on the luminance of the stimulus and the grating patterns have the advantage of allowing contrast to be varied in a sinusoidal fashion without affecting the average stimulus luminance and making possible isolation of specific channels of retinal neurons that respond optimally to that given spatial frequency. The experimental use of sinusoidal gratings in this fashion has been a key to the development of our understanding of retinal function at the level of the retinal ganglion cell response to contrast (Enroth-Cugell and Robson, 1966).

The luminance contrast modulation of the sine-wave grating stimuli used in our custom CS perimetry was defined as the Michelson contrast:

$$c = \frac{L_{\max} - L_{\min}}{L_{\max} + L_{\min}} \tag{1.1}$$

where c, called contrast, is often expressed as a percentage and the luminance L values in candelas per square meter (cd/m^2). L_{max} is the maximum luminance and L_{min} is the minimum luminance of the grating.

The point at which grating detection is lost for a given spatial frequency is known as the contrast detection threshold (c) and it is the reciprocal of this value that identifies the CS. Contrast sensitivity measures are also expressed in decibels (dB), following a logarithmic scale that corresponds to the physiology of the visual system:

$$dB = 10 \times \log\left(\frac{1}{c}\right) \tag{1.2}$$

with c measured as a percentage as in (1.1).

In this thesis, CS was determined at each VF location by means of a logarithmic staircase procedure. CS was defined in terms of a decibel (dB) scale, so that 0 dB of CS refers to a stimulus of 100% contrast. Each decibel correspond to a 0.1 log unit change in contrast, so that 10 dB refers to a stimulus of 10% contrast, 20 dB refers to a stimulus of 1% contrast, 30 dB corresponds to 0.1% and so forth. Gratings with a very low contrast (below a limit of

0.3%) are not perceived; in fact, this limit is not the same for all spatial frequencies. See **Figure 1.3** that represents the real limit curve for a viewing distance of 40 cm.

Another important parameter of CS is the temporal dimension. The study of the temporal response to contrast or dynamic contrast, can be made with a grating stimulus that is reversed periodically (white bars replacing black bars and vice versa). The temporal frequency is usually given in hertz (Hz) or in cycles per second (cps). Flicker is a specific example of dynamic contrast where the spatial frequency of the grating is so low that only one bar is visible at a given time.

1.5. Colour vision

High resolution vision and trivariant colour vision evolved to enhance survival. The fovea formed to facilitate high resolution achromatic vision and a third opsin evolved from the original mammalian L-cone opsin to create a new dimension of colour in higher primates (Jacobs, 2008). The evolution of trivariant colour vision in higher primates increased the repertoire of colours we perceive and the power of spectral contrast to detect objects. The original blue/yellow form of colour vision was then accompanied by a parallel system of red/green colours occurring in the region of the spectrum where brightness is maximal (Mullen and Kingdom, 2002).

Normal human vision is trichomatic. Observers can match a test light of any spectral composition to an appropriately adjusted mixture of just three other lights. Consequently, colours can be defined by three variables: the intensities of the three primary lights with which they match. These are called *tristimulus values*. The trichromatic theory of colour vision was developed by Helmholtz and Young in the 19th century based upon the colour matching experiments of Maxwell (Helmholtz, 1924; Young, 1902). They stated that there must be three different types of photoreceptors sensible to red, green and blue light, respectively. Indeed the first careful quantitative measurements of colour matching and trichromacy were made by Maxwell. Trichromacy means that the colour-matching behaviour of an individual can be characterized as the intensities of three independent *primary lights* that are required to match a series of monochromatic spectral lights spanning the visible spectrum. Two experimental methods have been used to measure colour matches: the maximum saturation method and Maxwell's method. Most standard colour-matching functions (CMFs) have been obtained using the maximum saturation method (Brainard and Stockman, 2010). In this method, the observer is presented with a half field illuminated by a monochromatic test light of variable wavelength λ and an abutting half field illuminated by a mixture of red (R), green (G), and blue (B) primary

lights. It was used by Wright (1929) and Guild (1931) to obtain the matches that form the basis of the CIE 1931 colour-matching functions. Many of the CMFs are available online in tabulated form at URL http://www.cvrl.org/.

In 1878, the physiologist Ewald Hering proposed the opponent-colour theory, in apparent contradiction with Young-Helmholtz trichromatic theory. Hering advanced his theory to explain various phenomena that could not be adequately accounted by trichromacy. Examples of such phenomena are the after-image effect (if the eye is adapted to a yellow stimulus the removal of the stimulus leaves a blue sensation or after-effect), the fact that some hues were never perceived to appear together (such as red-green or blue-yellow) and also the non-intuitive fact that an additive mixture of red and green light gives yellow and not a reddish-green. Hering proposed that yellow-blue and red-green represent opponent signals. The Young-Helmholtz-Hering dispute has an interesting resolution: both are plausible on a physiological basis. Colour vision is trichromatic at the photoreceptor level, while the opponent processes foreseen by Hering enter at the level of the ganglion cells of the retina, and are a feature of LGN and cortical processing of colour. Neurons of the retina encode the colour into three opponent signals. The output of the three cone types is combined to form the achromatic signal or luminance channel (L + M), the red-green signal (L - M) and the yellow-blue signal (- L - M + S), see Stockman and Brainard (2010).

Visualizing colour data and producing graphical representations of colour data is a very challenging issue, since colour coordinates are three-dimensional, it is difficult to plot them on a two dimensional way. Chromaticity diagrams are very useful for plotting colour data by reducing the dimensionality of the data representation. The Commission internationale de l'éclairage (CIE) 1931 *xy* chromaticity diagram has been the most widely used in the past, but it does suffer from one important disadvantage, the lack of uniformity, as observed by MacAdam. To avoid this non-uniformity, CIE recommended a new CIE 1964 diagram based mainly on the 10º CMFs of Stiles and Burch (1959), to be used with constant luminance levels and in 1976 the CIE defined two other colour coordinate systems: the CIELUV (Lu´v´) and the CIELAB (L*a*b*). CIE 1976 (Lu´v´) uniform colour space was defined as nonlinear transformation of the CIE 1931 (xy) space that maps equal differences in colour to equal distances. The MacAdam colour discrimination ellipses became circles after this transformation, obeying the principle of uniformity.

1.5.1. Contrast and Opponent Spaces

Cone coordinates are useful because they make explicit the responses of the initial physiological mechanisms thought to mediate colour vision. A number of investigators have begun to use representations that attempt to represent the responses of subsequent postreceptoral mechanisms. Two basic ideas underlie these representations. The first is the general opponent processing model. We call representations based on this idea opponent colour spaces. The second idea is that stimulus contrast is more relevant than stimulus magnitude. We call spaces that are based on this second idea modulation or contrast colour spaces.

Cone space - To derive coordinates in the cone contrast colour space, the stimulus is expressed first in terms of its cone coordinates. The cone coordinates of a white point are then chosen. Usually, these are the cone coordinates of a uniform adapting field or the spatio-temporal average of the cone coordinates of the entire image sequence. The cone coordinates of the white point are subtracted from the cone coordinates of the stimulus and the resulting differences are normalized by the corresponding cone coordinates of the white point. The cone contrast space is based on the assumption that cone excitations are subsequently coded as contrast relative to some background signal; more precisely Weber-style normalization is assumed. Let L, M and S represent the excitations of the three cone types. Thus, the corresponding differential responses ΔL; ΔM; ΔS with respect to a background, producing an excitation on the three cone types of L_o; M_o and S_o respectively are:

$$\begin{bmatrix} \Delta L \\ \Delta M \\ \Delta S \end{bmatrix} = \begin{bmatrix} L - L_o \\ M - M_o \\ S - S_o \end{bmatrix} \tag{1.3}$$

Macleod-Boynton space - In this two-dimensional space the coordinates are the projections of the space (*L*, *M*, *S*) in a plane parallel to the S axis passing through L=1 and M=1. This space is based on the Smith and Pokorny (1975) cone spectral sensitivities *l(λ)*, *m(λ)* and *s(λ)*, with s(λ) scaled by the constant 0.01608 for graphical convenience. These sensitivities represent corneal spectral sensitivities which are different from the sensitivities at the retina level, obtained by discounting the effect of the eye media (lenses, macular pigment). The assumption that l(λ) + m(λ) gives the photopic sensitivity implies that colour is represented in a uniform luminance plane and then the physiological diagram represents the relative cone excitations given by:

$$l_\lambda = L_\lambda /(L_\lambda + M_\lambda)$$
$$m_\lambda = M_\lambda /(L_\lambda + M_\lambda) \quad (1.4)$$
$$s_\lambda = S_\lambda /(L_\lambda + M_\lambda)$$

The chromaticity diagram suggested by MacLeod and Boynton (1979) consists on vertical variations which imply variations only in the yellow-blue chromatic channel and the horizontal variations correspond to the red-green chromatic channel. Tritan confusion lines are vertical lines (parallel to ordinate axis). The protan confusion lines (constant M and S) converge in the copunctal point (the locus of the missing fundamental) (0, 1) and deutan lines (constant L and S) in the point (0, 0).

DKL (Derrington, Krauskopf, and Lennie) space - The DKL colour opponent modulation space was introduced by Derrington, Krauskopf and Lennie (Derrington et al., 1982; Krauskopf et al., 1984) and is now widely used to characterize the output of the human vision opponent-colour model. This space is closely related to the chromaticity diagram suggested by MacLeod and Boynton (1979). So, this is a spectral opponent space that is consistent with the opponency of the P pathways of the primate retina and LGN. It is a linear transformation of the cone space centred in the coordinates corresponding of a white field to which the observer is adapted. To derive coordinates in the DKL colour space, the stimulus is first expressed in cone coordinates. As with cone contrast space, the cone coordinates of a white point are then subtracted from the cone coordinates of the stimulus of interest. It is particularly suited to experiments in which the observer is adapted to an equal-energy white field plotted in the origin of the space. The axes (from the origin) in terms of the Smith and Pokorny sensitivities are: L+M, L-2M and S-(L+M). These axes isolate variations in luminance, in the ratio of L to M cones at constant luminance and in S cones at constant luminance, respectively.

Acquired colour vision deficiencies can affect the coding of chromatic information at any level from the outer segments of the photoreceptors to the inferotemporal cortex. Because conventional colour vision procedures are based largely on principles derived from studies of normal colour vision and congenital dyschromatopsia, they often fail to adequately describe acquired colour vision deficiencies. Approximately 8% of the male and 0.4% of the female population have congenital colour vision anomalies in which one or more of these cone types is either absent or exhibits an altered spectral absorption. Abnormalities of the long-, medium-, and short-wavelength photopigments result in protan, deutan, and tritan defects, respectively.

1.6. The visual field

The VF can be defined as the area of space that one eye can see in stable fixation at any given instant. The term VF is sometimes used as a synonym to field of view, though they do not designate the same thing. Field of view is everything that at a given instant causes light to fall onto the retina. This input is processed by the visual system which computes the VF as the output. The study of VFs has always been of great interest in the field of ophthalmology, as a method of diagnosis. Visual acuity (VA) is the most common measure of visual function. Advances in understanding the functional anatomy of the visual pathways, have made it increasingly clear that vision is a multidimensional modality and that VA measures only a limited aspect of a single dimension of vision: spatial resolution. VA is the spatial resolving capacity of the visual system which can be defined both psychophysically and electrophysiologically, using for example Sweep Visual Evoked Potentials (SVEP). There are various ways to measure and specify VA, depending on the type of acuity task used. It can be measured with simple letter stimuli but sinusoidal gratings can also be used advantageously because with these stimuli one can isolate distinct spatial frequency channels which can then be related with distinct neural channels. However, there is an increasing recognition of the need to evaluate visual function beyond the limited extent afforded by VA. Other sub-categories of visual function also include: CS, colour perception, stereoacuity (depth perception), fixation stability and VF. A variety of new and lesser-used techniques for measuring visual function exist that complement VA assessment, each of which has been shown to detect visual dysfunction in patients with normal VA.

1.6.1. The retinotopic representation of the visual field

The spatial relationships among the ganglion cells in the retina are maintained in most of their central targets as “maps of visual space”. Most of these structures receive information from both eyes, requiring that these inputs be integrated to form a coherent map of individual points in space. As a general rule, information from the left half of the visual world, whether it originates from the left (OS) or right (OD) eye, is represented in the right half of the brain, and vice versa. Understanding the neural basis for the appropriate arrangement of inputs from the two eyes requires considering how images are projected onto the two retinas, and the central destination of the ganglion cells located in different parts of the retina. Each eye sees a part of visual space that defines its VF. For descriptive purposes, each retina and its corresponding VF are divided into quadrants. The surface of the retina is subdivided by vertical and horizontal lines that intersect at the centre of the fovea (**Figure 1.4 Upper panel)**. The vertical line

divides the retina into nasal and temporal divisions, while the horizontal lines divide the retina into superior (dorsal) and (ventral) divisions. Corresponding lines (also called meridians) in visual space intersect at the fixation point (which is the point in visual space that falls on the fovea), and define the quadrants of the VF (see **Figure 1.4 Lower panel**). The passage of light rays through the pupil of the eyes results in images of objects that are inverted and left-right reversed on the retinal surface. As a result, objects in the temporal part of the VF are seen by the nasal part of the retina and objects in the superior part of the VF are seen by the inferior retina (**Figure 1.4**).

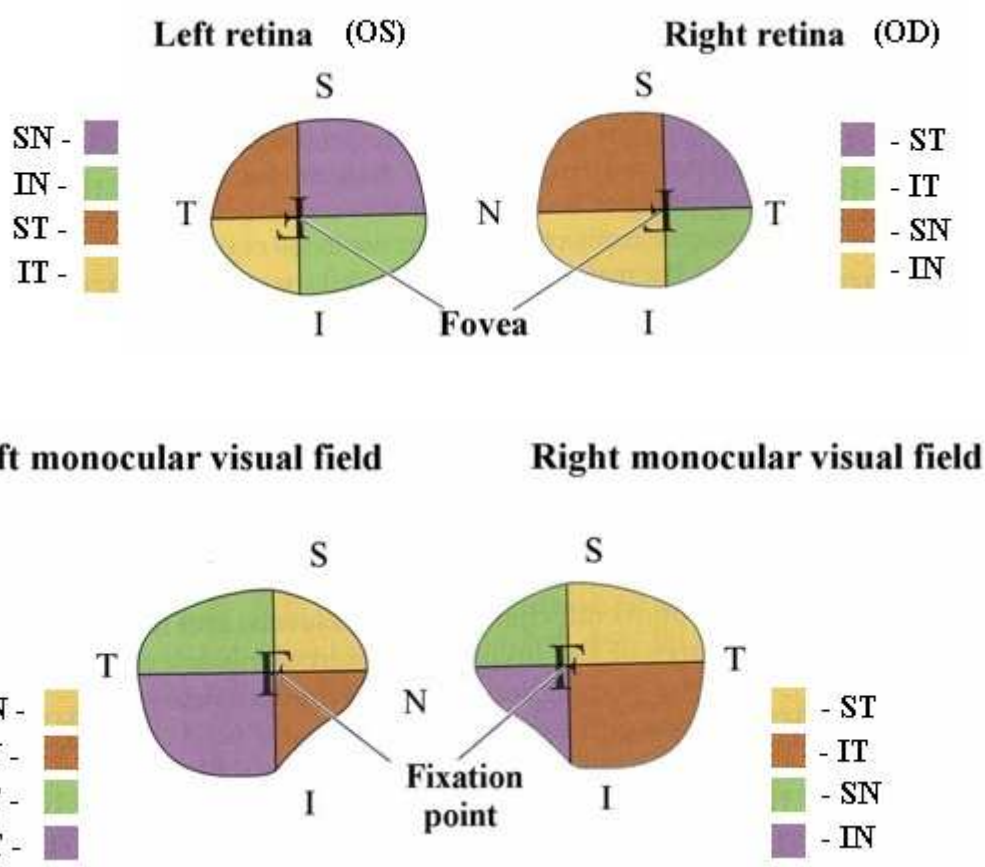

Figure 1.4. Upper Panel: Retinal quadrants (lines drawn through the centre of the fovea). **Lower Panel:** Vertical and horizontal lines drawn through the point of fixation define VF quadrants (note the inversion of quadrants in terms of VF). Colour coding illustrates corresponding retinal and VF quadrants. ST, superotemporal; IT, inferotemporal; SN, superonasal; IN, inferonasal. (Adapted from Purves D, Augustine GJ, Fitzpatrick D, Hall WC, LaMantia AS, McNamara J, Williams SM. In: Sinauer Associates, Inc., MA., 3rd edition, *Neuroscience*).

When both eyes are open, the two foveas are normally aligned on a single target in visual space, causing the VFs of both eyes to overlap extensively, in this way the binocular field of view consists of two symmetrical left and right visual hemifields (**Figure 1.5**). The temporal VFs are more extensive than the nasal ones, reflecting the size of the respectively nasal and temporal retinas, divided at the fovea. The sensitivity of the eye is not constant across the whole VF. It varies with eccentricity, adaptation level and the nature of the test stimulus. The normal human monocular extent of the VF for a bright stimulus is 60° superiorly, 75° inferiorly, 100° temporally and 60° nasally, although this can be affected by facial contours (Henson and Morris, 1993). As a result, vision in the periphery of the binocular field of view is strictly monocular, mediated by the most medial portion of each nasal retinas. Most of the rest of the field of view can be seen by both eyes; in particular, the inferior nasal VFs are less extensive than the superior nasal fields, consequently the binocular field of view is smaller in the lower VF than in the upper, see **Figure 1.5**. It is worth noting, that the shape of the face and nose can impact the extent of this region of binocular vision. The binocular field increases the horizontal extent of this field to approximately 200°. The clinical recording of VFs is called perimetry and is used to determine whether the VF is affected by diseases that cause local scotoma or a more extensive loss of vision or a reduction in sensitivity (threshold).

Images of objects in the binocular portion of the left visual hemifield fall on the nasal retina (the temporal VF) of the left eye (OS) and the temporal retina (the nasal VF) of the right eye (OD) (**Figure 1.5**); and the axons from ganglion cells in these regions of the two retinas project through the right optic tract. Objects in the binocular portion of the right visual hemifield fall on the nasal retina (temporal VF) of the OD and the temporal retina (nasal VF) of the OS; the axons from ganglion cells in these regions project through the left optic tract. Objects that lie in the monocular portions of the left and right VFs fall on the left and right nasal retinas, respectively (see **Figure 1.5**).

Thus, ganglion cells that lie in the nasal division of each retina give rise to axons that cross in the optic chiasm, whereas those from the temporal retina do not (see **Figure 1.5**). As a result, information from the left visual hemifield is carried in the right optic tract, and information from the right visual hemifield is carried in the left optic tract. Optic tract axons terminate in an orderly fashion within their target structures thus generating well ordered maps of the contralateral hemifield.

For the primary visual pathway, the map of the contralateral hemifield that is established in the LGN is maintained in the projections of the LGN to the striate cortex. Thus, the area of central vision (the foveamacular region) is represented over a disproportionately large part of the caudal portion of the occipital lobe, whereas peripheral vision is represented more

anteriorly. The superior VF is mapped below the calcarine sulcus, and the inferior VF above it. The amount of cortical area devoted to each unit area of the visual sensory surface is not uniform, but reflects the density of receptors and sensory axons that supply the peripheral region. V1 has a topographic map of the VF. There is a 'neural image' which retains the spatial layout of the pattern of light incident in the retina. This mapping is referred to as retinotopy. Information presented in the left half of the VF is detected by the nasal half of the left retina and the temporal half of the right retina. Fibres from these retinal areas project on to the right cerebral hemisphere and vice versa (**Figure 1.5**). Input from the upper VF is incident on the inferior retinal quadrants which project on to the lower lip of the calcarine sulcus. The inferior VF is represented on the calcarine sulcus upper lip. Information presented to the central VF is processed by a greater number of neurons and hence a much larger volume of visual cortex than information presented to more peripheral regions. This phenomenon is described as cortical magnification, and corresponds to the superior visual performance of the central VF, implying that retinotopic mapping is non-linear.

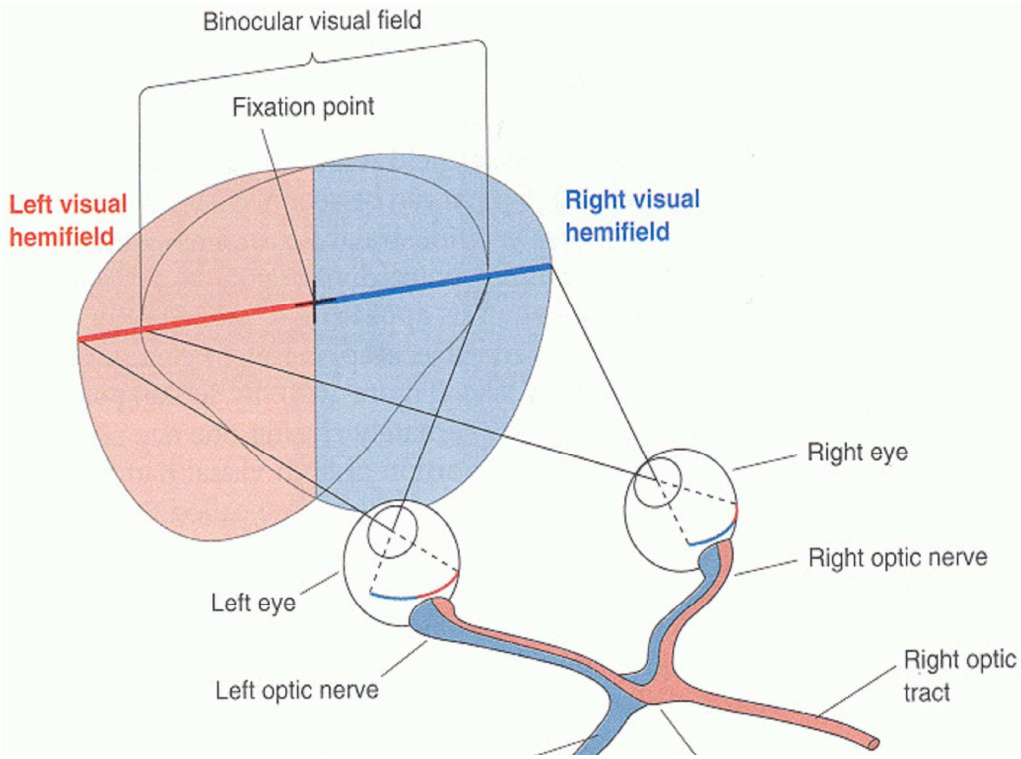

Figure 1.5. Projection of the binocular field of view onto the two retinas and its relation to the crossing of fibers in the optic chiasm. (From http://fourier.eng.hmc.edu/).

1.7. Visual field measures

1.7.1. Perimetric techniques that try to isolate functional pathways

A variety of techniques have been developed to functionally assess peripheral vision, these generally assess visual function in different locations of the more peripheral field and at and near the fovea and fall under the general heading of VF tests, or perimetry. The conventional perimeters are not specific to stimulate different types of ganglion cells and the redundancy present in the visual system makes it difficult to detect early functional loss. Following this theory, a special diagnostic method can be optimized for testing the functioning of a particular cell system. Perimetric tasks that evaluate the performance of specific ganglion cell types have been shown to be superior to standard automated perimetry (SAP) for the detection of early visual field loss (for example in glaucoma, see Johnson *et al*., 1993; Johnson and Samuels, 1997; Casson *et al*., 1993; Sample *et al*., 1993,1997).

Based on the anatomical and functional data presented above, many methods have been developed to study the visual function by targeting the M, P and/or K pathways. Presently the following methods are available to serve this purpose:

Magnocellular pathway:

a) Flicker perimetry. In the flicker perimetry technique (Matsumoto *et al*., 1998), the Critical Fusion Frequency threshold is measured locally at different locations in the VF (central 30º). The Critical Fusion Frequency is the value in Hz where the flickering stimulus fuses into a seemingly continuous light. During the test the flicker (temporal) frequency is varied in steps, depending on the strategy selected, from slow (1-5 Hz) to very fast (until 50 Hz). The patient must answer the question whether the stimulus is flickering or is seen as a continuous light, which is more difficult to answer compared to a simple detection task whether one sees or not the stimulus. For this reason the stimulus duration is one second in order to allow sufficient decision time. Important characteristics of Critical Fusion Frequency perimetry are that it is measured more efficiently in the early stages of visual field loss; is much less influenced by media opacities in the optical pathway and blur (Lachenmayr and Gleissner, 1992; Matsumoto *et al*., 1997; González *et al*., 1999). However a normative database is lacking in most devices.

b) Frequency doubling perimetry (FDP) is a CS discrimination method and has been implemented clinically and consists of patterns of flickering, achromatic, vertical, sinusoidal gratings. The test measures the amount of contrast necessary to detect the gratings when they

are presented in a series of locations in the central and peripheral field. In the normal eye at a certain level of contrast, the spatial frequency appears to double; this is called the frequency doubling illusion (Kelly, 1966). However the apparent spatial frequency of the gratings is not tested. It is a very sensitive technique suited to detect retinal dysfunction and is even used as golden standard for detection of early functional loss in glaucoma (Johnson and Samuels, 1997; Cello *et al*., 2000; Landers *et al*., 2000; Trible *et al*., 2000; Paczka *et al*., 2001).

c) Motion perimetry: Like contrast perception, motion perception plays an important role in this thesis. Numerous techniques have been developed for measuring the threshold of detection and recognition of movement in the VF. The motion tests can include global and/or local (at different eccentricities) aspects of motion perception. The different psychophysical tasks can be direction discrimination (indicating the motion direction), motion detection, and motion localization (pointing to the area of movement). The most commonly used stimuli are dynamic sparse random kinematograms dots (RDKs) generated on a computer screen. Such stimuli are usually used to measure the minimum and the maximum perceived displacements, referred as Dmin and Dmax (Fitzke *et al*., 1987, 1989; Westcott *et al*., 1999), called Motion Detection Threshold (MTD) test. Other example is the ability to report or detect the motion of a subset of coherently moving dots within a population of randomly moving dots, called coherent local motion perimetry (for a review on motion perception tests see Shabana *et al*., 2003).

Parvocellular pathway: High-pass resolution perimetry (HRP), see Frisen L (1992). HRP uses spatially high-pass filtered ‘‘ring’’ targets to measure detection and resolution thresholds (Martinez-Bello *et al*., 2000). HRP is a peripheral VA test involving targets that consist of a dark ring surrounding a light centre region and appears similar to Landolt C’s. The test varies the size of the targets while holding the contrast fixed and measures resolution thresholds at 50 locations across the VF. This technique is usually used to detect uninvolved and involved eyes in patients with optic neuritis (Wall *et al*., 1991) and glaucoma progression (Chauhan *et al*., 1999).

Koniocellular pathway: Short Wavelength Automated Perimetry (SWAP), also known as blue-yellow perimetry, is a chromatic perimetry and a modification of the automated static perimetry, in which a carefully chosen wavelength of blue light (440 nm) is used as the test spot, whereas a bright yellow light (530 nm cut-off-filtered, 315 apostilb equivalent to 100 cd/m^2) provides an adapting background (Risse, 1999). This technique is a variant of Stiles’ two-colour increment threshold technique, in which the yellow background desensitizes the middle-wavelength (green) and long-wavelength (red) sensitive cone pathway, so that the blue

test flash measures the sensitivity of the isolated blue/yellow (S-cone) pathway (Trick, 2003). SWAP has been shown to be more valuable in detecting early damage in diabetic retinopathy than conventional perimetric methods (Remky *et al*., 2000). Thus, blue-yellow perimetry has been suggested to specifically test the blue cones, their retinal ganglion cell connections, and their associated higher pathways.

1.7.2. Non-perimetric techniques that try to isolate functional pathways

Achromatic contrast discrimination technique: Pokorny and Smith (1997) developed a psychophysical achromatic contrast discrimination technique with the *pulsed-pedestal*, *steady-pedestal* and *pedestal-*Δ*-pedestal* paradigms to assess the P and M pathway function, respectively. This strategy was designed initially to separate the pathways on the basis of their different contrast gain properties (Kaplan and Shapley, 1986). In both paradigms, the stimulus array consists of four 1º squares with small separations in a larger uniform surround, but with different interstimulus adaptation. Contrast thresholds were measured in pulses that were incremented or decremented from the average retinal illuminance. The *steady-pedestal paradigm* consists of the brief presentation of a test stimulus against a continuously presented luminance pedestal. This paradigm is thought to favour the M pathway for test targets of low to intermediate spatial frequencies, because the test target is presented briefly. While the *pedestal-*Δ*-pedestal* one is identical to the steady-pedestal condition in all aspects except that during the trial, the retinal illuminance of all 4 squares was incremented or decremented with the test square differing in luminance from the other three. It is used to assess the contrast gain signature of the inferred M and P pathways. The *pulsed-pedestal* paradigm consists of the simultaneous brief presentation of a test stimulus and luminance pedestal. The pulsed-pedestal paradigm is thought to bias processing toward the P pathway because the abrupt onset of the luminance pedestal drives the M pathway toward saturation. Psychophysical data acquired using these two paradigms have the contrast response properties and temporal summation characteristics associated with the M and P pathways described electrophysiologically (Kaplan and Shapley, 1986; Leonova *et al*., 2003; Pokorny and Smith, 1997). Additionally, the results obtained under these paradigms have strong parallels with previous work examining pattern versus motion thresholds (Kulikowski, 1978), and sustained versus transient visual mechanisms (Harwerth, Boltz, and Smith, 1980; Kulikowski and Tolhurst, 1973; Legge, 1978. Recently, these paradigms have been however modified to assess the luminance spatial CS of the presumed M and P pathways (Kachinsky *et al*., 2003; Leonova *et al*., 2003; Gualtieri *et al*., 2006; Checkerboard test: Benoff *et al*., 2001; Costa and Ventura, 2005). The *steady-* and *pulsed-pedestal* paradigms have been used to examine CS

deficits in patients with retinal disease (Alexander *et al*., 2004; McKendrick *et al*., 2004), M and P function in schizophrenia (Delord *et al*., 2006), the visual pathways mediating particular visual illusions (McAnany and Levine, 2005; Puts, Pokorny, and Smith, 2004), the equivalency of common optotypes (McAnany and Alexander, 2006) and in a group of patients with Parkinson Disease (Feitosa-Santana, 2008). Although these studies had very different goals, the results obtained in each of these studies under the *steady-* and *pulsed-pedestal paradigms* are consistent with mediation of visual sensitivity by the M and P pathways, respectively.

Chromatic contrast discrimination technique: Cambridge Colour Test (CCT) [Cambridge Research Systems (CRS), Rochester, UK] is a commercially available version of the Mollon-Reffin colour discrimination test (Mollon and Reffin, 1989; Mollon and Regan, 2000; Regan *et al*., 1994, 1998). It is a computerized colour vision test (Regan *et al*., 1994) designed for rapid determination of colour discrimination thresholds by evaluating P and K pathways. Preliminary normative data for the CCT were described by Ventura *et al*. (2003a) for adults ranging from 18 to 30 years of age with normal colour vision (independently assessed by the Farnsworth-Munsell 100-Hue test). The CCT has been a useful tool for the assessment of colour discrimination in a variety of studies with different clinic populations, even in early stages of several diseases: Simunovic *et al.* (1998), for patients with dominant optic atrophy; Regan *et al*. (1998) for Parkinsonian patients; Ventura *et al*. (2002) for patients treated with chloroquine; Ventura *et al*. (2003b) for diabetic patients; Ventura *et al*. (2004, 2005) for individuals with mercury intoxication; Castelo-Branco *et al*. (2004) for glaucoma patients; Ventura *et al*. (2007) for carriers of Leber's hereditary optic neuropathy; Costa *et al*. (2007) for patients with Duchenne muscular dystrophy, as well as with individuals without pathologies (Costa *et al*., 2006).

In its short test version (Trivector), subjects are tested for the three main cone-confusion axes (i.e. along the protan, deutan, and tritan colour confusion lines) simultaneously and in an interleaved manner, by modulating chromaticity in CIE 1976 u´v´ colour space (Castelo-Branco *et al*., 2004; Campos *et al.*, 2005), isolating L, M and S cone responses. A longer version of the test can determine "areas of colour confusion" (called discrimination ellipses) which evaluates damage along areas of impairment instead of axes of damage.

Chapter 2

2. Study-specific introduction

2.1. Early retinocortical contributions to perceptual anisotropies: evidence from anatomy, psychophysics and physiology

Given the layout of the retina, with specific rod and cone distributions and different populations of bipolar and retinal ganglion cells, spatial and temporal qualities of the retina are not uniform but rather depend on which parts are stimulated and under what conditions. Hence, at least from a retinal perspective, VA and CS will depend not just on “optical” factors such as refractive error and pupil size but also on “neural” factors such as photoreceptor density, stimulus contrast and luminance and the region of the retina being stimulated (Perry and Cowey, 1985; Thibos *et al*., 1987; Dacey and Petersen, 1992; Altpeter *et al*., 2000). It is well established that sensitivity is not necessarily equivalent at isoeccentric locations across the VF. Acuity is highest in the central field, and worsens toward the periphery. There are also clear nasal-temporal differences, a difference that has not been explored as thoroughly is that between the superior and inferior visual hemifields. However, asymmetries in terms of VF have been widely established for high-level psychophysical tasks (for comprehensive reviews see Ivry and Robertson, 1998; Hugdahl and Davidson, 2003).

Although anatomical and physiological data is available for anisotropies in early visual pathways including cortical retinotopic areas and the retina it is important to clarify this apparent dissociation between anatomy, physiology and psychophysics, in particular if one considers the emphasis that has been assigned to the biological foundations of functional asymmetries in the field of cortical lateralization research.

2.1.1. Anatomical anisotropies within the primate retina

Previous anatomical asymmetries within the retina have been well documented in many species (Andrade da Costa and Hokoc, 2000; Chandler, Smith, Samuelson, and MacKay, 1999; Kryger, Galli-Resta, Jacobs, and Reese, 1998; Packer, Hendrickson, and Curcio, 1989; Perry and Cowey, 1985; Wikler and Rakic, 1990a; Wikler, Williams, and Rakic, 1990b), including the human eye (Curcio and Allen, 1990a; Curcio *et al*., 1990b; Østerberg, 1935). In particular, variation of rod and cone densities of the human eye and along naso/temporal axes is well documented both in terms of eccentricity as well as of radial asymmetries (Osterberg, 1935; Curcio *et al*, 1987; Curcio *et al*., 1990b; Jonas *et al*., 1992). In Osterberg´s data the difference between nasal and temporal cone density is namely, 80000/mm^2 nasal versus 56000/mm^2 temporal at 23° eccentricity. Cone density in the nasal retina (temporal VF) is close to the density in the temporal retina for small eccentricities, but starts to become slightly larger at about 5º and this difference increases up to 40º, where the nasal density is 40 to 45% higher than the temporal density. And there is a slightly higher density of cones in the midperipheral inferior retina compared to superior retina (Curcio *et al*., 1990b). Accordingly, highest rod density is found 12º above the fovea to the nasal side in healthy eyes (Curcio *et al*., 1990b). Curcio *et al*. (1993) found the highest rod density 4-5 mm above the fovea in healty eyes. The cone density declines more sharply along the vertical meridian (VM) than along the horizontal meridian (HM), so that at 3.5º the density is 20.000 cones/mm^2 on the HM and 16.000 cones/mm^2 on the VM (Curcio *et al*., 1990b).

There is also a ganglion cell density bias favouring the nasal retina (temporal VF) which, at eccentricities greater than 15º, has 300% more retinal ganglion cells (Curcio and Allen 1990a; see also Perry and Cowey, 1985 for data in monkeys) compared to the temporal retina (nasal VF). Retinal naso/temporal asymmetries are cancelled out in the cortex, due to the nature of left/right representation of visual hemifields.

The superior/inferior anisotropy is emphasized both in retina and cortex, since the superior retina (inferior VF) has 12% more visual cortex at eccentricities greater than 2.5º (Van Essen *et al*., 1984) and at eccentricities greater than 15º has 60% more retinal ganglion cells (Curcio and Allen, 1990a; Croner and Kaplan, 1995) compared to the inferior retina (superior VF).

The anisotropies in neural representations are further propagated to subsequent processing streams (Connolly and Van Essen, 1984; Van Essen *et al*., 1984). Connolly and Van Essen found that neural representations were larger for LGN laminae corresponding to the nasal retina (temporal VF) in both the M and P layers, which is in line with differences in ganglion cell densities seen in the macaque and human. There is already some evidence on

how radial (eccentricity dependent) asymmetries are distributed within M and P pathways. Dacey (1993) found that midget ganglion cells (P) make up about 95% of the total in central retina, falling to about 45% in the periphery. Anatomical studies on macaques indicate that 10% of the retinal ganglion cells projecting to the LGN terminate in the M layers (Perry *et al*., 1984). Both M and P ganglion cells increase in size from the fovea toward the retinal periphery. However M dendritic fields are generally about 2 to 3 times larger than P dendritic fields in all primate species (Perry *et al*., 1984, Dacey and Petersen, 1992; Yamada *et al*., 2001). In all primates studied so far, the dendritic field size of M and P ganglion cells located in the nasal retinal is smaller than at similar eccentricities (Perry *et al*., 1984, Dacey and Petersen, 1992; Ghosh *et al*., 1996; Yamada *et al*., 2001). M and P ganglion cells in owl monkeys present (Silveira *et al*., 1994) larger dendritic fields than those of diurnal primates (Yamada *et al*., 1998, 2001). The fact that ganglion cells in primates with predominant nocturnal vision (with higher CS) have larger dendritic fields than those of diurnal primates suggests that larger dendritic trees may yield better CS (contrast sensitivity). Towards the retinal periphery of the owl monkey, temporal ganglion cells tend to have larger dendritic fields than nasal cells (Yamada *et al*., 2001). Then this might represent a neuronal correlate of higher CS for that part of the retina. Asymmetries in dendritic field size have also been described in human, macaque and marmoset retina (Dacey and Petersen, 1992; Dacey, 1993; Ghosh, Goodchild, Sefton and Martin, 1996) and in the periphery of the capuchin monkey retina (Yamada *et al*., 1996). In all studies the nasal cells are smaller at similar eccentricities. Asymmetries in dendritic field size may also lead to differences in M-scaling and perceptual performance.

2.1.2. Evidence for left-right and dorso-ventral performance anisotropies – The “dual frequency filter” model of visual processing

High-level spatial anisotropies in visual performance have been previously documented (Nakayama and Mckeben, 1989; Edgar and Smith, 1990; Previc, 1990; Rubin *et al*., 1996; Carrasco et al., 1998, 2001, 2004; Ivry and Robertson, 1998; Talgar and Carrasco, 2002; Hugdahl and Davidson, 2003). Visual left-right lateralization effects have also been often described and postulated to be mediated by attentional mechanisms and not by hardwired low-level receptoral differences (Kosslyn *et al*., 1994; Ivry and Robertson, 1998). Accordingly, the right hemisphere (RH) has a bias to filter visual information through large attended areas, in contrast to the left hemisphere (LH) which favors processing of small attended areas (Kosslyn *et al*., 1994; Ivry and Robertson, 1998; Kitterle *et al*., 1990; Kitterle and Christman, 1991;

Sergent, 1991). These asymmetries have become known as the “low and high spatial frequency” processing biases, due to the fact that they can be demonstrated when attention is deployed to simple supra-threshold sinusoidal gratings. This labeling would seem to suggest a low-level mechanism, but in fact it is believed that it reflects an attentional bias, that is incorporated in a “dual spatial frequency filter” model of visual processing (Ivry and Robertson, 1998), that also generalizes to auditory temporal frequency perception. In this model, sensory representations are generated prior to a frequency filtering first stage, which implements attentional selection of task relevant information. In the second stage, asymmetric processing of selected information occurs in the two hemispheres. Most of the previous work of visual lateralization has emphasized the “double spatial frequency filter” model postulated by Ivry and Robertson (1998), who asserted that the left hemisphere has an attentional bias for processing information contained in relatively high spatial frequencies whereas the right hemisphere has a high-level bias for processing information contained in relatively low spatial frequencies. This model is based on high-level task dependencies (Kitterle *et al*., 1990; Kitterle and Christman, 1991; Ivry and Robertson, 1998; but see Rao *et al*., 1981).

This framework leaves open the question whether these hemispheric asymmetries are due to the way the cerebral hemispheres treat differently M and P information, or whether there are true anatomophysiological asymmetries in the way these pathways connect to the two structures (for a discussion on these possibilities see Laeng *et al*., 2003; Roth and Hellige, 1998). The reported attentional biases seem to be very much task-dependent, which may explain some failures for replication (Sergent, 1991; for a review see Laeng *et al*., 2003). For these reasons it is likely that the “double frequency filter” hypothesis does in fact embed high-level mechanisms, and is revealed by complex tasks, requiring discrimination or identification processes. The evolution of the human visual system has resulted in biological arrangements designed to meet the needs of complex environmental demands. Some of the previous work has emphasized the ecological relevance of dorso-ventral anisotropies and focused on particular visual meridians and many authors have reported a general inferior VF (visual field) advantage (Carrasco, Giordano, and McElree, 2004; Carrasco *et al*., 2001; Liu, Heeger, and Carrasco, 2006; Skrandies, 1987; Talgar and Carrasco, 2002; Cameron, 2005; He *et al*., 1996; Levine and McAnany, 2005a, 2005b; McAnany and Levine, 2004a, 2004b; Previc, 1990). These asymmetries make sense if we consider that, the inferior VF is where the hands work at fine tasks like separating seeds and peels from fruit, or capturing small prey. Fine colour and contrast discriminations would be important for such tasks, as would sensitivity to small lateral motions. The superior VF may be somewhat more concerned with approaching dangers: low tree branches, swooping predators. Recognition of depth could be important to avoid these

threats. So, it could be reasonable to assume that our visual systems have evolved to meet these needs.

2.1.3. Evidence for low-level retinal sources of asymmetry and cortical hemispheric asymmetry

It is surprising that few of the former studies (Carrasco *et al*., 2001) investigating perceptual anisotropies did explicitly investigate whether they may be determined by visual constraints at an early cortical level, independently of the attentional modulatory effects mentioned above. Carrasco *et al*. (2001), analyzed performance at particular locations in the horizontal and vertical meridians and intermediate axes, for orientation discrimination, detection and localization tasks, while manipulating a number of visual factors and attention. The authors suggested that performance fields are determined by visual cortical constraints, rather than by transient high level attentional constraints (see also Carrasco *et al*., 2004). This work provided evidence for spatially asymmetric processing networks prior to the double spatial frequency filtering stage postulated by Ivry and Robertson. A retinal contribution was however not isolated and separately investigated in the studies of Carrasco *et al*, because performance was analyzed under binocular conditions. This fact precluded the possibility to explore naso/temporal biases, which would provide direct evidence for additional independent retinal mechanisms underlying functional asymmetries. Retinal naso/temporal asymmetries may indeed interact with left/right cortical binocular representations; however this fact was not taken into account in earlier studies. Nevertheless, laterality effects have never been found in simple detection tasks with sinusoidal gratings.

2.2. Non-motor manifestations in Parkinson´s disease – from vision to motion perception

Multisensory deficits have been documented in Parkinson's disease (PD), in particular within the visual domain. The neural origin of such deficits still remains controversial. It has also been questioned that the reported deficits are truly sensory, since ageing factors related to the brain and also to ocular structures could explain some of the reported results. Non-motor symptoms and in particular sensory impairment in PD are of outstanding interest for the research and clinical communities. In this section, we present a short review on non-motor manifestations essentially those concerning visual impairment (including motion perception) and the role of dopamine (DA) in PD.

2.2.1. Parkinson´s disease

Growing ageing population and related neurodegenerative disorders, such as PD, are increasingly common realities in our society. PD is a degenerative disorder of the central nervous system, characterized by a progressive loss of dopaminergic neurons (Parkinson, 2002; Kempster *et al*., 2007). PD maybe idiopathic or familial (with some of the genetic causes already identified, see reviews by Hardy *et al*., 2006; Gasser, 2007; Yang *et al*., 2009) and is one of the most common neurodegenerative disorders in the developed world, after Alzheimer's disease, affecting about 1% of world population aged over 60 years (de Lau *et al*., 2006). It affects people of all ethnic origins and both sexes with slight preponderance for males. Its incidence increases with age and age is itself a risk factor, the disease manifesting itself around the fifth or sixth decade of life, and only exceptionally earlier.

During recent years researchers in the field of PD and of other movement disorders have made extraordinary advances in understanding the cellular mechanisms of neurodegeneration, diagnosis and treatment of movement disorders. The studies of Antal *et al*. (2008) and Jankovic (2008) can be found most of the important findings of PD are particularly remarkable in this respect. Although the tryad of tremor, rigity and bradykinesia are the hallmark of PD (as James Parkinson's original description of "the shaking palsy" in 1817) a more complete picture of the clinical phenotype of PD has emerged nowadays as a "multi-system neurodegenerative disorder" with a wide variety of motor and non-motor symptoms.

It is known for a long time that striatal function largely includes non-motor aspects (Bodis-Wollner and Yahr, 1984). Non-motor functions not based in the basal ganglia have also deserved attention (Raskin *et al*., 1990) in particular visuospatial orientation, which is impaired in PD. In some cases, the non-motor aspects may precede the motor ones, even before therapy (Hunt *et al*., 1995; Becker *et al*., 2002; Crucian and Okun, 2003; Geldmacher, 2003; Amick *et al.,* 2007). In this context, visual deficits have been demonstrated in PD patients without treatment (Bloem *et al.,* 1992; Buttner *et al.,* 1995c, 1995d; Muller *et al.,* 1997, 1999, 2003; Sartucci *et al.,* 2003, 2006; Sartucci and Porciatti, 2006; Sprengelmeyer *et al.,* 2003).

Prominent among non-motor aspects are mood disturbance (Cummings and Masterman, 1999; Lemke *et al.,* 2004; Martinez-Martin *et al.,* 2007), cognitive decline and dementia (Levy *et al.,* 2002; Aarsland *et al.,* 2003; Foltynie *et al.,* 2004; Janvin *et al.,* 2006), sleep disorders (Comella, 2006), hyposmia (Bohnen *et al*., 2007) and autonomic failure (Allcock *et al*., 2006; Lucetti *et al*., 2006; Wullner *et al*., 2007). Concerning the visual domain, the most common symptoms in PD include: ocular symptoms such as visual blurring, fatigue and dry eye; sensory deficits such as decreased chromatic and achromatic CS; abnormal perceptual

phenomena, including visual hallucination (VH) and illusions (Repka *et al*., 1996; Fenelon *et al*., 2000; Barnes and David, 2001; Holroyd *et al*., 2001; Biousse *et al*., 2004; Johnson *et al*., 2004; Davidsdottir,*et al*., 2005; Bodis-Wollner and Jo, 2006; Castelo-Branco *et al*., 2009; Van Asselen *et al*., 2009). In fact, evidence has been accumulating regarding this issue, suggesting early changes of visual function even at the retinal level (see review by Archibald *et al*., 2009. Involvement of visual cortical pathways is also likely in this disease (Castelo-Branco *et al*., 2006, 2007, 2009; Van Asselen *et al*., 2009).

Concerning striatal circuits, nowadays there is increasing evidence that the caudate nucleus contributes to learning and memory, including tasks that involve goal-directed action not necessarily related to motor aspects (Grahn *et al*., 2008). This implies that the basal ganglia are relevant not just for motor and procedural learning, but also for other aspects of cognitive processing which include visual learning. It has recently been demonstrated that PD patients are unable to learn implicit information contained in visual scenes (Van Asselen *et al*., 2009). This loss leads to less efficient attentional search of an object within a subsequently repeated visual scene. The basal ganglia are believed to be involved in movement control, associative learning, planning, working memory, and emotion (Obeso *et al*., 2008). Indeed, the dissection of all these subcomponents will require carefully controlled studies.

Finally, normal ageing results in a multitude of physiological changes that could contribute to sensory impairments not necessarily caused by a disease process. A distinction between normal ageing and disease has diagnostic and potential therapeutic relevance in PD, since alterations in the spatial and temporal proprieties of the ocular structures and of the brain could potentially confound studies of vision in PD (Antal *et al*., 2008).

2.2.2. Retinal dopaminergic decrease in PD patients

Some studies have shown that the pathogenesis of the visual impairment in PD is caused by dopaminergic deficiency (Price *et al*., 1992; Buttner *et al*., 1994; Peters *et al*., 2000). Others have suggested that the deficiency of DA in the visual system is independent of the one found in the basal ganglia (Buttner *et al*., 1995b, Muller *et al*., 1998; Johnson *et al*., 2004). Further evidence for a differential pattern of dopamine concentration in foveal and peripheral regions of the retina is available from animal studies (Mariani *et al*., 1984). Indeed, animal studies, particularly in the primate (Ghilardi *et al*., 1989; Bodis-Wollner and Tzelepi, 1998), have proven to be extremely useful in advancing a coherent hypothesis for dopaminergic actions at a retinal level. Frederick *et al*. (1982) were the first to examine post-mortem human retinas of PD patients describing the content, synthesis, uptake, localization, and release of DA in the human retina and substantiating a neurotransmitter role for DA in that site, while

Nguyen-Legros (1988) was the first to note its relevance in PD. His study of dopamine neurons in the retina of five PD patients, as labelled by their tyrosine hydroxylase immunoreactivity, led to the demonstration of reduced dopamine innervation in the central retina of these patients (Nguyen-Legros, 1988). Harnois and Di Paolo (1990) verified post mortem the level of DA in the retinas of eight PD patients. This study was the first direct evidence that retinal DA concentration was decreased in PD. In this study, the PD patients were divided into two groups according to their last dose of L-dopa, the group that had not received L-dopa presented lower DA levels than patients exposed to the treatment before death. This study concluded that DA concentration at the retina is diminished in PD, in addition to the known reduction in the nigrostriatal pathway. This may explain the abnormal visual responses and their possible normalization after dopaminergic therapy (Harnois and Di Paolo, 1990). Later on, Nguyen-Legros (1993) found a severe degeneration of the foveal DA innervation for PD patients without L-dopa treatment a few days before death. Also a decrease in the endogenous rate of DA, and morphological deterioration of the peri-foveal dopaminergic plexus in some patients have been reported (Masson *et al*., 1993).

Abnormalities of colour discrimination in PD may be expected (Djamgoz *et al*., 1997), since DA seems to affect photoreceptor-horizontal cells transmission and functioning, which may contribute to chromatic processing in the retina. Because the short-wavelength cone receptors are sparse in the retina, they were believed to have elevated susceptibility to retinal damage caused by the progressive loss of dopaminergic cells in the retina. Also, changes in CS may be observed upon the transition from high to low luminance levels (Wink and Harris, 2000), suggesting a possible contribution of the dopaminergic circadian clock. Dopamine controls the transition between scotopic (dark) and photopic (bright) conditions and, when this fails, there is inadequate adaptation to darkness.

2.2.3. Evidence for deficits in sensory systems with a focus on vision

Early evidence has indicated a biochemical and electrophysiological disorder in the retina in PD patients (Nightingale *et al*., 1986) and nowadays, it has even been suggested that PD and macular degeneration may have a partly common etiology (Dantzig, 2006). The changes in visual function might suggest structural alterations at a microscopic or macroscopic level in the retina. Psychophysical, electrophysiological and morphological data have provided solid evidence for disruption of retinal structure and function, although a complete hierarchical evaluation of dysfunction at several levels at the visual pathway in PD and other neurological disorders is far from being established (Mendes *et al*., 2005; Castelo-Branco *et al*., 2006, 2009). Despite the fact that retinal dopaminergic dysfunction is reflected by the low tyrosine

hidroxylase imunorreactivity in central retinal dopaminergic cells (Nguyen-Legros, 1988), the dopaminergic innervation of LGN and visual cortex (Garcia-Cabezas *et al*., 2009) raises the question that these structures may also be directly affected. In light of the increasing evidence that cortical and sub-cortical visual pathology also plays a role in these abnormalities, development of tools to probe the retina in isolation becomes increasingly important. Non-invasive techniques are now available to probe retinal structure, such as optical coherence tomography (OCT) which provides high-resolution cross-sectional data on the retina. It is possible to assess peripapillary retinal nerve fiber layer (RNFL) thickness using this technique, thereby providing an estimation of retinal ganglion cell nerve fiber integrity. RNFL thinning has been found in PD, albeit in relatively small numbers of patients (Inzelberg *et al*., 2004; Altintas *et al*., 2007). Such studies require repetition in larger cohorts to ensure reproducibility and the functional implications of this structural change are still unknown.

Next, we will discuss the current standards in assessing visual function in PD across early visual pathways.

2.2.4. Damage across early visual pathways

In the initial study of Regan and Maxner (1987) with PD patients, a dependence of low spatial frequency horizontal gratings visual detection loss at mid temporal frequencies (4 - 8 Hz) combined with the sparing of VA was found, and the authors proposed that the results were congruent with the suggestion that the ‘‘dynamic visual channel’’ (the M pathway) was primarily deficient in PD. It has been suggested that the M system may suffer more damage in PD than the P stream (Regan and Maxner, 1987; Hutton *et al*., 1993; Hunt *et al.,* 1995). However, some studies (Hutton *et al*., 1999, Pieri *et al*., 2000 and Langhienrich *et al*., 2000) have found a reduction for intermediate and high spatial frequencies therefore suggesting that the P pathway is more affected than the M one. CS assessment has usually been done by simple charts, which lack temporal modulation that is required to activate the M pathway, except for the backward masking task in the work of Amick *et al*., 2003. Recently, Feitosa-Santana (2008) compared P, K and M performance, thereby paving the way for separating disease susceptibility of different pathways. In this study, the M and P pathways were probed with computerized psychophysical tests: the Pedestal test (Pokorny and Smith, 1997; Gualtieri *et al.,* 2006) and the Checkerboard test (Benoff *et al.,* 2001; Costa and Ventura, 2005), where spatial CS was evaluated. Their results confirmed the findings of previous studies and indicated that both pathways were compromised by the disease (i.e., Hutton *et al.,* 1999; Pieri *et al.,* 2000; Sener *et al.,* 2001; Muller *et al.,* 2002; Uc *et al.,* 2005).

Also, using CCT a selective loss was found of the red-green axis (P pathway) in PD with preservation of the tritan thresholds (K pathway).

2.2.5. Neurophysiological evidence of visual dysfunction in PD

2.2.5.1. Visual evoked potential (VEP) recordings

The first confirmed type of visual impairment in PD was abnormal pattern VEP (PVEP) responses (Bodis-Wollner and Yahr, 1976). The origin was believed to be retinal (although this measure represents in general the arrival of the visual signals at the cortex). This study, demonstrated a delay in the VEP latency to sinusoidal gratings at a mid-spatial frequency and these findings have been replicated in a number of subsequent studies using a variety of spatial and temporal stimulus parameters (Gawel *et al*., 1981; Regan and Neima, 1984; Marx *et al*., 1986; Nightingale *et al*., 1986; Tartaglione *et al*., 1987; Ikeda *et al*., 1994). Indeed, Bodis-Wollner *et al*. (1986) found that DA-related VEP delays were dependent on the spatial and temporal frequencies of stimulation and showed that in general, contrast responses were affected in PD. This study stated that PD directly affected the afferent visual system and not just the basal ganglia. Although PD causes an abnormal PVEP response, the origin is believed to be retinal, which is supported by the electrophysiologic and psychophysical studies described next.

2.2.5.2. Flash and pattern electroretinograms (ERG)

The flash electroretinogram (FERG) reflects the integrity of functioning in the outer retina (especially photoreceptor health). The effect of PD on the FERG is mixed. Some studies reported that the amplitude of the FERG response was reduced in treated patients with PD compared to controls (Iudice *et al*., 1980; Nightingale *et al*., 1986; Gottlob *et al*., 1987; Jaffe *et al*., 1987). Only one study (Iudice *et al*., 1980) found that untreated patients with PD exhibited normal responses, whereas another (Gottlob *et al*., 1987) found abnormal responses. The latency of the b-wave increased in patients with PD (Jaffe *et al*., 1987; Ellis *et al*., 1987; Ellis and Ikeda, 1988). Jackson and Owsley (2003) suggested that contradictory FERG findings indicate that PD does not affect the photoreceptors uniformly, which is probably the result of indirect modulation of photoreceptor function by the dopaminergic neurons in the retina.

Meanwhile, the effects of PD on pattern electroretinogram (PERG) are more consistent. It is believed that the origin of the PERG response is predominantly from the retinal ganglion cells, the post-receptoral layer in the inner retina (Maffei *et al*., 1985; Harrison *et al*., 1987;

Bach, 2001). The PERG is affected by alterations in retinal ganglion cells or retinal changes that affect their input. PD related changes in retinal processing caused by changes in the dopaminergic amacrine, horizontal and interplexiform cells may alter the receptive field composition of the ganglion cells, thereby altering the PERG response (Jackson and Owsley, 2003). Like other measures, the PERG response is highly dependent on the spatial, temporal and contrast characteristics of the stimuli used, such as gratings or checkerboards. However, studies have consistently shown alterations in both latencies and amplitudes of PERGs in PD (Nightingale *et al*., 1986; Gottlob *et al*., 1987; Peppe *et al*., 1992, 1998; Langheinrich *et al*., 2000; Sartucci *et al*., 2006). In contrast to a global reduction in amplitude of PERG response, to a variety of sinusoidal grating spatial frequencies, in age-matched controls compared to young controls, PD patients have shown a specific medium-frequency deficit (Tagliati *et al*., 1996), the region of peak sensitivity of CS for a normal observer. These changes respond to administration of levodopa (L-dopa) and may be progressive (Ikeda *et al*., 1994; Peppe *et al*., 1995, 1998).

2.2.6. Visual acuity

Reports of impaired VA in PD patients first emerged in the early 1990s in a small cross-sectional study (Jones *et al.,* 1992). Although patients with even mild PD have been reported to complain of visual problems, the visual impairment is not evident on routine eye examination since it consists of a high-contrast VA testing, the most commonly used measure of vision, and VA is typically unaffected, if it is well corrected with glasses. The clinical significance of diminished VA is highlighted by the finding that it can represent a risk factor for VH in PD (Holroyd *et al.,* 2001; Matsui *et al.,* 2006) and in Alzheimer's disease (McShane *et al.,* 1995; Chapman *et al.,* 1999). It is known that visual function declines with the normal course of ageing, even in the absence of ocular pathologies. Since VA is related to resolution power, it can be influenced by many ageing factors (Jackson and Owsley, 2003), such as lens changes and other changes in the optics of the eye and intrinsic "neural" factors such as ganglion cell/photoreceptor density, retinal eccentricity and stimulus related factors. This implies a complete knowledge of normal and pathological ageing of these ocular structures (Klein *et al.,* 1992; Mangione *et al.,* 1994; Johnson, 2001 and Castelo-Branco *et al.,* 2004) in PD studies.

2.2.7. Contrast Sensitivity

CS measures can complement VA as a test of central achromatic vision at low contrast and it increases the sensitivity of detecting optical and retinocortical lesions, which may spare high contrast vision. Specific changes of CS in PD patients has been implicated in falls, difficulties in reading and driving performance and other daily activities (Owsley and Sloane, 1987; Ivers *et al*., 1998; West *et al*., 2002; de Boer *et al*., 2004; Kooijman and Cornelissen, 2005; Davidsdottir *et al*., 2005; Lord, 2006; Kesler and Korczyn, 2006; Worringham *et al*., 2006; Moes *et al*., 2009). Abnormalities of colour vision and luminance (achromatic) CS visual deficits have been widely reported (Haug *et al*., 1995; Pieri *et al*., 2000; Bodis-Wollner *et al.,* 2002; see also reviews by Brandies and Yehuda, 2008; Archibald *et al*., 2009) and only two studies (Haug *et al*., 1994; Buttner *et al*., 1996) have shown no difference of achromatic CS in PD compared to the control group.

CS is an indirect measure of center surround interactions in ganglion cell receptive fields and may be tested for different stimuli resolutions expressed in terms of spatial frequencies and/or in terms of temporal frequencies. It is well documented that PD patients demonstrate impairments in the spatial and temporal domain of low-level CS visual tasks (for a review see Harris, 1998). Initial studies used letter charts, similar to Snellen VA cards, with contrast variations (Regan and Neima, 1984). Further studies using vertical gratings with a sinusoidal luminance profile have shown CS loss at a variety of spatial frequencies (Bulens *et al*., 1986; Delalande *et al*., 1996; Harris *et al*., 1992; Langheinrich *et al*., 2000). Bodis-Wollner and Onofrj (1987) reported that PD patients present accentuated loss around 4.8 cpd (the peak of normal adult spatial CS function, CSF), which they related to the spatial characteristics and extent of the dopaminergic deficit in the retina. The abnormal tuning of the spatial CS loss in PD has been similar to the selective loss found with PERG studies. In spatiotemporal CS tasks, the thresholds are measured for a range of spatial frequencies at different rates of flicker. The normal spatiotemporal CS function has a single peak and is attenuated at low and high frequencies in both the spatial and temporal domains (Robson, 1966; Kelly, 1969; Masson *et al*., 1993;). Disrupted spatiotemporal CS in PD has been observed using psychophysical and electrophysiological measures of retinal and higher-level visual pathway functioning (Bodis-Wollner and Yahr, 1978; Marx *et al*., 1986; Skrandies and Gottlob, 1986; Bodis-Wollner *et al*., 1987; Regan and Maxner, 1987; Mestre *et al*., 1990a, b; Bodis-Wollner and Regan, 1991; Harris *et al*., 1992; Delalande *et al*., 1996; Mestre *et al*., 1996; Tagliati, Bodis-Wollner and Yahr, 1996; Tebartz van Elst *et al*., 1997; for reviews see Bodis-Wollner, 1990, 2003; Harris 1998; Langheinrich *et al*., 2000; Pieri *et al*., 2000; Diederich *et al*., 2002). Similar to spatial CS, PD patients exhibit a selective abnormality at the peak of human sensitivity (8 Hz) and less

attenuation of sensitivity is observed at 16 Hz (Bodis-Wollner *et al*., 1987) or at 2 and 12-16 Hz (Regan and Maxner, 1987). We should also refer that spatiotemporal CS declines with age, particularly at intermediate and high spatial and temporal frequencies (Jackson and Owsley, 2003). This loss is caused in part, by optical factors in combination with retinal neural factors.

Usually, luminance CS is probed by clinical semi-quantitative tests based on simple charts, such as Pelli-Robson test charts and Vistech test charts, which do not allow for computerized quantitative assessment, (Regan and Maxner, 1987; Price *et al*., 1992; Buttner *et al*., 1995, 1996; Pieri *et al*., 2000; Diederich *et al*., 2002; Uc *et al*., 2005). These charts varied from study-to-study from static gratings with a sinusoidal luminance profile to contrast charts with letter optotypes of diminishing contrast. Static measures of CS are attractive due to their ease of application in a clinical setting, as well as their intuitive familiarity to patients, but they have been criticized for their lack of test-retest reliability (Reeves *et al*., 1991). Also, in the Amick *et al*. (2003) study no gross difference was found between PD and healthy participants when comparing their CS profiles using a standard chart, in contrast to the data cited above. They attributed this finding to the fact that the chart test used was not sensitive enough to detect the functional impairment in CS. This information may be important to patients, because CS, when examined in the clinic, is measured almost exclusively with wall charts. Scores in the normal range may mask subtle impairments that impact upon performance in the visuocognitive processing domain.

Meanwhile, it remains to be established into which extent CS abnormality has a predominant retinal nature, in spite of the claims for preserved cortical adaptation to changing stimuli (Tebartz van *et al*., 1997).

2.2.8. Colour Vision

Deficits in colour vision in PD have suggested involvement of different colour-opponent pathways and are probably due to retinal dysfunction as subsequently corroborated by chromatic and achromatic PERG measures in PD patients compared with a control group and with patients with Multiple System Atrophy (Sartucci *et al*., 2006). A general cautionary note is important here: one should not assume that classical ERG provides evidence for specific chromatic damage, because full-field stimulation with standard flashes or pattern stimuli will activate all colour pathways, unless isoluminance is ensured. This is only possible in some parts of the display, due to spatiotemporal variation in colour vision (Wyszecki and Stiles, 1982). This is mainly because colour matching functions are only available for 2º and 10º visual fields.

Thereby measures taken with ERG will only be reliable in focal parts of the display. This will render comparisons concerning differential impairment only valid for local equiluminant regions.

Extensive evidence about colour vision deficits in PD is available (see reviews by Brandies and Yehuda, 2008, Archibald *et al*., 2009). The clinical Farnsworth–Munsell 100-hue (FM 100-test) and Lanthony D-15 colour vision tests are the most widely used, requiring participants to arrange coloured discs into a smoothly graduated colour sequence. PD patients demonstrate significantly higher error rates on the FM-100 test than age-matched controls, where the most prominent deficits have been found along the blue and green axes (Price *et al*., 1992; Pieri *et al*., 2000). Computerized methods of colour vision that do not require the patient to make motor movements, a potential confounding variable of the clinical tests, showed mixed results. Only the work of Regan *et al*. (1998), showed that the colour vision function was not impaired compared to the control group, whereas previous studies (Haug *et al*., 1994; see also Haug *et al*., 1995) identified a tritan axis deficiency, in agreement with the results of Price *et al*. (1992) with the FM-100 test. The predominant affection of the blue-yellow pathway in PD has been the most reported. One should note that the ageing process in colour vision is typically characterized by a loss of colour discrimination in particular along this pathway, possibly due to opacified lens absorption of short wavelength light and cone dysfunction. Confounding factors should therefore always be taken into account.

Simultaneous studies of colour vision and luminance CS have also analyzed the influence of disease progression on performance, where all results were significantly related to the duration of disease (Price *et al*., 1992; Buttner *et al*., 1994) and temporal evolution of these deficits in PD, with evident progression in one longitudinal follow-up study over 20 months (Diederich *et al.,* 1998, 2002).

2.2.9. Visual hallucinations

VH in PD have often been argued to represent an iatrogenic effect of L-dopa treatment. They can be classified based on content (simple and complex: Gellar and Bellur, 1987; Feinberg and Rapcsack, 1989) and occur while the patient is alert with the eyes open, lasting a few seconds (Cummings, 1991). Complex VH are more often observed than simple VH, and the underlying mechanism is still poorly understood (Manford and Andermann, 1998), although the work of Ffytche *et al*. (1999) suggests a role for extrastriate visual cortex.

Cognitive impairment is not necessarily predictive of the occurrence of hallucinations since PD patients with and without hallucinations revealed no group differences in Mini-Mental

State Examination (MMSE) (Matsui *et al*., 2006). In this case, the hallucinations observed in PD (Diederich *et al*., 2000), may be related to the Charles Bonnet Syndrome (Santhouse *et al.,* 2000 and references therein) e.g. hallucinations in the absence of brain disease and where VA is classically impaired. Accordingly, PD patients presenting hallucinations demonstrate a lower CS and colour discrimination, suggesting that retinal dysfunction contributes to the appearance of VH in PD (Diederich *et al*., 1998). Diederich *et al*., (2005) emphasize the multifaceted phenomenology of hallucination that is part of the chronic complications of PD and are present in 30 to 60% of the patients. This study also suggests that hallucinations should be considered as an imbalance in the filter of relevant stimuli in the visual scene involved in the construction of perception. Antal *et al.* (2002) found electrophysiological evidence for visual object categorization deficits in PD, suggesting a potential link to object processing deficits and VH.

2.2.10. Motion Perception

In addition to changes in VA and CS, motion perception impairment in PD has also been found (Trick *et al*., 1994; Giaschi *et al*., 1997; Amick *et al*., 2003; Mosimann *et al*., 2004; Uc *et al*, 2005). Clinical support for a specific deficit of motion perception was provided by Lee and Harris (1999), who found that PD patients had difficulties in judging motion in everyday experience. The studies of Amick *et al*. (2003) and Uc *et al*. (2005) attempted the strategy of dissection of hierarchical deficits in M and low/high level motion processing in PD. however they used only one class of motion tests, thereby preventing truly hierarchical measurements of visual motion processing. Studies of higher-level visual functions requiring motion integration of moving surfaces and temporal processing have so far yielded conflicting results (Trick *et al.*, 1994; Amick *et al*., 2003; Uc *et al*., 2005).

In addition, there is also a marked effect of ageing on visual processing of moving objects, with older adults exhibiting decreased ability in motion discrimination (Ball and Sekuler, 1986), and decreased sensitivity in detection of moving targets (Gilmore *et al.,* 1992). Recently, it has been demonstrated that older subjects show greater impairment on sinusoidal grating and dot kinematogram tests of motion perception (Willis and Anderson, 2000; Billino *et al*., 2008; Conlon and Herkes, 2008). Such tasks assess motion perception processing in retinal, sub-cortical and cortical visual areas although the relative contribution of low-level retinal deficits make to such changes still remains unclear. These deficits were very similar to the reported motion deficits in PD, and could not be explained by optical changes in the aged eye or by cognitive factors, implying they had a basis in ageing-related changes in the visual neural pathway. The correlation between impaired visual perception and cognition argues in favor of both retinal and cortical components to the breakdown in visual perception. PD

patients have demonstrated impairments of visual attention, spatial and motion detection compared to age-matched controls (Uc *et al*., 2005). Group differences persisted for visual speed processing tasks with alternative measures of visual attention, supporting a cortical contribution to such perceptual disturbances as well. Also, the study of Uc *et al*. (2005) highlights the link between impairments of motion perception and motor function, with impaired performance on simple and complex finger-tapping tasks correlating with motion perception measures in the former and severity of postural instability and gait disorders correlating with impairments in visual speed of processing in the latter.

In addition, a disease-specific “motion blur” in contrast perception (Masson *et al*., 1993; Mestre *et al*., 1990) has been found in PD, where spatiotemporal CS to moving gratings was diminished, with a different deficit pattern being observed in comparison to the reductions seen in age-matched controls.

2.3. The role of dopamine

Retinal dopamine-related impairment is widely accepted to alter retinal visual processing primarily by changing the receptive field properties of ganglion cells (Jackson and Owsley, 2003). DA is believed to be involved in the control of centre-surround interactions and of the effective receptive field size, which may partly be due to the role of dopamine in the control of gap junction opening and its consequences on effective receptive field size and CS (Bodis-Wollner, 1990a, b). Certain visual impairments occur commonly in PD, in conjunction with loss of dopamine-producing retinal amacrine cells in the inner nuclear and ganglion cell layers and secondary depletion of the dopaminergic fiber plexus of the inner plexiform layer (Masson *et al*., 1993). Retinal dopaminergic dysfunction is likely the greatest contributor to visual syndromes associated with PD; however we should note that DA is found within several structures subserving vision such as the LGN (Papadopoulos and Parnavelas, 1990) and the visual cortex (Reader and Quesney, 1986; Parkinson, 1989; Bodis-Wollner, 1990a, b), in addition to the retina (Corbe *et al*., 1992; Witkovsky and Dearry, 1992). Some authors have proposed a dopaminergic deficiency in the retina (Mitchel, & Howe, 1986; Peppe et al., 1992, 1998; Price *et al.,* 1992; Haug *et al.,* 1994; Buttner *et al.,* 1995a; Lieb *et al.,* 1999; Muller, 2000; Nightingale et al., 2000; Crevits, 2003; Jackson and Owsley, 2003) while others indicated that this deficiency could also include other areas of the visual system (Buttner *et al.,* 1993, 1994a; Hutton et al., 1993; Flowers and Robertson, 1995; Ebersbach et al., 1996; IngsterMoati et al., 1996; McDowell and Harris, 1997; Muller et al., 1997; Harris, 1998; Rodnitzky, 1998; Lieb et al., 1999; Peters et al., 2000; Brandies and Yehuda, 2007).

The functions of DA in the visual system are not fully understood and most of the knowledge of their role is in studies with the retina, indicating the involvement of D1 receptors to D5 at this level. One of the most important types of neuron in PD is the striatum median spiny neuron which bears receptors for the two most common types of dopaminergic receptors. The D1 receptor family is associated with adenil-ciclase and therefore has stimulating activity, and the D2 family is connected to G-proteins which inhibit adenil-ciclase, leading to decreased AMP-ciclic levels, with ensuing inhibitory action. Each receptor family may also be divided in two subtypes. The D1 family may be divided in D1 and D5 receptor subtypes, while the D2 family may be divided in D2, D3 and D4 subtypes. The striatum median spiny also possesses receptors for the neurotransmitterr glutamate, as well as receptors for NMDA and D2A receptors for adenosine. Therapeutic modulation of these receptors offers an interesting potential in treating this condition (Jenner, 2003).

DA acts in the outer and inner retina at multiple levels, producing alterations to the flow of visual information. The dopaminergic neurons act as a chemical messenger for light adaptation and promote the flow of information through cone circuits while diminishing that through rod circuits (see reviews of Witkovsky, 2004 and Brandies and Yehuda, 2007). DA is expressed in the retina in the A18 cell type, which is a wide-field amacrine cell, with extensive dendritic branching, and extending through several neighbouring layers (Mariani, 1990,1991; Kolb *et al*., 1992; Witkovsky *et al*., 2005). The densely packed network of A18 amacrine cells leaves few rings for other cell bodies and dendrites to pass their information (Kolb *et al*., 2008). Another feature of dopaminergic cells can only be seen after dye injection (Dacey, 1990) or immunostainning (Kolb *et al*., 1990), revealing that A18 dendrites emit long axon like processes that run in different strata of the Inner Plexiform Layer, in the ganglion cell layer and even in the Outer Plexiform Layer (Kolb *et al*., 2008). DA neurons contact to two other types of amacrine cell belonging to the rod pathway—the AII and the A17 amacrine cell (Bloomfield and Dacheux, 2001). This suggests that DA plays also an important role in night vision.

2.3.1. Medical treatment and its effects on visual function in PD

The effect on the visual system of the treatment with drugs that provide a reduction in dopaminergic deficiency in the nervous system is very controversial. Some studies concluded that the treatment improves visual function in PD (Corbe *et al*., 1992, Jones *et al*., 1992; Peppe, Stanzione, and Pierelli, 1992; Hutton, Morris, & Elias, 1993; Barbato *et al*., 1994, Buttner *et al*., 1994a, 1995a; IngsterMoati *et al*., 1996; Buttner *et al*.,, 2000), while others suggest a reduction of these functions (Tagliati *et al*., 1996; Hutton *et al*., 1999; Peters *et al*., 2000, Pieri *et al*., 2000). The more definitive treatment of early PD is with either a dopamine

agonist (such as bromocriptine, cabergoline, ropinirole and pramipexole) or L-dopa. The L-dopa precursor treatment allows the DA reposition in the central nervous system, but may take several days depending on disease stage and site of damage (Bokobza *et al*., 1984; Ogasahara *et al*., 1984). The fact that the decline in CS within PD can at least in part, be reversed by the administration of L-dopa is well known for a long time (Bulens et al., 1987; Tebartz van Elst et al., 1997) but it is rather obvious that a reversal in decline does not imply better thresholds, and this is a critical point that goes often unrecognized. This relates to Bodis-Wollner (1990, 2003) tenet that "studies showing correlation between reduced levels of neurotransmitters and behavioural deficits should be complemented with data on kinetics of the same substances in health and disease states". We do however point out that one should be careful about difficulties in detecting a beneficial therapeutic effect as evidence for their non-existence. In fact, a decisive test for such an effect can only be done by applying a repeated measure design (Peppe *et al*., 1998), which takes into account within subjects variability and prevents between subjects confounding sources of variability. This was indeed done in the work of Buttner and colleagues (1994, 1995, 2000). There is also widespread evidence for beneficial effects of dopamine agonists in many repeated measures approaches (before and after therapy; see also the animal work of Ghilardi *et al*., 1989, for a review see Tebartz van Elst *et al*., 1997). Such designs are easier to apply in short term studies, (see the work of Jaffe *et al*., 1987, who studied the effect of L-dopa intravenous infusion) but remains a challenge to apply them for long term studies.

Still in order to evaluate treatment effects of PD, Buttner *et al*., (1994a) showed that the performance of colour vision in the tritan confusion axis of patients improved after treatment with L-dopa. Later, the same group (1995a, 1995b) identified a reduction in the performance of colour vision in "de novo" diagnosed groups suggesting early impairment.. The studies that support beneficial effects of L-dopa administration in CS (improving CS) (Bulens *et al*., 1987, 1989; Hutton *et al*., 1993) claim that DA may have an essential role in receptive field organization. Colour vision has indeed been improved with L-dopa administration (Buttner *et al*., 1994) and slightly by apomorphine (Buttner *et al*., 2000). However, colour vision was unaffected by amantadine sulfate therapy, and N-metil-D-aspartate (NMDA),antagonist believed to cause an enhanced DA release and turnover (Buttner *et al*., 1995b). The differential effects of these medications suggested that the colour deficiency probably may involve directly the visual system (Buttner *et al*., 1994), and that the pathophysiology of dopaminergic pathways in the visual system differs from that of the basal ganglia, given the beneficial effects of amantadine in motor symptoms (Buttner *et al*.,1995b).

2.4. Neuroimaging in PD

In this section, we will introduce briefly the main neuroimaging techniques applied nowadays in PD and their role in understanding disease pathophysiology. Structural imaging has been used to elucidate some of the neural correlates of dysfunctional states in PD. Accordingly, Ramírez-Ruiz *et al.*, 2007 documented brain changes on magnetic resonance imaging (MRI) in non-demented PD patients with VH using voxel-based morphometry. In this study the PD patients with VH, when compared with both controls and non hallucinating PD group, showed significant grey matter volume reductions in the lingual gyrus and superior parietal lobe. The novel MRI techniques such as spectroscopy, diffusion weighted imaging, diffusion tensor imaging and magnetization transfer have shown superior sensitivity compared to conventional MRI in detecting abnormal features in neurodegenerative parkinsonian disorders (Seppi and Schocke, 2005; Au *et al*., 2006).

Functional MRI (fMRI) and molecular studies such as positron emission tomography (PET) or single positron emission computed tomography (SPECT) appear to be more informative concerning striatal regions (Au *et al*., 2006) because the first gives insights concerning whole brain functional analysis while the latter provides neurochemical information. Indeed, fMRI can provide valuable information on the pathophysiology of PD, as shown in Cerasa *et al*. (2006) work that assess functional changes in the activity of cerebellum and frontostriatal regions during externally and internally timed movement (volunteers performed a continuation paradigm with a visual metronome). In this study, patients could store and reproduce movement frequencies but with larger latencies. Blood-oxygen-level dependent (BOLD) response differences were found when comparing the continuation with the preceding synchronization phase and vice versa, only for activity in visually related regions, in both groups. They also reported that during the synchronization phase, PD patients exhibited an overall signal increase in the cerebellum and frontostriatal circuit (i.e. putamen, supplementary motor area and thalamus) activity together with specific brain areas (right inferior frontal gyrus and insula cortex) that are also implicated in primary timekeeper processes. The only neural network involved to a greater extent by the PD group was the cerebello-thalamic pathway. Otherwise no major differences were found, suggesting that rhythmic externally and internally guided movements engage similar neural motor networks in PD and healthy matched controls. In this way, it is relevant to look at pathophysiology in other brain areas, such as visual and cerebellar ones. In sum, it is not easy to separate real non-motor from motor deficits in PD.

A good example is the fMRI study of Rieger *et al*. (2008) which attempted the dissection of the cortical functional anatomy of voluntary saccades in PD. They found saccade related BOLD-activation in PD and healthy participants in the superior parietal cortex and the occipital cortex,

aside from remarkable hypoactivity of the frontal and supplementary eye fields in PD patients. Abnormal frontal and supplementary eye fields and normal superior parietal cortex responses were found suggesting a higher vulnerability of the oculomotor frontal planning network.

Molecular imaging tool such as PET are also useful to investigate pre- and postsynaptic dopamine function in relation to the cognitive processes in PD. Dopaminergic markers allow for the study of pre- and postsynaptic nigrostriatal integrity (Brooks, 2008). A recent review (Nandhagopal *et al*., 2008) on the role of molecular imaging in PD recognized its potential role in the neurobiological basis of motor and non-motor complications. Cropley *et al*. (2008) examined the dopamine system within the frontostriatal circuitry with [(18)F]FDOPA (Fluorine-18-L-dihydroxyphenylalanine) for dopamine synthesis and [(11)C]NNC 112 (8-chloro-5-(7-benzofuranyl)-7-hydroxy-3-methyl-2,3,4,5-tetra-hydro-lH-3-benzazepine) for D1 receptors. This study had however some methodological problems related to reference tissue model assumption but still it was able to infer that striatal dopamine denervation may contribute to some frontostriatal cognitive impairment on moderate stage of PD. The future will elucidate the role of these techniques in understanding visual dysfunction in PD.

Part II

Methods

Chapter 3

3. Methodological overview

3.1. Novel psychophysical perimetric techniques – CS apparatus

When planning this thesis we concluded that it was necessary to create an open multifunction device, controlled photometrically and able to study different physiological functions of the central and peripheral VF, such as sensitivity to achromatic and chromatic contrast. In this way, the work of the thesis began with the development of an instrument, a custom-built system based on a Visual Stimulus Generator (VSG2/5, Cambridge Research Systems (CRS) Ltd.; Rochester, England) capable of performing the required tasks. The experimental work developed in this thesis quantifies several aspects of the human visual system by using calibrated stimuli that evaluates independently, P, K and M pathway function with adjustable parameters. The prototype of the perimeter designed for this purpose, which bears the name of Custom perimetry was installed on a Dell Pentium4 PC computer of 1.8 GHz with 768 MB of RAM. A customized program was written in Object Pascal (Drag & Drop Components, Delphi 7.0 environment, Borland) in a Microsoft Windows XP Professional platform. This perimetric strategy with eye tracking was generated by means of a visual stimulus generator video card (VSG2/5) and displayed on a gamma-corrected 21 inch Trinitron Sony GDM-F520 colour monitor (frame rate: 100 Hz, resolution of the monitor was set to 800 by 600 pixels). Stimuli were used as detection targets in multiple locations of the VF and subject's responses were recorded with a CT3 four button response box with millisecond (ms) resolution (from CRS).

First, we introduce a contrast discrimination technique that reveals P and M pathway function by taking advantage of their differences in achromatic contrast response. This strategy allowed us to evaluate spatiotemporal processing for these pathways using achromatic stimuli assessing two spatial frequency channels, low spatial frequency (LSF) and intermediate spatial frequency (ISF): we call these methods the LSF CS testing (also called FD perimetry) and the ISF CS testing approaches (parvocellular perimetry), respectively.

3.2. Psychophysics

Psychophysics is the science of relating the physical measurements of stimuli with the sensations and perceptions that those stimuli evoke. Psychophysical experiments have produced most of the knowledge we have of human visual system and visual phenomenology. This technique is used to extract quantitative data from perceptual experiences that are subjective.

However, if a psychophysical experiment is properly designed and controlled for, it could be as objective and precise as any other physical measurement. In order to properly set up a psychophysical test, one should plan a strict protocol that governs the experiment. This protocol is required to cover as many factors affecting the results of the threshold test as possible. The process of setting up a psychophysical test consists of six basic steps:

1. *Selection of the stimulus*. One should plan the size of the stimulus and its properties such as spatial and temporal frequencies.

2. *Preparation of the stimuli*. The number of trials to be presented is a very important factor. It should be large enough to allow an accurate convergence of the staircase, but not so much as to induce the observers to loose interest.

3. *Selection of observers*. The number of observers is another key factor for the development of a psychophysical test.

4. *Determination of the observer task*. The instructions should be clear and should communicate what is exactly the judgement task. Our CS tests were implemented in the form of a psychophysical detection task.

5. *Presentation of stimuli to observers for the experiment.* The principal variables to be considered are the viewing conditions and the mode of presentation. We presented our stimuli in a completely dark room. The stimuli were displayed within a grey background that provided a constant visual reference. The viewing distance was fixed to 36 cm. One should also consider environmental factors, such as psychological and physical comfort, noise and

surround that could distract the observers. Subjects should take pauses every 20 min to relax, and the most comfortable viewing position is chosen by each observer. In all CS custom tests the pre stimulus wait time was 500 ms. Thus the inter stimulus interval (ISI) ranged from 500 ms to a maximum value of 2800 ms for LSF and 2300 ms for ISF test. In this way, the response time of LSF test was 2300 ms, while for ISF testing the patient had 1800 ms to give the answer. For all tests the stimulus duration was 200 ms.

6. *Conducting the psychophysical test*. A logarithmic staircase procedure was used to estimate the thresholds. Small-size trials were used to test and debug the experimental protocol and to set up the psychophysical test. Our computerized methods used interleaved staircases, keeping, in this way, attention homogeneously distributed over the VF and preventing putative artefacts.

When developing a psychophysical test for the functional analysis of the retina, one should take into account also the following objectives:

- Isolation of the physiological response of different cellular types;
- Establishment of a quantifiable relation between the psychophysical performance and the number of cells involved;
- Decreasing as much as possible contribution of a cortical mechanism to the stimulus response.

All of these aspects were carefully considered and analyzed in order to perform a reliable psychophysical experiment and to control as many sources of uncertainty as possible. Indeed, quantitative psychophysical computerized methods are much more sensitive and reproducible than most of the clinical tests (which have limited quantification power, do not allow for the extraction of participants reliability parameters, and have in general poor calibration and lack of randomization). This results from the fact that testing steps can be calibrated and dynamically changed in a random manner, in a way that is unpredictable for the observer, allowing for the extraction of confidence parameters concerning subjects' performance and reliability.

3.3. Visual Stimulus Generators (VSG) 2/5 card

The VSG2/5 32 MB programmable high performance graphics card made by CRS (http://www.crsltd.com/) is designed specifically for vision experiments, where it is necessary to deliver complex spatial patterns (such as gratings) or carefully controlled colours. It is controlled by a host personal computer (PC) and controls a stimulus display device, usually a high-end Cathode-Ray-Tube (CRT) monitor. This system is designed to run autonomously

from the host computer, so that, when stimulus generation has begun, the VSG2/5 needs very little intervention. This way, the PC can be dedicated to operations such as running the experiment or controlling data collection. In the VSG2/5, the video synchronization and timing control are done at hardware level, via an embedded microprocessor. Therefore, the timing is accurately controlled. The stimulus presentation time is guaranteed to frame resolution and is independent of windows timing. This PC plug-in card can be placed in a fixed setup and permits eye tracking with video Eyetracker Toolbox (VET). The VSG2/5 is controlled using a multi-layer VSG Software Library, which at the top layer allows stimuli to be generated without knowledge of the underlying hardware architecture. Custom stimuli can be generated using the drag & drop components and the object inspector functionalities (typical stimulus properties: size and position, colour and contrast, spatial and temporal frequency, drift velocity, can easily be controlled). This card is different from a conventional graphics card in many ways. Normal PC graphics cards have 8 bits output resolution for each of the three colour channels, resulting in a resolution of one part in 256 for each colour. When using this resolution to represent a spatial waveform with a contrast of 0.5%, there will not be that many luminance levels left to define it (one or two). The dual 8-bit video digital-to-analogue converters (DACs) of the VSG2/5 hardware system provides 15 bits of output resolution per colour channel (15-bit resolution across the full scale voltage range), but only 256 sets of RGB values simultaneously. DAC files store the output voltage characteristics used to drive the monitor and are specific to each VSG and only used during gamma correction. The number of discrete levels that we can display is dependent on the calibration and the performance of the whole system around the mean level that we are modulating. Next, we present the calibration process used in this setup. All configuration settings of VSG2/5 were done with the software application supplied with the video card (VSG Desktop library, vsgDesktop version 8.0).

3.3.1. Calibration - Gamma Correction by vsgDesktop

CRTs have a nonlinear transfer function (equation 3.1) between voltage (V) and luminance (Y) so that voltage steps near the top end of the voltage range produce a far greater change in luminance than those near the bottom. Instead, the luminance produced by a CRT is proportional to the input voltage raised to the power γ, following the relation:

$$Y = k.(V - V_o)^{\gamma} \qquad (3.1)$$

where Y is the measured luminance, V_o represents a cut-off digital video value below which no incremental light is emitted, V is the digital value that can assume values from 0 to 255, k is a constant and γ is the gamma parameter to be estimated.

This nonlinear transfer equation is usually called *gamma function*. It varies from monitor to monitor and changes over time as the monitor ages. *Gamma correction* is an important part of monitor calibration and allows the system to simulate an approximately linear relationship between input value and phosphor luminance, in order to achieve a correct linearized reproduction of colour intensity. It is also important to use brightness and contrast controls on the display device itself to ensure that the entire range of input voltages produces a change in luminance.

The VSG2/5 integrates an automatic gamma correction system that corrects the nonlinearity of the display. Our monitor (Sony Trinitron) was gamma corrected and linearized with lookup tables using the standard calibration routine of the VSG Desktop library (version 8.0). The standard voltage-phosphor luminance measurements were obtained from CRS ColorCAL colorimeter (Minolta, Osaka, Japan) (see **Figure 3.1)**. Coordinates and luminance values were verified with ColorCAL.

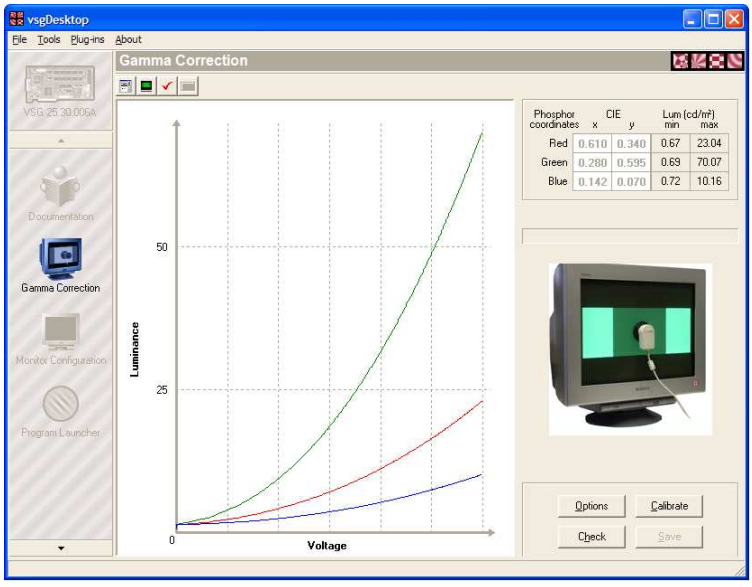

Figure 3.1. ColorCAL attached on the Sony display superimposed on vsgDesktop software display. This software is used for calibration of the display, to measure the displays gamut, creates files, known as LUT files, used by the VSG to linearise the display and has a colour check facility, for checking the accuracy of the colours produced.

ColorCAL has a luminance range between 0.2 - 200 cd/m^2 with repeatability of ± 0.3 % in the range of 0.2 < Y < 1.0 cd/m^2. It is used to perform *gamma correction* of the computer display and monitor the CIE (x, y) coordinates and luminance (Y, cd/m^2) of the stimuli throughout the experimental period. The monitor was calibrated regularly for luminance with ColorCAL and before each testing in mesopic conditions, to ensure the correct luminance values. The first step when using a colour display is to turn it on and allow sufficient warm up time for colour stability (around 30 min). However, to obtain the *gamma correction* some care is required. The readings must be taken in a dark room with the brightness control of the device adjusted so that a zero voltage input gives a just-black screen, and the contrast control adjusted so that, with the maximum voltage, the display achieves peak output but doesn't saturate (Robson, 1999). Later, inadvertent adjustment of these settings must be avoided. The CIE chromaticity coordinates for each RGB phosphor component are automatically measured at the end of the gamma correction procedure. The *gamma function* uses the LUT files created by the *Gamma Correction* plug-in inside vsgDesktop to measure luminance *vs*. DAC values for each phosphor, to calculate the transfer functions and to produce RGB gamma correction look-up tables. Once calibrated, the VSG automatically gamma-corrects the display so that colours appear with the correct brightness. Each time the user defines a pixel-levels colour (VSG Software library) the VSG will automatically convert the Red, Green and Blue colour components into the gamma-corrected equivalents.

3.4. Monitoring eye movements - Video Eyetracker Toolbox

In all CS tests implemented, it was possible to follow eye movements. Usually standard perimetric tests, such as the FDT, use the coarse method of verifying stimulation of the blind spot. However, this method is not very sensitive and is only usable when we want to have eye fixation during the test, giving us only coarse information of the fixation loss. In this study, monitoring eye movements was done via video Eyetracker Toolbox (VET) provided by CRS and based on the images of Purkinje (see **Figure 3.2**). This recording system of eye movements consists basically on an infrared camera (with two infrared diodes attached), mounted on a structure which function is to maintain the position of the head stable and comfortable. The two diodes are located on opposite sides of the chamber to create two reflections in the image acquired by the camera, the images of Purkinge. The estimation of the eye position at each moment is done using the position information of the pupil and the two Purkinge images. VET requires calibration before each testing section. This calibration consists on the recognition, by the system, of the eye position by up to 20 different points on the screen and is specific to each subject in a certain position and distance from the monitor.

With this information a calibration matrix is estimated for further analysis. The software libraries of VET were added to the custom software code, the interfaces and the necessary instructions for the test were done with a real time follow-up. The system integration of eye tracker in the custom perimetric test provides real time follow-up of the eye position during perimetric testing.

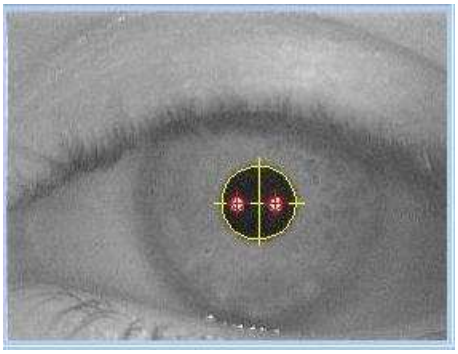

Figure 3.2. Purkinge images obtained by VET.

3.5. Achromatic CS stimuli

Sine-wave gratings gained their popularity after Blakemore and Campbell (1969) introduced the idea of the visual system as a set of “spatial-frequency channels”. These so-called “spatial-frequency channels” were suggested to form the basis of a visual Fourier analysis of the retinal image (Robson, 1975). Indeed Fourier (1822) showed that any visual scene could be described as the sum of elementary gratings characterized each by a spatial frequency, a contrast, an orientation and position (phase). Sine-wave (sinusoidal) gratings have been widely used in visual detection and discrimination tasks (Wilson and Wilkinson’s review, 1997). In all our CS detection tasks, stimuli were patches of vertically oriented sine-wave gratings. All tests of contrast are dependent on the luminance of the stimulus and the grating patterns have the advantage of allowing contrast to be varied in a sinusoidal fashion without affecting the average stimulus luminance. In general, the luminance profile of a sine-wave grating, in which the luminance variation occurs in only the horizontal dimension, is given by:

$$L(x) = L_m[1 + c\sin(2\pi f(x) + \phi)] \tag{3.2}$$

where $L(x)$ is the luminance at position x, L_m is the mean luminance, c is the contrast, *f* is the spatial frequency and Φ is the spatial phase.

A sinusoidal grating is also more useful for studying the thresholds of the visual system than any other waveform because it is composed of a single spatial frequency, allowing isolation of specific channels of retinal neurons that respond optimally to that given spatial frequency, unlike square-wave gratings that are composed of many different spatial frequencies. The spatial frequency of a sinusoidal grating is specified in terms of the number of cycles per degree (cpd) of visual angle, i.e., the number of cycles of the grating that the eye can see under a visual angle of 1º. One cycle corresponds to the smallest pattern made of a black and a white bar. The highest spatial frequency that can be perceived is in the order of 30 cpd, which corresponds to a VA of 1.0 (20/20).

All stimuli developed in the CS tasks were specified in visual angle units. To draw stimuli correctly we must set the viewing distance, which is the distance between the subject's eye and the display screen. The fixed viewing distance is required to control the spatial frequency of the stimulus and to ensure uniform viewing conditions, in order to reduce any source of variability. The stimulus was approximately 10º of visual angle. The stimulus presentation pattern is illustrated below (**Figure 3.3**) with four 10º diameter square targets per quadrant and a central 5º radius circular target.

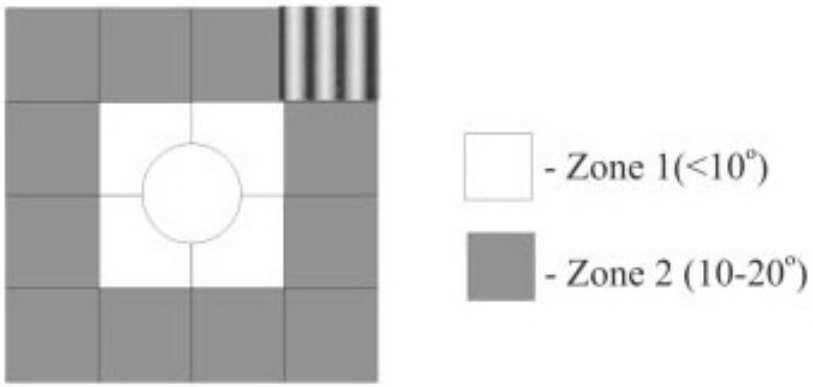

Figure 3.3. Scheme of tested locations of the sinusoidal grating stimulus. Stimuli were presented within 17 locations that were organized into two zones: zone 1, with a central circular 5º radius stimulus (which we refer latter to Zone 0) and 4 paracentral square stimuli, and zone 2, with 12 peripheral square stimuli. Zone 1 extended over 10º eccentricity and zone 2 between 10º and 20º.

3.5.1. LSF Stimulus: Frequency-doubling illusion

We currently assessed achromatic CS discrimination within the magnocellular system using a perimetric strategy inspired on frequency-doubling (FD) technology.

FD technology is based on the “frequency-doubling” effect or illusion phenomenon, which is generally observed when low spatial frequency (less than 1 cpd) sinusoidal gratings undergo high temporal frequency (greater than 15 Hz) counterphase modulation (**Figure 3.4**). This produces a perceived image that is twice the actual spatial frequency, i.e., there appear to be twice as many light and dark bars in the grating than are physically present (Kelly 1996).

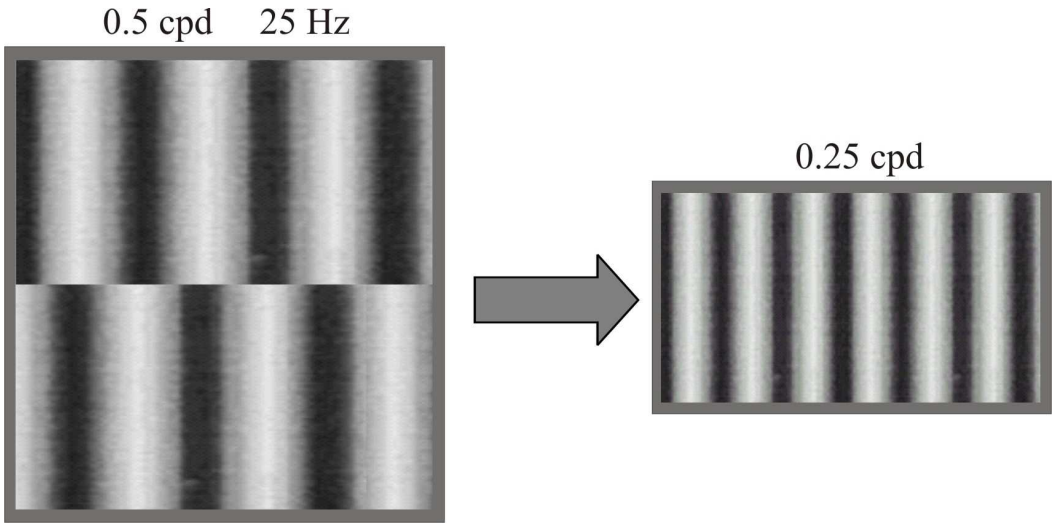

Figure 3.4. Representation of the stimuli used in the FD perimetry. Left: the stimulus of 0.5 cpd shown in phase and counterphase (figure top and bottom); Right: the FD phenomenon after temporary modulation.

It was initially believed that the FD effect was mediated by retinal ganglion cells within the visual pathways that had nonlinear response properties. Maddess and Henry (1992) proposed that FD selectively measures the activity of that subset of cells in the M pathway, called My cells, which represent approximately 3-5% of all retinal ganglion cells (Kaplan and Shapley 1982). Some authors have questioned this, and have suggested that, unlike Y-cells in cats, the spatially non-linear My retinal ganglion cells may not be the substrate of FD illusion in primates (Bosworth *et al*., 1999; White *et al*., 2002), while others have shown that, at contrast threshold, all M cells are likely to respond to the FD stimulus (Anderson and Johnson 2002). Recent studies, however, indicate that higher order cortical visual areas are also involved and that the appearance of this effect is usually fractional (between 1 and 2.5 times the physical frequency) rather than doubled (White *et al*., 2002; Zeppieri *et al*., 2008). It appears that the neurophysiological substrate for FD has yet to be determined and may lie at higher levels of processing. Fortunately, the standard and custom FD perimetry test does not depend on the appearance of the target but rather on the minimum contrast needed to detect the stimulus at different locations in the VF. In both our custom-based approach and N-30-F perimetric

strategy, inducing stimuli were patches of 0.25 cpd vertically oriented sinusoidal gratings, undergoing 25 Hz counterphase flicker. A fixation point was displayed in the center of the screen in order to ensure that the same region of the retina was recruited for stimulus detection.

3.5.2. ISF Stimulus

The spatial profile of the stimulus used in the ISF CS test was a sinusoidal grating at zero temporal and intermediate spatial frequency (3.5 cpd). The strategy implemented measures simultaneously visual performance in the central and peripheral regions (central 20°) and makes the best compromise to measure visual sensitivity across multiple regions in visual space. ISF CS testing conditions were optimized to allow testing within the limits of acuity for peripheral vision, which is quite relevant in particular for myopic eyes under mesopic conditions. The rationale for the choice of Intermediate Spatial Frequency (ISF) testing conditions is based on the fact that this spatial frequency is near to the acuity limit for peripheral vision, thereby best isolating the parvocellular (high resolution system) in that part of the VF. That same spatial frequency is near to the peak sensitivity in central vision in spite of less specifically isolating the parvocellular system near the fovea. Accurate correction of peripheral refractive error was critical to these experiments, contrary to what happened at low spatial frequencies (LSF testing).

Spatial chromatic CSs software (probing red-green and blue-yellow pathways) was also developed, but was not used in this project (for details on implementation, see Appendix A).

3.6. Psychophysical Parameters

3.6.1. Staircase protocol

In order to characterize the human achromatic and chromatic contrast detection mechanisms, we have used a threshold experiment, which is particularly appropriate to measure the detectability of a stimulus (Fairchild *et al*., 1998). In fact, with such experiments one can measure the just-perceptible change in a stimulus and thus estimate a detection threshold for that stimulus. The inverse of threshold is referred to as sensitivity, since low thresholds require high sensitivities. The staircase method represents a compromise between the method of limits and the method of constant stimuli. A logarithmic staircase adaptive procedure (vsgLogStaircase) was used to compute psychophysical thresholds, in which one correct response was required to change to a more difficult condition (i.e. decrease contrast)

but only two consecutive errors would change to an easier condition. Unlike a linear staircase, the step sizes get more refined as the test progresses. The value to be used for a trial is calculated using the previous trial value plus or minus the step size in dB. The initial step size was 3 dB. Staircases were run for a total of four reversals, with the contrast at the final two reversals being averaged to estimate the contrast threshold. In all perimetric tests pseudo-randomly interleaved staircases (vsgLogStaircase from VSG software library) were implemented in order to keep attention homogeneously distributed over the VF and to avoid observer bias and errors of anticipation and habituation. In our experiment, we have used around 40-60 stimuli for each staircase, which takes about 1 to 2 min to be completed.

3.6.2. Limits for reliability

Limits for reliability of data from the CS testing were set by the rate of fixation loss, the false negative rate and the false positive rate:

Fixation stability could be monitored by observing the participant directly through a closed circuit IR video system.

False Positive Errors were used to check that the patient is responding to seen targets. Blank targets at 0% contrast are periodically tested to check if the patient responds even when no stimulus is presented. Subjects that are anxious or “trigger happy” tend to give high false positive results.

False Negative Errors are evaluated by presenting targets at maximum contrast (100%).

For threshold testing, recommended limits for reliability are under 33% for each type of error, similar to SAP (Anderson and Johnson, 2003).

All subjects underwent a comprehensive ocular examination. This exam consisted of best-corrected visual acuity (VA-Snellen chart), IOP measurement (Goldman applanation tonometer), slit lamp examination of anterior chamber, angle and fundus examination (Goldman lens). Exclusion criteria included the following: cataract or other eye disease that might interfere with fundus examination, retinal diseases, neuro-ophthalmologic pathology, high ammetropia (sphere dpt > 4 and cylinder dpt > 2), diabetes, even in the absence of retinopathy, or other systemic diseases that might affect visual function and congenital colour vision disorders. Children known to have attention deficit disorder and children receiving

amphetamines, stimulants, or sedatives were excluded from this study. Also excluded from the study were children with a prior history of eye surgery or eye trauma, with amblyopia, with past or current strabismus, or with any ocular or systemic disease. All normal volunteers were naive to the purpose of the tests performed, and had normal best corrected visual acuity (VA > 0.6).

3.6.3. Data analysis

Statistical analysis was performed with the STATVIEW and SPSS software (version 15.0 for Windows) packages (SAS, Cary, NC and SPSS, Inc., Chicago, IL, respectively). Violations of ANOVA statistical assumptions were verified using the Kolmogorov-Smirnov normality check and Levene homogeneity tests. In all tests, we used a significance interval of 95% ($p<0.05$). The data did not significantly deviate from normal distributions in the control group, but this was often not the case for the disease group. Moreover, variance of the respective distributions was in general not homogeneous across the two groups. So, when this was the case, we have chosen to apply non-parametric statistical methods, although many times we verified that parametric approaches would not have changed the main conclusions, thereby indicating that lack of power was not an issue in these nonparametric analyses.

3.7. Motion Perception

The motion battery tests were developed from a high-end system of Vision Research Graphics (Durham, NH, USA) and sensitivity was measured by a discrimination method called “2-Alternative Forced Choice” (2-AFC) following a *staircase* algorithm. In particular, it is important to separate processes that are related to local motion perception (at the level of the retina) and motion integration processes (at the level of the cortex). We have developed methods to assess the contribution of each of these levels of processing in the visual system.

3.7.1. Psychophysical technique to address local motion - Local Speed Discrimination

A computerized Local Speed Discrimination Task adapted from PC-based Vision-WorksTM for Windows (Vision Research Graphics, Wisconsin, U.S.A.) was developed to measure local motion sensitivity. It is based on velocity comparisons of two widely separated dots moving with random trajectories, across four meridians (horizontal 0º, vertical 90º and oblique meridians 45º, 135º) with eccentricities between 7.5º and 15º (**Figure 3.5**). At the horizontal meridian a relatively small (7.5º) eccentricity was used, while the oblique ones were

15º and the vertical meridian 10º. Eccentricity here is defined as the distance between the center of the screen and the area of stimulation. Viewing distance was 56 cm. The stimuli used were random dots kinetograms (RDKs) presented within a circular spatial window called aperture (1º of diameter). Each test consisted of two apertures on the same meridian (with a single RDK dot moving randomly inside of each of them) and equal eccentricity with the fixation point located halfway between them (see **Figure 3.5**). During the test, two points (single dots; pixel size was 0.056 deg^2 and dot size was 3×2 pixels) are presented in two distinct opposite zones moving at different speeds, one is called the standard stimulus, with a constant speed during the test and the other is the test stimulus, whose speed varies according to the response of whom performs the test.

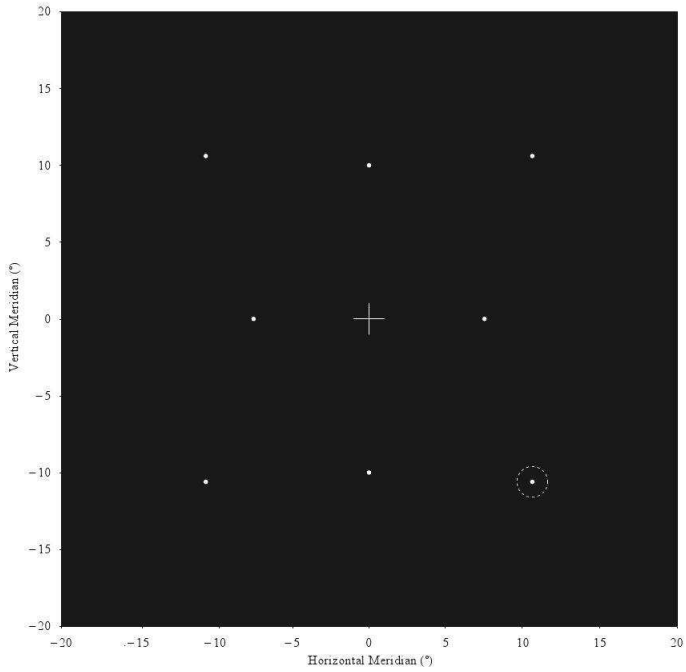

Figure 3.5. Schematic of the stimulation paradigm at various eccentricities. Stimuli move within a circular area designated aperture. The two stimuli (standard and test stimulus) are shown to the subject in one of the four meridians at equal eccentricity. The fixation point located halfway between them.

This test is implemented in a way that at the end of the experiment, visual speed thresholds (º/s) are determined in different areas of the VF. Visual speed thresholds where obtained with a two-alternative forced-choice (spatial 2-AFC) staircase method with 12 reversals (6 practice and 6 experimental). All results were given as a geometric mean of the experimental reversals. Steps were 0.01 log units in size and the number of steps was 1 down and 4 up for correct and uncorrect answers, respectively. The initial speed of the test stimulus

was 50º/s and the standard stimulus was moving at 15º/s. Stimuli had a fixed presentation time of 200ms (15 frames). Since no reaction time parameters were being measured, subjects responded verbally (right/left or up/down) which was the fastest moving dot and the experimenter introduced the response. The speed varies throughout the test until the difference between the speeds of the two points becomes imperceptible to the subject performing the test. All subjects are instructed to keep their eyes fixed on the fixation point at the center screen. The tests were performed under dark ambient illumination conditions, monocularly (first eye tested was randomly chosen) and displayed in a Trinitron GDM-F520 21" monitor (refresh rate was 75 Hz). The background luminance was ~ 0 cd/m^2 and average luminance of each aperture was 0.13 cd/m^2, while each single dot had a brightness value of 15% of the maximum output of each of the red, green and blue CRT guns. Fixation point was a white (0.34 cd/m^2) 0.4º cross-hair with 0.05º arm thickness.

3.7.2. Psychophysical technique to address global motion perception

The same motion battery with RDKs from Vision-WorksTM was used to probe different aspects of global motion perception (see below in **Figure 3.6** the stimulus used for all tasks of planar surfaces) by measuring the following parameters:

1 – *Global speed discrimination thresholds* (in º/s) between two coherent surfaces (spatial 2-AFC);

2 – *2D Motion coherence thresholds* (% coherence) for surfaces with random global motion, which rendered the test more difficult than other conventional measures of motion coherence (temporal 2-AFC);

3 – *Direction discrimination thresholds* (in º) of global motion direction of coherent surfaces (2-AFC).

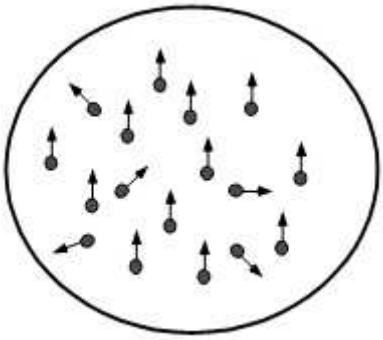

Figure 3.6. Basic sketch of stimuli (for motion coherence testing many surface directions were possible). The higher the percentage of dots defining a surface in relation to noise dots, the higher the coherence. The lower the % coherence required to perform the task, the better the performance.

Stimuli were presented within a circular spatial window of 6º visual angle in a calibrated Sony Trinitron GDM-F520 monitor and viewing distance was 56 cm. For all tests, the background luminance was ~ 0 cd/m^2 and a 2-AFC staircase method (temporal or spatial) was used (with 12 reversals, 6 practice and 6 experimental) to determine thresholds. Steps were 0.01 log units in size, unless otherwise stated. Durations of fixed stimulus presentations were of 1.133 s, after which a grey background appeared, and was present until the subject responded and the next trial commenced.

3.8. Data base of custom perimetries

An important factor in the development and validation of any clinical diagnostic test procedure, particularly one that evaluates visual function, is to establish a database for evaluation of results for individual normal subjects and patients, and also establish the changes that occur as a function of normal ageing process. A set of control experiments for different test configurations spanning at least 9 visual locations in a large group of individuals over a large span of ages was performed to construct a database for each test. Accordingly, we determined the normal population characteristics of each technique. All subjects underwent a comprehensive ocular examination and both eyes were tested in most of the time.

3.8.1. Demographic distribution of the Custom LSF task

Psychophysical study of the function of the M system in a population of normal controls was assessed by LSF testing, with hardware and software developed for this purpose:

- Implementation of computerized "staircases" in a randomized order with appropriate hardware and software (CRS, VSG2/5 visual stimulus generator).

- A system for recording eye movement (VET) was also integrated in the system of visual stimulation;

- Production of visual stimuli filtered in time and space in order to isolate the M system function, such as FD stimuli;

- Creation of a database for the computerized psychophysical method developed in our laboratory.

We generated a database of FD-CS thresholds using a custom-based approach that is comparable to commercially available FD perimetry (such as Humphrey C20, 30-2 and Matrix N-30-F). The mean background luminance (61.7 cd/m^2) for the custom-FDT method was lower than for the standard approach which likely explains the resulting lower custom CS values.

The participant's demographic data regarding LSF custom perimetric assessment were: 157 eyes (42 male and 47 female) with mean age 38 ± 19 years (mean ± SD) (range 5-75 years), see also **Figure 3.7**. The factors analyzed for the construction of LSF database were age, gender and eye. Considering the VF locations separately, the effect of simultaneously interaction (Manova) between all parameters age * gender * eye in each of the regions studied is summarized in **Table B.1** (appendix B). No global interaction effect was found. Considering each parameter individually, we observed that the most significant changes, and in almost all regions assessed, are due to age and not to chosen eye or gender effects (see main effects in each region in **Table B.2**).

The subject distribution according to age was as follows:

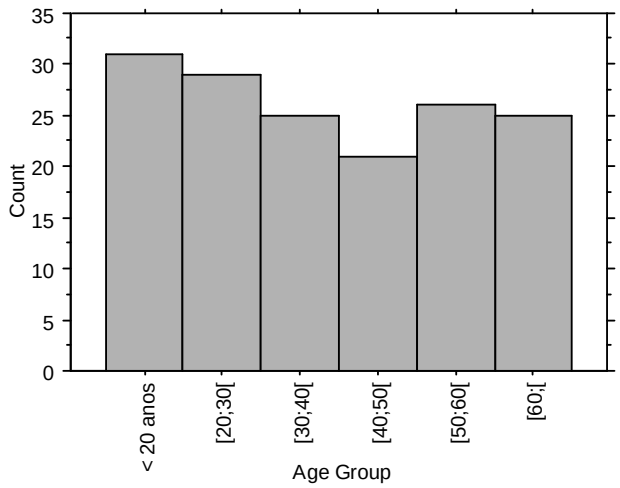

Figure 3.7. Distribution by age group of 157 eyes of normal subjects.

CS per decade of age for Zone 0 (central 5º) and global mean values in normal subjects is shown below in **Figure 3.8**.

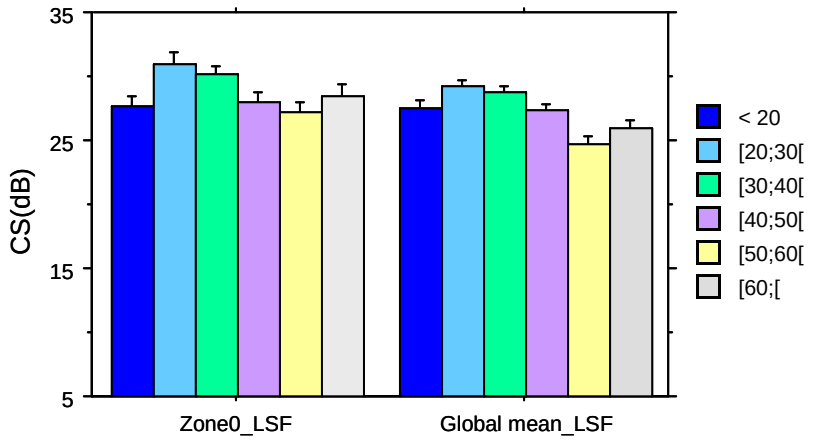

Figure 3.8. CS distribution for the central region (zone 0) and global mean values per decade of age. Error bars represent the standard error of the mean (SEM) in each zone.

On average values, for each decade of ageing, there is a decrease of 0.6 dB to 0.7 dB, depending on the region (see **Table B.3**). This normal ageing effect for FD perimetry is similar to the one found for standard FDT perimetry (Adams *et al*., 1999) and for conventional automated static threshold perimetry using Goldmann stimulus size III, averaging about 0.6 dB per decade. We did not evaluate differences in CS between the first and second eyes tested, since we considered a rest period of 5 min between testing the two eyes, cancelling in this way the central dichoptic adaptation effect (Anderson and Johnson, 2002). The first eye was choosed always randomly. We analyzed the eye effect in terms of being the right or left eye.

3.8.2. Demographic distribution of Matrix N-30-F participants

Technical collaboration with PG-Hitec Zeiss helped to validate the custom methodology implemented, by performing the standard perimetric test to a population of normal controls of different age groups (Matrix N-30-F). The Humphrey Matrix perimeter has its own normative database and their characteristics are well described (see Adams *et al*., 1999 and references therein). A statistical analysis package based on this normative database is included, providing mean deviation (MD) and pattern standard deviation (PSD) VF measures and a total deviation plot along with probability levels for these values. We constructed our database excluding all

subjects with False Positives or Negatives > 33%; Fixation errors > 20%; MD < -2 dB and PSD >+5 dB (exclusion of outlier criteria).

The total of subjects performing this task was 172 eyes, with mean age of 34 ± 19 years (range 10-83 years):

Children, with n= 44 subjects (53 eyes; 34 OD and 19 OS; 23 male, 21 female), mean age of 14 ± 1 years (range 10-17 years).

Adults, with n=48 subjects (88 eyes, 44 OD and 44 OS; 23 male and 25 female), mean age of 33 ± 10 years (range of 21- 60 years).

Adults (>=60 years), with n= 23 subjects (31 eyes; 18 OD and 13 OS; 12 male, 11 female), mean age of 66 ± 6 years (range 60-83 years).

Figure 3.9 shows the distribution of all subjects per decade of age. The group with 40-50 is too small at this time point and should be considered as providing little weight. The parameters analyzed for the construction of this database were also age, gender and eye. Considering each parameter individually, we observed that the most significant changes, and in all regions assessed, are due to age and not to chosen eye or gender effects (see main effects in **Table B.4**). As confirmed by the effect of simultaneously interaction (Manova) between all parameters age*gender*eye, where no global interaction effect was found (which is summarized in **Table B.5**).

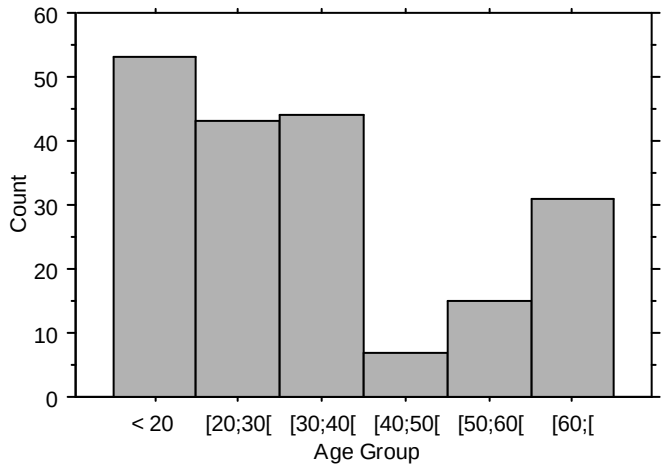

Figure 3.9. Number of subjects tested as a function of age (per decade).

A clear age-dependent performance in these tasks is also evident (see **Figure 3.10)** with older subjects presenting lower CS.

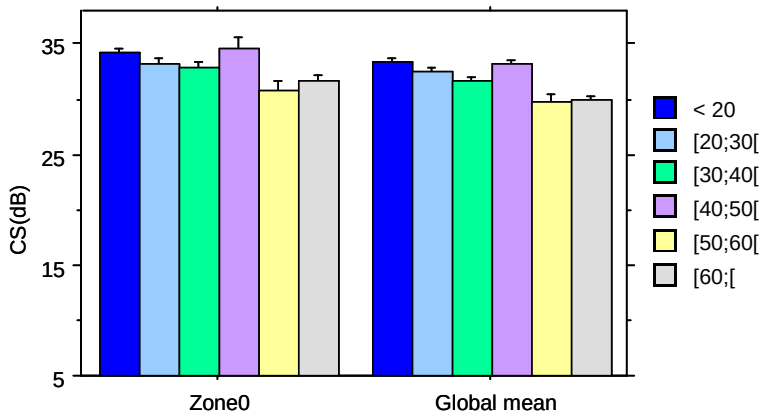

Figure 3.10. CS distribution for the central region (zone 0) and global mean values per decade of age.

For each decade of ageing, there is a decrease of 0.5 dB to 0.8 dB, depending on the region (see **Table B.6**). This normal ageing effect for FD perimetry is similar to the one found for our custom and standard FDT perimetry (Adams *et al*., 1999).

3.8.3. Bland-Altman analysis

In order to verify the agreement between the two FD versions with adult subjects (n=13) with normal vision, statistical analysis following the methods proposed by Bland and Altman (1987, 1999) were evaluated (see **Figures 3.11** and **3.12)**.

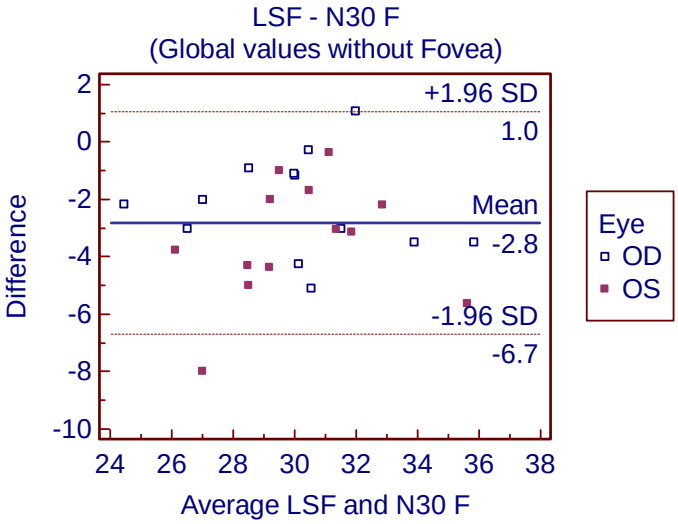

Figure 3.11. Results of the comparisons between global values without fovea made with standard FD (N-30 F) and custom FD (LSF) versions, split by eye. Data are in dB (CS).

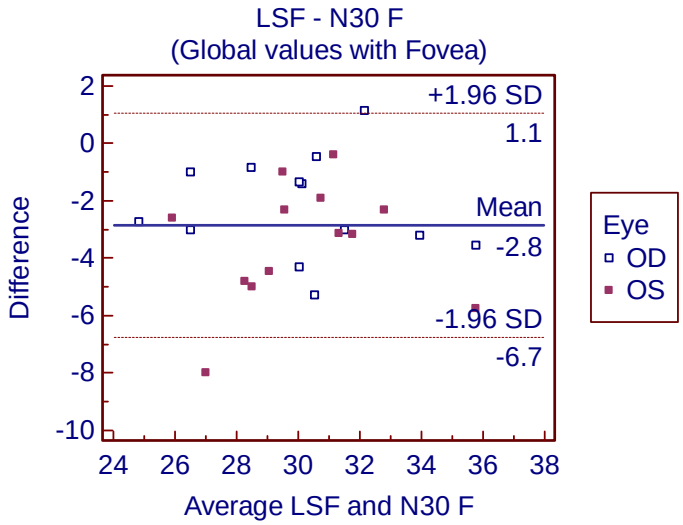

Figure 3.12. Results of the comparisons split by eye between global values with fovea measurements made with standard FD (N-30 F) and custom FD (LSF) version. Data are in dB (CS). The individual who appears below the -1.96 SD is the same, when assessing the fovea without or with the fovea, as well as the one that appears on the line +1.96SD. Thus, it appears 1 case out of the confidence limits at 95% (3.8%).

In Bland-Altman's analysis the agreement between two methods can be quantified with the aid of graphical methods using the differences between the outcomes of each method for the same subject. It is common to compute the "limits of agreement" during Bland-Altman analysis. This is usually specified as the mean difference ± 1.96 STD (mean difference ± 1.96 standard deviation of the differences). Analyzing **Figures 3.11** and **3.12** it appears that N-30 F returns, on average, a higher value by about 2.8 units than LSF custom test.

3.8.4. Demographic distribution of the Custom ISF task (ISF_photopic)

The demographic data regarding ISF custom perimetric assessment was: 191 eyes (43 male and 76 female) with mean age 35.95 ± 17.46 years (mean ± SD) (range 7 - 72 years). The age distribution of this normal population is presented below in **Figure 3.13**.

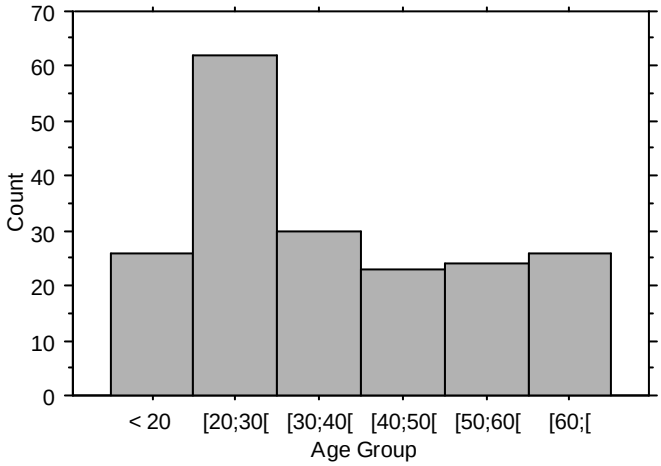

Figure 3.13. The age distribution of subjects enrolled in the construction of the ISF normative data base.

Next we show the change in sensitivity with age.

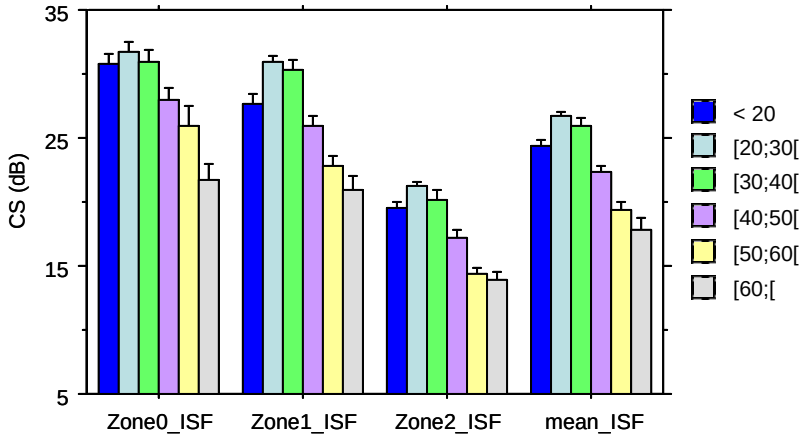

Figure 3.14. CS distribution per decade of age in normal subjects over all central (Zone 0 and Zone 1) and peripheral (Zone 2) regions, and for global mean values.

Considering all locations as a whole, an interaction exists between all factors, that is between age*gender*eye (λ_{Wilks}= 0.843; p = 0.033, Manova), which is mainly due to the interaction between age*gender (λ_{Wilks}= 0.803; p = 0.043), rather than the interaction between the eye*gender (λ_{Wilks}= 0.930; p = 0.070) or eye*age (λ_{Wilks}= 0.473; p = 0.139). Note that there is no significant effect of each factor separately in this condition (such as eye: λ_{Wilks}= 0.374; p = 0.626; age: λ_{Wilks}= 0.350; p = 0.189; gender: λ_{Wilks}= 0.893; p = 0.107). However, considering each zone and hemifield separately, it appears that there is no effect of

global interaction (age*gender*eye) in each of these regions. The only area affected by pairs of interactions such as age*eye or eye*gender is the nasal hemifield ($p < 0.001$ and $p = 0.040$, respectively). See **Table B.7**, with the first interaction explaining 45% of the variability in the values obtained in nasal hemifield ($\eta^2 = 0.450$) and the second explaining 2.5% of the same ($\eta^2 = 0.025$).

Graphically, it can be noted that in the nasal hemifield, regardless of the gender, it seems that the performance of the right eye is significantly better until about age 50, from which the values obtained for the nasal hemifield are identical as shown in **Figure 3.15**.

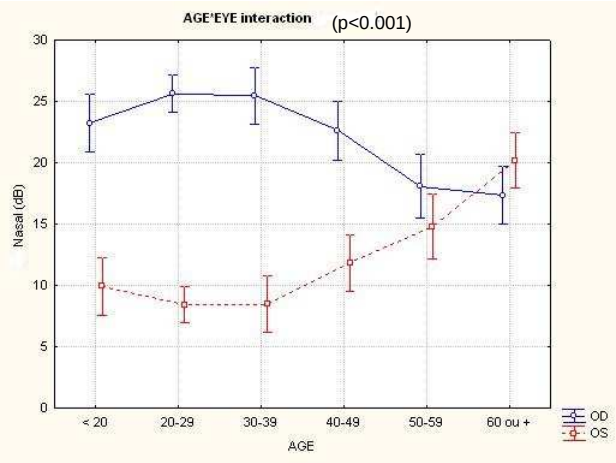

Figure 3.15. Age*eye interactions for the nasal hemifield.

Moreover, in this region, the right eye has a better performance in both the male gender as female, regardless of age of the individuals (see **Figure 3.16**).

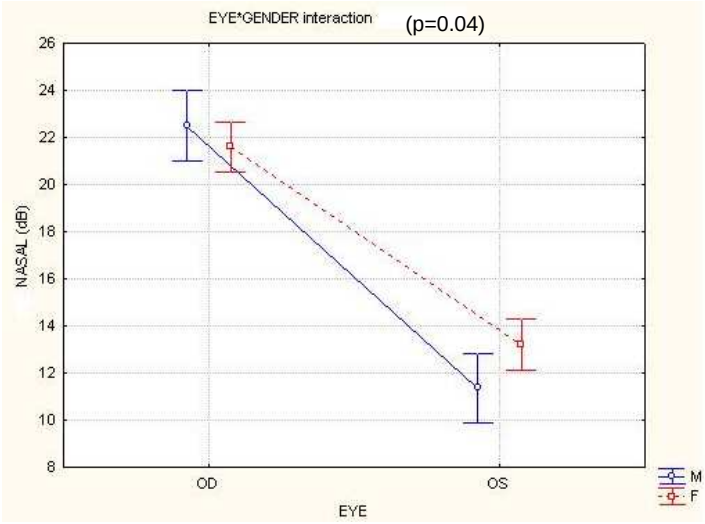

Figure 3.16. Eye*gender effect for the nasal hemifield.

So, visualizing the interaction age*eye in each gender (see below in **Figure 3.17**), it appears that, in fact, there is a significant difference between the performance of both eyes up to 50 years, being cancelled after this age, regardless of gender of the individual.

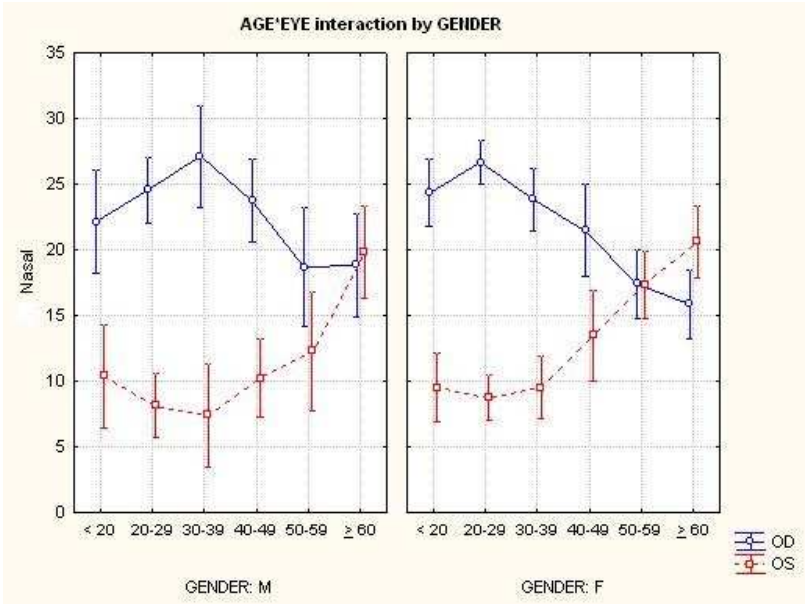

Figure 3.17. Age*eye effect split by gender for the nasal hemified.

Considering each parameter individually, we observed that the most significant changes and in almost all regions assessed are due to age and not to chosen eye or gender. In fact, the eye chosen only interferes with vision in the nasal hemifield, which is the only region not affected

by ageing (see **Table B.8**). The influence of age, gender and eye in each region by iterative multiple regression analysis is summarized in **Table B.9**.

So, the nasal hemifield is the only region influenced by the eye, having the right eye, on average, better performance by about 11.10 dB. This is likely due to the interaction with hemispheric factors. This is the only region where age is not a predictor of change in values. On average every 10 years, there is a decrease of 1.5 dB to 2.0 dB in average values, depending on the region studied (see **Table B.9**). Also, in some regions it is observed that the male gender is a better predictor of performance. The most notorious is in the superior hemifield (-1.33 dB, female), in Zone 1 (-1.36 dB, female) and for the overall, the average ISF (-1.02 dB, female, $p = 0.050$).

Regarding left and right visual hemifields, two main points should be taken into account (see **Figure 3.18**):

- Left and right VF profiles are identical for OD, regardless of gender;

- Left and right visual profiles are different up to 50 years (in the OS), for both genders (identical profile in men and women but higher variability in men). This is again likely to be due to the interaction with hemispheric factors.

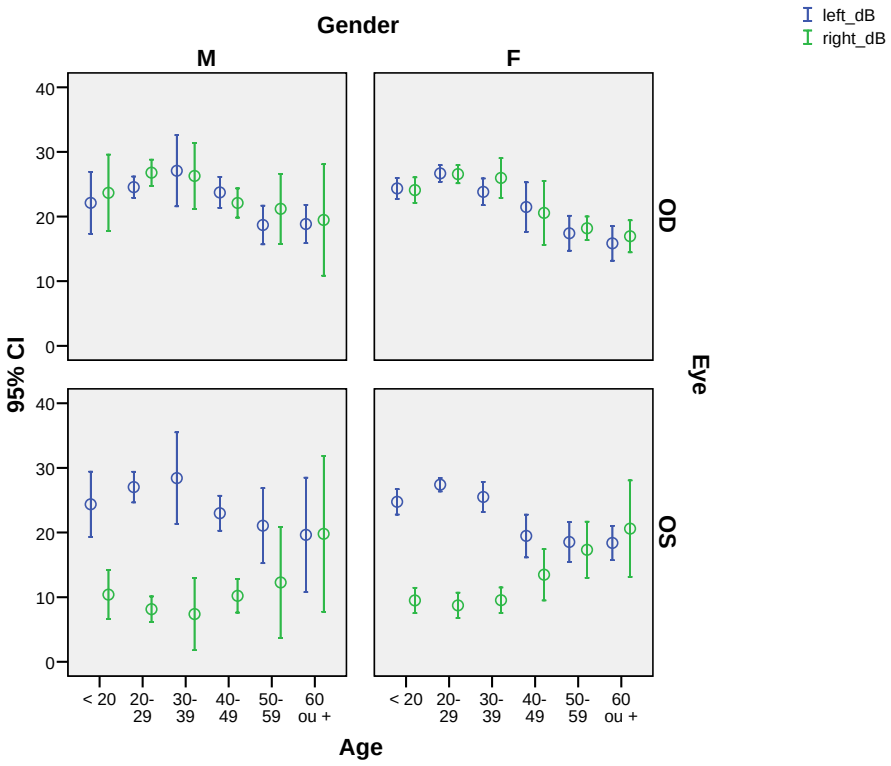

Figure 3.18. Main effects in left and right hemifields. Error bars with 95% of confidence intervals.

Part III

Results

Chapter 4

4. Retinal and cortical patterns of spatial anisotropy in CS

4.1. Summary

It has often been postulated that asymmetries in performance within the visual field (VF) are not characteristic of early visual processing. Here, human retinal (naso/temporal), cortical (left/right) and superior/inferior patterns of asymmetry were explored with achromatic contrast sensitivity (CS) tasks, that probed distinct spatiotemporal frequency channels. Low spatial, high temporal frequency stimuli (eliciting illusory frequency-doubling (FD) perception of stimulus stripes) yielded superior and temporal field disadvantage. We found independent right and nasal visual hemifield patterns of disadvantage when probing an intermediate spatial frequency (ISF) channel, with stationary sinusoidal gratings. These findings show that asymmetries in spatial vision are explained by two independent mechanisms with retinal and cortical origin.

4.2. Introduction

Psychophysical performance has often been assumed to be symmetric in terms of early level visual function, although visual field (VF) asymmetries have been established for higher level psychophysical tasks (Edgar and Smith, 1990; Hugdahl and Davidson, 2003; Ivry and Robertson, 1998; Nakayama and Mackeben, 1989; Previc, 1990; Rubin *et al*., 1996). This is quite surprising, given the available anatomical and physiological data for anisotropies in early visual pathways including cortical retinotopic areas and the retina (see below). Previous studies, such as in letter identification (Mackeben, 1999), visual acuity (Altpeter *et al*., 2000) and attentional conjunctive visual search tasks (He *et al*., 1996), have emphasized the ecological relevance of dorso/ventral anisotropies (above and below the horizon) and focused on cardinal visual meridians, raising the question whether these asymmetries could generalize to other VF locations. An early cortical contribution to asymmetric visual performance has also been recently considered (Carrasco *et al*., 2001; Carrasco *et al*., 2004) independently of attentional biases. A retinal contribution was however not isolated and separately investigated in these studies (Carrasco *et al*., 2001, 2004), because performance was analyzed only under binocular conditions. This fact precluded the possibility of exploring naso/temporal biases, which could provide direct evidence for independent retinal mechanisms underlying functional asymmetries. Retinal naso/temporal asymmetries are indeed canceled out within left/right cortical binocular representations, due to the normal crossing of visual pathways (for instance, the left hemifield corresponds to the nasal retina of the left eye, OS and the temporal retina of the right eye, OD), and this fact was also not taken into account in earlier studies using CS tasks (Rijsdijk *et al*., 1980; Rovamo and Virsu, 1979). However, a possible role for naso/temporal asymmetries in CS, in particular, in hyper acuity tasks was noted (Fahle and Schmid, 1988).

Previous anatomical findings suggest a possible neural basis for performance anisotropies of retinal origin. For example, differences in cell density can be related to relative magnification factors (M-scaling, e.g., mm of cortical surface per degree of visual space) of visual representations (Myerson *et al*., 1977; Van Essen *et al*., 1984; Virsu and Rovamo, 1979). It is also well established that differences in retinal cell density can explain differences in visual performance (Drasdo, 1977; Levi *et al*., 1985; Rolls and Cowey, 1970; Rovamo *et al*., 1978; Schein, 1988; Thibos *et al*., 1987; Weymouth, 1958; Williams and Coletta, 1987). All of these studies are consistent with strong naso/temporal biases: cone and ganglion cell densities are larger in the nasal retina (temporal VF) and these anisotropies in neural representations are further propagated to subsequent processing streams (Connolly and Van

Essen, 1984; Van Essen *et al*., 1984). These anatomical asymmetries are also consistent with documented electrophysiological data in humans (Marmor *et al*., 2003).

4.2.1. Psychophysical separation of asymmetries within the parvocellular and magnocellular pathways

We aimed to investigate early level visual asymmetries by measuring achromatic CS under conditions that provide a different mango (M)/parvocellular (P) activation bias. Previous work suggests that the M and P pathways are functionally separable given their distinct roles in temporal and spatial vision (Merigan *et al*., 1991, Merigan and Maunsell, 1993; Baseler and Sutter, 1997; Allison *et al*., 2000; Ellemberg *et al*., 2001; Maddess *et al*., 1999; Leonova *et al*., 2003). The functional characterization of the M/P pathways is conventionally performed using temporal and spatially modulated sine wave gratings as test stimuli (Robson, 1966; Derrington and Lennie, 1984). Accordingly, the parvo-biased stimuli used in our experiments were static sinusoidal gratings of relatively high spatial frequency, considering the visual eccentricities that were studied (3.5 cpd) and 0 Hz temporal frequency. This spatial frequency only provides relative isolation (mixed P-test), in particular in central VF locations. It is, however, relatively high for the more peripheral locations (beyond central 5º), which were the focus of our analyses of CS asymmetries. We have performed the P-biased test (ISF test) under both photopic and mesopic conditions, to get distinct levels of relative P isolation. Accordingly, under photopic conditions cone/parvocellular isolation is better achieved (Lee *et al*, 1996). Under mesopic luminance conditions, rod intrusion is more prominent as well as at low temporal frequencies (Lee *et al*., 2000).

To explore the M pathway (high temporal and low spatial frequency (LSF) channel) we used grating stimuli at low spatial frequency (0.25 cpd) and counterphasing at a temporal frequency of 25 Hz. These properties are appropriate to isolate the M pathway (Merigan *et al*., 1991, Merigan and Maunsell, 1993) and, in addition, it is believed that these stimuli activate more strongly a specific subset of M ganglion cells, the M/Y cells (Johnson and Samuels, 1997). These cells display non-linear responses to sinusoidal gratings flickering at high temporal frequencies. Under these conditions, perception of “frequency doubling” phenomena may occur (Kelly, 1966, 1981). The number of perceived stripes is indeed duplicated for every subject, and for this reason CS measurement techniques using such M-biased stimuli are frequently labelled as Frequency Doubling (FD) psychophysical methods. We will label this technique as LSF task.

All of our low-level visual CS tasks were performed with conditions that keep attention homogeneously distributed over the VF, by running randomly interleaved staircases in space and time, in order to unravel separate retinal and cortical mechanisms underlying anisotropies in spatial vision.

The main goal of this study was therefore to test for the presence of asymmetries in low-level visual CS tasks in terms of left/right (interhemispheric), superior/inferior, and nasal/temporal (retinal) hemifields, concerning distinct spatiotemporal frequency channels. We took into account in our approach the interaction between different types of asymmetry. For example right/left anisotropies should interact with naso/temporal asymmetries in an eye-dependent manner: in case of putative temporal and left field advantages, effects should summate for the OS, because they coincide, and cancel out for the OD. This study separates for the first time retinal and cortical mechanisms underlying psychophysical anisotropies, and shows that they are distinct in temporal and spatial vision.

4.3. Methods

4.3.1. Ophthalmological examination

A complete ophthalmological examination was done to all individuals by two ophthalmologists (from the Center for Ophthalmology, IBILI-Faculty of Medicine). This exam consisted of best-corrected visual acuity (VA - Snellen chart), IOP measurement (Goldman applanation tonometer), slit lamp examination of anterior chamber, angle and fundus examination (Goldman lens). The following exclusion criteria were applied: pseudophakic and aphakic eyes, medium significant opacification (corneal leucoma or cataract), retinal diseases, neuro-ophthalmologic pathology, VA <0.6, high ammetropia (sphere dpt > 4 and cylinder dpt > 2) and pupil diameter ≤ 2.0 mm.

4.3.2. Participants

Informed consent was obtained from all participants. This study was conducted in accordance with the tenets of the Declaration of Helsinki, and followed the guidelines of the Ethics Committee of the Faculty of Medicine of Coimbra. All subjects were right-handed and naive to the tests performed with normal or corrected-to-normal VA and wore, when necessary, a correction appropriate for the 36 cm viewing distance. To avoid biases related to perceptual learning, groups performing different types of tasks were independent.

4.3.2.1. Participants of the ISF task

Concerning ISF task (P-biased perimetry) for both luminance conditions, the subject distribution was as follows: ISF_photopic, n = 18 subjects (36 eyes; 8 male and 10 female) with mean age 25 ± 3 years (mean ± SD) (range 22 - 34 years) for monocular testing and n = 18 under binocular conditions; ISF_mesopic, n= 22 subjects (39 eyes; 9 male and 13 female) with mean age 27 ± 5 years (range: 21 - 44 years) under monocular and n = 10 (5 male and 5 female) under binocular conditions (mean age 27 ± 5 years; range: 23 - 33 years).

4.3.2.2. Demographic distribution of the LSF task

FD perimetry was performed using two standards and one custom-made test: **T1.Matrix N-30-F**, **T2.Humphrey N-30** and **T3.Custom C20**. The demographic distribution for all tasks performed was as followed:

T1.Matrix N-30-F: perimetric assessment with n=48subjects (88 eyes, 44 OD and 44 OS; 23 male and 25 female), mean age 33 ± 10 years (range: 21- 60 years).

T2.Humphrey N-30: n= 29 subjects (47 eyes; 27 OD and 20 OS; 15 male and 14 female), mean age 35 ± 9 years (range: 26 – 67 years).

T3.Custom C20: n= 20 subjects (36 eyes; 20 OD and 16 OS; 8 male, 12 female subjects), mean age 27 ± 4 years (range: 20 – 34 years), age-matched with the group of ISF task. Thirteen subjects performed also **T1.Matrix N-30-F** standard test.

4.3.3. Perimetic CS assessment

4.3.3.1. ISF contrast sensitivity test

To explore an ISF channel, we used static sinusoidal gratings of 3.5 cpd (intermediate spatial frequency). The ISF CS perimetric test was performed under photopic (background luminance of 51 cd/m^2) and high mesopic (1 cd/m^2) conditions (**ISF_photopic** and **ISF_mesopic** tests, respectively). The stimulus was used as a detection target and presented pseudo-randomly within 9 locations (for more details, see Methods and Experiments in Part II). Subjects were instructed to fixate the black square (1ºx1º) in the centre of the screen and report the presence of ‘‘striped’’ targets by means of a button press. Participants’ reliability was

evaluated by randomly interleaving false positive (FP) with 0% contrast stimuli and negative (FN) with 100% contrast trials. We excluded all results with FP and FN errors ≥ 33%, according to standard criteria (Caprioli, 1991; Brusini *et al*., 2006). Fixation loss was monitored with our custom eye-tracking methodology (CRS device) which provides detailed measurements of eye position. This perimetric task was performed in a monocular way (an opaque black patch was used to occlude the non-tested eye to be similar with the patch used in FD standard perimetry) for both eyes, with the first tested eye being chosen in a random manner (since ocular dominance does not appear to affect VF test results, see Spry *et al*., 2002). To replicate the left/right asymmetry observed under monocular conditions, this task was also performed under binocular conditions.

4.3.3.2. LSF contrast sensitivity - FD test

The spatiotemporal profile of the stimulus used in the LSF task (FD test) was optimized to independently isolate the M pathway. In brief, the FD test stimulus consists of a sinusoidal grating of low spatial frequency undergoing counter phase flicker at high temporal frequency, projected on a dim background; contrast is either increased or decreased to determine the threshold. The contrast threshold value for each test location is defined as the minimal contrast at which the pattern is perceived. FD perimetry was performed by standard and custom-made tests: **T1.Matrix N-30-F**, **T2.Humphrey N-30** and **T3.Custom C20**. In all detection target strategies, stimuli were patches of 0.25 cpd vertically oriented sinusoidal gratings, undergoing 25 Hz counterphase flicker. This LSF task was generated in a perimetric strategy, by means of either FD Technology (standard tests) or by a video board (Cambridge Visual Stimulus Generator, VSG2/5; Cambridge Research Systems [CRS]) for the custom-made approach (Mendes *et al*., 2005; Silva *et al*., 2005). The stimulus, in the custom mode was displayed on a gamma-corrected 21-inch colour Trinitron GDM-F520 monitor (frame rate 100 Hz). While the standard approach was performed with both FDT instruments, the N-30 full-threshold test (Welch Allyn FDT, Skaneateles Falls, New York; Carl Zeiss Meditec, Dublin, California, USA), and Humphrey Matrix Instrument (Humphrey Matrix perimeter, Welch Allyn, Skaneateles, NY; Zeiss–Humphrey, Dublin, CA) with N-30-F full-threshold test ((Johnson and Samuels 1997; Anderson *et al*., 2005). The FD stimuli were used as detection targets in all techniques and presented pseudo-randomly within 19 VF locations, including 2 additional nasal locations, testing 30º nasally and 20º temporally (see **Figure 4.1**). The 9 locations tested in the custom task matched 9/17 locations tested in the standard approach.

T1.Matrix N-30-F program is identical to the previous one (**T2.Humphrey N-30**). In fact, several authors have reported that there are no significant differences with regard to within-test variability (short-term fluctuation) between the two instruments (Johnson *et al*. 1999; Spry and Johnson 2002). The 19-point threshold test includes: 18 squares 10º×10º targets (16 of which are central and two are in the nasal periphery), and one 10º×10º central circular target (**Figure 4.1**). The **T1.Matrix N-30-F** uses a two-reversal modified binary search (MOBS) staircase strategy (instead of four reversals of the Humphrey task) for determining full threshold which tends to be a more efficient time saving algorithm. Threshold testing gives comprehensive quantitative information by providing the minimum CS needed to detect the FD stimulus at each location. Results incorporate a scaling factor to resemble normal sensitivity values found in standard automated perimetry Humphrey Viusal Field Analyzer (SAP, Carl Zeiss Meditec, Inc), and are given in dB of sensitivity (Anderson *et al*., 2003):

$$\log\left(\frac{2048}{c}\right)\times 10\times H \tag{4.1}$$

where c is the Michelson contrast and ranges from 1 (minimum contrast) to 2048 (maximum contrast) and H, the Humphrey scaling factor which is approximately 2.

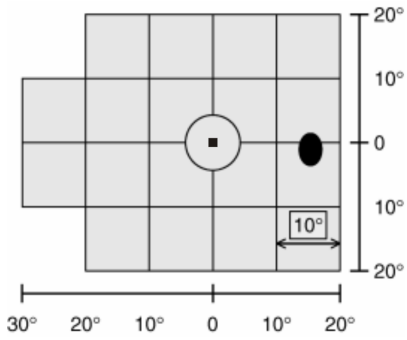

Figure 4.1: T1.Matrix N-30-F and **T2.Humprey N-30** test patterns for OD.

The range of possible threshold level values is between 0 dB (maximum contrast) and 38 dB (minimum contrast) for **T1.Matrix N-30-F** and 56 dB for **T2.Humphrey N-30** test. All test characteristics are specified in **Table 4.1,** including: target locations (Locs), Central field of view (FV), background luminance (BckL), test strategy (Strategy), as well as stimulus duration (D) and spatial (SF) and temporal frequency (TF). **T3**, **ISF_photopic** and **ISF_mesopic** are similar custom tests performed at different background luminances to isolate visual pathways. **T3** and **ISF_mesopic** stimulate specifically M and P pathways, respectively, while **ISF_photopic** stimulates both pathways.

Table 4.1 Test specifications for all perimetric approaches.

Tests	Locs	Central FV (º)	SF (cpd)	TF (Hz)	BckL (cd/m)	Strategy	D (ms)
ISF_photopic	9	20	3.5	0	51.2	vsgLogStaircase	200
ISF_mesopic	9	20	3.5	0	1.0	vsgLogStaircase	200
T1.Matrix N-30-F	19	30	0.25	25	100	Optimized MOBS (2 reversals)	300
T2.Humphrey N-30	19	30	0.25	25	100	MOBS (4 reversals)	200-400
T3.Custom C20	9	20	0.25	25	61.7	vsgLogStaircase	200

As FD perimetry is unaffected by blur of up to 6 diopters, patients can wear their normal spectacle correction to take the test, even if they have a bifocal added. The Matrix instrument has a video eye-monitoring device and performance reliability was assessed by monitoring fixation loss with the Heijl–Krakau method (for the custom approach see previous section). A total of 2.3% fixation errors were found. All results with global statistical indices as Mean Deviation (MD) < -2 dB and Pattern Standard Deviation (PSD) > 5 dB as well as fixation loss ≥ 20%, FN and FP responses ≥ 33% (2/6) were excluded. Subjects, as in the ISF experiment, were instructed to fixate the black square in the centre of the screen and report, by button press, the presence of ‘‘striped’’ targets. All participants performed the tests under monocular conditions and the first tested eye was chosen in a random manner. Since no left/right asymmetry was observed under monocular conditions, no replication was needed in this case for binocular conditions. OS results were converted into OD format for the analysis.

4.3.4. Magnification (M – scaling) factor analysis

Equations used to account for functional magnification factors (Virsu and Rovamo, 1979) were:

Nasal: $M_N = (1 + 0.33\ E + 0.00007\ E^3)^{-1}\ M_o$, $(0 \leq E \leq 60^o)$; (4.2)

Superior: $M_S = (1 + 0.42\ E + 0.00012\ E^3)^{-1}\ M_o$, $(0 \leq E \leq 45^o)$; (4.3)

Temporal: $M_T = (1 + 0.29\ E + 0.000012\ E^3)^{-1}\ M_o$, $(0 \leq E \leq 80^o)$; (4.4)

Inferior: $M_I = (1 + 0.42\ E + 0.000055\ E^3)^{-1}\ M_o$, $(0 \leq E \leq 60^o)$; (4.5)

where, E refers to eccentricity and M_o is the value of magnification (7.99 mm/º) for the most central fovea).

4.3.5. Statistical analysis

To examine spatial perceptual asymmetries we have used parametric statistics both for pairwise/quadrantwise assessment of VF asymmetries (paired t-test when analyzing hemifield patterns of asymmetry and/or repeated measures ANOVA for quadrantwise analyses), after verifying that the data did not significantly deviate from normal distributions. The central 5º radius region of higher CS was excluded in all data analyses of spatial asymmetries, since it gives a homogeneous contribution for all quadrants and hemifields, and is therefore irrelevant to the analysis of anisotropy. Note that for the LSF testing condition, 9 locations were tested in the custom approach as compared to 17 locations (9 of which matching exactly the ones used in the custom approach) in **T1** and **T2** standard methods (2 additional nasal locations were excluded so that comparisons between all approaches were made in matched locations within the same range of eccentricity, 20º). Statistical analysis was done with the STATVIEW and SPSS software packages (SAS, Cary, NC and SPSS, Inc., Chicago, IL, respectively).

4.4. Results

4.4.1. Results for ISF test

4.4.1.1. Retinal naso/temporal VF asymmetries in the ISF task under photopic and mesopic conditions

Measurements of monocular and binocular CS across VF, were done using ISF stimuli under photopic and mesopic conditions. For ISF_photopic (cone photoreceptor and parvocellular - isolating) and ISF_mesopic (activating both rods and cones) tasks, we have found mean CS values of 24.7 dB ± 6.2 and 16.7 dB ± 6.3 (mean ± SD), respectively. These distinct sensitivities were, as expected, from the physiological properties of the predominantly activated cell populations, and, accordingly were also considerably lower than the ones found for the LSF test conditions (see below). Representative individual CS maps are illustrated in **Figure 4.2**.

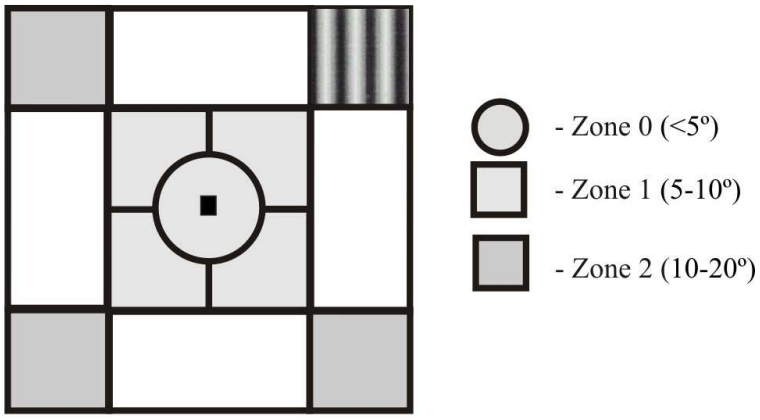

Figure 4.2. Top inset: Basic scheme of VF locations, tested in the custom approach in a pseudorandomly interleaved manner (continued below).

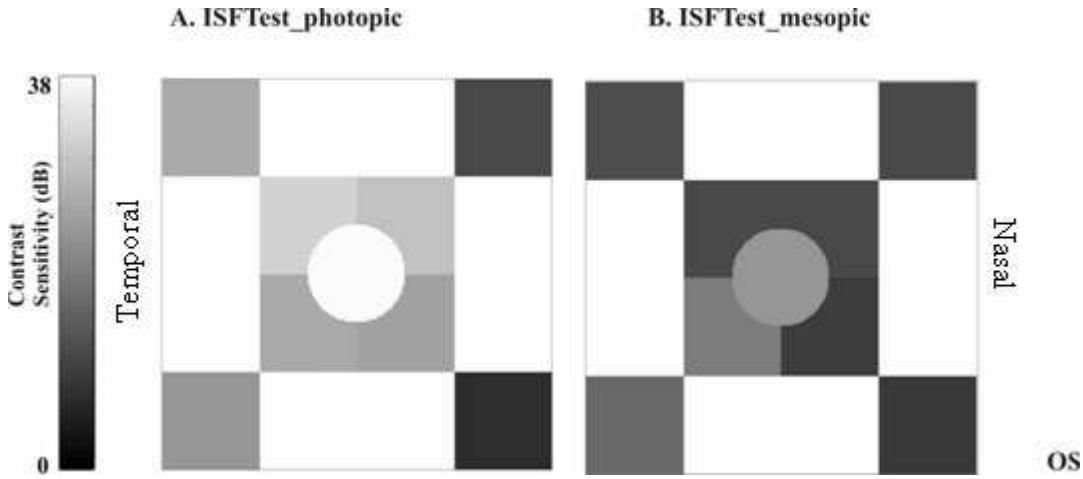

Figure 4.2. Lower panel (continued): Gray scale CS maps (OS) for ISF stimuli tested in 9 locations for both luminance conditions, depicted from a representative subject with strong asymmetry (due to synergistic summation of left/right and naso/temporal asymmetries in left monocular testing – for details see Text). Darker regions correspond to areas of lower CS (the central region is very bright due to high CS).

The group analysis of hemifield asymmetries (**Figure 4.3**) showed a significant naso/temporal pattern of VF anisotropy), with a stronger effect for the photopic condition (paired *t*-test: photopic, $p = .0002$; mesopic, $p = .0055$; lower CS in the nasal hemifield).

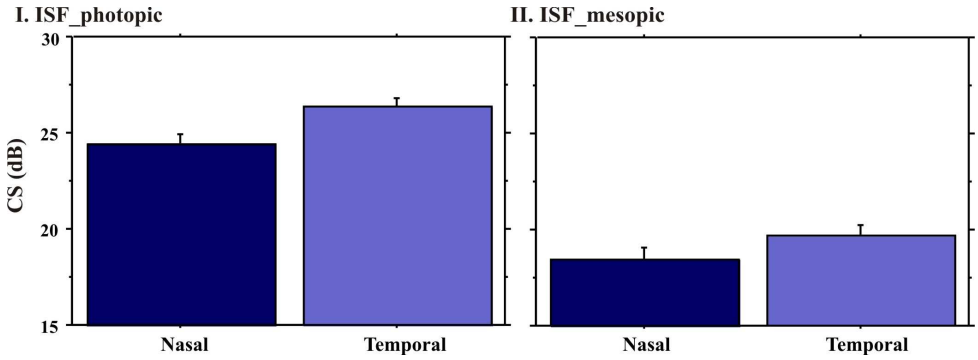

Figure 4.3. Comparisons of performance in nasal and temporal VF regions, for the ISF task under photopic and mesopic conditions. Error bars correspond to 1 standard error of the mean (SEM), in all figures. A naso/temporal pattern of asymmetry (nasal field disadvantage, lower CS) was found for both luminance conditions (paired *t*-test: $p_{photopic} = .0002$, $p_{mesopic} = .0055$).

We have also performed analysis split by VF quadrants, because most cortical areas beyond V1 are organized into separate quadrant representations and to further document whether the strength of naso/temporal asymmetries was modulated by a dorso/ventral

(superior/inferior) factor. This analysis did confirm, as expected, significant differences in performance across visual quadrants (repeated measures ANOVA with n = 4 levels: $p_{photopic}$ = .001, $p_{mesopic}$ = .005). Accordingly, we found predominant $IN_{photopic}$ (inferonasal) and $SN_{photopic}$ (superonasal) field disadvantage (corresponding to supero and inferotemporal retina) in comparison to $IT_{photopic}$ and $ST_{photopic}$ regions. Differences between IN and, in particular, region IT, were significant ($p_{photopic}$ < .0001, $p_{mesopic}$ < .002) even after correction for multiple comparisons.

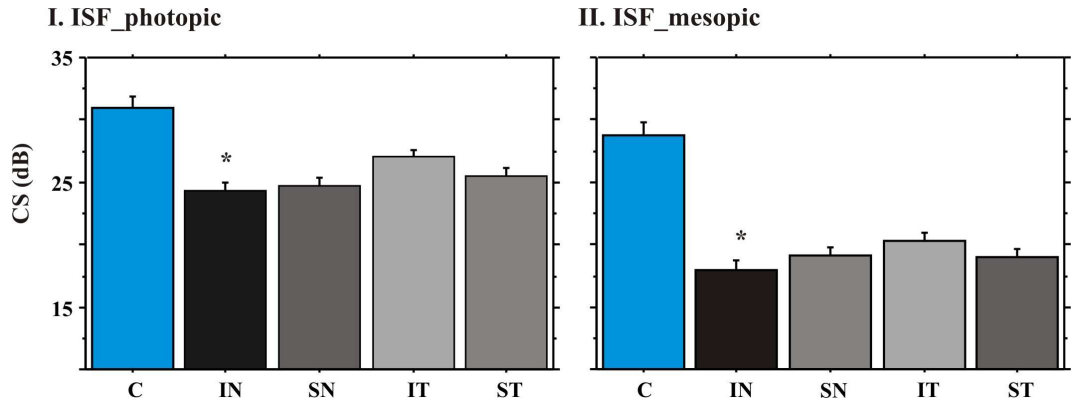

Figure 4.4. Bar plots depicting CS for each quadrant: IN - inferonasal; IT - inferotemporal; SN - superonasal; ST - superotemporal; C - central 5º radius region, for both luminance conditions. A IN pattern of disadvantage (superotemporal retina) was found.

4.4.1.2. Cortical left/right VF asymmetries in the ISF task

A significant cortical hemifield effect (performance in the left hemifield being significantly better than the right) was found (**Figure 4.5;** paired *t*-test for left/right hemifield comparisons: I. ISF_photopic, p = .013; II. ISF_mesopic, p = .024). This was further confirmed when considering experiments performed under binocular conditions (**Figure 4.5**; photopic, p = .0071; mesopic, p < .0001). Superior/inferior asymmetries were not present for binocular conditions. Hemifield (interhemispheric) performance was then analyzed separately for each eye, to better understand the interaction between naso/temporal field asymmetries (that can better be separated by considering each eye separately) and cortical left/right anisotropies (since the left hemifield includes the nasal VF of OD and the temporal VF of OS).

When the analysis of naso/temporal asymmetries was split by eye, significance was found specifically for the OS (photopic, p < .0001; mesopic, p = .0023; see **Figure 4.5**). Note in **Figure 4.5**, that the left panel represents data pooled across eyes, but the source of the effect

becomes clearer in the right panel. The effect was indeed strongest for OS, and binocular conditions. However it was not present or even occasionally reversed for OD.

This was expected from our interaction hypothesis that the left field advantage should summate with the corresponding temporal VF advantage in OS, and should cancel out with the corresponding nasal VF disadvantage in the OD. If this were the case, a significant interaction between the left/right VF asymmetry and tested eye should be observed. This was indeed the case (p = 0.002, concerning analysis of the interaction between these factors).

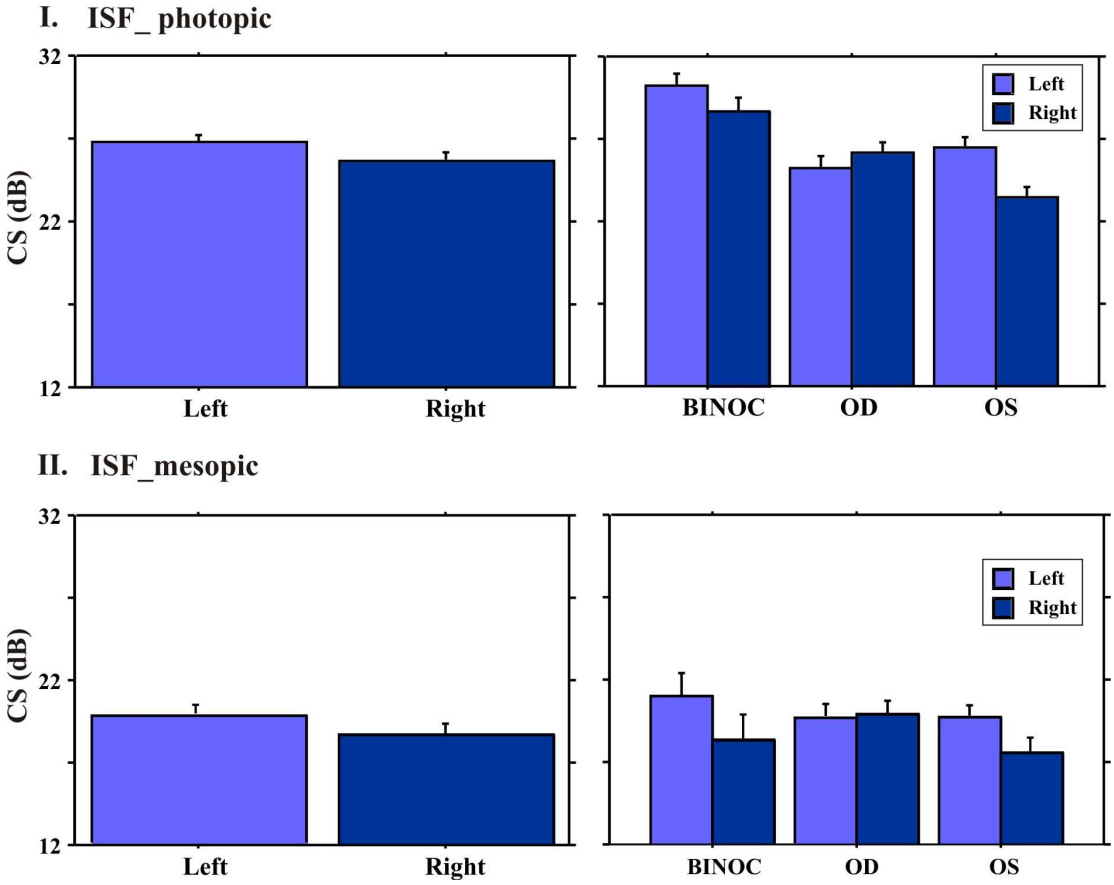

Figure 4.5: Left/right performance asymmetries (of likely cortical origin) were observed in our parvo-biased ISF test, reaching significance under both photopic (I) and mesopic (II) conditions (paired *t*-test for left/right hemifield: photopic, p = .013; mesopic, p = .024). When analysis was split by eye, significance was found for OS but not for OD, under both conditions (photopic: p < .0001, OS); mesopic: p = .0023, OS). Binocular (BINOC) control testing showed the same pattern of cortical left hemifield advantage (photopic, p = .0071; mesopic, p < .0001).

4.4.2 Results for LSF standard tests

The spatiotemporal profile of the stimulus used in this task was optimized to independently isolate the M pathway. We have measured monocular CS across the VF using FD stimuli. The commercial FDT perimeter exhibited decibel values 2.0 to 3.5 times higher than those reported for the custom perimeter approach. However, the representive maps were similar. The custom CS was on average slightly higher when compared with the ISF task, which probed a higher spatial frequency. The similarity of representative CS maps obtained with distinct LSF approaches can be appreciated in Figures below (standard and custom approaches).

Table 4.2: CS values (mean ± SD) in dB for C (5º radius central region) and global mean (without C), for all LSF tests.

Tests of CS (dB)	C (5º)	Global mean(without C)
T1.Matrix N-30-F	33.03 ± 3.19	31.66 ± 2.56
T2.Humphrey N-30	31.36 ± 3.65	30.04 ± 1.97
T3.Custom C20	30.13 ± 3.52	28.01 ± 3.73

4.4.2.1 Naso/temporal and dorso/ventral VF asymmetries in the LSF task

It is interesting to note that a quadrant-like pattern of asymmetry was found, which is likely due to the combination of naso/temporal and dorso/ventral anisotropies (see representative examples below). It is worth noting that the pattern of temporal field disadvantage observed for this task was opposite to the one observed for the ISF task confirming that the distinct stimulus properties tap separate mechanisms. In terms of cortical left/right anisotropy, nothing was found for all groups ($p > .05$, ns) so no control binocular tests were done for the LSF channel. We did observe a worse performance in the superotemporal (ST) quadrant. In method **T1.Matrix N-30-F**, superior/inferior asymmetry was present as well as a pattern of naso/temporal anisotropy ($p < .0001$, for both). For **T2.Humphrey N-30** we found only a naso/temporal asymmetry ($p = .009$).

However, the retinal naso/temporal anisotropy was not found with the **T3.Custom C20** strategy (p = .1686, ns; ANOVA repeated measures, n=4 with Bonferroni correction). Surprisingly, a strong superior/inferior asymmetry appeared (p = .0098).

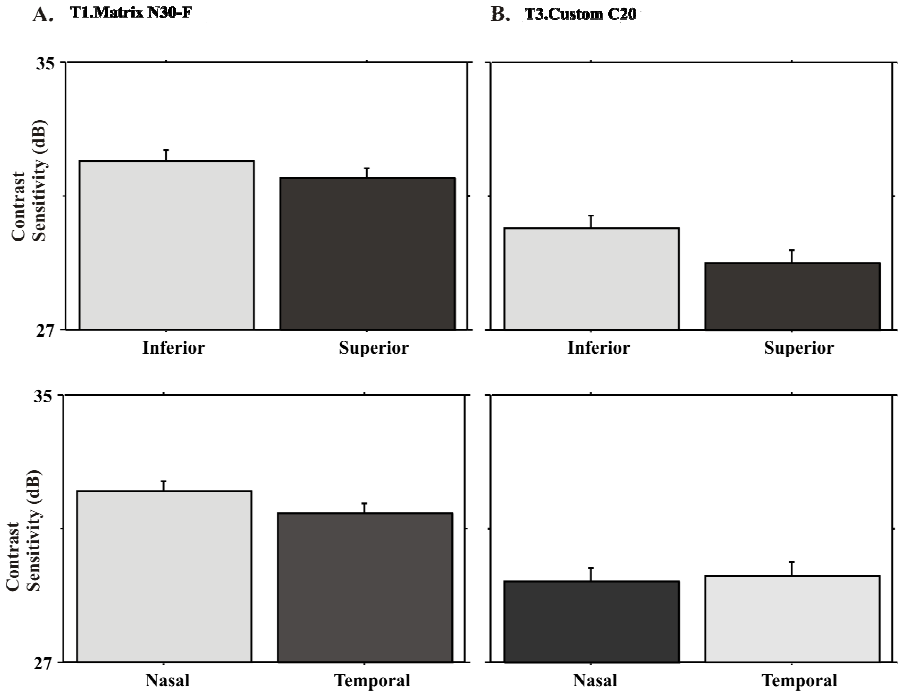

Figure 4.6. Naso/temporal and superior/inferior patterns of performance are summarized in bar plots for tests. **(A)** A strong naso/temporal asymmetry (temporal field disadvantage) was found for both standard approaches (**T1.Matrix N-30-F**: p < .0001 and **T2. Humphrey N-30**: p = .009, not represented in Figure). Significant superior/inferior asymmetry (p <.0001, superior field disadvantage) field was present only in standard **T1** Matrix N-30-F. **(B)** In **T3.Custom C20** task the nasal/temporal asymmetry was not significant, but a superior/inferior asymmetry appeared (p = .0098). In all figures, darker bars correspond to lower CS.

Analyses split by VF quadrants confirmed the ST pattern of disadvantage (inferior nasal retina) for all probing methods, (see representive plots below in **Figure 4.7**). In **T1.Matrix N-30-F**, p < .0001, **T2.Humphrey N-30**, p = .003 and **T3.Custom C20**, p = .001; repeated measures ANOVA, with n = 4. These effects remained significant after correction for multiple comparisons. In the **T1** approach, differences for Bonferroni-Dunn *post-hoc* comparisons were significant in particular between ST and all other quadrants (p < .0001). In **T2**.**Humphrey N-30**, significance was found between ST and SN (p = .023) and IN (p = .011). For the custom approach, significance was found only between ST and IT (p < .0001).

T1. Matrix N-30-F

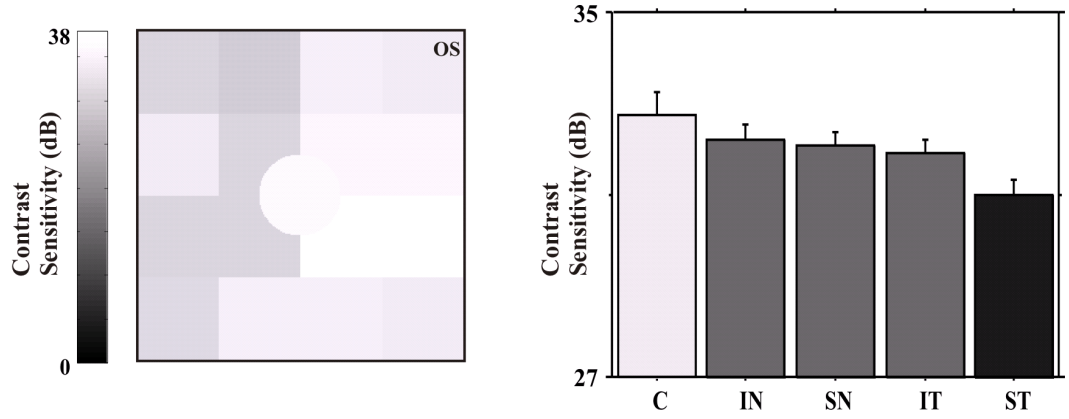

T2. Humphrey N-30

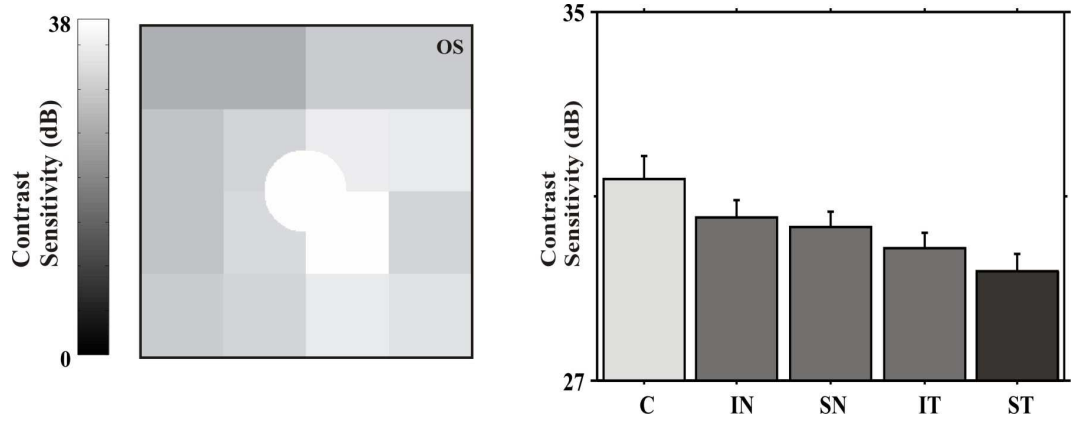

T3. C20 Custom

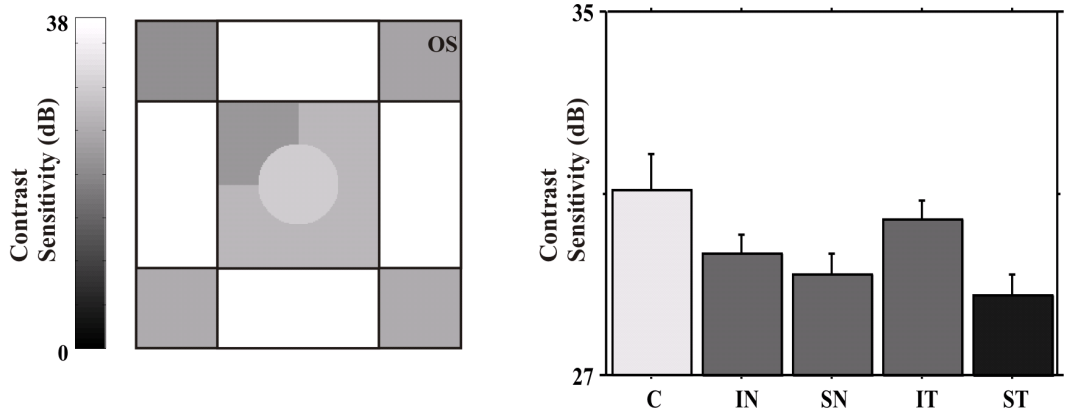

Figure 4.7. Left panels: CS maps from OS eyes of representative normal subjects (using standard and custom LSF tests; for details see text). **Right panels**: bar plots depicting CS for each quadrant: IN, inferonasal; IT, inferotemporal; SN, superonasal; ST, superotemporal; C, central 5º region. For all LSF tests, a ST pattern of disadvantage (inferior nasal retina) was found.

4.4.3 Center-periphery CS differences across distinct sensory mechanisms

Comparisons of CS in our custom tasks (ISF and LSF) across regions of different eccentricities are plotted below in **Figure 4.8**. It is worth noting the relatively flat profile of eccentricity dependence observed for performance in the LSF test when compared with ISF test. This suggests that eccentricity dependence of CS in LSF channel and its relation to M-scaling (mm of cortical surface/º) is less prominent than for the ISF channel. When M-scaling our Custom CS maps, using the equations described before (Virsu and Rovamo, 1979) we have found an overestimation of peripheral performance for the LSF channel task as shown next in **Figure 4.8.**

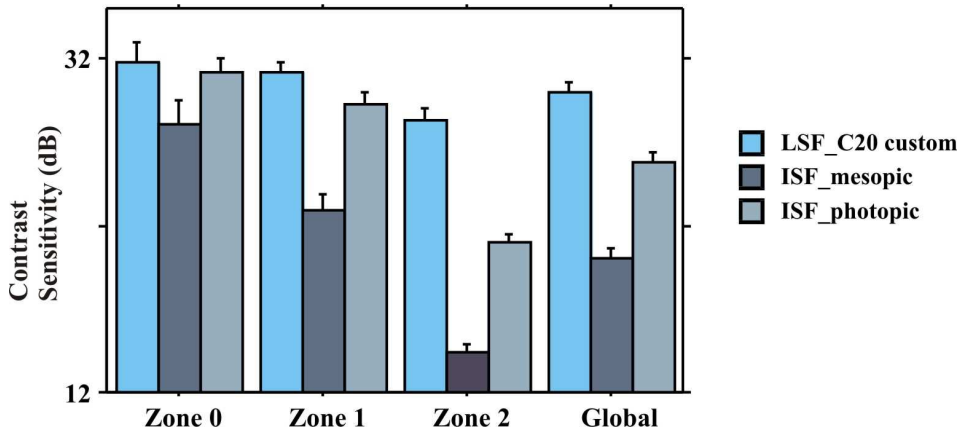

Figure 4.8. CS shows distinct dependence on eccentricity for magno (**LSF_C20 custom** or **T3.Custom C20**) and parvo-biased (**ISF_mesopic** and **ISF_photopic**) tasks. Zones are as defined in top inset of **Figure 4.2** and "Global" measure corresponds to an average across the three zones. The relatively flat profile observed for the LSF (M) test explains why classical M-scaling procedures would lead to deviations in correct CS estimation.

This previously unreported effect is, therefore, likely due to the case that the M pathway has a distinct magnification profile as suggested by the plots in **Figure 4.8**. In other words, the LSF channel has likely a less steep magnification profie than the pathways related to the ISF channel.

4.5 Discussion

This study demonstrates perceptual anisotropies of low-level cortical (left/right) and retinal (naso/temporal) or mixed (dorso/ventral) origin which are distinct within the two tested spatiotemporal frequency channels. Combinations of different types of hemifield asymmetries also yielded quadrant-like patterns of anisotropy. In our custom ISF (intermediate spatial frequency) task, we found that retinal mechanisms are modulated by a surprising left hemifield advantage of cortical origin, which was not previously reported for such low-level detection tasks (Hugdahl and Davidson, 2003; Ivry and Robertson, 1998).

Our experimental design was able to render attention homogeneous across space, by interlacing tests simultaneously across the VF, thereby rendering stimulus presentation unpredictable. All results (right and nasal hemifield patterns of disadvantage when assessing the ISF channel and quadrant-like superotemporal pattern of asymmetry for the LSF channel) showed unequivocal evidence for pre-attentive low-level visual anisotropies that includes early contrast processing, contradicting traditional postulates of pure high-level asymmetries (Hugdahl and Davidson, 2003; Ivry and Robertson, 1998). Some previous studies were performed under binocular conditions, which precluded analysis of the contribution of low-level retinal factors and thereby missing naso/temporal asymmetries (see however the findings of Fahle and Schmid, 1988; Fahle and Wehrhahn, 1991 concerning hyperacuity and motion tasks). Furthermore, we have verified that retinal naso/temporal asymmetries interact significantly with left/right cortical binocular representations (summating, as expected from the anatomical arrangement and monocular psychophysical asymmetry patterns, synergistically for the OS and antagonistically for the OD, an effect that is independent of eye dominance). Indeed right/left anisotropies should interact with naso/temporal asymmetries in an eye-dependent manner: in case of temporal and left field advantages effects, as found, should summate for the OS, because they coincide, and cancel out for the OD. The temporal disadvantage observed with the LSF task combines with the also observed dorso/ventral asymmetry (inferior field superiority) related with the LSF channel, which routes predominantly to the visual dorsal stream. This finding generalizes previous reports suggesting enhanced anatomical representation of the lower VF (Van Essen *et al*., 1984), with better performance in this region for several tasks.

The superior/inferior asymmetry in the LSF condition mirrors the pattern observed for other previously described tasks (Altpeter *et al*., 2000; Carrasco, McLean, Katz, and Frieder, 1998; Carrasco *et al*., 2004; Mackeben, 1999; Rubin *et al*., 1996). Better performance in the inferior visual hemifield is not surprising, since ganglion cell densitiy is higher in the superior

retina (Curcio and Allen, 1990a) and the fact that most interesting visual events occur below the line of horizon (Previc, 1990, for review).

It is surprising that the magno-biased LSF test gives a pattern of naso/temporal asymmetry opposite to the ISF task. It remains to be explored whether such performance differences observed for LSF tests are related to anatomical asymmetries such as naso/temporal size differences in primate ganglion cell dendritic arborizations (Dacey and Petersen, 1992; Silveira and Perry, 1991; Yamada, Silveira, Perry, and Franco, 2001). This would imply a distinct explanation not based on cell number as was the case for the ISF task. In fact, Silveira and Perry (1991) noted that M-ganglion cells in the nasal region of the retina (temporal field) have relatively smaller dendritic trees. Dacey and Petersen (1992) have previously correlated larger dendritic field sizes of human M (parasol) cells, with a lower resolving ability and an increased sensitivity to luminance contrast than their equivalents in the macaque. Concerning the different VF performance observed for the magno task we can, therefore, speculate that it is likely related to naso/temporal size differences in primate ganglion cell dendritic arborizations. Indeed, temporal ganglion cells tend to have larger dendritic fields than nasal cells (Yamada *et al*., 2001). Furthermore, P (midget) and M (parasol) ganglion cells in owl monkeys have larger dendritic fields than those of diurnal primates (Silveira, Yamada, Perry, and Picanco-Diniz, 1994; Yamada, Marshak, Silveira, and Casagrande, 1998). The fact that ganglion cells in primates with predominant nocturnal vision (requiring higher CS) have larger dendritic fields than those of diurnal primates further supports the idea that larger dendritic trees may yield better CS. Indeed, larger dendritic trees imply sampling of a larger number of photoreceptors and thereby larger sensitivity (see also the classical evidence for the relation between spatial summation and CS: Shapley, Kaplan, and Soodak, 1981). If this is also the case for the human retina, then this might well represent a neuronal correlate of the higher CS we have observed for that part of the retina.

Concerning the ISF channel, the novel and surprising pattern of left hemifield advantage suggests that an interhemispheric effect can powerfully modulate performance even for low-level CS tasks. This extends the previously known right hemispheric dominance for high-level spatial vision tasks (Hugdahl and Davidson, 2003) also to early vision mechanisms.

This is specifically true for the ISF task which is probably related to the fact that spatial vision mechanisms are more heavily recruited with higher spatial frequency stimuli. The enhanced nasal VF disadvantage provides direct evidence for an additional retinal mechanism contributing to anisotropic performance, and is consistent with the correspondingly lower cone/ganglion cell density profiles in the temporal retina (Curcio and Allen, 1990a; Curcio *et al*., 1990b; Dacey, 1993; Drasdo, Millican, Katholi, and Curcio, 2007).

Anatomical anisotropies within the retina have been well documented and are consistent with our own optical coherence tomography and multifocal electrophysiology data (presented in the next Chapter, see also Marmor *et al*., 2003). In sum, the left hemifield advantage observed for the ISF test mirrors the well known right hemisphere specialization in spatial vision, and the nasal field disadvantage may reflect the less stringent need to better resolve that part of the VF under monocular conditions.

The observed differences in VF performance suggest different ecological constraints and that distinct magnification factors should be applied for each spatiotemporal channel. Accordingly, when comparing CS for ISF and LSF custom tasks across regions of different eccentricities we have found that LSF (magno) sensitivities fall off less quickly with increasing eccentricity than their ISF (parvo) sensitivities (on the issue of corresponding parvo/magno anatomical naso-temporal asymmetries at the level of the retina and LGN see Dacey and Petersen, 1992 and Connolly and Van Essen, 1984, respectively).

As discussed above, the distinct CS's found for custom (LSF and ISF) test conditions suggest that the two types of stimulus paradigms used can provide different activation bias concerning P and M visual pathways. We speculate that ISF condition taps more the peripheral P pathway (at least compared to the magno-like LSF condition). The lower CS observed for the ISF task could possibly reflect the lower ganglion cell convergence within the P pathway (Perry and Cowey, 1985; Yamada *et al*., 2001). Accordingly, we have observed the expected higher CS at all eccentricities at high temporal frequencies imposed by our M-like LSF task conditions. Furthermore there is also evidence that LSF-like stimuli favor the M pathway (Derrington and Lennie, 1984; Lee *et al*., 1993; Maddess *et al*., 1999).

In conclusion, our findings shed new light on the role of low-level spatial vision on functional asymmetries in visual perception. Future studies should further elucidate the relative role of such functional anisotropies in different visual tasks and contexts.

Chapter 5

5. Asymmetry of visual sensory mechanisms:

Electrophysiological, structural and psychophysical evidences

5.1. Summary

Psychophysical visual field asymmetries are widely documented and have been attributed to anatomical anisotropies both at the retinal and cortical levels. This debate on whether such differences originate within the retina itself or are due to higher visual processing may be illuminated if concomitant anatomical, physiological, and psychophysical measures are taken in the same individuals. In the current study, we have focused on the study of objective functional and structural asymmetries at the retinal level and examined their putative correlation with visual performance asymmetries. Forty healthy participants (80 eyes; 13 male and 27 female subjects) were included in this study. Objective functional/structural asymmetries were probed using the multifocal electroretinogram (mfERG) technique and optical coherence tomography (OCT), respectively. A nasal/temporal pattern of asymmetry (nasal visual hemifield disadvantage) was found for all methods (retinal thickness, contrast sensitivity, and mfERG P1 amplitude). Furthermore, superior/inferior asymmetries could be documented only with psychophysics and structural measures. These patterns likely arise at different levels of the retina as inferred by partly independent correlation patterns.

We conclude that patterns of structural/functional asymmetries arise at different levels of visual processing with a strong retinal contribution.

5.2. Introduction

Spatial asymmetry in the neural density and population responses of visual neurons may lead to psychophysical spatial anisotropies. Even in normal subjects, visual spatial performance is indeed asymmetrical (Carrasco, Giordano, and McElree, 2004; Carrasco, Talgar, and Cameron, 2001; Silva *et al*., 2008). A wide range of tasks has proven to yield superior/inferior anisotropies (Altpeter, Mackeben, and Trauzettel-Klosinski, 2000; Edgar and Smith, 1990; He, Cavanagh, and Intrilligator, 1996; Levine and McAnany, 2005; McAnany and Levine, 2007; Previc, 1990), all suggesting better performance in the superior hemiretina (inferior VF) over the inferior hemiretina (superior VF). Although some of these performance differences have been attributed to cortical processing, functional retinal asymmetries could also be documented. Accordingly, Miyake, Shiroyama, Horiguchi, and Ota (1989) have demonstrated an asymmetry of the focal electroretinogram (ERG) in the human macular region, with disadvantage of the inferior retina. This asymmetry was also confirmed by Nagatomo, Nao-i, Mariuiwa, Arai, and Sawada (1998), using mfERG in normal subjects.

Nasal/temporal asymmetries have also been documented namely in hyperacuity tasks (Fahle and Schmid, 1988). We have previously documented a disadvantage of the temporal retina (nasal hemifield), using contrast sensitivity CS task, with gratings at 3.5 cycles per degree (cpd). This retinal anisotropy could be functionally separated from a right cortical hemispheric dominance pattern (Silva *et al*., 2008). Concerning objective electrophysiological data on naso/temporal asymmetries, early studies used focal cone ERGs (e.g., Miyake, 1990; Miyake *et al*., 1989). Interestingly, distinct patterns of nasal/temporal differences are found concerning the amplitude of focal and multifocal oscillatory potentials (OPs), such that OPs in the temporal retina are larger than those in the nasal retina (Bearse, Shimada, and Sutter, 2000; Fortune, Bearse, Cioffi, and Johnson, 2002; Miyake, 1990; Miyake *et al*., 1989; Rangaswamy, Hood, and Frishman, 2003; Wu and Sutter, 1995). This pattern is more conspicuous and opposite to the asymmetry observed for the P1 wave amplitude (see normative data in the studies of Kondo *et al*., 1996; Nagatomo *et al*., 1998; Parks *et al*., 1996). The study of Sutter and Tran (1992) was particularly revealing, since a nasal/temporal asymmetry was observed in all subjects with higher response densities in the nasal retina (temporal hemifield) within the central 23º outside the blind spot. The implicit time topography of mfERG has been less explored (see Parks *et al*., 1996, and Seeliger, Kretschmann, Apfelstedt-Sylla, and Zrenner, 1998, work in normal control groups).

It is unknown whether such differences originate within the retina itself or are due to higher visual processing. Some answers to this question have been suggested by studying the standing potential of the eye (Skrandies and Baier, 1986), which reflects the function of the retinal pigment epithelium and is also larger in the superior retina; or by the anatomical asymmetry of the human retina, since it is known for a long time that there is a higher density of ganglion cells in the superior retina (Croner and Kaplan, 1995; Curcio and Allen, 1990; for cone data, see Curcio, Sloan, Kalina, and Hendrickson, 1990). It is also known that, at equivalent eccentricities, cone density is higher in nasal compared to temporal retina (Curcio *et al*., 1990; Curcio, Sloan, Packer, Hendrickson, and Kalina, 1987; Jonas, Schneider, and Naumann, 1992), as well as for ganglion cells (Curcio and Allen, 1990).

Scarce data are available concerning direct comparison of relationships between local psychophysical and mfERG measures. Most studies have only examined eccentricity dependent psychophysical performance (Seiple and Holopigian, 1996; Seiple, Holopigian, Szlyk, and Wu, 2004; Virsu and Rovamo, 1979, see also references therein). Seiple *et al*. (2004) mapped acuity, CS, and temporal sensitivity in terms of retinal eccentricity and meridian but did not study specifically VF asymmetries. They also compared psychophysical data with local electrophysiological data and to Humphrey VF thresholds.

The focus of this study was to probe objective functional and structural asymmetries at the retinal level and examine their putative correlation with visual performance asymmetries. Visual CS was examined using intermediate spatial frequency (ISF) 3.5 cpd stimuli (Silva *et al*., 2008). In this study, we separated for the first time retinal and cortical mechanisms underlying psychophysical asymmetries of visual CS. Retinal function was objectively assessed by using the multifocal ERG (mfERG, Castelo-Branco et al., 2007; Hood, 2000; Lam, 2005; Sutter, 2001; Sutter and Tran, 1992) and thickness of neural layers by optical coherence tomography (Stratus OCT3) to probe whether superior and nasal quadrants were thickest (Castelo-Branco *et al*., 2007; Chan, Duker, Ko, Fujimoto, and Schuman, 2006) and correlated with psychophysical function.

5.3. Material and Methods

5.3.1. Participants

Forty healthy participants (80 eyes; 13 male, 27 female subjects) with mean age of 43 $\pm$ 16 years were included in this study. They were submitted to a complete ophthalmic examination, including best-corrected visual acuity (VA-Snellen chart), IOP measurement (Goldman applanation tonometer), slit lamp biomicroscopy and fundus examination (Goldman

lens). Central visual (macular) function was tested by mfERG and ISF test, and macular thickness was determined by OCT.

Exclusion criteria included the following: cataract or other eye disease that might interfere with fundus examination, retinal diseases, or optic nerve pathology, and high ammetropia (sphere dpt > 4 and cylinder dpt > 2). In this study all subjects were right-handed and naive to the purpose of the tests performed, and had normal best corrected visual acuity.

The study followed the tenets of the Declaration of Helsinki. Informed consent was obtained from each patient after procedures of the research had been fully explained.

5.3.2. Optical Coherence Tomography

Optical coherence tomography (OCT) is a high-resolution cross-sectional imaging technique that allows in vivo measurement of tissue thickness. We have used an OCT device (Stratus OCT 3, Carl Zeiss Meditec, Dublin, CA, USA) to obtain cross-sectional images centred in the macula (Brancato and Lumbroso, 2004; Castelo-Branco *et al*., 2007; Eriksson and Alm, 2009; Polito, Del Borrello, Isola, Zemella, and Bandello, 2005) with axial resolution ≤10 µm, transversal resolution of 20 µm, and 2 mm of longitudinal scan range.

The Fast Macular Thickness Protocol (FMTP) was used to obtain macular thickness measurements, which we will refer to retinal thickness (RT) measures. This measure does take into account only the neural layers of the retina. Using FMTP, 6-radial 6 mm in length line scans, 30º apart and of 128 A-scans each were obtained in 1.92 s. Stratus OCT 3 software calculates retinal thickness as the distance between the vitreoretinal interface and the junction between the inner and outer segments of the photoreceptors, which is just above the retinal pigment epithelium. In **Figure 5.1** we show the zones where RT was analyzed.

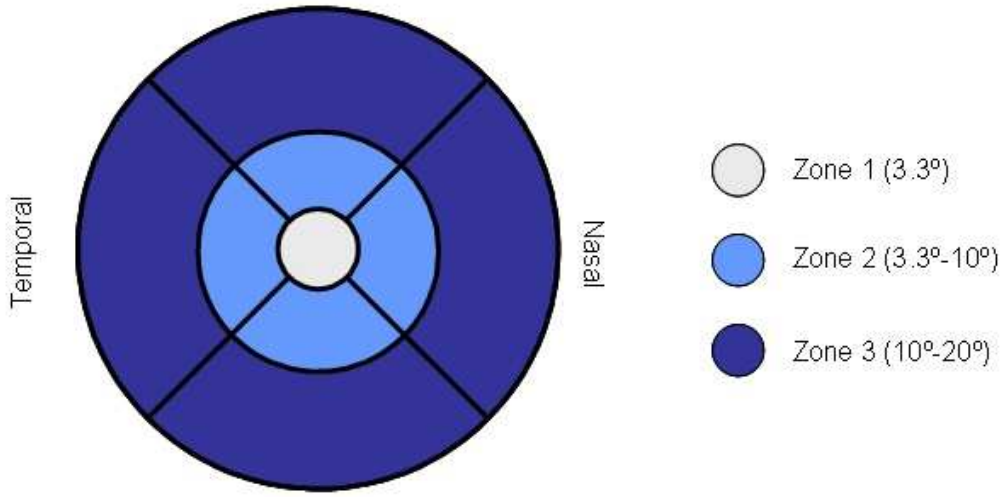

Figure 5.1. Layout of the OCT zones where RT was analyzed.

Three concentric circles with default diameters of 1 mm (3.3º), 3 mm (3.3º-10º) and 6 mm (10º-20º), were used to divide the macular thickness map into three zones: fovea (zone 1), inner macula (zone 2) and outer macula (zone 3), with the aim of verifying retinal morphometric asymmetries at different eccentricities (see **Figure 5.1** above).

5.3.3. Electrophysiological Recordings

We recorded mfERG with a RETIscan System (Roland Consult, Wiesbaden, Germany). The stimulus used in the mfERG consisted of 61 hexagons, covering a VF of up to 30º of radius and presented on a 20 inch monitor at a viewing distance of 33 cm. Maximum luminance was 120 cd/m^2. The hexagon areas increased with eccentricity in order to compensate for local differences in signal amplitude due to differences in cone density across the retina (leading to a fourfold change in hexagon area size). Each hexagon was temporally modulated between light and dark according to a binary m-sequence (frame rate: 60 Hz). Observers were instructed to fixate a small red cross in the centre of the stimulus. Fixation was continuously checked by means of online video-monitoring during the approximately 8 min recording sessions. To improve fixation stability, sessions were broken into 47 s segments and 8 trials were recorded in total. Signals were amplified with a gain of 100.000 and band-pass filtered (5-100 Hz).

We used DTL fiber electrodes (recording electrodes), after a light adaptation of 10 min and pupil dilation with tropicamide 1%. The reference and ground electrodes were attached to

the ipsilateral outer canthus and forehead, respectively. The surface electrode impedance was less than 10 kΩ. Refractive errors were corrected. Analyses were performed with the system software (RETIscan; Roland). First-order kernels were used for mfERG evaluation. First-order kernels were analyzed because of their closer correlation with the function of the outer retina and to avoid temporal adaptation mechanisms that are generally considered to influence higher-order kernel analyses (Hood, Seiple, Holopigian, and Greenstein, 1997). The local ERGs responses were normalized by the area of the stimulus delivery in order to obtain a density response (nV/deg^2). For analysis of mfERG data, the peak amplitude of P1 (defined as the difference between N1 and P1 amplitudes) of each hexagon was calculated.

Local 61 mfERG responses were also divided in five regional areas in order to evaluate these asymmetries at distinct eccentricities (see **Figure 5.2** and **appendix C**): zone 1 (4.4º diameter), zone 2 (4.4º-13.6º), zone 3 (13.6º-25.8º), zone 4 (25.8º-40.8º), and zone 5 (40.8º-58.7º).

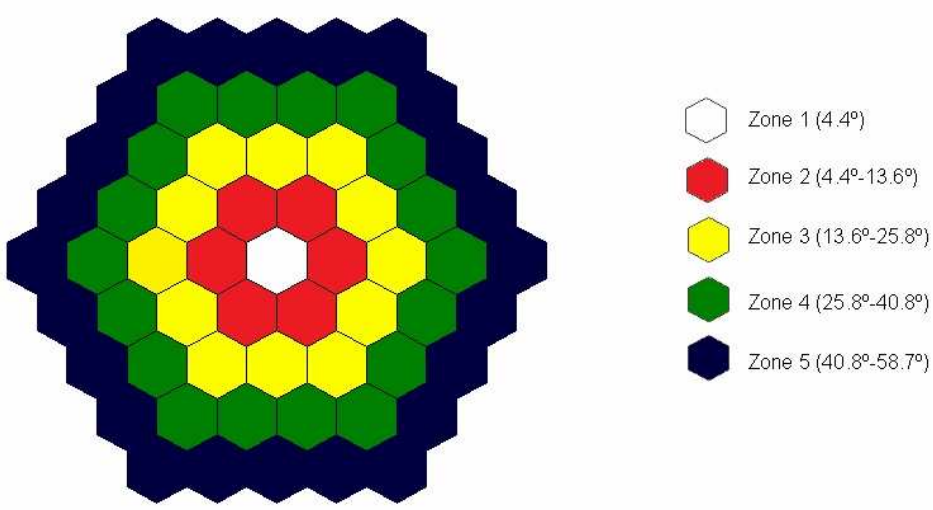

Figure 5.2. Layout of local stimulus hexagons and division in five analysis zones, according to eccentricity with Zone 1 being the central region.

To perform spatial asymmetries analysis, central region, blind spot region, and horizontal or vertical midline regions were excluded (for testing superior/inferior or nasal/temporal asymmetries, respectively), to prevent contribution of regions that are irrelevant to the concept of asymmetry or (in the case of the blind spot) may even lead to erroneous results (see **Figure 5.3**).

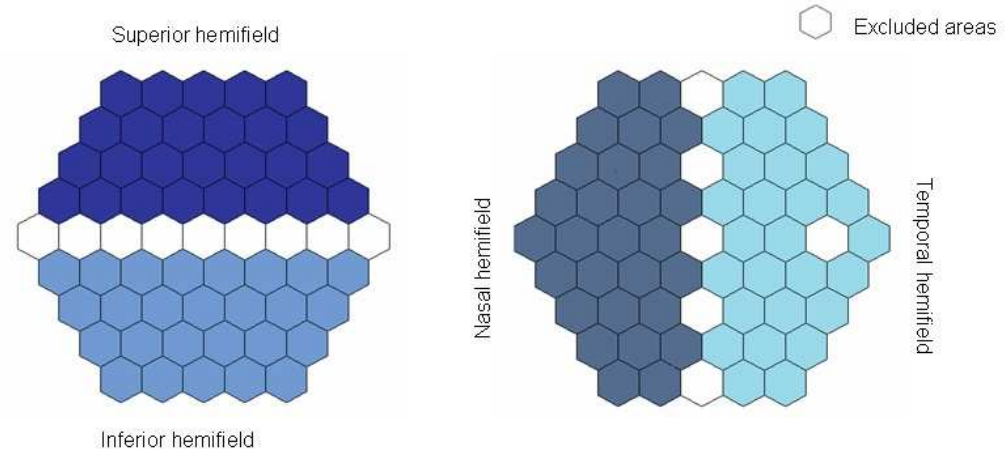

Figure 5.3. Scheme of analyzed asymmetries, white regions has been excluded from the analysis (see text).

5.3.4. Intermediate Spatial Frequency (ISF) Contrast Sensitivity Test

We have applied CS multiple interleaved staircase testing at multiple locations, where stimuli were patches of 3.5 cpd of vertically oriented sinusoidal gratings and 0 Hz temporal frequency (Maia-Lopes *et al*., 2008; Silva *et al*., 2005, 2008), displayed on a gamma corrected 21 inch Trinitron GDM-F520 Sony colour monitor (frame rate 100 Hz) with background luminance of 51 cd/m^2 and viewing distance of 36 cm. The details on implementation and calibration of this test can be found in Chapter 3. Results were expressed in terms of dB units, dB = 20 * log (1/c), with c = Michelson luminance contrast (%). This spatial testing procedure was performed monocularly, and both eyes were tested in all participants, the first eye being randomly chosen (since ocular dominance does not appear to affect VF test results, see Spry *et al*., 2002). Subjects were instructed to fixate a black square (1º x 1º) in the centre of the screen and report the presence of vertical "striped" targets (detection task) by means of a button press. Participant's reliability was evaluated by the inclusion of false positive and negative "catch trials", and all the results with false positive and false negative errors ≥ 33% were excluded, according to standard criteria (Caprioli, 1991; Clement, Goldberg, Healey, and Graham, 2009). Fixation loss was monitored with our custom eye-tracking methodology (CRS device) which provides detailed measurements of eye position.

In sum, CS was assessed independently for each random location (see all tested 9 locations in **Figure 5.4**). For analysis purposes, 3 zones were defined: Zone 1 (10º diameter of visual field); Zone 2 (10º- 20^o) and Zone 3 (20º- 40^o).

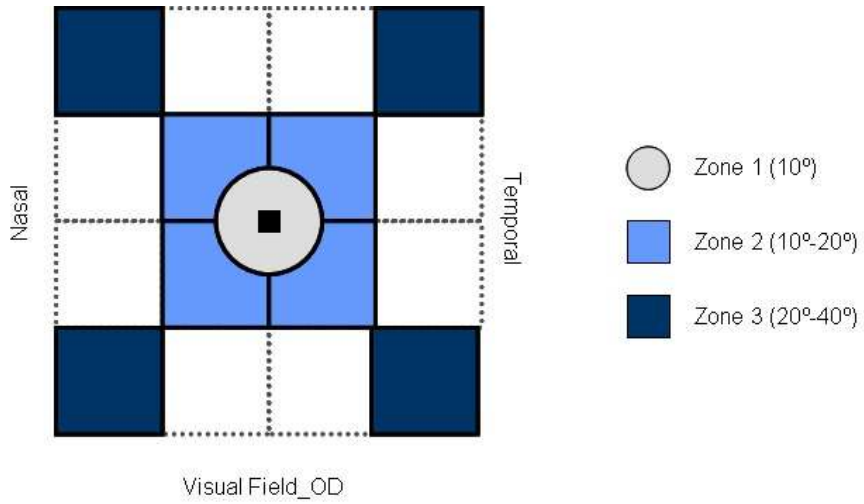

Figure 5.4. Basic scheme of the nine VF locations tested in our CS ISF task. Sinusoidal gratings were used as detection target stimuli (for details see Chapter 3 Methods section).

5.3.5. Statistical Analysis

Two analysis steps were conducted in this study. In the first step, visual spatial asymmetries of RT, CS, and P1 amplitude (using OCT3, ISF, and mfERG techniques, respectively) were independently assessed. It is important to note that all results from the left eye were converted into right eye (retina) format (orientation) for analysis. Asymmetries were analyzed using a multivariate approach for the 4 retinal hemifields, i.e., superior, inferior, nasal, and temporal. After verifying the normality assumption for the different parameters among the 4 hemifields (Kolmogorov–Smirnov test), an ANOVA repeated measures analysis was conducted using a Bonferroni correction for multiple comparisons. We have used a standard statistical measure of effect size, Cohen's d, in addition to % differences (Cohen, 1992).

In the second step the correlation between structural and functional parameters was assessed by the Pearson correlation coefficient. All statistical analysis was performed using the SPSS software version 16.0 (SPSS Inc., Chicago, IL, USA). Statistically significant results were considered at a cut-off *p*-value of 0.05.

5.4. Results

A naso/temporal asymmetry pattern was found for all studied outcome measures, with nasal hemifield disadvantage (see **Tables 5.1** and **5.2**). With respect to superior/inferior asymmetry, present only for the ISF-CS task and OCT measures. Mean RTs by area are shown in **Figure 5.5** for a representative individual and the global values (mean ± SEM) in **Tables 5.1 and 5.2**.

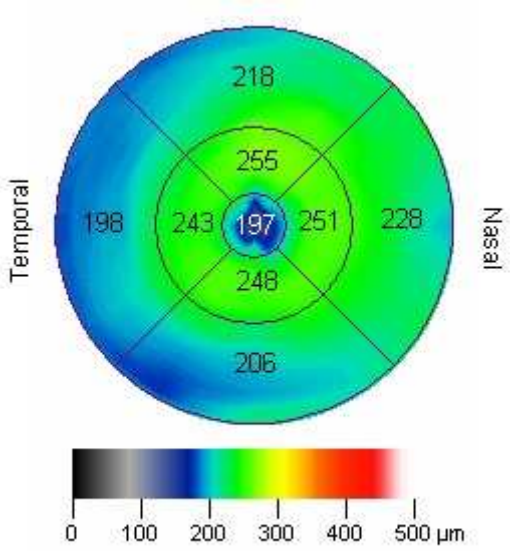

Figure 5.5. Retinal thickness map (µm) of a representative individual (OD) with strong nasal/ temporal and superior/ inferior asymmetries for all zones in terms of retina (colour-coded map: red, high value; black, low).

The analysis of structural retinal asymmetries (OCT measures) demonstrated significant naso/temporal and superior/inferior global asymmetries, with reduced thickness of temporal and inferior retina (nasal and superior VFs). These asymmetries were also present in Zones 2 and 3 (see **Tables 5.1** and **5.2**).

Table 5.1. Mean values of superior and inferior VF hemifields for RT (OCT), CS (ISF), P1 wave amplitude and implicit time (mfERG) per zones. Statistically significant results were considered for $p < 0.05$ (ANOVA repeated measures with Bonferroni correction).

Methods	**Zones**	**Superior VF** (Inferior R)	**Inferior VF** (Superior R)	***p value***
OCT (µm)	Global average	254.1 ± 1.5	261.0 ± 1.5	<0.0001
	Zone 2	274.8 ±1.7	281.1±1.7	<0.0001
	Zone 3	233.4±1.7	240.9±1.6	<0.0001
ISF (dB)	Global average	21.9 ± 0.6	23.2 ± 0.5	<0.0001
	Zone 2	26.4 ± 0.6	28.0 ± 0.6	<0.0001
	Zone 3	17.4 ± 0.6	18.5 ± 0.5	0.054
mfERG (nV/deg^2)	Global average	19.8 ± 0.4	19.6 ± 0.4	n.s.
	Zone 2	38.7 ± 0.8	39.1 ± 0.9	n.s.
	Zone 3	26.1 ± 0.6	26.7 ± 0.6	n.s.
	Zone 4	18.1 ± 0.5	17.3 ± 0.3	n.s.
	Zone 5	14.7 ± 0.4	14.4 ± 0.3	n.s.
mfERG(ms)	Global average	34.8 $\pm$ 0.14	35.4 $\pm$ 0.14	<0.0001
	Zone 2	36.1 $\pm$ 0.23	36.8 $\pm$ 0.25	n.s.
	Zone 3	34.9 $\pm$ 0.16	35.6 $\pm$ 0.15	<0.0001
	Zone 4	34.4 $\pm$ 0.15	35.1 $\pm$ 0.15	<0.0001
	Zone 5	34.8 $\pm$ 0.16	35.4 $\pm$ 0.17	<0.0001

Using mfERG, as expected we found the higher P1 amplitudes in the central ring (4.4º), with a mean value of 77.9 ± 2.0 nV/deg^2. The inter-individual variance in response density is greatest at the central fovea, reducing towards more peripheral locations. A naso/temporal asymmetry was found for global hemifield means, with vulnerability of temporal retina (i.e. in the nasal hemifeld, see **Table 5.2**).

This asymmetry was significant in zones 2 and 3 (13.6º and 25.8º), disappearing in the most eccentric ones (40.8º and 58.7º; see **Table 5.2**).

Table 5.2. Mean values of nasal and temporal VF hemifields for RT (OCT), CS (ISF), P1 wave amplitude and implicit time (mfERG) per zones. Statistically significant results were considered for $p < 0.05$ (ANOVA repeated measures with Bonferroni correction).

Methods	**Zones**	**Temporal VF** (Nasal R)	**Nasal VF** (Temporal R)	***p* value**
OCT (µm)	Global average	270.6 ± 1.6	243.9 ± 1.5	<0.0001
	Zone 2	280.0 ± 1.6	264.8 ± 1.5	<0.0001
	Zone 3	261.2 ± 1.9	223.0 ± 1.6	<0.0001
ISF (dB)	Global average	23.2 ± 0.5	21.9 ± 0.5	<0.0001
	Zone 2	27.5 ± 0.6	26.8 ± 0.6	*n.s.*
	Zone 3	18.9 ± 0.6	16.9 ± 0.5	<0.0001
mfERG (nV/deg^2)	Global average	20.7 ± 0.4	20.1 ± 0.4	0.003
	Zone 2	40.8 ± 0.9	38.9 ± 0.8	0.001
	Zone 3	26.6 ± 0.6	25.4 ± 0.5	0.002
	Zone 4	17.4 ± 0.4	17.9 ± 0.4	*n.s.*
	Zone 5	14.8 ± 0.3	14.4 ± 0.3	*n.s.*
mfERG (ms)	Global average	35.3 $\pm$ 0.14	35.2 $\pm$ 0.14	n.s.
	Zone 2	36.7 $\pm$ 0.19	36.7 $\pm$ 0.25	n.s.
	Zone 3	35.4 $\pm$ 0.15	35.4 $\pm$ 0.15	n.s.
	Zone 4	34.7 $\pm$ 0.15	34.8 $\pm$ 0.15	n.s.
	Zone 5	35.2 $\pm$ 0.17	35.0 $\pm$ 0.16	n.s.

In **Figure 5.6**, we show for the mfERG technique, a representative individual with nasal/temporal asymmetry for P1 amplitude. In terms of P1 implicit time, a superior/inferior asymmetry was found (except for Zone 2), with higher values in the superior retina (mean: 35.4 ± 0.2 ms) and no statistical difference between the nasal and temporal retinas.

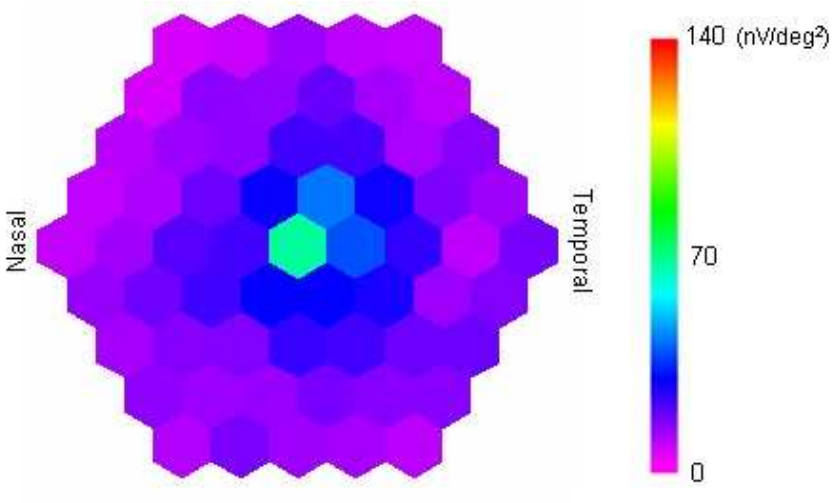

Figure 5.6. P1 wave amplitude map of mfERG (nV/deg^2) in terms of VF, obtained from a representative individual (OD). Note a significant nasal/temporal VF asymmetry specifically for Zones 2 and 3.

VF anisotropies were found also for CS testing, with temporal and inferior retinas presenting lower CS mean values (see **Tables 5.1**, **5.2** and also **Figure 5.7,** for a representative subject in terms of VF, where one can see reduction of the CS in nasal and superior hemifields).

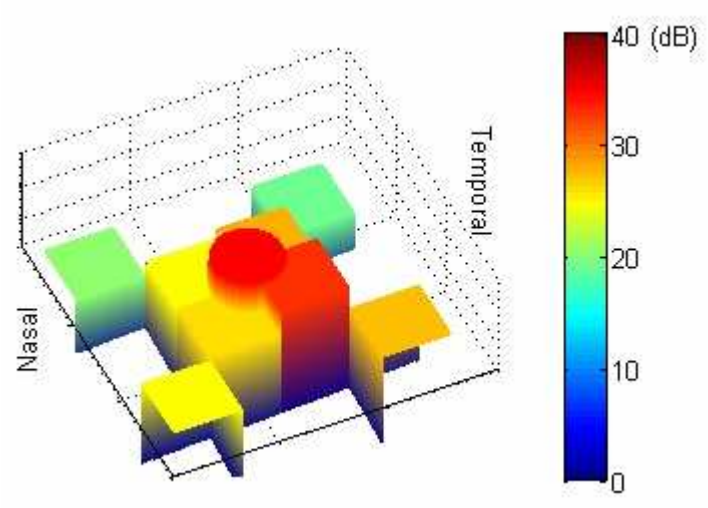

Figure 5.7. Representative CS map (OD) obtained using the ISF-CS test (in dB) in terms of VF coordinates. Dark blue regions correspond to areas of lower CS (the central region is red due to high CS value). In this task superior/inferior and nasal/temporal asymmetries are present in Zones 2 and 3.

5.4.1. Analysis of size effects

Analysis of effect sizes using both % differences and Cohen's *d* showed that OCT structural measures yielded large effects in particular for naso/temporal asymmetries, which is consistent with the notion that this type of asymmetry is generated in the retina (Cohen's *d* well above 1 - 2.1 and 3.6 for inner and outer naso/temporal asymmetries - which surpasses the 0.8 criterion for large effects). mfERG measures (which sample photoreceptor and bipolar cell populations) showed a moderate effect (Cohen's *d* of 0.42 and 0.44). Taken together these findings show that naso/temporal asymmetries have a retinal origin and dominate in the inner retina (ganglion cell level). These findings were corroborated using measures of % change, which confirmed that effects are stronger in the periphery (with 17% effect in terms of structural measures and 16% concerning psychophysical measures of naso/temporal asymmetry). These findings confirm the notion that behavioral performance is partly explained by retinal asymmetries in particular (but not exclusively) concerning inner retinal layers (which is confirmed by Cohen's *d* values above 0.5, for the CS task). Concerning inferior/superior asymmetries, Cohen´s measures were in the moderate range and effect sizes were percentually smaller concerning structural measures (~3%) that for psychophysical measures (~ 8 - 10%) suggesting that psychophysical up/down asymmetries has an additional significant cortical contribution.

5.4.2. Correlation Analysis

To further evaluate whether psychophysical and electrophysiological measurements conveyed independent information, we performed correlation analysis between functional ISF-CS and mfERG measures. Significant correlations were present between global values of CS and implicit time of the P1 component (r = -0.619, p < 0.0001). Pearson's analysis between corresponding areas revealed significant correlations (psychophysical ISF-CS measures and physiological mfERG implicit times), within inner pericentral zones, r = -0.537, p < 0.0001, and outer pericentral zones, r = -0.641, p < 0.0001. Correlations between CS and implicit time (P1) measures, in terms of hemifields for the corresponding areas, are shown in **Table 5.3**. A simultaneous representation of the corresponding zones for all methods used in this study can be found in **appendix C**.

Table 5.3. Correlation coefficients (*r*) between CS and implicit time of P1 measures per corresponding zone in visual hemifields, with the *p*-values in parenthesis.

Hemifields	Zone 2 (CS)– Zone 3(mfERG)	Zone 3 (CS)– Zone 4 (mfERG)
Superior	- 0.483 (p < 0.0001)	- 0.64 (p < 0.0001)
Inferior	- 0.388 (p = 0.0003)	- 0.496 (p < 0.0001)
Nasal	- 0.478 (p < 0.0001)	- 0.575 (p < 0.0001)
Temporal	- 0.451 (p < 0.0001)	- 0.603 (p < 0.0001)

As expected, the analysis between non-corresponding areas revealed only weak correlations. Between Zones 2 of both functional techniques, r = -0.232, p = 0.0377, while a moderate one was found between the Zones 3 (r = -0.467, p < 0.0001). Finally, no significant correlations were found between central areas (Zone 1) of both methods (ISF-CS and mfERG). We also performed correlation analysis between morphological data obtained by OCT and objective functional parameters of mfERG (P1 amplitude and implicit time). Only a weak correlation was found between RT measures and P1 amplitude for Zone 1 (r = -0.374, p = 0.001). The weak correlations between macular thickness (OCT) and physiological/behavioural measures may be due to the fact that they measure non-overlapping retinal components. In general, patterns of asymmetry likely arise at different levels of the retina as inferred by the observed partly independent correlation patterns (only part of the explained variance being common to all measures).

5.5. Discussion

Here we have demonstrated for the first time concomitant and partially correlated retinal asymmetries, identified by psychophysics, structural imaging and neurophysiology.

The specific relationship between behavioural, structural and physiological effects is well illustrated by the observed correlation patterns, which suggest that some of the behavioural effects have a retinal origin.

The extent into which these measures are related is also explained by which part of the retinal circuitry contributes to each measure. mfERG measures are mostly dominated by outer retina (photoreceptor and bipolar cell components) and showed the smallest contribution to the naso/temporal asymmetry effects. Psychophysical measures were accordingly better explained (but not exclusively) by the efferent output (inner part) of retina.

The notion that behavioural performance is partly explained by retinal asymmetries was jointly corroborated by correlation and effect size analyses.

Concerning inferior/superior asymmetries, effect size measures suggested that psychophysical up/down asymmetries have an additional significant cortical contribution. It is worth pointing out that nasal/ temporal asymmetries are inherently retinal and are dissociable from left/right cortical asymmetry patterns (see also Silva *et al*., 2008). The findings that naso/ temporal asymmetries have a retinal origin and dominate in the inner retina (ganglion cell level) are consistent with the notion that there are 300% more retinal ganglion cells in the nasal retina (Curcio and Allen, 1990). A contribution of retina mechanisms to psychophysical performance patterns was already observed before in patients (see also Castelo-Branco et al., 2007). Our findings are therefore consistent with the notion that cortical contributions are mostly relevant concerning left/right and up/down asymmetries (Connolly and Van Essen, 1984; Van Essen, Newsome, and Maunsell, 1984) but cannot explain nasal/temporal asymmetries (see also Silva *et al*., 2008).

This study does therefore provide further elucidation on the sensory contribution to the interplay between visual and attentional factors in the generation of functional asymmetries and visual performance fields (Carrasco, Giordano, and McElree, 2004).

Multidimensional mapping of structure and function of the healthy visual system is an important starting point for understanding the perceptual consequences of visual disease. Even a slight reduction in local contrast can have an adverse effect on reading performance, mobility, orientation, and other daily visual activities. Given the layout of the retina, with specific rod and cone distributions and different populations of bipolar and retinal ganglion cells, it is expectable that the spatial and temporal sensitivities of different parts of the retina are not uniform (Altpeter *et al*., 2000; Dacey and Petersen, 1992; Perry and Cowey, 1985; Silva *et al*., 2005, 2008; Thibos, Cheney, and Walsh, 1987). Our photopic CS testing conditions were validated in previous studies (Maia-Lopes *et al*., 2008; Silva *et al*., 2008) and yielded results consistent with anatomical studies of photoreceptors and ganglion cell distribution in the human retina. Concerning ganglion cell densities, they are higher in the superior retina as compared to the inferior part, as well as in the nasal retina as compared with the temporal counterpart (Croner and Kaplan, 1995; Curcio and Allen, 1990). These known anatomical facts are consistent with our results of ISF-CS, which showed a pattern of nasal/temporal asymmetry, significantly higher in the 20º – 40º eccentricity range, with lower CS in the temporal retina (nasal hemifield); as well as a superior/inferior asymmetry, with lower CS in the inferior retina (superior hemifield). In our previous work (Silva *et al*., 2008), similar naso/temporal patterns were found, although no superior/inferior asymmetry was present.

This difference may be explained by the fact that our sample is higher in the present study with increased statistical power (see also the results of Carrasco *et al*., 2004, 2001).

Anatomical anisotropies within the retina (Curcio *et al*., 1990) are also consistent with our own mfERG data. A nasal/temporal asymmetry was found for global means with disadvantage of the temporal retina (nasal hemifield). This asymmetry reflects the fact that cone density is 40 – 45 % higher in the nasal retina and suggests that asymmetric distribution of cone receptors in the retina is more remarkable near the fovea (Curcio, Sloan, and Meyers, 1989; Curcio *et al*., 1990; Osterberg, 1935). In addition, the topography of ERG responses (photopic luminance response) found in Sutter and Tran's (1992) study shares all these expected properties based on the known density of retinal cones.

Finally, our structural data confirmed the predictions of previous anatomical studies (Curcio and Allen, 1990; Curcio *et al*., 1990; Dacey, 1993; Drasdo, Millican, Katholi, and Curcio, 2007; see also Chan *et al*., 2006; Hee *et al*., 1995). An outstanding question in our study was whether there was any significant structure-function correlation between the concomitantly measured variables. Our analysis showed that these measures shared common variance but also diverged to some extent, suggesting that patterns of asymmetry likely arise at different levels of the retina and even of the cortex, as revealed by the partly unexplained variance observed in the case of psychophysical measures.

It is however worth pointing out that central mechanisms are also important as determined by comparing naso/temporal versus left/right performance patterns (Silva *et al*., 2008) and from functional imaging studies of cortical retinotopic anisotropies (Liu, Heeger and Carrasco, 2006). This is important in particular in which concerns up/down patterns of asymmetry. Anatomical asymmetry patterns in the LGN (Connolly and Van Essen, 1984) and cortex (Van Essen, Newsome, and Maunsell, 1984) provide important evidence for the additional role of central structures.

Finally, it is important to point out that distinct temporal dynamics at different locations of the VF (temporal performance fields, Carrasco, Giordano, and McElree, 2004) may combine with the spatial psychophysical patterns described here.

5.6. Conclusion

In conclusion, functional asymmetries can be concomitantly documented at multiple levels of the human visual system, within a significant retinal contribution, as assessed by comparison of psychophysical, electrophysiological, and structural measures. Our results are consistent with the different anatomical anisotropies in terms of cone and ganglion cell densities and suggest an inner retinal dominance in terms of the origin of naso/temporal asymmetries and a dual retinal and cortical contribution to up/down asymmetries. The results of this study are relevant for the design of psychophysical paradigms and development of clinical training programs, such as the case of patients with heterogeneous VF loss and who need reuse the most functional parts of their retina.

Chapter 6

6. Independent patterns of damage across retinocortical pathways in Parkinson's disease

6.1. Summary

Sensory deficits have been documented in PD, in particular within the visual domain. However, visual ageing factors related to the brain and to neural and non-neural ocular structures should also be taken into account, which has often not been the case in previous studies.

This study addressed visual impairment attributable to the M (luminance), P (red-green) and K (blue-yellow) pathways in a population of PD patients. To avoid potential age-related confounding factors, all subjects underwent a full neurophthalmological assessment which led to exclusion of subjects with increased intraocular pressure, diabetes, even in the absence of retinopathy, and ocular abnormalities (from a total of 72 patients eyes, 12 were excluded). Both P and K pathways were studied by means of CS measurements along protan, deutan and tritan axes and also by fitting chromatic discrimination ellipses using eight measured contrast axes. M function was assessed, using stimuli that induce a FD illusion, in 17 locations in the fovea and periphery. Achromatic (luminance modulation) thresholds were significantly higher in PD, both in foveal and peripheral locations. A significant impairment was observed along protan and deutan axes, but only marginally along the tritan axis. These results were corroborated by a significant elongation of chromatic discrimination ellipses in our PD group.

Correlation analysis showed that achromatic and chromatic CS measures were independent, which implies that multiple visual pathways are affected independently in PD. M impairment was significantly correlated with age and disease stage, in contrast to the measured chromatic deficits. We conclude that in PD, independent damage occurs in low-level M and P pathways. Furthermore, traditional K probing strategies in PD may be confounded by ageing factors. This may reconcile the previously reported controversial findings concerning chromatic impairment in PD.

6.2. Introduction

Among the non-motor effects of the idiopathic PD, visual aspects are still not well understood. The nature of previously described visual deficits in PD has been questioned mainly on the ground that the reported deficits do not reflect a sensory deficit, but rather confounding cognitive factors (Crucian and Okun, 2003; Geldmacher, 2003). Moreover, many previous studies have probed chromatic and luminance contrast sensitivity (CS) using clinical semi-quantitative tests, such as the Lanthony D-15, FM 100-test, Pelli-Robson test charts and Vistech tables (Regan and Maxner, 1987; Buttner *et al*., 1995; Pieri *et al*., 2000; Diederich *et al*., 2002).

One should emphasize the methodological importance of measuring CS with quantitative psychophysical methods in PD (Bodis-Wollner *et al*., 1987; Bodis-Wollner and Regan, 1991; Harris 1998; Regan *et al*., 1998; Bodis-Wollner, 2003). Indeed, most of the clinical tests are more prone to artefacts and do not allow for extraction of subject reliability parameters, thereby providing limited quantification power. In fact, Regan *et al*. (1994) have previously compared computerized approaches with the current clinical tests. In general, clinical tests, such as FM 100-test or D-15 test are much less sensitive and less reproducible in comparison with techniques that allow for very fine contrast adjustments using randomly interleaved staircases (Regan *et al*., 1994; Castelo-Branco *et al*., 2004, 2006, 2009; Campos *et al*., 2005). Roth and Lanthony (1999) provide a good description of the limitations of FM 100-test, where 30% changes in test-retest could occur, which was confirmed by Birch *et al*. (1998). Reeves *et al*. (1989) have also documented that a difference in global score would only be significant if the difference is > 50. This led Roth and Lanthony (1999) to conclude that the FM 100-test is just a semi-quantitative evaluation test. Accordingly, it has been postulated that commonly used clinical colour tests are not suitable for the early detection or monitoring of treatments in PD (Birch *et al*., 1998). Furthermore, it is also important to use psychophysical tests that do not rely on higher level visuospatial abilities, such as orientation discrimination (Regan and Maxner, 1987; Bulens *et al*., 1988).

In addition, ageing factors related to the brain, and also to the retina and other ocular structures (Wyszecki and Stiles, 1982; Pokorny *et al*., 1987; Werner *et al*., 1990; Packer and Williams, 2003), might explain some of the previously described results, in particular the widely reported deficits in the K pathway (for a review see Haug *et al*., 1994, 1995; Harris 1998; Pieri *et al*., 2000; Birch *et al*., 1998; Regan *et al*., 1998). Common age-related and progressive ocular diseases in older adults, such as cataract, age-related maculopathy, glaucoma and diabetic retinopathy, are often associated with sensory deficits (Jackson and Owsley, 2003; Castelo-Branco *et al*., 2004; for a comprehensive review of the older literature see Roth and Lanthony, 1999). To account for these methodological problems, we have used age-matched controls (eliminating ageing as a between-group confound) and both groups underwent the same type of careful ophthalmological examination, with exactly the same conservative exclusion criteria (e.g. diabetes in pre-retinopathy stage, ocular hypertension in pre-glaucomatous stage, fundus signs of age-related macular degeneration). It should also be understood that age-matching is not a sufficient measure to prevent confounding from age related diseases, and should be complemented with strict exclusion criteria, to prevent that control subjects with subclinical disorders, typical of a particular age group are included. These disorders may lead to achromatic and chromatic deficits that are completely unrelated to PD. In sum, our methodological procedure helped to highlight the marked difference between normal ageing and PD in terms of retinal function.

In spite of such potentially confounding factors, there is strong previous evidence that spatiotemporal CS deficits do occur in PD (Bodis-Wollner and Yahr, 1978; Marx *et al*., 1986; Skrandies and Gottlob, 1986; Bodis-Wollner *et al*., 1987; Regan and Maxner, 1987; Mestre *et al*., 1990a, b; Bodis-Wollner and Regan, 1991; Harris *et al*., 1992; Delalande *et al*., 1996; Mestre *et al*., 1996; Tebartz van Elst *et al*., 1997; for reviews see Bodis-Wollner, 1990, 2003; Harris 1998; Langheinrich *et al*., 2000; Pieri *et al*., 2000; Diederich *et al*., 2002).

The purpose of this study was to analyse visual performance in PD within multiple visual channels, both in the fovea and the periphery, using computerized psychophysical tests that access the function of visual pathways in an independent manner. No clear-cut efforts for separation of different retinocortical pathways had been attempted prior to this work. Our novel strategy allows for the analysis and comparison of relative patterns of damage within M, P and K pathways in PD. To study chromatic CS performance, we adopted a new methodological approach, based on work of Regan *et al*. (1994), using randomly interleaved psychophysical staircases with spatial and luminance noise (see Castelo-Branco *et al*., 2004; Campos *et al*., 2005). Stimulus parameters were adjusted along colour modulation axes in order to separate dysfunction within P and K systems. This strategy allowed independent and non-biased assessment of the relative damage of these pathways and relied only on chromatic properties

and not on spatiotemporal criteria. This choice was based on neurophysiological and lesion studies in primates, which show that chromatic criteria are by far the best to provide isolation (Lee, 1996). Indeed, isolation based on spatial vision often fails, and vernier acuity may be preserved even after destruction of P cells, suggesting incomplete isolation of the P mechanism in this case (Lynch *et al*., 1992). This led us to choose chromatic properties as the isolating criteria.

To probe the M pathway at early retinotopic levels we applied a CS task that uses a sinusoidal grating stimulus at high temporal and low spatial frequency as the probing stimulus. This spatiotemporal profile of the stimulus is, in general, appropriate to activate the M pathway but may not be sufficient to isolate its function, unless one uses stimulus parameters such that an illusory duplication of number of stripes is perceived (Kelly, 1981). This frequency-doubling (FD) illusion reflects a non-linearity that resembles the response properties of the M/Y system (Shapley and Victor, 1980). Between 5 and 20% of LGN M cells respond with this non-linear Y-type response (Kaplan and Shapley, 1982; Derrington and Lennie, 1984; Purpura *et al*., 1988, 1990). Neurophysiological evidence has also shown that these stimuli differentially activate M neurons (Derrington and Lennie, 1984; Merigan and Maunsell, 1993; Lee, 1996). Given the low percentage (low functional redundancy) of responding M/Y neurons, this approach provides functional isolation and improves the likelihood of detecting early level impairment due to reduced compensation by redundancy mechanisms. The value of FD stimuli to assess retinotopic M damage as early as the retina stage has already been applied in glaucoma, because large retinal ganglion cell fibres (most of which are of M origin) are preferentially affected in this disease (Quigley *et al*., 1987, 1988; Maddess and Henry, 1992; Glovinsky *et al*., 1993; Merigan and Maunsell, 1993; Johnson and Samuels, 1997; Maddess *et al*., 1999; Cello *et al*., 2000; Landers *et al*., 2000; Trible *et al*., 2000; Paczka *et al*., 2001; Shabana *et al*., 2003; McKendrick *et al*., 2003, 2004, 2007; Clement *et al*., 2009). Based on this evidence, we adopted the FD paradigm to study early M function in PD.

In our study, we have obtained multiple test measures for distinct pathways: 17 achromatic test thresholds were obtained in independent locations, 3 chromatic test thresholds were obtained along cone-isolating axes in colour space and eight chromatic colour test thresholds were still obtained along eight additional axes in colour space, to provide measures unbiased to cone spaces. This allowed for testing multiple visual processing pathways, using up to 28 distinct threshold measurements for each subject. It is also noteworthy to point out that all of these measures were obtained in a random, interleaved manner, which allowed for simultaneous comparisons across visual mechanisms. Furthermore, it was possible to extract reliability criteria, such as false positives and false negatives.

6.3. Methods

6.3.1. Patient selection and classification

All PD patients were recruited from the Neurology Department of Coimbra University Hospital. Control subjects were patients' spouses, age-matched staff, or relatives, with normal or corrected to normal refraction. Informed consent was obtained from all participants, and the study was conducted in accordance with the tenets of the Declaration of Helsinki, and approval of the procedures by our local ethics committee. Neurological examination was performed in the Neurology Department. Dementia was excluded by analysis of MMSE scores (Portuguese adapted version by Guerreiro *et al*., 1994 following Folstein *et al*., 1975) and clinical interview. For exclusion of depression, the Hamilton Depression Rating Scale 17 (cut-off 14) was used. A total of 36 PD patients were included in our study.

Both groups underwent full ophthalmological examination, which consisted of best-corrected visual acuity (VA; Snellen chart), slit lamp examination of anterior chamber, IOP measurement (Goldman applanation tonometer), angle and fundus examination (Goldman lens), cataract grading by the Lens Opacities Classification System II (LOCS II) and the assessment of subjective visual complaints. The following exclusion criteria were applied: neurological/psychiatric conditions other than PD, fundus signs of age-related macular degeneration, diabetes, even in the absence of retinopathy, increased intraocular pressure, even in the absence of glaucoma, congenital colour vision disorders, VA < 0.6 , high ammetropy (sphere dpt > 4 and cylinder dpt > 2), cataract (LOCS ≥ 2) and other ophthalmological diseases. We excluded 6 PD patients (3 with diabetes in absence of retinopathy, 2 with glaucoma and 1 patient with high ocular hypertension).

PD patients were classified in Stages [1 to 3] of the modified Hoehn and Yahr (H & Y) clinical scale [1.9 ± 0.5 (mean ± SD) for both eligible subsets of chromatic and achromatic testing]. The motor Unified Parkinson's Disease Rating Scale (UPDRS) was also applied [UPDRS motor score, 25.0 ± 8.4 (chromatic testing) and 23.9 ± 9.3 (achromatic testing)].

6.3.2. Participants

The final subset (n = 30) of PD patients (14 male and 16 female) had a mean illness duration of 4.6 ± 3.0 years. Concerning chromatic assessment, participant's distribution was as follows: Control subjects (n = 32; 13 male, 19 female) with mean age of 57.9 ± 7.6 years and PD subjects with mean age of 61.1 ± 10.4 years. For achromatic CS testing: Control subjects

(n = 21; 13 male and 8 female), mean age of 58.5 ± 9.5 years; PD subjects (n= 24; 11 male and 13 female), mean age of 60.0 ± 10.8 years.

Our patient and control populations had age and gender distributions that were not significantly different under all testing procedures (ANOVA, non-significant (ns)). Mean education level was similar across groups and was not significantly correlated with sensory performance. Ten PD patients were newly diagnosed and were tested free from therapy. The others were receiving conventional levodopa therapy (mean dose of L-dopa: 544 ± 238 mg daily; other agonists: 7 patients with bromocriptine, 7.5 mg; 6 patients with ropinirole, 3.5 ± 0.84 mg). The medicated patients were all tested best-on state.

6.3.3. Statistical analysis

Mann-Whitney U-tests were used to compare chromatic and achromatic (luminance modulation) performance between the two groups (Control and PD), given the lack of data homoscedascity. Statistical independence was analysed using standard correlation methods (Han *et al*., 2004). If two measures are statistically uncorrelated (using appropriate testing criteria) they must have a different neural source or mechanism, as explained and explored by Han *et al*. (2004). It is important to note that partial correlation models are essential if multiple parameters show correlations that are significantly different from 0, as applied in Castelo-Branco *et al*., 2004 and Campos *et al*., 2005 studies. Independence was measured in terms of cross-sectional performance and not in terms of time course. Given the data distribution, we used Spearman rank correlations (Siegel and Castellan, 1988).

6.3.4. Psychophysical techniques to address the function of parvo- and koniocellular pathways

We have probed the P and K pathways in PD with an alternative psychophysical strategy based on the version of the computer controlled psychophysical method developed by Regan et al. (1994) and taken from the Cambridge Colour Test (CCT) a commercially available test [Cambridge Research Systems (CRS), Rochester, UK]; which we will refer to by modified CCT and has two different protocols: the Trivector and the Ellipse test. The Trivector test presents a rapid testing procedure in which three thresholds are obtained, respectively in a protan, a deutan and a tritan line, and is used for a rapid screening (**Figure 6.1**). The Ellipses test which is a longer testing procedure in which 3 MacAdam ellipses are determined, either along a tritan or along a deutan-protan line. Since CCT is a computerized test, its construction allows easy

change in stimulus parameters and permits threshold determination of the discrimination between any pair of target and background hues. Both tests use a luminance noise strategy that forces the subject to rely exclusively on colour cues to identify the position of a gap in a Landolt-like C-shaped ring (see **Figure 6.1, right inset**; gap size: 1.6º, outer diameter: 7.6º, inner diameter: 3.81º, viewing distance: 1.8 m).

Implementation and calibration procedures were performed with software and hardware provided by CRS (Minolta colorimeter; calibration software and CRS/VSG 2/5 graphics card with 15-bit contrast resolution per pixel). Stimuli were displayed on a 21 inch monitor (GDM-F520; Sony, Tokyo, Japan) that was gamma-corrected. As in the Ishihara test, both the target (visual stimuli) and the background (stimulus patches) were made up of small disks of variable size and luminance.

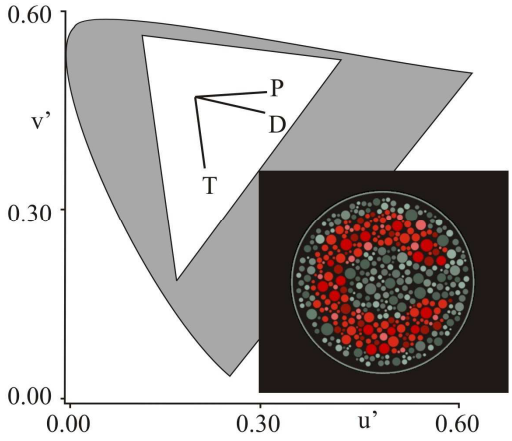

Figure 6.1. Right inset: Schematic illustration of the luminance noise stimulus. The Landolt C shape is visible due to the presence of high chromatic contrast in this image. **Left Graph** depicts axes (confusion lines in CIE 1976 u´ v´ colour space) along which colour contrast is modulated, in order to study cone function human subjects. P, protan; D, Deutan and T, Tritan axes (corresponding to L, M and S cones).

The background chromaticity was fixed while the colour of the target was varied in order to determine a discrimination threshold (see below). Luminance and size variation of stimulus patches (see **Figure 6.1**, right inset) forced the subject to use specific colour cues, since he/she could not use spatial or luminance cues to infer the embedded shape. These patches were randomly assigned six different luminance noise levels (8, 10, 12, 14, 16 and 18 cd/m^2; see also right inset in **Figure 6.1**, which illustrates the patches in different shades of grey). Neutral background coordinates (CIE 1976 *u´, v´* coordinates are shown, respectively): 0.197, 0.469; minimum excursion: 0.002 unit's *u´ v´* was superimposed on the noise levels, to define

the chromatic shape; protan confusion (copunctal) point: 0.678, 0.501; deutan confusion (copunctal) point: -1.217, 0.782; and tritan confusion (copunctal) point: 0.257, 0.0. Maximum excursion for trivector test: 0.1100 units (**Figure 6.1**, left Graph). We performed the 8-vector ellipses test version, only for one ellipse centred on the neutral background (white point of the test), along the tritanopic confusion line: 0.197, 0.469 u´v´ units. The ellipses fitting method which was developed by Regan et al. (1994), produces an ellipse that is centred on the neutral background; and is obtained by minimizing the sum of squares of the log distances between the ellipse and the fitted point, which is a geometric solution for producing discrimination ellipses.

The PD population of this study was probed monocularly for chromatic pathways (n = 30 patients PD eyes; n = 33 age-matched control eyes). The tested eye was chosen in a random manner. All participants viewed with refraction corrected for viewing distance, when necessary. The viewing conditions were such that the macular area of the retina was the one that subserved chromatic comparisons.

To further emphasize accuracy versus speed in the measurement of psychophysical responses, all participants were instructed that they had up to 20 s to report their decision. Also given the subjects' average age, and to exclude confounding factors such as motor errors, the experimenter recorded subjects' oral responses (indicating one out of four possible gap positions of the C ring stimulus: bottom, top, left and right) using a 4-button response box (CRS). A complete session would last around 40 min per eye, with 10 min (time out of 20 s) for the Trivector test and 30 min for the 8-vector ellipse determination. This technique of assessment of colour discrimination is easy to perform and reproducible in different setups. We developed our own normative database for the modified CCT test and excluded all normal subjects, with trivector discrimation thresholds above the CCT manual limits of 100 x 10^{-4} *u´v´* units for the protan and deutan lines and of 150 x 10^{-4} *u´v´* units for the tritan line. The "ellipse" test for normal subjects yields small discrimination ellipses, without a large axis ratio: the latter will typically be less than 2.0.

Chromatic performance along the classical cone axes (protan, deutan and tritan confusion vectors) was explored first by the Trivector test followed by the Ellipse test. One of the major methodological innovations of our study was that by using chromatic discrimination ellipses (measured in eight evenly spaced directions) we were able to avoid the sampling bias that is inherent to any procedure that only measures along one or two axes along cone spaces. We found no significant worsening of performance (no fatigue) or learning effects when PD patients moved from the trivector version of the test to the ellipse method. This strategy allowed testing all colour axes simultaneously, which makes comparisons concerning relative damage of chromatic pathways more reliable. This strategy has also been applied

successfully in early glaucoma (Castelo-Branco *et al.*, 2004). The chromaticity of the Landolt C shape was adjusted according to a staircase procedure. On each axis, the separation between the background and target chromaticities was initially large, and was decreased after each correct response on that axis and increased after each error. Since the tests were measuring multiple colour axes randomly (independent interleaved staircases), and since there was no fixed order, attentional biases could be prevented. The test terminated after 11 reversals of each of the three individual staircases; and the mean of the last seven reversals was taken as the threshold estimate for a given confusion line. The step size is computed in units of the CIE 1976 uniform chromaticity space and is a function of the number of reversals completed, and of the separation of test and background chromaticities. Small subsets of trials, randomly intermixed with the test trials, were used as control trials to detect malingering and to provide the subject clear cases when he or she is near threshold. The results are called confusion vector lengths and expressed in 10^{-4} *u´v´* units of 1976 CIE colour space. In the Ellipses test, "areas of colour confusion" (discrimination ellipses) were determined; see **Figure 6.2**, which allows evaluating damage along areas of impairment instead of axes of damage. Larger ellipses correspond to increased colour "confusion area" and impaired performance.

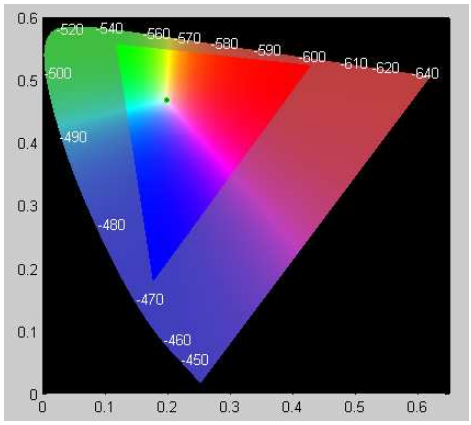

Figure 6.2. Chromatic discrimination ellipse (raw discrimination vectors and fitted ellipses) taken from a control subject. Colour rendering (which is only approximate in the printed version) is based on the sRGB (IEC1996 2.1) standard; the white point set to the white point of the test and the monitor gamut set to the gamut of our SONY GDM-F520 monitor equipped with Trinitron phosphors. Parameters extracted from fitted ellipse of the representative control: Ellipse Length: 0.0082 Axis ratio: 1.244 Angle: 50.1.

Our four alternative spatial forced-choice (4-AFC) procedure allowed the extraction of the following quantitative parameters: confusion vector length, ellipse length, axis ratio and angle. The ellipse length (long diameter) helps in quantifying the magnitude of chromatic CS deficit and varies inversely with performance while the axis ratio (ratio of long and short diameters) estimates the specificity of damage and the angle provides an indication of the most affected type of chromatic pathway (red-green or blue-yellow paths). Unlike other colour tests such as Lanthony D-15 (Hovis *et al*., 2004) and FM 100-test, the CCT thresholds are not affected by binocularity, eye dominance or learning (Costa *et al*., 2006).

In most cases, the chromatic function is evaluated with the ellipse test in a neutral background, but it is also possible to perform it in colour saturated environment (that is under red, blue or green background). When the individual is subject to a red background, blue, or green, the respective cones adapt to or enter into fatigue. In this study a parallel set of adaptation experiments under saturated blue background (x = 0.02530 and y = 0.1920, CIE 1931) were further performed in 8 PD patients.

6.3.5. Psychophysical technique to address the function of the M pathway

The spatiotemporal profile of the sinusoidal grating FD stimulus was optimized to activate the M pathway (Mendes *et al*., 2005; Castelo-Branco *et al*., 2006) and assessed with a custom-based approach. FD stimuli were generated directly from CRS/VSG 2/5 graphics card (with 15-bit contrast resolution per pixel) using CRS object animation library, this is the best possible method to avoid flicker (see McKendrick *et al*., 2003; *Silva et al*., 2004). Stimuli were displayed on a gamma corrected 21 inch colour Trinitron GDM-F520 monitor (frame rate, 100 Hz). Each stimulus was a 10º x 10º patch of 0.25 cpd sinusoidal grating vertically oriented, undergoing 25 Hz counter phase flicker. Mean background luminance was 61.7 cd/m^2. Stimuli were randomly presented within 17 localizations to mimic as closely as possible the standard strategy of Humphrey FDT C-20, which includes the central foveomacular 5º (radius) region of the VF and a distinct outer peripheral VF region (> 5º to 20º). Luminance contrast threshold was expressed according to the Michelson formula and obtained by adaptive logarithmic staircase strategy from CRS object animation library. The value to be used for a given trial was calculated using the previous trials value plus or minus the step size in dB. The initial step size used was 3 dB. Staircases were run for a total of four reversals, with the contrast at the final two reversals being averaged to obtain the threshold estimate. FD perimetry was done under monocular conditions (an opaque black patch was used to occlude the non-tested eye) for both eyes in 21 PD patients and in 24 age-matched controls. The first eye tested was chosen in a random manner. We did not find any significant differences in performance between the two

eyes, and we therefore pooled these data. Subjects were instructed to fixate the black square (1º x 1º) in the center of the screen and report the presence of ‘‘striped’’ targets and the experimenter converted the subjects’ oral response into a button response (4-button CRS box). Subjects wore, when necessary, a correction appropriate for the 36 cm viewing distance. Participants reliability was evaluated by intermittently including false positive (FP) and negative (FN) “catch trials” and we excluded all results with FP and FN errors ≥ 33%.

6.4. Results

6.4.1. Retinal assessment of parvo- and koniocellular damage

Representative examples of chromatic discrimination ellipses are shown in **Figure 6.3**, both for control and PD patients in different stages of the motor UPDRS and the modified H&Y clinical scale. In order to isolate relative damage of different chromatic pathways we measured contrast thresholds not only along the three main colour axes (protan, deutan and tritan) that isolate cone function, but also along eight evenly oriented vectors that define discrimination ellipses. This novel approach in PD allows to fit chromatic *confusion areas* (ellipses, which represent regions in colour space that look perceptually identical to the subject) to individual data, and to estimate in an unbiased way relative damage across chromatic channels. Inspection of the plots in **Figure 6.3** clearly shows that there is not a fixed axis of impairment, and that multiples axis can be found. The measured length and orientation of ellipses axes can be used to compare damage along K (blue-yellow opponent channel) and P pathways (red-green opponent channel). It is worth emphasizing that ellipses have variable length and orientation in the PD examples, suggesting evidence for heterogeneous patterns of damage. This was further confirmed by testing homogeneity of variances in the PD group.

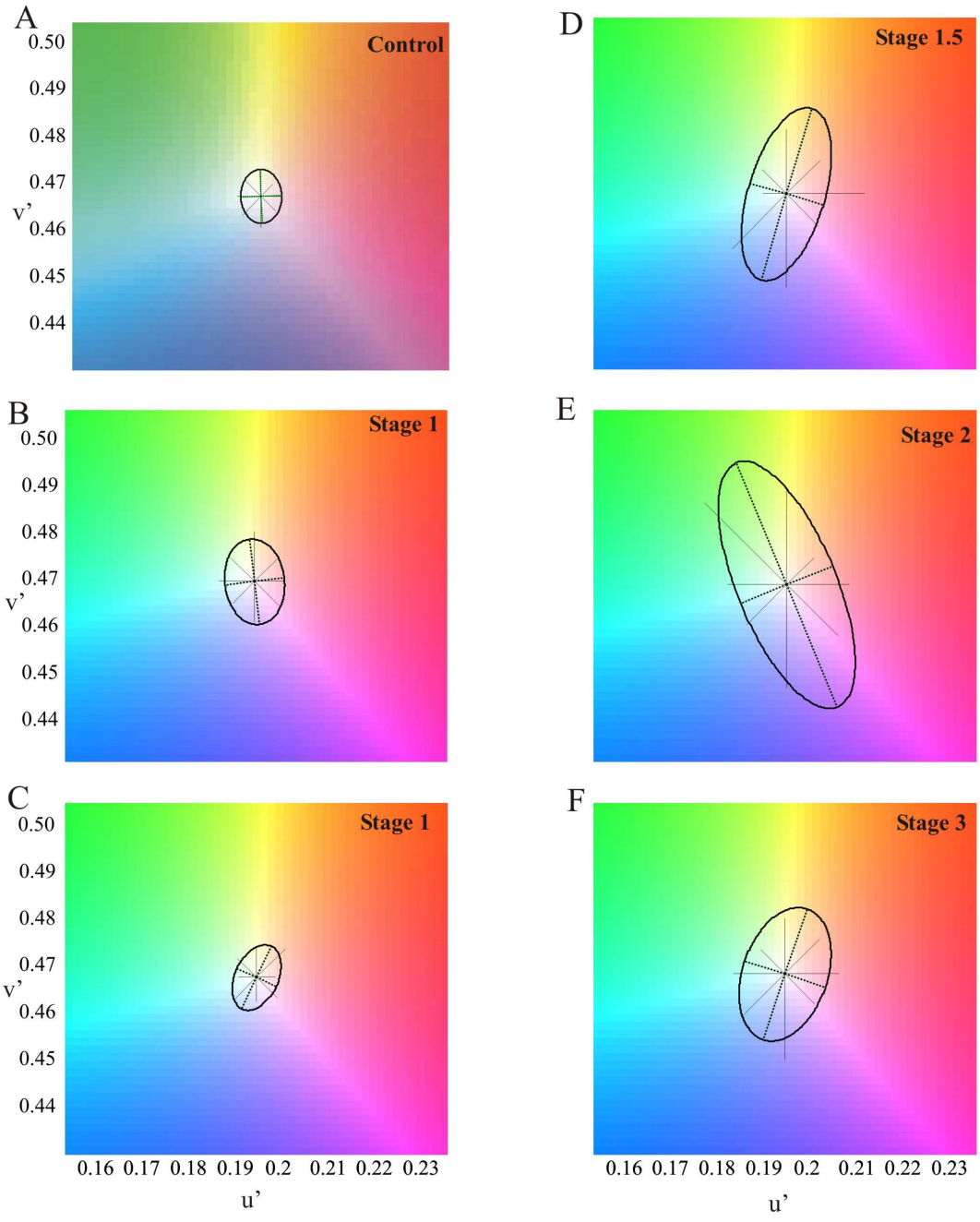

Figure 6.3. Representative examples of chromatic discrimination ellipses (raw discrimination vectors and fitted ellipses) in PD, over Stages 1 to 3 of the modified H&Y clinical scale (motor UPDRS: **B**, 11; **C**, 13; **D**, 18; **E**, 28; **F**, 40). Solid straight lines: 8 measured colour vectors. Curved solid line: fitted ellipse. Colour rendering (which is only approximate in the printed version) is based on the sRGB (IEC1996 2.1) standard, with the white point set to the white point of the test and the monitor gamut set to our Trinitron monitor. Parameters extracted from fitted ellipses were as follows (length, axis ratio and angle, respectively): **(A)** 0.0116, 1.316, 92º; **(B)** 0.0184, 1.439, 97º; **(C)** 0.0147, 1.594, 65.5º; **(D)** 0.0382, 2.334, 73.6º; **(E)** 0.0565, 2.673, 112,3º; **(F)** 0.0295, 1.636, 71.5º.

The latter showed significantly increased variability (*F*-test, $p < .001$ for all parameter comparisons). Note that one of the patients in Stage 1, shown in **Figure 6.3B** had nearly normal performance, and that all patients above Stage 1.5 showed increased length of both minor and major axes, as compared to a representative normal control. Chromatic damage was confirmed by statistical analysis of ellipses main parameters (**Figure 6.4**): a significant elongation of ellipses length was found (**Figure 6.4A**, Mann-Whitney, $p < .0001$). In contrast, axis ratio (a measure of specificity of damage) was not significantly different from the control population (**Figure 6.4B**, Mann-Whitney, ns), indicating damage across both P and K chromatic pathways.

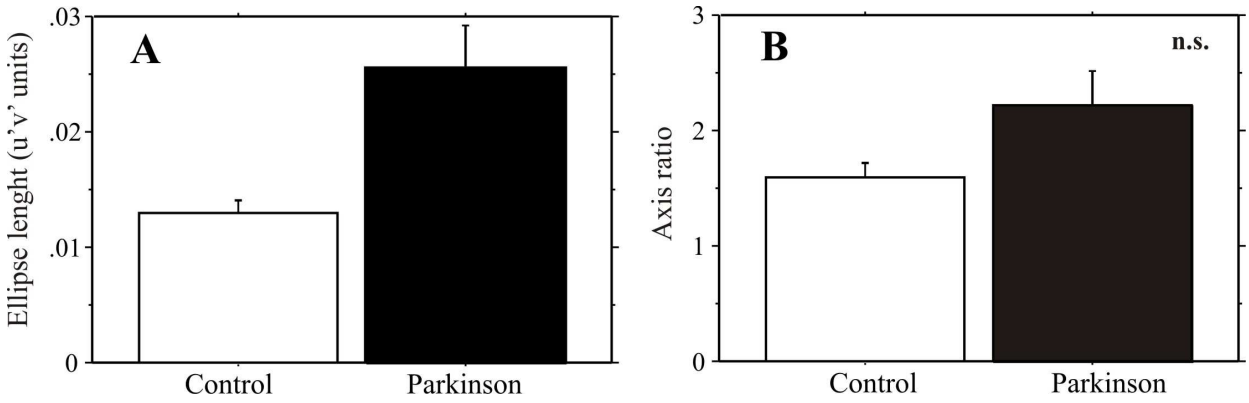

Figure 6.4. (A) Length of discrimination ellipses is significantly different between control and PD groups ($p < .0001$, Mann-Whitney). **(B)** Axis ratios of discrimination ellipses are not significantly different from the control group (ns, Mann-Whitney). In all figures error bars correspond to 1 SE.

In order to investigate whether or not patterns of damage are different along axes that isolate specific cone pathways, we independently analysed performance for protan, deutan and tritan colour axes. We found significant impairment of chromatic sensitivity in PD, in particular along the protan and deutan confusion lines (Mann-Whitney: $p = .0003$ for the protan axis, and .0021 for the deutan axis, $p = .0591$ for the tritan axis, which is only close to marginal significance; see **Figure 6.5**).

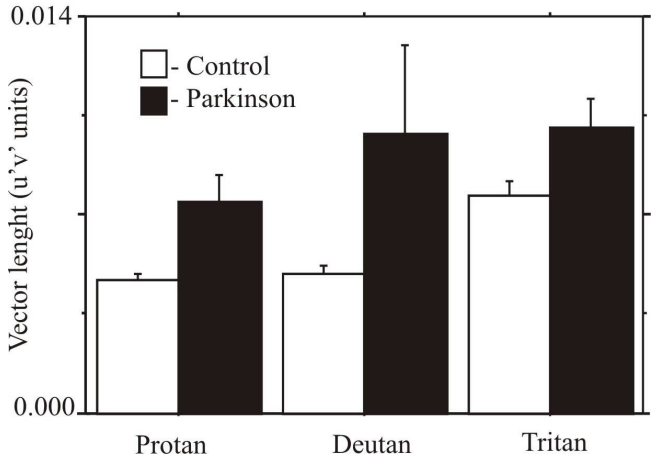

Figure 6.5. Lengths of protan, deutan and tritan vectors are significantly different between control and PD groups (except for the tritan axis).

6.4.2. Chromatic parameters vs. clinical parameters

No correlations were found between age and chromatic performance (Spearman's rank correlation, $p \leq 0.05$ for all measures). More importantly, no significant correlation was found between the duration of disease and the chromatic measured parameters. Interestingly, also no significant correlation was found between motor UPDRS scale and psychophysical performance, as measured by Spearman's rank correlation coefficients. The effect of dopaminergic medication was also analysed and no significant correlations were found between L-dopa and trivector measured parameters, as well as with the ellipse measured parameters.

6.4.3. Adaptation experiments under saturated blue background

In another set of control experiments, designed to verify whether results generalized under blue cone (pre-ganglionic) adaptation conditions (Shevell, 2003) we tested chromatic performance in eight PD patients. The parameters (length, axis ratio and angle) extracted from the fitted chromatic adaptation ellipses were as follows in **Table 6.1**.

Table 6.1. Parameters from the fitted adaptation ellipses for all subjects.

	Parameters of fitted adaptation ellipses		
	Length	**Axis ratio**	**Angle**
Subject 1 (A)	0.061	4.122	99.1
Subject 2 (B)	0.025	2.283	98.6
Subject 3 (C)	0.031	2.254	95.0
Subject 4 (D)	0.031	2.975	101.7
Subject 5 (E)	0.176	14.014	104.4
Subject 6 (F)	0.037	3.736	92.9
Subject 7 (G)	0.018	2.220	97.0
Subject 8 (H)	2.425	200.990	106.4

Ellipses were larger than for control subjects, but this increase was proportional to the baseline impairment, suggesting that adaptation per se does not amplify patterns of damage. Representative examples of chromatic adaptation discrimination ellipses are shown next in **Figure 6.6**.

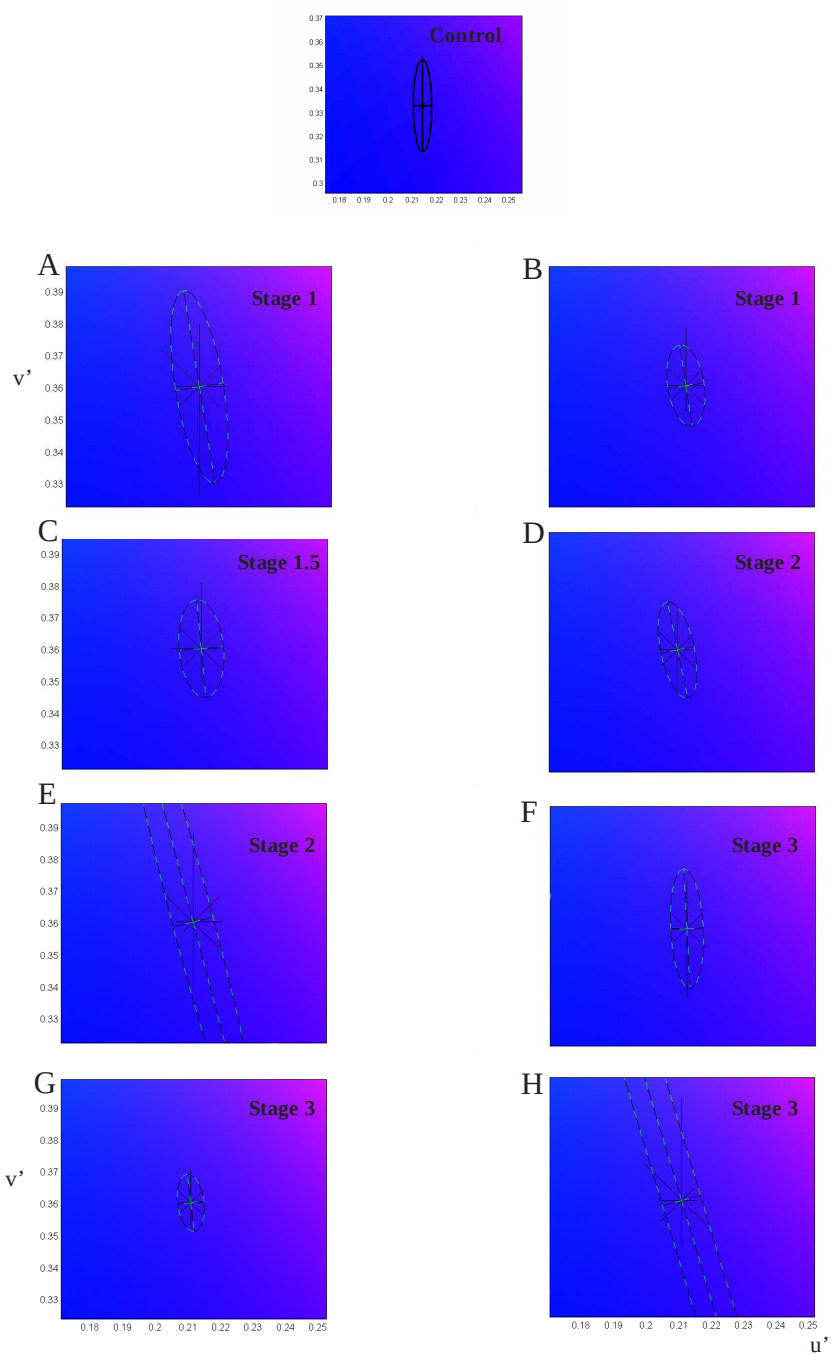

Figure 6.6. Top inset: representative example of a normal control chromatic discrimination ellipse from an adaptation experiment under saturated blue background. Chromatic adaptation in the PD group over Stages 1 to 3 of the modified H & Y clinical scale (motor UPDRS: **A**,11; **B**, 13; **C**, 21; **D**, 31; **E**, 21; **F**, 33; **G**,45; **H**,41). Subject 1 (**A**) corresponds to the same PD subject shown in **Figure 6.1B**, while Subject 2 (**B**) is the same shown in **Figure 6.1C**.

6.4.4. Perimetric assessment of magnocellular function

The spatiotemporal profile of the stimulus used in the achromatic FD perimetry was optimized to independently isolate the M pathway.

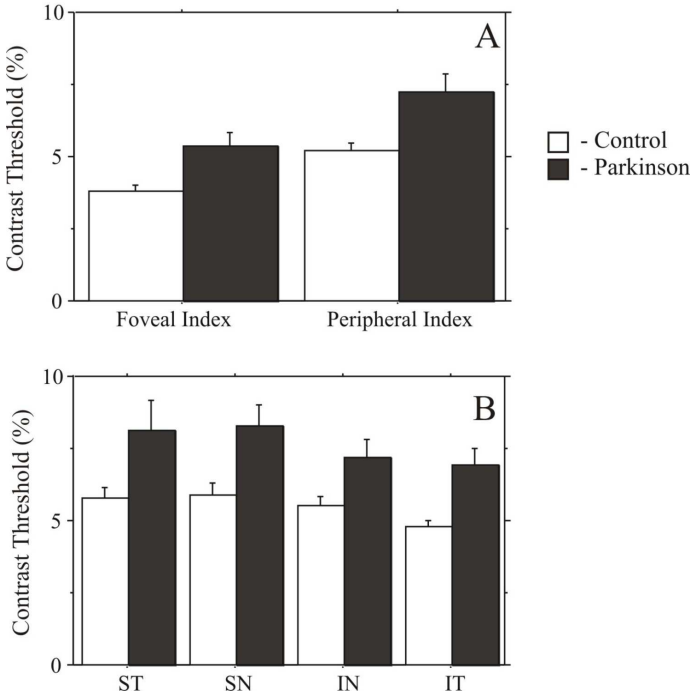

Figure 6.7. (A) Both Foveal Index and Peripheral Index Measures are significantly different between control and PD groups. **(B)** Achromatic contrast detection thresholds compared across visual field quadrants for each group of subjects.

We have found significant impairment in PD patients for both the central vision region (fovea) and periphery, as documented by the Foveal Index Measure which includes the foveomacular 5º region and the Peripheral Index Measure which corresponds to the average of the 16 peripheral locations (Mann-Whitney: p =.029, Foveal Index Measure and p = .012, Peripheral Index Measure; see **Figure 6.7 A**).

Differences in effect size maybe related both to relative density of different cell types in the retina and their spatiotemporal tuning properties (foveomacular M cells respond less well to high frequency flicker than peripheral cells). Threshold comparisons remained significant even when the analysis was performed separately for each visual field quadrant, except for the IN quadrant (**Figure 6.7 B**; Mann-Whitney tests: ST, p = .037; SN, p = .016; IN, p = .082 (ns); IT, p = .0030). This is a conservative statistical approach since it does not take into account that multiple locations were measured independently in each quadrant.

Representative examples are shown in **Figure 6.8**, demonstrating, in contrast with **Figure 6.3**, a clear worsening over stages. CS was significantly less homogeneous in PD than for control subjects (*F*-test across quadrants: superior temporal field (ST), inferior nasal (IN), inferior temporal (IT), superior nasal (SN), $p \leq .0001$ for all comparisons).

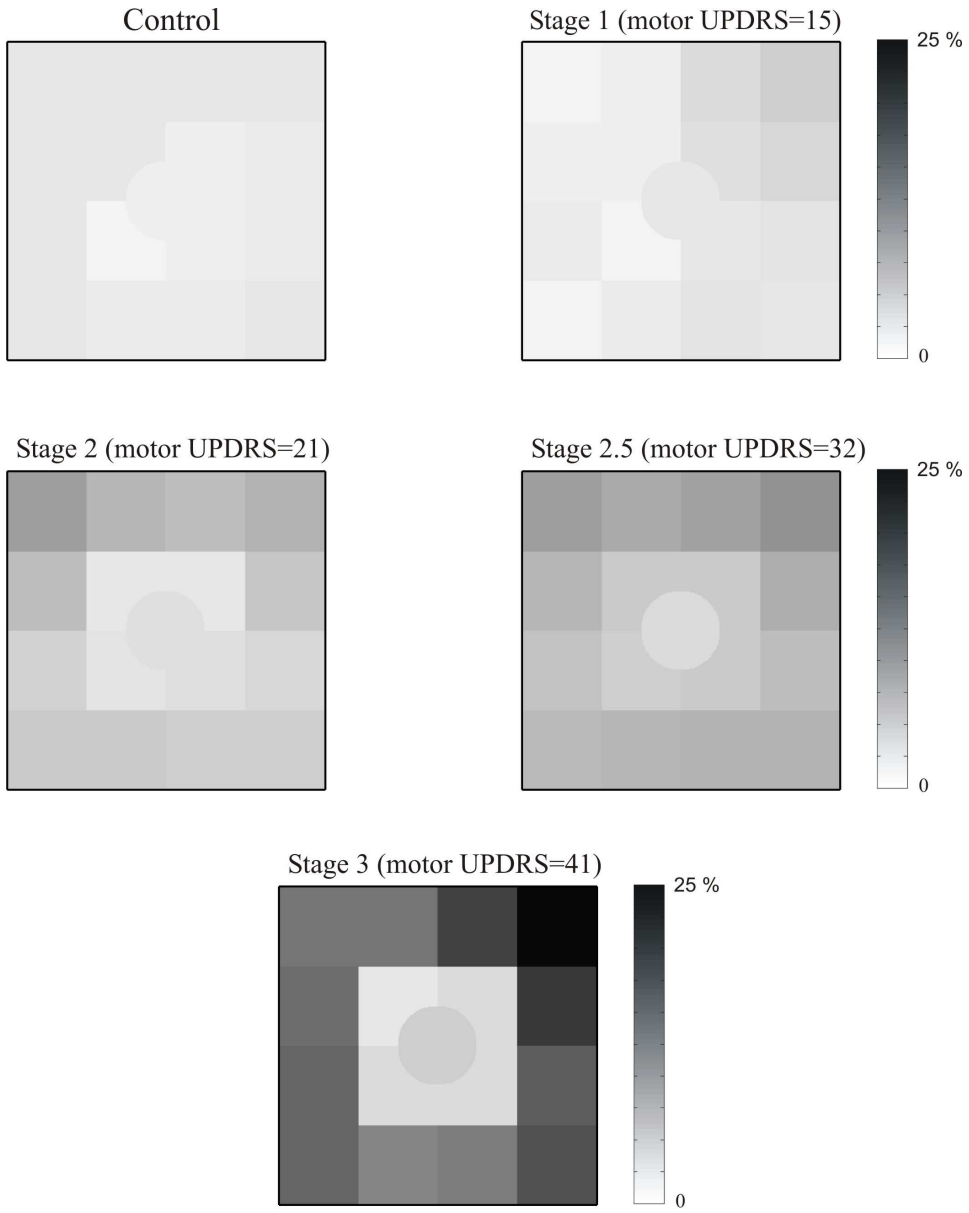

Figure 6.8. Representative examples of achromatic contrast sensitivity plots (left eye), where darker grey regions correspond to higher (lower CS) contrast thresholds (%). Grey level scale bar depicts % contrast thresholds. Note the clear-cut deterioration across stages.

6.4.5. Correlation between achromatic psychophysical performance and disease progression

In contrast with our findings for the chromatic tests, psychophysical performance for the achromatic test showed a significant correlation with age only within the PD group (in the control group, ns for all correlations): Foveal Index Measure, $\rho_{spearman}$ = 0.47, *p* = .0024; Peripheral Index Measure, ρ = 0.49, *p* = .0017). These effects in the PD group remained significant even when analysis was split according to visual quadrants (ST: ρ = 0.40, p = 0.0106; SN: ρ = 0.44, p = 0.0046; IN: ρ = 0.35, p = 0.0233; IT: ρ = 0.41, p = 0.0085). This was corroborated by Spearman correlation analyses between the duration of disease and achromatic parameters (contrast threshold, CT) as shown below in the **Table 6.2**. We have then computed correlations between modified H & Y stage and achromatic psychophysical thresholds.

Table 6.2. Spearman correlation coefficients (ρ) between contrast threshold and disease progression clinical parameters. The upper values correspond to ρ and the respective p values are in parenthesis (statistically significant correlation between contrast threshold and clinical parameters when p < 0.05).

	Contrast Threshold [%]					
	Peripheral Index	**Foveal Index**	**SN**	**IN**	**ST**	**IT**
Disease Duration [years]	0.60 (.0001)	0.49 (.0016)	0.54 (.0006)	0.66 (<.0001)	0.45 (.0038)	0.57 (.0003)
modified H & Y [0-5]	0.38 (.0304)	0.41 (.0201)	0.47 (.0073)	0.44 (.012)	0.27 (ns)	0.35 (.044)
motor UPDRS	0.43 (.0061)	0.49 (.0019)	0.46 (.0032)	0.39 (.014)	0.35 (.030)	0.35 (.025)

We found that all correlations were significant between Foveal and Peripheral Index Measure and further analysis revealed that nasal visual quadrants were the most significantly affected by stage. Again correlation analyses (**Table 6.2**) between the motor UPDRS and the achromatic performance (luminance modulation) confirmed these results, that is, a clear worsening over stages.

The SN visual quadrant was the most significantly correlated with the motor UPDRS. The effect of medication (L-dopa) in test performance showed no significant patterns (Mann-Whitney, ns).

6.4.6. Correlation between CS tests: Achromatic vs. chromatic parameters

It is important to test whether our measures of damage within M, P and K pathways in PD are indeed independent, as would be expected if parallel pathways were being separately explored. The results of this analysis showed that there was no evidence of an association between chromatic and achromatic contrast measurements. Indeed, our correlation analysis showed that all of our measurements of chromatic and achromatic CS were independent (Spearman correlations between Foveal/Peripheral Index Measures and Protan, Deutan and Tritan were ns; Foveal/Peripheral Index Measures and ellipses length, also ns), which allowed for an unbiased comparison of damage within these pathways.

6.5. Discussion

6.5.1. Independent assessment of multiple visual pathways and implications for understanding disease pathophysiology

In the present study, we found clear evidence of independent visual deficits within the P, K and M pathways in PD in line with previous work that suggested independent impairment of both colour and contrast discrimination (Pieri *et al*., 2000). Our measures of assessing sensory performance within the different pathways were independent, which allows for unbiased comparison of damage within these pathways. We use the term independent in a strict statistical sense: multiple measures of chromatic and achromatic thresholds were statistically uncorrelated, which is by definition a criterion for independence. This means that performance subserved by one pathway cannot predict performance by another pathway. Such statistical independence was not surprising, given the considerable amount of evidence that our spatiotemporal method isolates the M pathway (Purpura *et al*., 1988, 1990; Mendes *et al*., 2005; Castelo-Branco *et al*., 2006, 2009). In any case, the value of our M stimuli in assessing retinotopic M damage as early as at the retina level has already been demonstrated in glaucoma (Maddess *et al*., 1992, 1999; Johnson *et al*., 1997; Landers *et al*., 2000; Trible *et al*., 2000; Paczka *et al*., 2001; Shabana *et al*., 2003). There is also direct neurophysiological evidence that these stimuli differentially activate M neurons (Derrington and Lennie, 1984; Merigan and Maunsell, 1993; Lee, 1996). In sum, the high CS at high temporal frequencies, observed under our M test condition is a hallmark of M isolation (see also Mestre 1990b, Lee, 1996). While, the strategy used in the pure chromatic CS modulation test isolates two distinct colour vision pathways (Regan *et al*., 1994; Pearson *et al*., 2001; Shevell, 2003). It could be argued that the absence of correlations between chromatic and luminance modulation

measures might be due to involvement of different retinal areas. However, correlations remained close to zero even when spatially averaged (global) measures were used.

6.5.2. Patterns of damage across M, P and K pathways

We have observed involvement of chromatic pathways in PD even in some recently diagnosed patients. Surprisingly, predominant effects were found in measures of the function of the P pathway. K involvement found in previous reports may have been overestimated due to ageing effects. This may help to explain the results of Birch (1998), who concluded that clinical tests for tritan colour deficiency are unlikely to be helpful in identifying PD (see Haug *et al*., 1995). These observations are also compatible with the notion that ageing processes within ocular structures, such as the retina and the lens, are more prone to affect tritan measures (Wyszecki and Stiles, 1982; Pokorny *et al*., 1987; for reviews see Werner *et al*., 1990; Packer and Williams, 2003). Thus, it is important to ensure that neither significant lens opacification is present nor age-related senile changes are observed in fundus examination, even when groups are age-matched. Our careful ophthalmological examinations allowed exclusion of these and other confounding factors such as increased intraocular pressure. Even control subjects underwent the same type of careful assessment, with exactly the same exclusion criteria. All tests were measuring multiple colour axes randomly (multiple interleaved staircases), and since there was no fixed order there is no possibility that an attentional bias could have occurred during the tests. Measuring chromatic performance along only one or two axes in colour space and finding impairment does not mean that any of these two axes are the most impaired. Our discrimination ellipses represent a 4-fold improvement in colour space orientation resolution compared to previous studies, which avoids biased measurements/conclusions. The measured length, axis ratio and orientation of ellipses axes can be used to compare damage along K (blue-yellow opponent channel) and P pathways (red-green opponent channel). In contrast to what might have been expected, axis ratio measurements indicated damage across both P and K chromatic pathways. This finding was further substantiated by analysis of the relative distribution of ellipses orientation. We suggest that the assessment of P pathway may be more promising than the traditional K strategy, even when chromatic discrimination ellipses show a tritan tilt. Also, the adaptation experiments along the tritan axis showed effects that did not differ from the elongation observed in control groups. One should, however, note that some PD patients may have entirely normal thresholds. Some studies have indeed pointed out that only a subset of PD patients (that may reach 22.7%) may show chromatic deficits (Birch *et al*., 1998; Regan *et al*., 1998). M thresholds, as measured using an achromatic CS task, were significantly higher in PD both

in foveal and peripheral locations. In any case, our findings imply a significant involvement of early M maps (probably in the retina) in PD (for details on their topography see Curcio *et al*., 1990; Silveira and Perry, 1991; Yamada *et al*., 2001). Our finding of M impairment is consistent with a previous result suggesting that visual processing of rapidly presented stimuli is normalized in PD when stimulus contrast is enhanced (Amick *et al*., 2003). Also, the study of Sartucci *et al*., (2003) is consistent with our own findings that achromatic, red-green and blue-yellow pathways are impaired. In fact this study states that "in PD patients, the PERG amplitude was significantly reduced (by 40 to 50% on average) for both chromatic and luminance stimuli", this was observed in spite of the fact that very different (non-pathway isolating) stimulus conditions were used (suprathreshold 90% contrast, reversed at 1 Hz).

It is not yet possible to obtain in vivo anatomical evidence for damage across multiple visual pathways in PD. In the study of Inzelberg (2004) which measured the circumpapillary RNFL in PD, a full thinning of the retinal layer was found. Given that the most abundant are the P ones, this population is likely to provide a substantial contribution to the observed thinning, but by no means a specific one.

These findings do thereby provide an anatomical substrate for our findings, predicting impairment of multiple pathways, and not just one, as also observed in glaucoma (Yucel *et al*., 2001a, b). Ganglion cell loss in glaucoma has now clearly been shown to affect all ganglion cell populations (see Castelo-Branco *et al*., 2004 and references therein, Yucel *et al*., 2001a, b), while it had previously been believed that the P (red–green) pathway was spared. The same applies to PD: if the underlying disease mechanism relates to contrast processing control, and since the red–green pathway is essentially a contrast-processing pathway, it becomes hard to argue that it should be spared. When procedures with unbiased colour sampling strategies are applied, which is one of the main innovations of our study it becomes obvious that multiple pathways are concomitantly affected. In fact, simple inspection of our chromatic discrimination ellipses (**Figure 6.3**), which allow for direct simultaneous comparisons of concomitantly obtained measures, show that selective sparing of the red-green pathway does not occur.

6.5.3. Retinal dopaminergic effect in PD

Retinal dopamine-related impairment is widely accepted to alter retinal visual processing primarily by changing the receptive field properties of ganglion cells (Jackson and Owsley, 2003). The significant change in foveal CS that we have found is consistent with evidence suggesting that dopaminergic innervation around the fovea is reduced in PD patients (Nguyen-Legros, 1988). An electrophysiological study from Ikeda *et al*. (1994), in newly diagnosed PD

patients (in Stage 1), suggests that the retina is a likely source of impairment as revealed by early changes in electrooculography. Follow-up of these patients revealed subsequent (Stage 2) global ERG abnormalities. We do also believe that the observed deficits are likely to be at least partially located in the retina. In the subset of 21 patients in which both eyes were tested using the M isolating stimuli, we observed a pattern of asymmetry very similar to the one typically observed in glaucoma which represents evidence for involvement at the level of the retina, as previously suggested by Harnois and di Paolo (1990). Retinal impairment could, in turn, lead to specific metabolic occipital glucose hypometabolism (Bohnen *et al*., 1999). The main source of the retinal deficit is probably at the ganglion cell level which is consistent with PERG literature (Tagliati *et al*., 1996) in PD, and the fact that PERG responses predominantly reflect the activity of retinal ganglion cells (Fiorentini *et al*., 1981; Harrison *et al*., 1987; Bach, 2001). This interpretation is consistent with the above mentioned evidence for retinal nerve fibre layer thinning in PD (Inzelberg *et al*., 2004). The work of Bodis-Wollner and Tzelepi (1998) is in this sense seminal, because it discusses the PERG spatial contrast response function in terms of the envelope output of retinal ganglion cells or the average or “equivalent” retinal ganglion cell population response. It also postulates the existence of a “push-pull” mechanism related to two dopamine-sensitive pathways with different weights for two classes of ganglion cells. One uses D1 receptors and is primarily affecting the “surround” organization of ganglion cells with large centres, while the other uses D2 post-synaptic receptors and contributes to “centre” response amplification of ganglion cells with smaller centres. A preganglionic mechanism is unlikely to contribute to the chromatic CS impairment as well.

6.5.4. Differentiation of disease related patterns of damage

The present study was designed to compare P, K and M performance, thereby paving the way for separating disease susceptibility of different pathways. Fortunately, exactly the same psychophysical method could be applied in related work in other retinal diseases (including photoreceptor and ganglion cell diseases) and here in PD as a strategy to differentiate patterns of damage in these distinct diseases of the retina (Castelo-Branco *et al*., 2004; Maia-Lopes *et al*., 2008a, b). Concerning colour vision assessment, it is relevant to point out that the pattern of colour vision impairment across multiple colour axes is more linear-like across, and thereby more predictable in across the natural history of glaucoma (Castelo-Branco *et al*., 2004) than in PD, with preserved main axes of impairment across disease stages in the former case. Concerning a disease model of photoreceptor function, a more accelerated pattern of deterioration of K and P pathways was observed (Campos *et al*., 2005).

This comparative analysis suggests that patterns of retinal impairment in PD can be separated from the ones observed in other eye diseases and have distinct neural substrates.

Interestingly, concerning M function, patterns of damage in other diseases of the neural retina tend to be more similar when the same method is applied as in PD, possibly because of the higher amount of convergence in this pathway within the whole vertical retinal circuitry (for photoreceptor degenerations where M function was studied see Maia-Lopes *et al*., 2008 a, b; for diseases implying the whole retina, see Castelo-Branco *et al*., 2007).

The comparison between age-related retinal changes and the degeneration seen in comorbid conditions affecting PD patients (i.e. glaucoma, age-related macular degeneration (AMD), diabetic retinopathy) is relevant to understand potential confounds. Comparing these diseases with early onset retinal degenerations, such as Best Macular Dystrophy and Stargardt disease, is also important. Although these diseases do occur in younger cohorts, they may occur in older age groups overlapping with PD and represent a genetic model of age-related retinal degeneration. Indeed, late onset Stargardt disease is now believed to represent a subset of AMD (Maia-Lopes *et al*., 2008a). Comparison of PD retinal degeneration with these forms of retinal degeneration (Maia-Lopes *et al*., 2008a, b) may help framing the distinctiveness of the retinal degeneration that is observed in PD and strengthens the suggestion that there is a genuine disease-specific pattern of retinal impairment in PD.

Most of our patients were in early disease stages, and some were even newly diagnosed without any medication (similarly to the study of Ikeda *et al*., 1994). We have seen no significant difference between the treated vs. the untreated *de novo* patients, although average scores were better for the treated group. These results are consistent with the idea that the dopaminergic treatment may partially compensate (Buttner *et al*., 1994) the progression of visual impairment. The study of Sartucci *et al*. (2003) showed that visual impairment may occur in PD even in the absence of therapy, which is in agreement with our results in the subsample of patients without therapy. In contrast with chromatic tasks, performance under luminance modulation conditions showed a significant deterioration with age, disease duration, modified H&Y stage as well with motor UPDRS.

In terms of ageing our results contradicts some previous studies in ageing where not the same standard of care was taken to exclude age related conditions. Furthermore most of these studies did not attempt as much effort as we put in our study to isolate distinct visual pathways (Page and Crognale, 2005). In Pieri (2000) study, CS deficits (not isolating a specific pathway)

but not colour discrimination deficits, correlated with age in both patients and controls, while we have found only a most significant age related deterioration within the (age-matched) PD group.

Some previous studies of colour discrimination and CS in PD have also analysed the influence of disease progression on performance (Hutton *et al*., 1991; Price *et al*., 1992; Buttner *et al*., 1994; Pieri *et al*., 2000; Diederich *et al*., 2000). Most of these studies showed that the deterioration in CS was correlated with PD duration, follow-up scores of H&Y stage and motor UPDRS assessments. Disease progression is used in the sense of disease stage and should not be mistaken with ageing (whose between-group effects can of course be studied in longitudinal studies). It seems that the deterioration of achromatic FD CS occurs in parallel with motor UPDRS, in agreement with other studies that generalize these findings and correlations to these and other visual functions (Mosimann *et al*., 2004; Uc *et al*., 2005). These studies make clear that even if there is a putative short term beneficial therapy effect, such an early effect will be probably cancelled out by intrinsic disease progression.

6.6. Final Conclusions

Taken together, our findings suggest a differential and independent involvement of P (red-green), K (blue-yellow) and M visual pathways in PD. This indicates that distinct mechanisms, possibly related to different patterns of dopaminergic modulation (Bodis-Wollner and Tzelepi, 1998; Buttner *et al*., 2000), contribute to sensory impairment in PD. Since we could show that our quantitative measures of chromatic and achromatic CS were independent, and differently related to stage, future studies should address the effect of medication in these different types of deficit, in distinct disease stages (Buttner *et al*., 1994, 2000; for a review see Bodis-Wollner, 1990, 2002; Mestre *et al*., 1990a, b, 1996). Future studies should also investigate the role of within-group ageing effects, since normal controls did not show any effect of age on M performance. We suggest that future studies should use random psychophysical staircases due to their improved sensitivity and robustness against cognitive confounding factors.

Future studies should further address the question of how PD may interact with age-related ophthalmological diseases such as cataract and AMD, as almost all studies to date have excluded patients with significantly diminished VA or identifiable ocular pathology. Whilst this has helped to clarify disease-specific disruption of visual processing in PD, this is not the “real world” found by clinicians and interaction patterns across different vision loss disease related mechanisms should be explored in the future. A better appreciation of how structural disease of the eye contributes to disability in PD is overdue, particularly as effective treatments

exist for many of the concomitant ocular disorders that may contribute to visual symptoms in PD. Successful intervention therefore offers the prospect of improvements in the quality of life of PD patients and their carers. It also seems important to move beyond traditional static methods of assessing visual function for a detailed assessment of some of the more subtle changes in visual function, allowing an earlier identification of patients at risk of developing visual, motor and cognitive complications of PD. In addition, understanding neurodegeneration at multiple levels of the visual system, both at a microscopic and macroscopic level, may provide a clearer window through which to view the disease process itself and its influence, not just on the eye, but also on visuoperceptual, visuocognitive and visuomotor performance as well. We would like to stress that we could define very objective and unbiased measures of visual function, following the tenet of Geldmacher (2003) that precise definitions are needed to characterize “visuospatial dysfunction”.

In conclusion, we believe that our approach, focusing on improved methodological assessment and rigorous patient and data sampling criteria, and using multiple independent measures of distinct visual pathways, represents a promising strategy to better understand patterns of visual impairment in this disease.

Chapter 7

7. Hierarchical approach to the study of magnocellular and dorsal stream processing in Parkinson's disease: relation between visual and motor patterns of impairment

7.1. Summary

Motion processing involves multiple hierarchical steps, from the M pathway, sensitive to high temporal frequency modulations, to subsequent motion integration within the visual cortical dorsal stream. We have tested whether motion integration deficits in mild PD can be explained by visual deficits in earlier processing nodes. CS deficits in the M pathway, were compared with speed discrimination of local dots moving in random directions, speed and direction discrimination of moving surfaces and motion integration as measured by 2D coherence thresholds (n=27, PD patients).

We have found that low-level M impairment in PD does not explain deficits in subsequent steps in motion processing. High-level performance was abnormal in particular for tasks requiring perception of coherently moving surfaces. Motion coherence deficits were predictive of visuomotor impairment, corroborating a previous magnetic stimulation study in normal subjects. We conclude that dorsal stream deficits in PD have a high-level visual cortical basis independent of low-level M damage.

7.2. Introduction

The retinocortical M pathway represents the main projection to the visual dorsal stream, where motion integration takes place (Tootell *et al*., 1997; Galleti and Fattori, 2003; Orban, Van Essen and Vanduffel, 2004; Castelo-Branco *et al*., 2002, 2006, 2007). Given that cortical, dorsal-stream areas are projections of lower-level, M areas, one could argue, based on the integrated approach of Van Essen *et al*., (1992) that both of these brain streams are part of the M pathway (being lower- and higher-level segments). However, and given the mechanistic differences in integrative processing, we refer to the high-level segment as the cortical dorsal stream.

We have previously found evidence for M impairment in PD (see previous Chapter), but it is important to understand how these deficits relate to low/intermediate- (motion detection, speed and direction discrimination) and high-level motion processing (requiring global integration of coherent motion cues). Concerning low/intermediate-level processing, PD patients have difficulties in detecting motion when the tasks require the indication of its direction (Trick, Kaskie and Steinman, 1994) or speed (Mosimann *et al*., 2004). Furthermore, there is evidence, from one case study, that speed perception in PD constrains performance in tasks that require the perception of simple shapes from motion cues (Giaschi *et al*., 1997).

The previous studies that have analysed motion coherence (Trick *et al*., 1994, Amick *et al*., 2003, Uc *et al*., 2005) have yielded inconclusive or even contradictory results, probably due to variations of cognitive demands or ceiling effects. For example, two-alternative forced choice (2AFC) experiments, in which subjects know a priori that only two directions of motion are possible, may lead to missed detection of motion deficits (Amick *et al*., 2003). Here, we have circumvented the problem of potential ceiling effects by introducing a simple motion coherence task, in which direction of motion was unpredictable.

Most importantly, it is relevant to compare performance across multiple low- and high-level tasks and understand their interdependence. Our approach was the first to use a range of hierarchical stimuli designed to bias responses from low-level (M) and high-level (dorsal stream) pathways. Previous studies (see above) attempted in part such a strategy, but only used one class of motion tests, thereby preventing hierarchical measurements of visual motion processing. In particular, it is important to use direct high-level dependent measures of motion integration in addition to speed and direction discrimination and M CS measures (Gilmore *et al*., 1994). This might explain why previous approaches have not been conclusive in terms of dissection of hierarchical deficits in M and low/high-level motion processing in PD.

In this study, we explored tasks requiring speed and direction discrimination of peripheral single dots and/or surfaces, as well as more high-level motion coherence detection paradigms that address dorsal stream function (see Mendes *et al*., 2005 and references therein). Therefore, the main goal was to establish a correlation between performance across these tasks recruiting different levels of visual analysis, clinical stage and the ability to perform accurate motor sequences.

The impact of CS on reading disability, driving ability, and other daily activities is well covered in the literature (de Boer *et al*., 2004; Ivers *et al*., 1998; Kooijman and Cornelissen, 2005; Lord, 2006; Owsley and Sloane, 1987; West *et al*., 2002; Worringham *et al*., 2006). However, the functional implications of CS alterations to motor functions in PD is less clear, and correlations of CS performance with specific motor functions may in fact reveal independence of damage of these sensory and motor domains (Castelo-Branco *et al*., 2009). This is quite an important finding because it may be generalized to other conditions where a link between CS and visuomotor ability had been claimed but probably does not hold true (Castelo-Branco *et al*., 2007).

7.3. Methods

7.3.1. Participants

A subset of PD patients (n=27, 14 female and 13 male) of the study referred in the previous Chapter performed motion/motor tasks and a group of age-matched control subjects (n=24, 15 female and 9 male) was used for both motion and CS tests. Prior to inclusion, all subjects underwent full ophthalmological and neurological examination, the exclusion criteria was the same as in previous Chapter. Informed consent was obtained from all participants, and the study was conducted in accordance with the tenets of the Declaration of Helsinki, and the guidelines of our local ethics committee. The PD patients had a mean illness duration of 4.83 ± 3.8 (mean ± SD) years and their age distribution (61.2 ± 11.2 years) was not significantly different from that of the control subjects (56.2 ± 11.15) (ANOVA; non-significant (ns)). PD was staged according to the modified H&Y clinical scale (1.90 ± 0.62). Motor UPDRS yielded the following mean score, 24.6 ± 10.45. Aside from 10 PD patients that were newly diagnosed and were tested free from therapy, the others were receiving conventional levodopa therapy orally (mean dose of L-dopa: 578.12 ± 306.57 mg daily; other agonists: 7 patients with bromocriptine, 7.5 mg; 4 patients with ropinirole, 3.0 mg). The medicated patients were all tested in the best-on state.

Subject characterization for assessment of M CS is described in methods of previous Chapter. Mean education level was similar across groups, and was not significantly correlated with sensory performance.

7.3.2. Statistical analysis

The data did not significantly deviate from normal distributions in the control group, but this was often not the case for the PD group (violations of ANOVA statistical assumptions were verified using the Kolmogorov-Smirnov normality check and Levene homogeneity tests). Moreover, variance of the respective distributions was in general not homogeneous across the two groups. We did therefore choose non-parametric statistical methods (although we verified that parametric approaches would not have changed the main conclusions, thereby indicating that lack of power was not an issue in these non-parametric analyses).

7.3.3. Low-level M processing task - high temporal/low spatial frequency channel

We have applied CS multiple interleaved staircase test strategies, where stimuli were patches of 0.25 cpd of vertically oriented sinusoidal gratings, undergoing 25 Hz counterphase flicker, that are best suited to assess the M system. All participants performed CS perimetry under monocular conditions, in central (5º) and peripheral (5 to 10º and 10 to 20º) visual locations and the first tested eye was chosen in a random manner (for details on implementation, calibration, viewing conditions and experimental parameters see Chapter of Methods and Experiments).

7.3.4. Assessment of low-level (M) and high-level (integrative dorsal stream) motion performance

Concerning motion stimuli we have used RDKs (random dot kinematograms) presented within a circular spatial window of 6º visual angle (except when otherwise stated) generated using Vision-WorksTM for Windows (Vision Research Graphics, Wisconsin, USA) in a calibrated Sony Trinitron GDM-F520 monitor. Viewing distance was 56 cm. For all tests, the background luminance was ~ 0 cd/m^2 and a 2AFC staircase method (temporal or spatial) was used (with 12 reversals, 6 practice and 6 experimental) to determine thresholds. Steps were 0.01 log units in size, unless otherwise stated. Durations of fixed stimulus presentations were

of 1.133 s, after which a grey background appeared, and was present until the subject responded and the next trial commenced. Visual thresholds were measured for the following specific tasks:

a) 2D Motion coherence: 100% noise dots alternated randomly within one aperture with variable coherent motion (manipulated through a staircase procedure) in a particular direction that varied pseudorandomly from trial to trial. Dots moved at 3 º/s. Subjects had to report the presence or absence of coherent motion;

b) Direction discrimination: The stimulus was presented within a single circular aperture in the middle of the screen and consisted of dot-defined surfaces moving coherently in a horizontal manner to the right (0º) or vertically downwards (270º) at 2.5 º/s. Subjects had to indicate whether dots were moving horizontally (0º). Staircase implementation was such that correct responses caused the vertical stimulus to change its direction of motion to approximate the horizontally moving stimulus (from 270º towards 0º). Step size was 0.02 log units;

c) Global (surface) speed discrimination (spatial 2AFC): two windows were positioned with 6º horizontal separation. Dots moved horizontally, rightwards with 100% coherence;

d) Local Speed discrimination (spatial 2AFC): two windows were positioned with 30º horizontal separations, with single dots moving within 1º apertures. The initial speed of the test stimulus was 50 º/s and the standard stimulus was moving at 15 º/s. **For both conditions c) and d) subjects had to indicate which aperture contained the fastest moving dots.**

7.3.5. Simple and Complex Motor Temporal processing

We also studied Simple and Complex Motor Temporal processing, using Brainmetric Software (Drexel Hil, PA, US). Simple motor speed was tested by requesting subject's to tap as quickly as possible on the space bar of the computer keyboard using the dominant and nondominant forefinger (10 trials of 5 s duration for each hand). The first type of complex tapping measurements involved the subject tapping alternately with the left and right forefinger on alternate sides of the keyboard (two-finger, interhemispheric task, with five 5 s trials for each hand; subjects could start with either finger (S and L keys). The second complex tapping task required the subject to tap a sequence of keys with each hand (four-finger sequences; five 10 s trials for each hand) in distinct parts of the keyboard. These sequences had opposite directions for each hand, and subjects were requested to perform the task by emphasizing accuracy. Subject started with the dominant hand (Sequence: forefinger, middle, third and last: Right hand keyboard letter sequence, VBNM; Left hand, VCXZ).

7.4. Results - Performance patterns in low- and high-level motion discrimination tasks:

7.4.1. Preferential impairment in tasks that require perceptual integration of moving surfaces

We did confirm and extend previous evidence that suggested motion discrimination deficits in PD (**Figure 7.1**, p = .017 for main effect of motion tests, Mann-Whitney test). However, post-hoc analyses showed these deficits were mainly due to deficits in tasks requiring integration and detection of motion coherence among noise (p = .020) and speed discrimination of motion defined surfaces (p = .030). The motion coherence task is the one that shows the most clear-cut differences across the two groups, as well as speed discrimination of moving surfaces. Note that these comparisons were performed for identical sample sizes. This pattern is further confirmed by observation of Percentile Box plots in **Figure 7.1** which show that the tasks requiring integration and/or speed discrimination of moving surfaces are the ones that show less degree of distributional overlap between the two groups. These results suggest that tasks posing stringent demands on motion integration are the most sensitive to detect dorsal stream dysfunction. Accordingly, no significant impairment was detected at a post-hoc level for tasks requiring discrimination of local motion attributes such as speed discrimination of single, randomly moving local dots. Furthermore, direction discrimination tasks showed only a non-significant trend of impairment in PD.

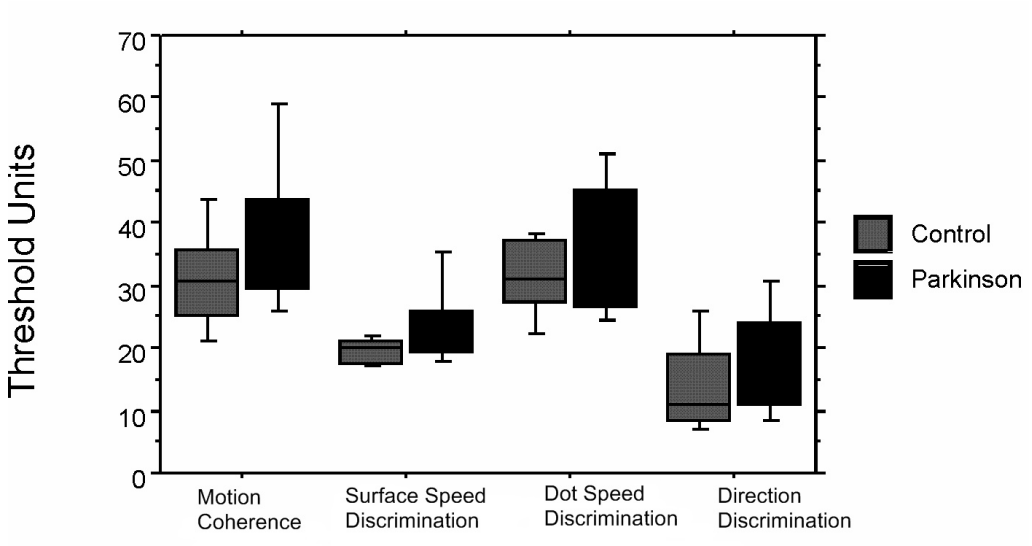

Figure 7.1. Evidence for motion processing impairment in PD. Motion integration (assessed by testing the minimum percentage of dot coherence necessary to perceive a moving surface) and speed discrimination of moving surfaces are the most prominently impaired in PD. Percentile Box Plots show that ranking of performance between PD and control groups reveals a better separation for Motion Coherence and Speed Discrimination of moving 2D surfaces tasks than for Speed Discrimination of single dots and Direction Discrimination tasks (box boundaries correspond to upper and lower 25th percentiles,outer bars to the 10th percentiles, and middle bar to the median).

7.4.2 Correlation analyses of between-task performance

Spearman correlation analyses of between-task performance predictability, revealed an interesting dissociation in PD as compared to the control group. In controls a significant correlation was found across motion coherence thresholds and performance in direction discrimination tasks ($\rho = 0.560$; $p = .010$). In contrast, in the patient group, performance was not correlated in these tasks ($p = 0.100$, ns), probably reflecting their differential impairment in PD. Exactly the same pattern of dissociation could be found when correlating speed discrimination of moving surfaces with direction discrimination. Again, a significant correlation was found only for the control group ($\rho = 0.490$; $p = .027$) but not for the PD group ($p = 0.420$), which further suggests a disease-related dissociation pattern. Interestingly, this dissociation was not present for the single dot task, which was predictive of performance in the other motion tasks in both groups, suggesting that it represents a common denominator in performance.

Evidence for specific disease related clustering of performance patterns was also found for high-level tasks. Indeed, only in the PD group did measures of motion coherence and

speed discrimination of moving surfaces (the tasks for which impairment was found) reach significant correlation (ρ = 0.530; *p* = 0.006), as compared to the control group. This finding suggests that these two tasks can be clustered in a disease related manner.

7.4.3 Correlation of motion performance measures with M contrast sensitivity

We have correlated motion sensitivity measures with two parameters of M performance in PD, the Foveal Index Measure (CS within the central foveomacular 5º region of VF and Peripheral Index Measure (in a distinct outer 10-20º peripheral VF region). In spite of the concomitant M CS impairment (see section of Results in previous Chapter), we have found rather weak, non significant correlations between all motion discrimination and CS tests. Correlation coefficients were indeed nearly zero for all comparisons. As an example, the scattergram in the lower panel of **Figure 7.2** shows no distinct pattern of correlation between CS performance and motion coherence, unlike the upper panel, which shows a clear correlation between CS performance in central and peripheral retina (see also significant linear regression line in plot).

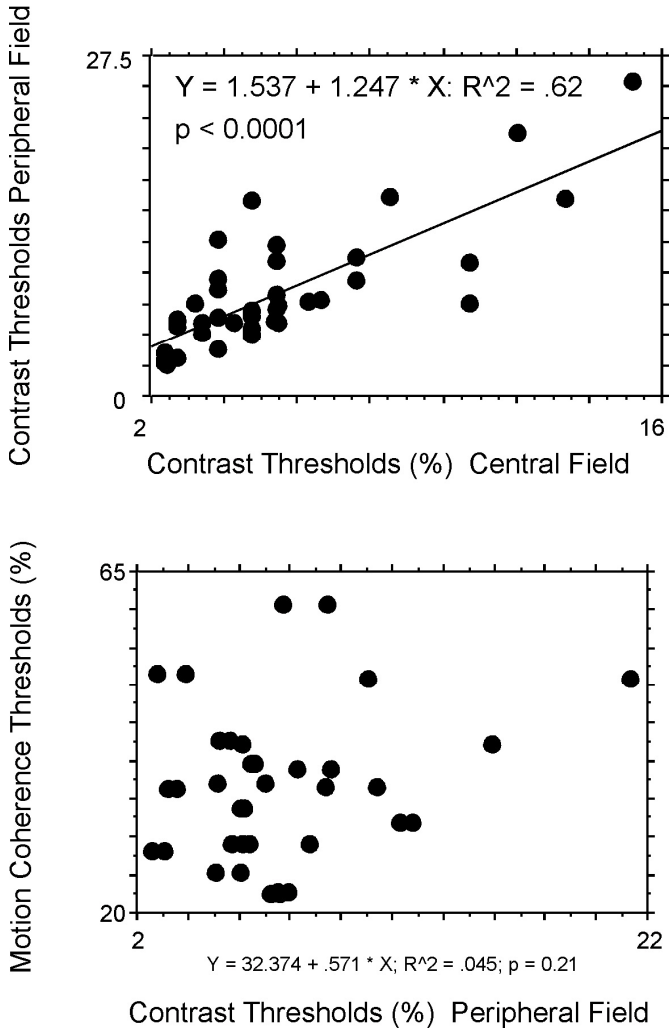

Figure 7.2. Motion coherence deficits are not correlated with M performance in PD. **Top panel**: Scattergram and fitted linear regression curves show that central and peripheral M CS´s are significantly correlated in PD (p < .0001, R^2 = 0.62). **Bottom panel**: no correlation is observed between motion integration performance and M performance in PD (p = .21, R^2 = 0.045).

7.4.4. Correlation of motion parameters with disease progression

Interestingly, none of the motion performance measures showed significant correlation with the UPDRS motor scale, unlike the M task, for which there was a clear correlation with this scale (see **Figure 7.3**). This pattern can be inspected in **Figure 7.3** (see also **Table 6.2**), which shows that Motor UPDRS scores are monotonically correlated with M performance. It is worth pointing out that higher value on CS psychophysical task (contrast thresholds in %) means poorer performance, which explains the positive correlation. Concerning correlations with L-Dopa therapy, the impairment that we found in motion coherence performance did not

show significant correlation with the dose of L-Dopa (this analysis being confirmed in a subset of 10 patients which were virgin from therapy). A similar pattern was observed for the other motion tasks and for the M tasks (except for a weak trend in peripheral CS).

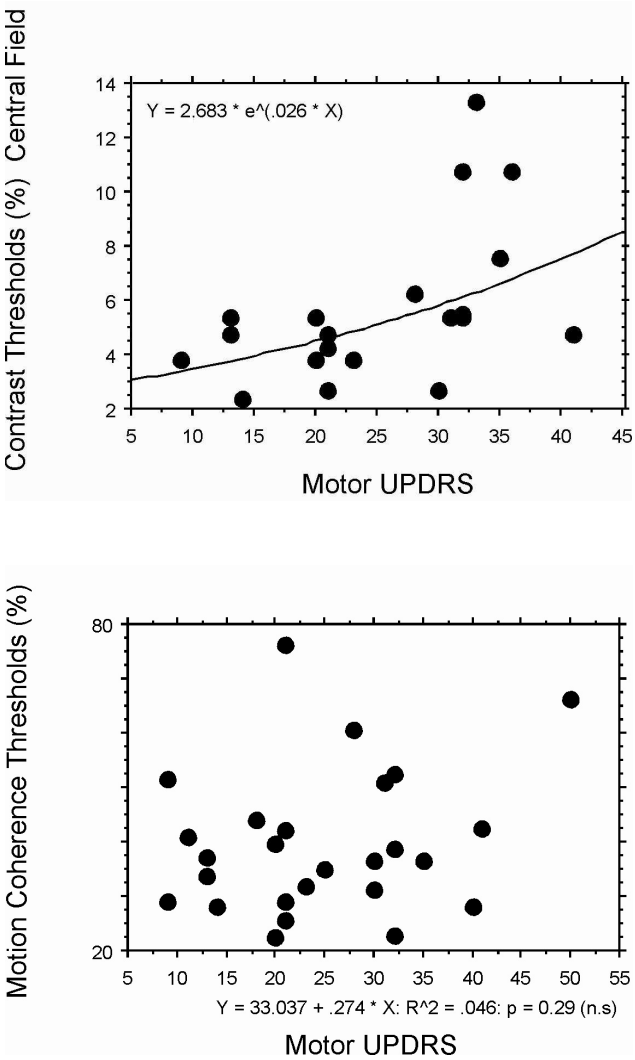

Figure 7.3. Motor UPDRS scores are monotonically correlated with M (top panel). Significant exponential fit (ln y = ln (b0) + b1x) for the central region, with p = .0006 and p = 0.017, for ln(b0) and b1 but not with motion integration performance (bottom panel).

7.4.5. Correlation with quantitative parameters of motor sequence execution

Interestingly, we have found that motion integration performance is correlated with the ability to perform motor sequences (**Figure 7.4**). Motion performance measures were not correlated with clinical UPDRS scores, but were nevertheless correlated with quantitative measures of motor sequence execution (Simple and Complex Motor Temporal processing, for details on these tasks see section 7.2.5 in Methods). This can be appreciated above in **Figure 7.4**, which illustrates an inverse monotonic relation between motion coherence scores and the ability to execute complex motor sequences: **A**: Complex Two-Finger Sequence, requiring interhemispheric coordination; **B**, Complex Four-Finger Sequence performed by the dominant hemisphere; **C**, Complex Four-Finger Sequence performed by the nondominant hemisphere; all fits significant with $p < .0001$ for ln(b0) and, concerning b1, $p = .0052$, $p = .0001$ and $p = .0021$, respectively, for the left panels). The right panels in **Figure 7.4** show that these correlations remained essentially the same regardless of whether errors were taken into account (these occurred at low rates because subjects were instructed to optimize accuracy versus speed).

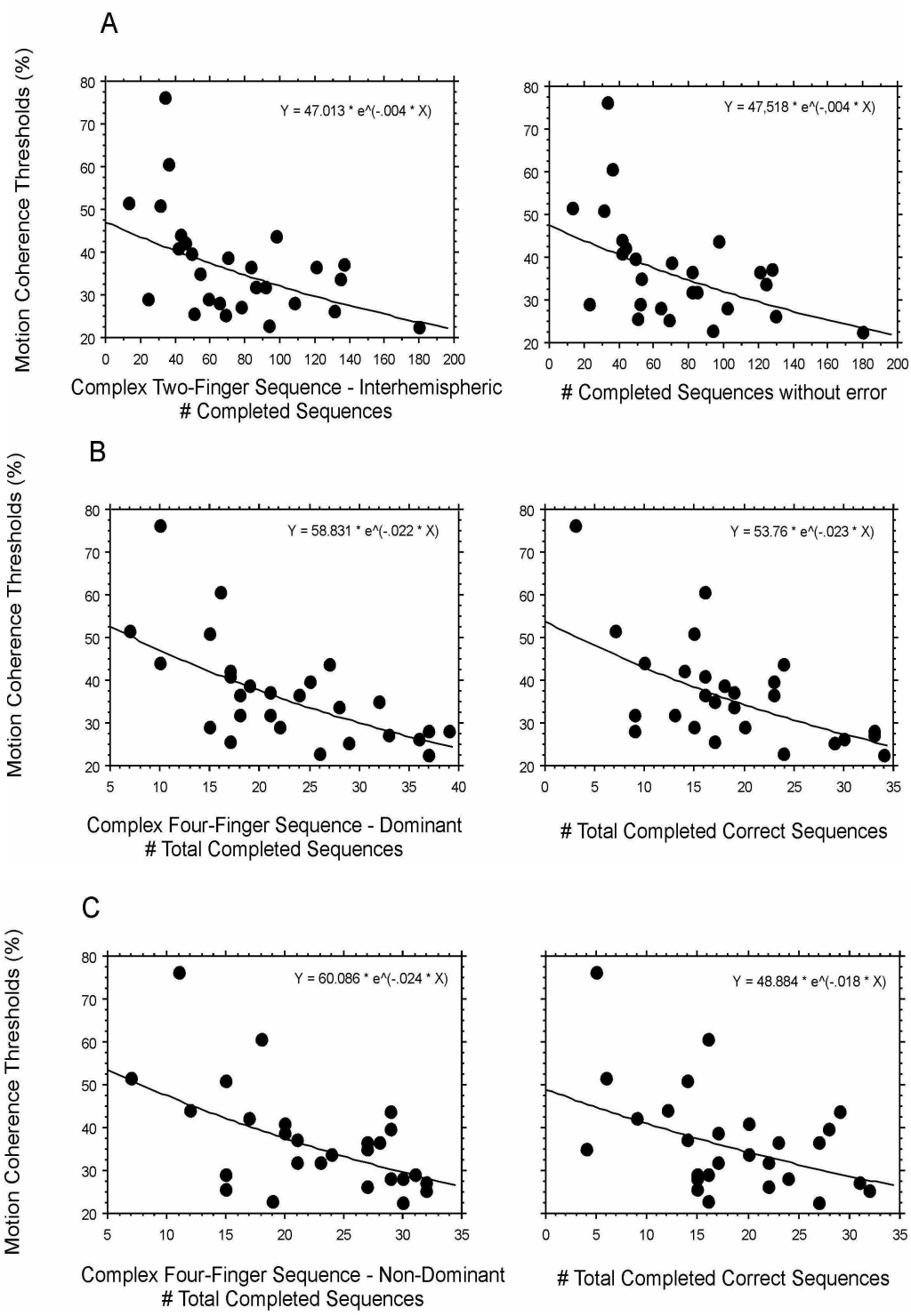

Figure 7.4. Motion integration performance is correlated with the ability to perform motor sequences. Left plots correspond to total number of completed sequences and right plots to number of correct sequences. **A**: complex Two-Finger Sequence, requiring interhemispheric coordination; **B:** Complex Four-Finger Sequence performed by the dominant hemisphere. **C:** Complex Four-Finger Sequence (continued below)

Figure 7.4(continued).performed by the nondominant hemisphere (all fits were significant; for details see Text).

When errors were discounted for, results remained essentially the same (**Figure 7.4A**, **B**, **C**, right panels: all fits significant with $p < .0001$ for ln(b0) and concerning b1, $p = .0052$, $p = .0006$ and $p = .015$, respectively). Spearman rank correlations confirmed the significant relationships between motion integration performance and motor sequence execution ability (Complex Two-Finger Sequence, requiring interhemispheric coordination: $\rho = -0.61$; $p = .0045$; Complex Four-Finger Sequence performed by the dominant hemisphere: $\rho = -0.67$; $p = .0017$; Complex Four-Finger Sequence performed by the non-dominant hemisphere $\rho = -0.54$; $p = .010$). Similar findings were observed for speed discrimination of single dots (Complex Two-Finger Sequence, requiring interhemispheric coordination: $\rho = -0.504$; $p = .018$; Complex Four-Finger Sequence performed by the dominant hemisphere: $\rho = -0.52$; $p = .014$; Complex Four-Finger Sequence performed by the non-dominant hemisphere $\rho = -0.46$; $p = .033$), speed discrimination of moving surfaces (the effect reaching significance only for the Complex Four-Finger Sequence performed by the non-dominant hemisphere: $\rho = -0.515$; $p = .0156$) and direction discrimination (the effect also reaching significance only for the Complex Four-Finger Sequence performed by the non-dominant hemisphere: $\rho = -0.52$; $p = .0148$).

CS M tasks did not show any correlation with the ability to perform motor sequences, which further emphasizes the distinction between this type of function and motion coherence/motor sequence performance skills in PD.

7.5. Discussion

In the present study, we have found that the significant involvement of early magno function occurring in PD is not predictive of motion integration deficits. This suggests that cortical convergence of M inputs maybe sufficient to compensate for peripheral loss of M inputs but is nevertheless not sufficient to overcome the intrinsic cortical motion integration deficits**.** In other words, functional damage of the M pathway, which serves as the primary input to cortical motion sensitive area hMT+/V5, does not contribute to deficits in motion tasks, suggesting that these have a high level neural substrate. This is consistent with evidence that indicates that the visual deficits found in PD patients are not solely related to retinal dysfunctions and that some of the deficits may be explained with generalized abnormal center-surround interactions of low- and high-level visual neurons as a consequence of dopaminergic deficiency, as suggested by human and animal studies (Bodis-Wollner, 1990; Schneider et al., 1992; Bodis-Wollner and Tagliati 1993; Zhao *et al*., 2001; Bodis-Wollner, 2003, Silva et al.,

2005). Previous studies have shown impaired space-motion perception in late stages of PD (accompanied with dementia, Mosimann *et al*., 2004), but our study has further explored motion perception in a comprehensive hierarchical manner (separating local from global motion perception), in early disease stages. Furthermore, we have explicitly correlated motion integration skills with M function. Impairment of more basic detection of local displacement had been reported previously, but the correlation with magno/dorsal stream dysfunction was not explicitly attempted (Haug *et al*., 1994; Trick *et al*., 1994, Bodis-Wollner and Tagliati, 1993).

The finding that cortical motion integration mechanisms are not related with peripheral retinotopic deficits in extracting local temporal information, has substantial implications concerning the understanding of mechanisms of disease in PD and other disorders that affect visuomotor function. These results do indeed challenge the prevailing view that motion coherence deficits are in general explained by a M deficit, such as in dyslexia (for the debate concerning this issue see Demb *et al*., 1998; Stein, 2001; Samar *et al*., 2007; Sperling *et al*., 2005, 2007). This conclusion is in agreement with the recent discovery of a novel phenotype in Williams Syndrome, where cortical deficits were proven to be unrelated to M deficits (Castelo-Branco *et al*., 2007).

However, the possibility still remains that spatiotemporal integration of motion cues can be correlated with time perception skills that are relevant to visuomotor integration. If this is true, deficits would be expected both in dyslexia and PD. We have found such patterns of correlation in PD, thereby providing support for this hypothesis, and it remains an open issue whether such patterns will also be found in dyslexia. This novel framework of impaired cortical integration of motion and its correlation with motor timing and sequence planning is also supported by the observation that motion performance impairments were more prominent for tasks requiring perception of coherently moving surfaces. Giaschi *et al*., (1997) had also previously proposed, based on one case study, that M function is not essential for the recognition of motion-defined form. Here we prove that this is the case in general for the integration of coherent 2D surfaces. Furthermore, our hierarchical design, allowed us to identify specific impairment of cortical motion integration (unlike the above mentioned previous studies). Only the study of Uc *et al* (2004) used dorsal stream function measures, but a hierarchical approach to the study of motion processing was not followed.

Our observation that motion integration measures are better correlated with computerized motor sequence scores than the UPDRS clinical score suggests that computerized quantitative methods provide added value in the characterization visuomotor dysfunction in PD. M measures were not correlated with motor sequence execution scores, further suggesting a consistent functional dissociation between magno-dorsal stream pathways and subsequent dorsal stream sequence planning networks. These findings nicely fit with the

recent discovery that direct current stimulation over hMT+/V5 (the human motion selective complex) enhances visuomotor coordination by improving motion perception in humans (Antal *et al*., 2004). In this study it was found that a diminution in excitability induced by cathodal stimulation improved the subject's perception of the direction of the coherent motion if this was presented among random dots. It is known that PD patients do not accelerate their predictions of trajectories with practice as fast as controls, a deficit that has been interpreted in terms of the fronto-striatal dysfunction (Schnider *et al*., 1995). These observations can be parsimoniously explained by the consideration that visuomotor transformations require the cross-talk between occipito-parietal and the above mentioned motor planning networks. In conclusion our findings challenge visual M theories that postulate a causal relation with local CS and visuomotor integration deficits in several cognitive disorders, and demonstrate the existence of a specific cortical-based motion integration deficit in PD that is predictive of motor sequence execution skills.

Part IV

Final Remarks

Chapter 8

8. Conclusion and Final Remarks

8.1. The relative value of novel psychophysical methods

Our new and comprehensive quantitative methodology to evaluate functional CS of macular and peripheral regions (up to 20º of VF) has shown several advantages:

1- Quantitative calibration (being possible to control precisely the luminance of the stimulus and background through proper calibration);

2- Presence of reliability criteria, such as False Positive and False Negative errors;

3- Reproducibility;

4- Multifocality (since it gathers data from many locations, central locations and in more peripheral regions, up to 20º of VF);

5- Randomly interleaved multiple staircases, minimizing the predictability of the stimulus and the factors of learning;

6- Control of quantitative and qualitative eye movements of each patient through a system of eye-tracker;

7- These tests are easy to understand and perform, since they are simple detection tasks. Answers are easily stored in a .txt file;

8- Its sensitivity is sufficient to detect even physiological asymmetries. Distinct patterns of VF asymmetries were found for each parvo/magnocellular task.

9- These methods are able to infer distinct perceptual magnification factors for both M and P tasks;

10- They allow for multidimensional mapping of the functional capabilities;

11- The protocols proved easy to adapt to clinical use and patients completed the tasks without difficulty;

12- They are appropriate to study selective mechanisms of functional impairment of photoreceptor/ganglion cell populations;

13- They allow for multimodal imaging comparisons with other functional methods like the mfERG and structural ones such as OCT3;

14- Our FD CS data does confirm the tenet that FD stimulus is best suited to isolate the M pathway. Accordingly, we have observed the expected higher CS at all eccentricities at the high temporal frequencies imposed by our M task condition.

8.1.1. Applications

These methods have allowed to understand pathophysiological mechanisms and suggested new ways to analyse impariment in diseases such as glaucoma, macular degeneration and neurological diseases such as Parkinson's disease, because they are quantitative. They are also useful at the more generic level of quality of vision testing.

These novel non-invasive CS methods were found to be appropriate to study selective mechanisms of functional impairment of photoreceptor populations. These strategies with quantitative electrophysiological approaches have been combined to phenotype visual impairment in genetic models of photoreceptor degeneration. The first model was subsequently applied to Stargardt Disease (SD), (Maia-Lopes et al., 2008a) to probe the M

and P pathways (Maia-Lopes *et al*., 2008a). Quantitative CS perimetry seems to be a promising phenotyping strategy in SD.

8.1.2. Implications of the findings of VF anisotropies in terms of segregation of parallel visual processing across pathways and space

The differences in terms of VF performance observed for M and P tasks suggest that distinct magnification factors (representation of visual angle per square mm of neurosensory tissue) should be applied for each of these pathways. Accordingly given the distinct eccentricity dependence of CS across M and P pathways, we concluded that using classical M-scaling procedures would lead to an overestimation of M thresholds in the visual periphery. This fact emphasizes the notion of pathway dependent magnification factors and is consistent with anatomical data. Variable retinotopic scaling across visual areas has also been previously discussed as a factor that may influence the eccentricity dependence of specific tasks. Indeed, monkey V1 cortical magnification factor falls off three to four times faster than CS and spatial resolution, suggesting that other areas, with distinct magnifications are relevant for these tasks.

In this thesis we provide evidence for novel parvo/magno cortical and subcortical mechanisms underlying perceptual anisotropies, yielding distinct perceptual magnification factors. This leads to a model that emphasizes right hemispheric dominance for low-level spatial vision and dorsal retinotopic dominance for early level temporal vision, prior to the dual spatial frequency filtering stages that occur at later cortical pathways underlying visual attention. Future studies should explore further the relative role of such functional anisotropies in different visual tasks and contexts.

In Chapter 5, we show that functional asymmetries can be concomitantly documented at multiple levels of the human visual system, including a significant retinal contribution, as assessed by comparison of psychophysical, electrophysiological and structural measures. Our results are consistent with the different anatomical anisotropies in terms of known cone and ganglion cell densities and suggest an inner retinal dominance in terms of the origin of naso/temporal asymmetries and a dual retinal and cortical contribution to up/down asymmetries.

The results of the visual asymmetry study have relevance in the design of psychophysical paradigms and clinical training programs for patients with heterogeneous VF loss and who need to reuse the most functional parts of their retina. The functional differences between the upper and lower visual fields could benefit rehabilitation training for patients who have lost central vision. In low-vision therapy, patients with central vision loss due to diseases such as macular degeneration are trained to use an eccentric retinal location as a surrogate fovea. The preferred retinal location for use as a surrogate fovea is often established either above or to the left (on the retina) of the scotoma (Guez *et al*., 1993; Seiple *et al*., 2005). It is of interest to note that patients with central field loss seem to have a tendency to naturally adopt a preferred retinal location in the inferior VF. The tendency to choose a preferred retinal location in the inferior VF may be driven, in part, by the enhanced sensitivity of this part of the VF.

8.1.3. Implications for early diagnosis of retinocortical diseases

All results (right and nasal hemifield patterns of disadvantage when assessing the ISF channel and quadrant-like combined ST (superotemporal) pattern of asymmetry for the LSF approach) showed unequivocal evidence for pre-attentive low-level visual anisotropies that includes early contrast processing. In terms of the cortical asymmetry, we have found evidence that even for low level visual tasks there is right hemispheric dominance.

The fact that the pattern of observed M disadvantage found was superior and temporal is consistent with a previous intriguing finding that local motion thresholds are first perturbed in that region in glaucoma. This particular ST disadvantage or vulnerability can therefore have implications for early diagnosis of diseases such as glaucoma. The better performance in the IT quadrant is in accordance with the fact that both temporal and inferior VFs set the broader field of vision in humans and with its role in tasks such as walking, grooming objects in their environment, etc.

It is important to recognize that when evaluating topographic structural and functional impairment in diseases such as diabetic retinopathy and glaucoma, one should consider that even in normal subjects, performance of retinal networks is asymmetrical in space. Visual maps and the correlations among measures as a function of retinal position serve as a baseline when examining disease effects throughout the retina. Accordingly, the development of vision rehabilitation programs focused on eccentric viewing training should consider these differential sensitivities of the peripheral retina.

8.2. Parkinsons´s Disease

We have shown that CS impairment is independent of motor dysfunction in PD, and correlations of CS performance with specific motor functions did in fact reveal independence of damage of these sensory and motor domains This is quite an important finding because it may be generalized to other conditions where a link between CS and visuomotor ability had been claimed but is likely to be proven wrong. Our approach was the first to use a range of hierarchical stimuli designed to bias responses from low-level (magnocellular) and high-level (dorsal stream) pathways. Interestingly, peripheral damage to the magnocellular pathway is not correlated with high-level motion perception, suggesting that low-level visual impairment does not predict high level dorsal stream impairment. In sum, low- and high-level impairments are dissociable, and only the latter are correlated with motor impairment.

8.3. Future work

We aim to take advantage os stimulus manipulation in terms of spatial and temporal frequency, in order to isolate and map processing channels separately, using electrophysiological and functional magnetic resonance imaging techniques. We will use these methods to map the brain areas that correspond to different neuro-sensory channels (parallel magno/parvo and koniocellular streams) which were isolated by the psychophysical techniques developed throughout this thesis. We also aim to investigate the neural correlates of the identified asymmetries using fMRI.

The strategies implemented can be applied to pathophysiological models of ganglion cell damage (such as ocular hypertension and glaucoma), photoreceptor dystrophies (monogenic degenerative diseases of the retina) and inflammatory optic nerve damage (optic neuritis). In order to validate models of structure-function, the psychophysical data obtained in these models will be correlated with structural data (imaging of the optic nerve).

In Chapter 2 strong evidence of structural and functional dysfunction of the visual pathways in PD was presented (with psychophysical, electrophysiological and morphological data). We have shown that selective impairment of retinal spatio-temporal visual processing and specific motion perception deficits found in PD are the result of the disease, not of aging per se. The inclusion of appropriate age-matched controls in many studies has marked the difference between normal ageing and PD in terms of retinal function.

However, it is not known how PD may interact with age-related ophthalmologic diseases such as age-related macular degeneration (AMD) or diabetic retinopathy since almost all studies have excluded patients with reduced VA and/or other ocular pathology. The role of molecular imaging in illuminating models of pathophysiological dysfunction in PD will definitely be an important research trend in the future. Nonetheless much of the current research is focused on motor impairment and in the future visual impairment should also be considered.

Future functional studies will be particularly important concerning the non-motor functions of the basal ganglia and their involvement in PD, by exploring modulation of activity in its entry points, the striatum and the subthalamic nucleus (STN), and its output, the globus pallidus pars internal (GPi), which connects to the cortex via the motor thalamus. Although many questions have been answered, many findings still remain unexplained. Most importantly, the involvement of non striatal dopaminergic pathways and other neurotransmitter systems will have to be clarified in the future. In fact, in spite of the existence of strong psychophysical, electrophysiological and morphological evidence for disruption of structure and function of visual pathways in PD, their link with striatal function is still unclear and should be explored with the newer methodologies that are now available.

Appendix A

Monitor Calibration and Calculation of the effective quantal catch based on the cone silent substitution technique

It is important to take into account when computing cone coordinates one has to use the formula s = S c. where cone coordinates are s (3 value vector)and c is the spectrum of the colour stimulus In other words one can compute l, m, and s quantal absorption rates corresponding phosphor spectra. To this end one must compute phosphor light intensities (finding r, g, and b values such that the mixture expresses the desired overall quantal absorption rates). It is very important to realize that this computation relies on measurements of the phosphor spectra but is independent of the gamma functions. The third step, gamma correction, finds DAC values R, G, and B that will produce the desired phosphor intensities r, g, and b. This computation is independent of the phosphor spectra.

A.1. Manual calibration of the Sony GDM-F520 Monitor

The procedure used to characterize the monitor employed for the psychophysical experiment of chromatic CS test is described in this section. Individual phosphor spectra (radiance units) of a 21 inch monitor (GDM-F520; Sony, Tokyo, Japan) where measured separately for distinct intensity levels with a Photo Research PR650 spectroradiometer [Photo Research PR-650-PC SpectraScan (Chatsworth, CA)] and with a matlab program developed in the laboratory. The program allows an automatic synchronization between the displaying of the

stimulus on the screen and the measure of the Minolta spectroradiometer. The measured spectra are shown in below in **Figure A.1**. The PR-650 measures spectral power distributions at 1-nm intervals in the range 380-780nm in W·sr−1·m−2.

For calculations of gamma functions, a procedure that is independent from the calculation of spectral distributions and quantal cataches, the stimuli used to make the measurements were square patches, which were displayed in the center of the screen in a completely dark room. We have measured three sets of coloured patches, red, green and blue, for colour numbers varying between 15 and 255 with a step of 15, that is, 17 measures have been taken for each colour. Moreover, grey patches have been measured in the range 0-255, taking thus 18 measurements. For example, a colour number of 255 for the red patch correspond to a stimulation of [255 0 0], this value corresponds to the most saturated red that the monitor can display. Thus, a grey number equal to 0 represents the monitor stimulation value [0 0 0], corresponding to the black of the screen, while a grey number of 255 corresponds to the stimulation [255 255 255], that indicates the reference white. Using such measures, we have estimated the gamma function (γ) for each gun red, green and blue. The gamma functions have been computed for normalized values of the stimulation (a measurement of ambient light was subtracted from each individual measurement. Then, for each measured spectrum, a scalar value was found that expressed that spectrum as a fraction of the spectrum *G(λ)* obtained from the maximum digital video value (*G* = 255). These scalars take on values between 0 and 1 and are the measured gamma function (γ).

For most CRT monitors, measured gamma functions are well fit by the functional form (e.g. for green phosphor, g):

$$g = [(G - G_0)/ (255 - G_0)]^{\gamma}, \quad \text{for } G > G_0$$

$$g = 0, \quad \text{for } G \leq G_0. \qquad (A.1)$$

parameter G_0, represents a cutoff digital video value below which no incremental light is emitted, and parameter γ describes the nonlinear form of the typical gamma function. The constant 255 normalizes the digital video value and is appropriate when *G* is specified by 8-bit numbers.

We have found the parameters that satisfy these equations using the Matlab function *lsqcurvefit* that solves nonlinear equations in the least square sense. The gamma values γ_R, γ_G, γ_B were 2.01, 2.12, 2.14 respectively (while parameters R_0, G_0, B_0: 54.9, 43.47, 47.68).

A.2. Silent Substitution Technique

The spectrum of Sony GDM-F520 phosphors is shown below in **Figure A.1**:

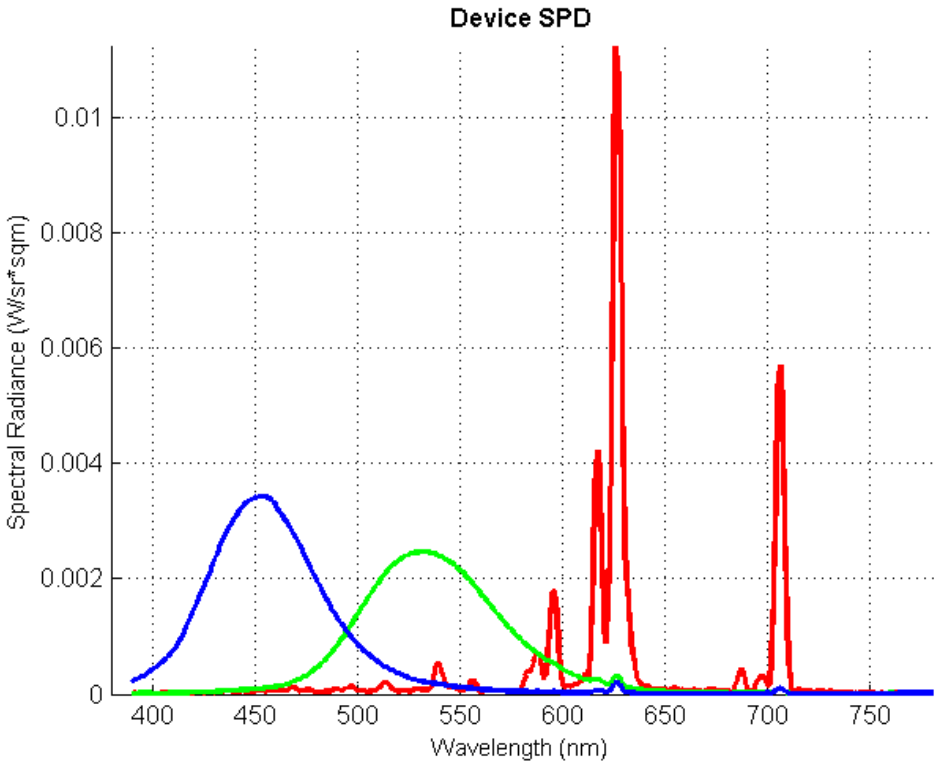

Figure A.1. Emission spectra of Spectral Power Distributions (SPD) of the phosphors of the display device, measured by PR-650. The blue phosphor has its peak at 452 nm, the green phosphor has its peak at 524 nm and the red phosphor has its primary peak at 628 nm and a secondary peak at 704 nm.

With the Planck's formula for radiant energy, the number of quanta (n) could be calculated:

$$\mathbf{n} = (E^*\lambda) / (h * c) \quad \text{(A.2)}$$

where, $h=6.626*10^{-34}$ J.s; $c=3*10^{8}$ m.s^{-1}

$$\mathbf{n} = E^* \lambda * 5.03*10^{24} \text{ (with } \lambda \text{ in m)} \quad \text{(A.3)}$$

$$\mathbf{n} = E^* \lambda * 5.03*10^{15} \text{ (with } \lambda \text{ in nm))} \quad \text{(A.4)}$$

Note: E em radiance units (W/m2/sr/nm); n = number of quanta/ m^2/ s/sr.

The quanta spectrum of Sony GDM-F520 phosphors is shown below in **Figure A.2**:

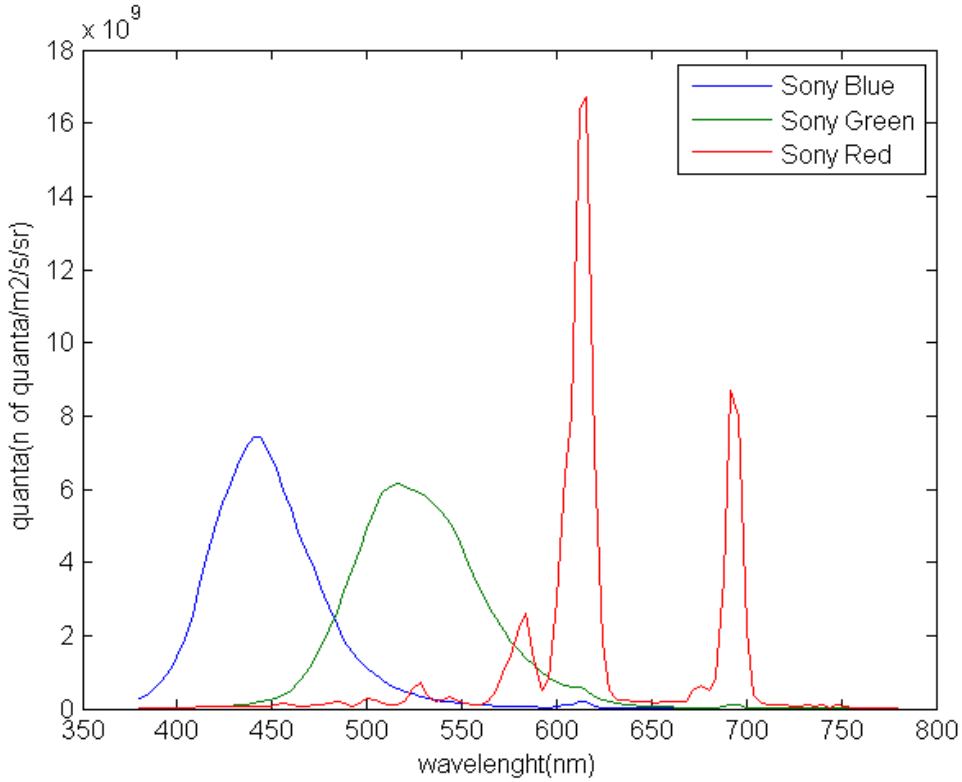

Figure A.2. Quanta spectrum of the three phosphors.

Estevez and Spekreijse (1982) firstly described a method of silent substitution, formerly called spectral compensation, in 1974, in which one of the cones is selectively stimulated, while the other cones are kept from responding to the stimulus. This method was based on the "principle of univariance" of Rushton, saying that for each class of cones the result of light stimulation depends upon the effective quantal catch, but not upon what quanta are caught (Mitchell and Rushton 1971a, b).

Rushton introduced the concept of effective quantal catch, which is the fraction of the quantal flux from a light source that actually produces pigment bleaching. Thus, only the amount of bleaching (and not e.g. the amount of quanta caught in a cone by passive pigments or transition photoproducts) leads to an intrinsic response of a cone contributing to a real visual response.

In the principle of trichromacy, any spectral light can be matched by a mixture of three fixed-colour primary lights, noted as the primaries R, G, and B. Thus, the spectral test light U

can be described as the addition of r units of primary R, g units of primary G and b units of primary B:

$$U = rR + gG + bB \quad (A.5)$$

The match is achieved when the amount of total quantal catch, which the three primaries produce in each of the three cone types, equals to the quantal catch produced by the spectral test light. This can be depicted in an equation as followed:

$$(rL_R + rM_R + rS_R) + (gL_G + gM_G + gS_G) + (bL_B + bM_B + bS_B) = rR + gG + bB \quad (A.6)$$

rL_R, rM_R, rS_R represent the effective quantal catch produced by the r units of primary R in the L-, M-, S-cone pigments (similarly gL_G, gM_G, gS_G by g units of primary G and bL_B, bM_B, bS_B by b units of primary B). Thus, the effective quantal catch produced in a single L-cone pigment by the spectral test light U is:

$$L = rL_R + gL_G + bL_B \quad (A.7)$$

Similarly, the effective quantal catch produced in a single M-cone pigment by the spectral test light U is

$$M = rM_R + gM_G + bM_B \quad (A.8)$$

And the effective quantal catch produced in a single S-cone pigment by the spectral test light U is:

$$S = rS_R + gS_G + bS_B \quad (A.9)$$

These linear relations (A.7; A.8; A.9) between the spectral test light U = rR + gG + bB and the effective quantal catch produced in each cone pigment can be written in a matrix notation:

$$\begin{pmatrix} L \\ M \\ S \end{pmatrix} = \begin{bmatrix} L_R & L_G & L_B \\ M_R & M_G & M_B \\ S_R & S_G & S_B \end{bmatrix} * \begin{pmatrix} r \\ g \\ b \end{pmatrix} \quad \text{(A.10)}$$

The conversion matrix will be referred as LMS_rgb, where each matrix coefficient represents the relative cone excitation produced by each phosphor primary.

The 3*3 matrix above results from the matrix multiplication S*c described above (r=g=b=1).

A.3. Cromatic CS tests - Cone contrast quantal catch tests -

In normal human colour vision, light is initially encoded in the quantal catch rates in three classes of photoreceptor, L-, M- and S-cones. The spectral sensitivities of these three systems are treated as linear single-valued functions and the values of these three functions are represented in LMS-cone excitation space. To evaluate independently red-green and blue-yellow pathways we used sinusoidal gratings similar to the ISF achromatic stimulus (static, 3.5 cpd) modulated along lines in colour space close to the three main axes of CIE (1931) x, y space (Campos et al., 2005; Regan et al., 1994) but with slight offsets from the isoluminant plane to ensure similar computed quantal catches across tasks (see below). This allowed for comparison with previous studies, where isoluminance was prioritized over quantal catch equivalence (Campos et al., 2005). We have used the same setup for stimuli generation, staircase procedure, viewing distance, subjects instructions and performance reliability as defined previous for the achromatic CS tests, which ensured test comparability. Manual calibration of the display monitor was performed for this task (see **A.1**), the emission spectra of the red, green, and blue phosphors of the monitor were measured separately in steps of 4 nm with a calibrated spectroradiometer (Photo Research PR650, SpectraScan, Chatsworth, CA).

Psychophysical chromatic sensitivity was tested in a randomly interleaved manner for each contrast axis. The red-green pathway was tested with two distinct procedures, by modulating contrast close to the protan and deutan axes (averages across these two axes being finally used as an estimate of red-green contrast sensitivity). Staircase vector extreme coordinates in the CIE (1931) x, y colour space were as follows: protan: x = 0.433, y = 0.295, and deutan: x = 0.371, y = 0.243. The blue-yellow stimulus was modulated close to the tritan axis (x = 0.254, y = 0.197).

The white starting point was x = 0.306, y = 0.314. Background luminance and stimulus luminance were equally set to 22.20, 41.50 and 6.75 cd/m^2 for protan, deutan and tritan axes, respectively, in order to obtain nearly identical average cone quantal catches at 2º and 10º (9.79 ± 0.64 (SD) log quanta.s^{-1}.$cone^{-1}$ for 2º stimulus and 9.82 ± 0.66 (SD) log quanta.s^{-1}.$cone^{-1}$ for 10º). Therefore, chromatic pathways (Kremers et al., 2003; Albrecht et al., 2002) could be compared, at approximately the same adapting level.

The effective quantal catch (number of absorbed quanta per cone per second) produced in each cone by each primary were calculated by multiplying the Stockman & Sharpe (2000) cone fundamentals for 2º or 10º with the emission spectra of the three phosphors and a constant k, and by integrating the product over wavelength (Wyszecki and Stiles, 1982; Pugh, 1988). The constant k is different for each cone, depending on the product of the ocular media transmittance and the absolute absorption coefficients for the wavelength of the maximal absorption probability for each cone (see **A.2**).

The chromatic contrast thresholds could be measured in five locations within 10º of VF (a central circular test field subtending 2º of visual angle called Zone 0 and 4 additional 5-10º testing locations, Zone 1 as displayed in **Figure A.1**).

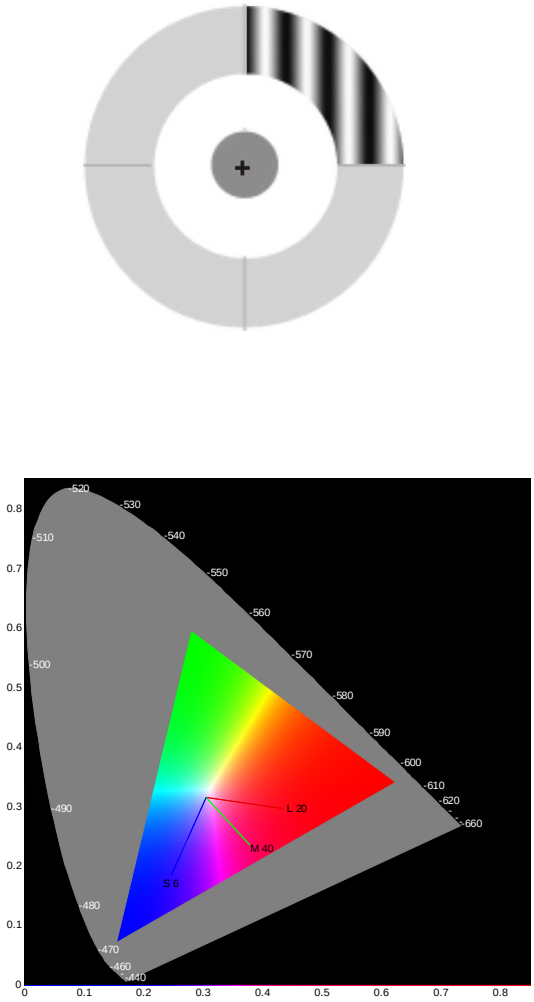

Figure A.1. **Upper panel**: Illustration of tested locations and stimulus layout for the chromatic CS test. CS obtained for each of the three colour axes tested was expressed in decibels. **Lower panel**: The CIE (1931) x,y chromaticity diagram showing the white (WP), protan (L20), deutan (M40) and tritan (S6) points. Note that luminance values were set to 22.20, 41.50 and 6.75 cd/m^2 for protan, deutan and tritan axes such that cone quantal catches remained constant.

This method can be used to quantify the chromatic performance and can even be used to establish percentile curves of chromatic function between different populations (controls and subjects with diseases, such as Best Macular Dystrophy).

Appendix B

B.1. Database characteristics of the Custom LSF task (T3.Custom C20)

The parameters analyzed for all custom tasks were age, gender and chosen eye. The zones were defined as Global mean (GM) corresponding to an average measure across all localizations; Zone 0 (central 5º region); visual hemifields: Superior, Inferior, Nasal and Temporal. The effect of the simultaneously interaction between all parameters (age*gender*eye) in each of the regions studied is resumed next in **Table B.1**.

Table B.1. Interaction effect (age*gender*eye).

Age*Gender*Eye	p	η^2
GM_LSF	0.923	0.010
Zone0_LSF	0.549	-0.029
Superior_LSF	0.866	0.014
Inferior_LSF	0.958	0.008
Temporal_LSF	0.982	0.005
Nasal_LSF	0.960	0.008

Considering each parameter individually, we observed that the most significant changes and in almost all regions assessed are due to age and not to chosen eye or gender (see **Table B.2** below). Finally, the influence of age in each zone studied (using iterative multiple regression analysis is shown in **Table B.3**.

Table B.2. Main effects in each region in terms of VF.

	AGE			EYE			GENDER		
Regions	F	p	η^2	F	p	η^2	F	p	η^2
GM_LSF	8.325	< 0.001	0.238	1.081	0.300	0.008	3.011	0.085	0.022
Zone0_LSF	2.885	0.017	0.098	0.569	0.452	0.004	0.519	0.473	0.004
Superior_LSF	9.530	< 0.001	0.264	1.702	0.194	0.013	0.068	0.068	0.025
Inferior_LSF	8.274	< 0.001	0.237	0.473	0.493	0.004	0.065	0.065	0.025
Temporal_LSF	8.482	< 0.001	0.242	0.664	0.417	0.005	0.063	0.063	0.026
Nasal_LSF	9.207	< 0.001	0.257	1.358	0.246	0.010	0.072	0.072	0.024

Table B.3. The influence of age per decade in each zone studied, using iterative multiple regression analysis The data was fitted by a linear regression equation (y= a +b * age).

	Total		AGE	
Regions	r^2	p	per decade	p
GM_LSF	0.093	< 0.001	-0.549	<0.001
Zone0_LSF	0.013	0.579	-	-
Superior_LSF	0.134	<0.001	- 0.682	< 0.001
Inferior_LSF	0.092	<0.001	-0.570	< 0.001
Temporal_LSF	0.093	<0.001	-0.577	< 0.001
Nasal_LSF	0.132	<0.001	-0.675	< 0.001

B.2. Database characteristics of the FDT task (MATRIX)

Table B.4 shows the main effects for each factor.

Table B.4. Main effects in each region.

	AGE			EYE			GENDER		
Regions	F	p	η^2	F	p	η^2	F	p	η^2
GM_FDT	18.792	< 0.001	.355	0.413	0.521	0.002	0.114	0.736	0.001
Zone0_FDT	7.027	< 0.001	.170	2.780	0.097	0.016	0.283	0.95	0.002
Superior_FDT	16.063	< 0.001	0.320	0.002	0.965	0.000	0.016	0.899	0.000
Inferior_FDT	18.869	< 0.001	0.356	0.128	0.721	0.001	0.095	0.758	0.001
Temporal_FDT	18.169	< 0.001	0.347	0.009	0.923	0.000	0.009	0.925	0.000
Nasal_FDT	17.086	< 0.001	0.333	0.227	0.634	0.001	0.261	0.610	0.002

The effect of the simultaneously interaction between all factors in each of the regions is summarized next in **Table B.5**:

Table B.5. Interaction effect (age*gender*eye) in each region in terms of visual field.

Age*Gender*Eye	p	η^2
GM_FDT	0.479	0.020
Zone0_FDT	0.099	0.044
Superior_FDT	0.557	0.017
Inferior_FDT	0.941	0.005
Temporal_FDT	0.696	0.013
Nasal_FDT	0.830	0.009

Considering next the age factor, the data was fitted by a linear regression equation (y= a + b *age):

Table B.6. The influence of age in each zone studied (using iterative multiple regression analysis).

	Total		AGE	
Regions	r^2	p	**per decade**	**p**
GM_FDT	0.244	< 0.001	-0.699	< 0.0001
Zone0_FDT	0.085	< 0.001	-0.526	< 0.0001
Superior_FDT	0.248	< 0.001	-0.751	< 0.0001
Inferior_FDT	0.239	< 0.001	-0.734	< 0.0001
Temporal_FDT	0.234	< 0.001	-0.707	< 0.0001
Nasal_FDT	0.258	< 0.001	-0.776	< 0.0001

B.3. Database characteristics of the Custom ISF task (T3.Custom C20)

Analyzing interactions between each two factors (considering factors as age. chosen eye and gender).

Table B.7. Interaction effect (age*gender; age*eye; gender*eye) in each region.

	Age * Eye			**Age * Gender**			**Eye * Gender**		
Regions	F	p	η^2	F	p	η^2	F	p	η^2
Zone0_ISF	0.175	0.972	0.005	0.183	0.969	0.005	0.295	0.588	0.002
Zone1_ISF	0.253	0.938	0.008	1.931	0.092	0.055	0.138	0.711	0.001
Zone2_ISF	0.143	0.982	0.004	1.800	0.115	0.051	0.755	0.386	0.004
Nasal_ISF	27.29	<0.001	0.450	0.510	0.769	0.015	4.304	0.040	0.025
Temporal_ISF	0.074	0.996	0.002	1.077	0.375	0.031	0.113	0.737	0.001
Superior_ISF	0.245	0.942	0.007	1.805	0.114	0.051	0.685	0.409	0.004
Inferior_ISF	0.354	0.879	0.010	1.834	0.109	0.052	0.136	0.712	0.001
Left_dB	0.878	0.497	0.026	3.107	0.010	0.085	0.409	0.523	0.002
Right_dB	25.075	<0.001	0.429	0.187	0.967	0.006	4.845	0.029	0.028

Analyzing separately each factor (age, chosen eye and gender):

Table B.8. Main effects in each region.

	AGE			EYE			GENDER		
Regions	F	p	η^2	F	p	η^2	F	p	η^2
Zone0_ISF	11.57	<0.001	.257	.040	.842	.000	3.914	.050	.023
Zone1_ISF	26.75	<0.001	.445	.331	.566	.002	8.671	.004	.049
Zone2_ISF	31.08	<0.001	.482	1.664	.199	.010	2.989	.086	.018
Nasal_ISF	1.015	.411	.029	219.89	<0.001	.568	.487	.486	.003
Temporal_ISF	31.89	<0.001	.488	.752	.387	.004	6.208	.014	.036
Superior_ISF	32.39	<0.001	.492	.053	.818	.000	11.103	.001	.062
Inferior_ISF	31.34	<0.001	.484	045	.832	.000	2.873	.092	.017
Left	30.27	<0.001		-	0.039			0.018	
Right	1.13	0.345		227.73	<0.001		.209	.648	

The influence of age, gender and eye in each zone with iterative multiple regression analysis is summarized below in **Table B.9**.

Table B.9. The influence of age in each zone studied (using iterative multiple regression analysis).

	Total		AGE		EYE		GENDER	
Regions	r^2	p	per decade	p	OS/OD	p	F/M	p
Zone0_ISF	0.241	< 0.001	-1.95	< 0.001	-	-		
Zone1_ISF	0.364	< 0.0001	-1.97	< 0.001	-	-	-1.36	0.044
Zone2_ISF	0.416	< 0.001	-1.59	< 0.001	-	-		
Nasal_ISF	0.509	< 0.001	-	-	-11.10	< 0.001		
Temporal_ISF	0.394	< 0.001	-1.81	< 0.001	-	-		
Superior_ISF	0.442	< 0.001	-1.97	< 0.001	-	-	-1.33	0.020
Inferior_ISF	0.365	< 0.001	-1.59	< 0.001	-	-		
Left_ISF	0.429	< 0.001	-1.84	< 0.001	1.13	0.039		
Right_ISF	0.429	< 0.001	-	-	-11.69	< 0.001		

Appendix C

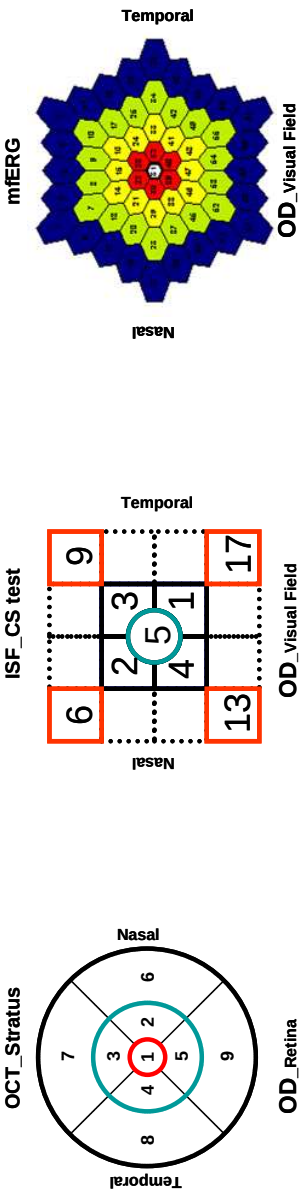

Regions in terms of visual field (VF)									
OCT- (corrected for VF)			ISF			mfERG			
ϕ (°)	Areas		ϕ (°)	Areas		ϕ (°)	Areas		
3.3° (R1) Zone1	1		-	-		4.4° (R1) Zone1	31		
10° (R2) Zone2	Superior	5	10° (R1) Zone1	5		13.6° (R2) Zone2	Superior	22 + 23	
	Inferior	3					Inferior	39 + 40	
	Temporal	2					Temporal	23 + 32 + 40	
	Nasal	4					Nasal	22 + 30 + 39	
20° (R3) Zone3	Superior	9	20° (R2) Zone2	Superior	3 + 2	25.8° (R3) Zone3	Superior	14 + 15 +16 + 21 + 24	
	Inferior	7		Inferior	4 + 1		Inferior	38 + 41 + 46 + 47 + 48	
	Temporal	6		Temporal	3 + 1		Temporal	16 + 24 + 33 + 41 + 48	
	Nasal	8		Nasal	4 + 2		Nasal	14 + 21 + 29 + 38 + 46	
-	Superior	-	40° (R3) Zone3	Superior	6 + 9	40.8° (R4) Zone4	Superior	7 + 8 + 9 +10 + 13 + 17 + 20 + 25	
	Inferior			Inferior	13+ 17		Inferior	37 + 42 + 45 + 49 + 52 + 53 + 54 + 55	
	Temporal			Temporal	9 + 17		Temporal	9 + 10 + 17 + 25 + 34(blind spot) + 42 + 49 + 54 + 55	
	Nasal			Nasal	6 + 13		Nasal	7 + 8 + 13 + 20 + 28 + 37 + 45 + 52 + 53	
-	-		-	-		58.7° (R5) Zone5	Superior	1 + 2 + 3 + 4 + 5 + 6 + 11 + 12 + 18 + 19 + 26	
							Inferior	36 + 43 + 44 + 50 + 51 + 56 + 57 + 58+59+60+61	
							Temporal	4 + 5 + 11 + 18 + 26 + 35 + 43 + 50 + 56 +60+ 61	
							Nasal	1 + 2 + 6 + 12 + 19 + 27 + 36 + 44 + 51 + 58 + 59	

Figure C.1. A simultaneous representation of the corresponding zones for all methods used in the study described in Chapter 5.

References

Albrecht, J., Jagle, H., Hood, D.C., & Sharpe, L.T. (2002). The multifocal electroretinogram (mfERG) and cone isolating stimuli: variation in L- and M-cone drives signals across the retina. *J Vis*; 2:543-558.

Altpeter, E., Mackeben, M., & Trauzettel-Klosinski, S. (2000). The importance of sustained attention for patients with maculopathies. *Vision Res*; 40:1539-1547.

Anderson, A.J., & Johnson, C.A. (2003). Frequency-doubling technology perimetry. *Ophthalmol Clin North Am*; 16:213-225.

Anderson, A.J., Johnson, C.A., Fingeret, M., Keltner, J.L., Spry, P.G., Wall, M., & Werner, J.S. (2005). Characteristics of the normative database for the Humphrey matrix perimeter. *Invest Ophthalmol Vis Sci*; 46(4):1540-1548.

Andrade da Costa, B.L., & Hokoc, J.N. (2000). Photoreceptor topography of the retina in the New World monkey Cebus apella. *Vision Res*; 40:2395-2409.

Antal, A., Kéri, S., Dibó, G., Benedek, G., Janka, Z., Vécsei, L., & Bodis-Wollner, I. (2002). Electrophysiological correlates of visual categorization: evidence for cognitive dysfunctions in early Parkinson's disease. *Brain Res Cogn Brain Res*; 13:153-158.

Archibald, N.K., Clarke, M.P., Mosimann, U.P. & Burn, D.J. (2009). The retina in Parkinson's disease. *Brain*; 132:1128-1145.

Arend, O., Wolf, S., Harris, A., & Reim, M. (1995). The relationship of macular microcirculation to visual acuity in diabetic patients. *Arch Ophthalmol*; 75:610-614.

Bach, M. (2001). Electrophysiological approaches for early detection of glaucoma. *Eur J Ophthalmol;* 11 Suppl 2:S41-9.

Bearse, M. A., Jr., Shimada, Y., & Sutter, E. E. (2000). Distribution of oscillatory components in the central retina. *Doc Ophthalmol*; 100:185-205.

Bearse, M.A., Jr, Han, Y., Schneck, M.E., Barez, S., Jacobsen, C., & Adams, A.J. (2004). Local multifocal oscillatory potential abnormalities in diabetes and early diabetic retinopathy. *Invest Ophthalmol Vis Sci*; 45(9):3259-3265.

Benardete, E. A., Kaplan, E. & Knight, B. W. (1992). Contrast gain control in the primate retina: P cells are not X-like, some M cells are. *Vis Neurosci;* 8:483-486.

Bidwell, L.C., Holzman, P.S., & Chen, Y. (2006). Aging and visual motion discrimination in normal adults and schizophrenia patients. Psychiatry Res; 145:1-8.

Billino, J., Bremmer, F., & Gegenfurtner, K. R. (2008). Differential aging of motion processing mechanisms: evidence against general perceptual decline. *Vision Res*;48:1254-1261.

Birch, J., Kolle, R.U., Kunkel, M., Paulus, W., & Upadhyay, P. (1998). Acquired colour deficiency in patients with Parkinson's disease. *Vision Res*; 38:3421-346.

Blakemore, C., & Campbell, F.W. (1969). On the existence of neurones in the human visual system selectively sensitive to the orientation and size of retinal images. *J Physiol (London)*; 203:237-260.

Bland, J. M. & Altman, D. G. (1987). Statistical methods for assessing agreement between two methods of clinical measurement. *Biochimica Clinica*; 11:399-404.

Bland, J. M. & Altman, D. G. (1999). Measuring agreement in method comparison studies. *Statistical Methods in Medical Research*; *8*:135-160.

Bodis-Wollner, I. (1990). Visual deficits related to dopamine deficiency in experimental animals and Parkinson’s disease patients. *Trends Neurosci*; 13:296-302.

Bodis-Wollner, I. (2003). Neuropsychological and perceptual defects in Parkinson's disease. [Review]. *Parkinsonism Relat Disord*; 9:83-89.

Bodis-Wollner, I., & Yahr, M.D. (1978). Measurements of visual evoked potentials in Parkinson's disease. *Brain*; 101:661-671.

Bodis-Wollner, I., Yahr, M.D., & Mylin, L.H. (1984). Non-motor functions of the basal ganglia. *Adv Neurol*; 40:289-298.

Bodis-Wollner, I., & Regan, D. (1991). Spatiotemporal contrast vision in Parkinson’s disease and MPTP-treated monkeys: the role of dopamine. Regan D., eds., Macmillan London. *Spatial Vision*; 250-260.

Bodis-Wollner, I., & Tzelepi, A. (1998). The push-pull action of dopamine on spatial tuning of the monkey retina: the effects of dopaminergic deficiency and selective D1 and D2 receptor ligands on the pattern electroretinogram. *Vision Res*; 38:1479-1487.

Bodis-Wollner, I., Marx, M.S., Mitra, S., Bobak, P., Mylin, L., & Yahr, M. (1987). Visual dysfunction in Parkinson's disease. Loss in spatiotemporal contrast sensitivity. *Brain*; 110: 1675-1698.

Bohnen, N.I., Minoshima, S., Giordani, B., Frey, K.A., & Kuhl, D.E. (1999). Motor correlates of occipital glucose hypometabolism in Parkinson's disease without dementia. *Neurology*; 52: 541-546.

Boycott, B.B., & Wässle, H. (1991). Morphological Classification of Bipolar Cells of the Primate Retina. *Eur J Neurosci*; 3:1069-1088.

Braddick, O.J., O'Brien, J.M., Wattam-Bell, J., Atkinson, J., & Turner, R. (2000). Form and motion coherence activate independent, but not dorsal/ventral segregated, networks in the human brain. *Curr Biol*; 10(12):731-734.

Brainard, D.H., Peli, D.G., & Robson, T (2002). Display characterization. In: Hornak J, editor. The Encyclopedia of Imaging Science and Technology. New York: John Wiley and Sons; pp. 172-188.

Brainard, D.H. & Stockman, A. (2010). Colorimetry. To appear in the OSA Handbook of Optics (3rd edition, M. Bass, ed). McGraw-Hill, New York, pp. 10.1-10.56.

Brancato, R., & Lumbroso, B. (2004). Guide to Optical Coherence Tomography Interpretation. Rome: Innovation-News-Communication.

Breitmeyer, B.G., & Ganz, L. (1977). Temporal studies with flashed gratings: inferences about human transient and sustained channels. *Vision Res*; 17(7):861-865.

Breitmeyer, B., & Julesz, B. (1975). The role of on and off transients in determining the psychophysical spatial frequency response. *Vision Res*; 15:411-415.

Bruyn, B.D., & Orban, G.A. (1988). Human velocity and direction discrimination measured with random dot patterns. *Vision Res*; 28:1323-1335.

Bulens, C., Meerwaldt, J.D., & Van der Wildt, G.J. (1988). Effect of stimulus orientation on contrast sensitivity in Parkinson's disease. *Neurology*; 38:76-81.

Buttner, T., Kuhn, W., Patzold, T., & Przuntek, H. (1994). L-dopa improves colour vision in Parkinson 's disease. *J Neural Transm Park Dis Dement Sect*; 7:3-9.

Buttner, T., Kuhn, W., Muller, T., Patzold, T., Heidbrink, K., & Przuntek, H. (1995a). Distorted color discrimination in 'de novo' Parkinsonian patients. *Neurology*; 45:386-387.

Buttner, T., Kuhn, W., Muller, T., & Przuntek, H. (1995c). Pharmacological effects of dopaminergics and amantadine on color discrimination in Parkinsons - disease. *Neuro - Opthalmology*; *15*(3):135−141.

Buttner, T., Kuhn, W., & Przuntek, H. (1995d). Alterations in chromatic contour perception in 'de - novo' Parkinsonian - patients. *Eur Neurol*; *35*(4):226−229.

Buttner, T., Kuhn, W., Muller, T., & Przuntek, H. (1996b). Visual hallucinosis: the major clinical determinant of distorted chromatic contour perception in Parkinson's disease. *J Neural Transm*; 103(10):1195−1204.

Buttner, T., Muller, T., & Kuhn, W. (2000). Effects of apomorphine on visual functions in Parkinson 's disease. *J Neural Transm*; 107:87-94.

Campos, S.H., Forjaz, V., Kozak, L.R., Silva, E., & Castelo-Branco, M. (2005). Quantitative phenotyping of chromatic dysfunction in Best macular dystrophy. *Arch Ophthalmol*; 123:944-949.

Casson, E.J., Johnson, C.A., & Shapiro, L.R. (1993). Longitudinal comparison of temporal-modulation perimetry with white-on-white and blue-on-yellow perimetry in ocular hypertension and early glaucoma. *J Opt Soc Am A*; 10:1792-1806.

Carrasco, M., McLean, T.L., Katz, S.M., & Frieder, K.S. (1998). Feature asymmetries in visual search: Effects of display duration, target eccentricity, orientation and spatial frequency. *Vision Res*; 38:347-374.

Carrasco, M., Talgar, C.P., & Cameron, E.L. (2001). Characterizing visual performance fields: Effects of transient covert attention, spatial frequency, eccentricity, task and set size. *Spatial Vision;* 15:61-75.

Carrasco, M., Giordano, A. M., and McElree, B. (2004). Temporal performance fields: visual and attentional factors. *Vision Res;* 44:1351-1365.

Chan, A., Duker, J.S., Ko, T.H., Fujimoto, J.G., & Schuman, J.S. (2006). Normal macular thickness measurements in healthy eyes using Stratus optical coherence tomography. *Arch Ophthalmol*; 124(2):193-198.

Chandler, M.J., Smith, P.J., Samuelson, D.A., & MacKay, E.O. (1999). Photoreceptor density of the domestic pig retina. *Veterinary Ophthalmology*; *2*:179-184.

Chauhan, B.C., House, P.H., McCormick, T.A., & LeBlanc, R.P. (1999). Comparison of conventional and highpass resolution perimetry in a prospective study of patients with glaucoma and healthy controls. *Arch Ophthalmol*; 117(1):24-33.

Caprioli, J. (1991). Automated perimetry in glaucoma. *American Journal of Ophthalmology*; 111: 235-239.

Carpenter, R.H.S., & Robson J.G. (1999). Vision research: a practical guide to laboratory methods. Oxford University Press.

Castelo-Branco, M., Faria, P., Forjaz, V., Kozak, L.R., & Azevedo, H. (2004). Simultaneous comparison of relative damage to chromatic pathways in ocular hypertension and glaucoma: correlation with clinical measures. *Invest Ophthalmol Vis Sci*; 45:499-505.

Castelo-Branco, M., Mendes, M., Sebastião, A. R., Reis, A., Soares, M., Saraiva, J., et al. (2007). Visual phenotype in Williams–Beuren syndrome challenges magnocellular theories explaining human neurodevelopmental visual cortical disorders. Journal of Clinical Investigation; 117:3720-3729.

Cello, K.E., Nelson-Quigg, J.M., & Johnson, C.A. (2000). Frequency doubling technology perimetry for detection of glaucomatous visual field loss. *Am J Ophthalmol*; 129:314-322.

Cerasa, A., Hagberg, G.E., Peppe, A., Bianciardi, M., Gioia, M.C., Costa, A., Castriota-Scanderbeg, A., Caltagirone, C., & Sabatini, U. (2006). Functional changes in the activity of cerebellum and frontostriatal regions during externally and internally timed movement in Parkinson's disease. *Brain Res Bull*; 71:259-269.

Clement, C.I., Goldberg, I., Healey, P.R., Graham, S. (2009). Humphrey matrix frequency doubling perimetry for detection of visual-field defects in open-angle glaucoma. *Br J Ophthalmol*; 93(5):582-588.

Cohen, J. (1992). A power primer. *Psychological Bulletin*; 112:155-159.

Conlon, E., & Herkes, K. (2008). Spatial and temporal processing in healthy aging: implications for perceptions of driving skills. Neuropsychol Dev Cogn B Aging Neuropsychol Cogn;15:446-470.

Connolly, M., & Van Essen, D. (1984). The representation of the visual field in parvocellular and magnocellular layers of the lateral geniculate nucleus in the macaque monkey. *J Comp Neurol*; 266:544-564.

Croner, L.J., & Kaplan, E. (1995). "Receptive fields of P and M ganglion cells across the primate retina." *Vision Res*; 35(1):7-24.

Crucian, G.P., & Okun, M.S. (2003). Visual-spatial ability in Parkinson's disease. *Front Biosci*; 8:992-997.

Curcio, C.A., Sloan, K.R., Packer, O., Hendrickson, A.E., & Kalina, R. (1987). Distribution of cones in human and monkey retina: Individual variability and radial asymmetry. *Science*; 236:579.

Curcio, C.A., Sloan, K.R., & Meyers, D. (1989). Computer methods for sampling, reconstruction, display and analysis of retinal whole mounts. *Vision Res*; 29(5):529-540.

Curcio, C.A., & Allen, K. A. (1990a). Topography of ganglion cells in human retina. *J Comp Neurol*; 300:5-25.

Curcio, C.A., Sloan, K.R., Kalina, R.E., & Hendrickson, A.E. (1990b). Human photoreceptor topography. *J Comp Neurol*; 292:497-523.

Curcio, C., Millican, L., Allen, K., & Kalina, R. (1993). Aging of the human photoreceptor mosaic: evidence for selective vulnerability of rods in central retina. *Invest Ophthalmol Vis Sci*; 34:3278-3296.

Dacey, D.M., & Petersen, M.R. (1992). Dendritic field size and morphology of midget and parasol cells of the human retina. *Proc Natl Acad Sci U S A;* 89:9666-9671.

Dacey, D.M. (1993). The mosaic of midget ganglion cells in the human retina. *J Neurosci*; 13:5334-5355.

Dacey, D.M., & Lee, B.B. (1994). The “blue-on” opponent pathway in primate retina originates from a distinct bistratified ganglion cell type. *Nature*; 367:731-735.

Dacey, D.M. (2000). Parallel pathways for spectral coding in primate retina, *Annu. Rev. Neurosci*; 23:743-775.

Dacey, D.M. (2004). Origins of perception: retinal ganglion cell diversity and the creation of parallel visual pathways. In: Gazzanigga MS (ed), *The Cognitive Neurosciences III*. Cambridge, MA: MIT Press; 281-301.

de Lau, L.M., Breteler, M.M. (2006). Epidemiology of Parkinson's disease. *Lancet Neurol*; 5:525-535.

Delalande, L., Destee, A., Hache, J.C., Forzy, G., Bughin, M., & Benhadjali, J. (1996). Visual evoked potentials and spatiotemporal contrast sensitivity changes in idiopathic Parkinson’s disease and multiple system atrophy. *Adv Neurol*; 69:319-325.

Derrington, A.M., & Lennie, P. (1984). Spatial and temporal contrast sensitivities of neurons in lateral geniculate nucleus of macaque. *J Physiol*; 357:219-240.

Derrington, A.M., Krauskopf. J., & Lennie, P. (1984). Chromatic mechanisms in lateral geniculate nucleus of macaque. *J Physiol*; 357:241-265.

Diederich, N.J., Raman, R., Leurgans, S., & Goetz, C.G. (2002). Progressive worsening of spatial and chromatic processing deficits in Parkinson disease. *Arch Neurol*; 59:1249-1252.

Drasdo, N. (1977). The neural representation of visual space. *Nature;* 266:554-556.

Drasdo, N., Millican, C.L., Katholi, C.R., & Curcio, C.A. (2007). The length of Henle fibers in the human retina and a model of ganglion receptive field density in the visual field. *Vision Res*; 47:2901-2911.

Edgar, G.K., & Smith, A.T. (1990). Hemifield differences of perceived spatial frequency. *Perception;* 19:759-766.

Enroth-Cugell, C., & Robson, J.G. (1966). The contrast sensitivity of retinal ganglion cells of the cat. J Physiol; 187:517-552.

Eriksson, U., & Alm, A. (2009). Repeatability in and interchangeability between the macular and the fast macular thickness map protocols: A study on normal eyes with Stratus optical coherence tomography. Acta Ophthalmologica; 87:725-730.

Fahle M., & Schmid M. (1988) Naso-temporal asymmetry of visual perception and of the visual cortex. *Vision Res;* 28:293-300.

Fahle, M. & Wehrhahn, C. (1991). Motion perception in the peripheral visual field. *Graefes Arch Clin Exp Ophthalmol*; *229*:430-436.

Fairchild, M.D. (1998). Color Appearance Models. Reading, MA: Addison-Wesley.

Fitzke, F.W., Poinoosawmy, D., Ernst, W., & Hitchings, R.A. (1987). Peripheral displacement thresholds in normals, ocular hypertensives and glaucoma. *Doc Ophthalmol Proc Ser*; 49:447-452.

Fitzke, F.W., Poinoosawmy, D., Nagasubramanian, S., Hitchings, R.A. (1989). Peripheral displacement thresholds in glaucoma and ocular hypertension. In: Heijl A, ed. *Perimetry Update 1988/1989.* Amsterdam: Kugler:399-405.

Fiorentini, A., Maffei, L., Pirchio, M., Spinelli, D., & Porciatti, V. (1981). The ERG in response to alternating gratings in patients with diseases of the peripheral visual pathway. *Invest Ophthalmol Vis Sci*; 21:490-493.

Folstein, M.F., Folstein, S.E., & Mchugh, P.R. (1975). Mini-Mental State: a practical method for grading the cognitive state of patients for the clinician. *J Psychiatr Res*; 12:189-198.

Fortune, B., Bearse, M. A., Jr., Cioffi, G. A., & Johnson, C. A. (2002). Selective loss of an oscillatory component from temporal retinal multifocal ERG responses in glaucoma. *Invest Ophthalmol Vis Sci*; 43(8):2638-2647.

Frisen, L. (1992). High-pass resolution perimetry: evidence for parvocellular neural channel dependence. *Neuro-ophthalmology;* 4:257-264.

Frizke, F.W., Poinoosawmy, D., Ernst, W., & Hitchings, R.A. (1987). Peripheral displacement thresholds in normals, ocular hypertensive and glaucoma. *Doc Ophthalmol Proc Ser*; 49:447-452.

Gasser, T. (2007). Update on the genetics of Parkinson's disease. *Mov Disord*; 22 Suppl 17:S343-50.

Geldmacher, D.S. (2003). Visuospatial dysfunction in the neurodegenerative diseases. *Front Biosci*; 8:428-436.

Gilmore, G.C., Wenk, H.E., Naylor, L.A., & Stuve, T.A., (1992). Motion perception and aging. *Psychology and Aging*; 7:654-660.

Glover, S. (2004). Separate visual representations in the planning and control of action. *Behav Brain Sci*; 27(1):3-24.

Glovinsky, Y., Quigley, H.A., & Pease, M.E. (1993). Foveal ganglion cell loss is size dependent in experimental glaucoma. *Invest Ophthalmol Vis Sci*; 34:395-400.

González de la Rosa M, Rodríguez J, Rodriguez M. 1999. Flicker-TOP perimetry in normals and patients with ocular hypertension and early glaucoma. In: Wall M and Wild J Perimetry update 1998/1999. Amsterdam: Kugler Publ; 59-66.

Goodale, M.A., & Milner, A.D. (1992). Separate visual pathways for perception and action.*Trends Neurosci*; 15(1):20-5.

Guerreiro, M., Silva, A.P., & Botelho, M.A. *Adaptação à população portuguesa na tradução do* "Mini Mental State Examination" (MMSE). *Revista Portuguesa de Neurologia;* 1, 9.

Guild, J. (1931). The Colorimetric Properties of the Spectrum. Philos Trans R Soc Lond A*;* 230:149-187.

Han, Y., Adams, A.J., Bearse, M.A. Jr., & Schneck, M.E. (2004). Multifocal electroretinogram and short-wavelength automated perimetry measures in diabetic eyes with little or no retinopathy. *Arch Ophthalmol*; 122:1809-1815.

Hardy, J., Cai, H., Cookson, M.R., Gwinn-Hardy, K., & Singleton, A. (2006). Genetics of Parkinson's disease and parkinsonism. *Ann Neurol*; 60:389-398.

Harnois, C., & di Paolo, T. (1990). Decreased dopamine in the retinas of patients with Parkinson's disease. *Invest Ophthalmol Vis Sci*; 31:2473-2475.

Harris, J.P. (1998). Vision in Parkinson's disease: what are the deficits and what are their origins? [Review]. *Neuro-Ophthalmology*; 19:113-135.

Harris, J.P., Calvert, J.E., & Phillipson, O.T. (1992). Processing of spatial contrast in peripheral vision in Parkinson’s disease. *Brain*; 115:1447-1457.

Harrison, J.M., O'Connor, P.S., Young, R.S., Kincaid, M., & Bentley, R. (1987). The pattern ERG in man following surgical resection of the optic nerve. *Invest Ophthalmol Vis Sci*; 28:492-499.

Haug, B.A., Trenkwalder, C., Arden, G.B., Oertel, W.H., & Paulus, W. (1994). Visual thresholds to low-contrast pattern displacement, color contrast, and luminance contrast stimuli in Parkinson's disease. *Mov Disord*; 9:563-570.

Haug, B.A., Kolle, R.U., Trenkwalder, C., Oertel, W.H., & Paulus, W. (1995). Predominant affection of the blue cone pathway in Parkinson's disease. *Brain*; 118:771-778.

He, S., Cavanagh, P., & Intrilligator, J. (1996). Attentional resolution and the locus of visual awareness, *Nature; 383*, 334–337.

Hee, M.R., Izatt, J.A., Swanson, E.A., Huang, D, Schuman, J.S., Lin, C.P., Puliafito, C.A., & Fujimoto, J.G. (1995). Optical coherence tomography of the human retina. *Arch Ophthalmol*; 113(3):325-32.

Hendry, S.H., & Reid, R.C. (2000). The koniocellular pathway in primate vision. *Annu Rev Neurosci*; 23:127-53.

Henson, D.B., & Morris, E.J. (1993). Effect of uncorrected refractive errors upon central visual field testing. *Ophthalmic Physiol Opt*; 13(4):339-343.

Hood, D. C., Seiple, W., Holopigian, K., & Greenstein, V. (1997). A comparison of the components of the multifocal and full-field ERGs. *Vis Neurosci; 14*(3):533-544.

Hood DC. (2000). Assessing retinal function with the multifocal technique. *Prog Ret Eye Res*;19(5):607-46.

Hugdahl, K., & Davidson, R. J. (2003). The Asymmetrical Brain (pp. 259–302). Cambridge, MA: MIT Press.

Ikeda, H., Head, G.M., & Ellis, C.J. (1994). Electrophysiological signs of retinal dopamine deficiency in recently diagnosed Parkinson's disease and a follow up study. *Vision Res*; 34:2629-2638.

Inzelberg, R., Ramirez, J.A., Nisipeanu, P., & Ophir, A. (2004). Retinal nerve fiber layer thinning in Parkinson disease. *Vision Res*; 44:2793-2797.

Irvin, G.E., Casagrande, V.A., & Norton, T.T. (1993). Center/surround relationships of magnocellular, parvocellular, and koniocellular relay cells in primate lateral geniculate nucleus. *Visual Neuroscience*; 10:363-373.

Ivry, R.B., & Robertson, L.C. (1998). The Two Sides of Perception (pp. 41–45, 77–82). Cambridge, MA: MIT Press.

Jackson, G.R., & Owsley, C. (2003). Visual dysfunction, neurodegenerative diseases, and aging. *Neurol Clin*; 21:709-728.

Jacobs, G.H. (2008). Primate color vision: a comparative perspective. Vis Neurosci; 25:619-33.

Jankovic, J. (2008). Parkinson's disease: clinical features and diagnosis. *J Neurol Neurosurg Psychiatry*; 79:368-376.

Johnson, C.A., Adams, A.J., Casson, E.J., & Brandt, J.D. (1993). Progression of early glaucomatous visual field loss for blue-on-yellow and standard white-on-white automated perimetry. *Arch Ophthalmol*; 111:651-656.

Johnson, C.A., & Samuels, S.J. (1997). Screening for glaucomatous visual field loss with frequency-doubling perimetry. *Invest Ophthalmol Vis Sci*; 38:413-425.

Jonas, J.B., Schneider, U., & Naumann, G.O. (1992). Count and density of human retinal photoreceptors. *Graefes Arch Clin Exp Ophthalmol*; 230:505-510.

Kaplan, E., & Shapley, R.M. (1982). X and y cells in the lateral geniculate nucleus of macaque monkeys. *J Physiol*; 330:125-43.

Kaplan, E., & Shapley, R.M. (1986). The primate retina contains two types of ganglion cells, with high and low contrast sensitivity. *Proc Natl Acad Sci U S A*; 83(8):2755-2757.

Kaplan, E. (2004). The M, P, and K pathways of the primate visual system. In: L.M. Chalupa, & J.S. Werner (Eds.), *The Visual Neurosciences,* Vol. 1 (pp. 481-493). Cambridge: MIT press.

Kelly, D.H. (1966). Frequency Doubling in Visual Responses. *J Opt Soc Am*; 56(11):1628-1632.

Kelly, D.H. (1981). Nonlinear visual responses to flickering sinusoidal gratings*. J Opt Soc Am*; 71:1051-1055.

Kempster, P.A., Hurwitz, B., & Lee, A. J. (2007). A new look at James Parkinson's Essay on the Shaking Palsy*. Neurology*; 69:482-485.

Kondo, M., Miyake, Y., Horiguchi, M., Suzuki, S., Ito, Y., & Tanikawa, A. (1996). [Normal values of retinal response densities in multifocal electroretinogram]. *Nippon Ganka Gakkai Zasshi*; 100(10):810-816.

Kremers, J., Maciej, W.S., Scholl, H.P., & Saito, C. (2003). Cone selective adaptation influences L-and M-cone drives signals in electroretinography and psychophysics. *Journal of Vision*; 3:146-160.

Kryger, Z., Galli–Resta, L., Jacobs, G. H., & Reese, B. E. (1998). The topography of rod and cone photoreceptors in the retina of the ground squirrel. *Visual Neuroscience, 15*:685–691.

Kurtenbach, A., Langrova, E., & Zrenner, E. (2000). Multifocal Oscillatory Potentials in Type 1 Diabetes without Retinopathy. *Invest Ophthalmol Vis Sci*; 41(10):3234-3241.

Lachenmayr, B.J., & Gleissner, M. (1992). Flicker perimetry resists retinal image degradation. *Invest Ophthalmol Vis Sci*; 33(13):3539-3542.

Lam, B.L. Electrophysiology of Vision: Clinical Testing and Applications. Boca Raton: Taylor & Francis, 2005.

Landers, J., Goldberg, I., & Graham, S. (2000). A comparison of short wavelength automated perimetry with frequency doubling perimetry for the early detection of visual field loss in ocular hypertension. *Clin Experiment Ophthalmol*; 28:248-252.

Laeng, B., Chabris, C.F., & Kosslyn, S.M. (2003). Asymmetries in encoding spatial relations. In K. Hugdahl and R. Davidson (Eds.), *The Asymmetrical Brain.* Chapter 9, pp. 303-339. Cambridge, MA: The MIT Press.

Langheinrich, T., Tebartz van Elst, L., LaGreze, W., Bach, M., Lücking, C.H., & Greenlee, M.W. (2000). Visual contrast response functions in Parkinson's disease: evidence from PERG, VEP and psychophysics. *Clin Neurophysiol*; 111:66-74.

Lee, B.B., Pokorny, J., Smith, V.C., Martin, P.R., & Valberg, A. (1990). Luminance and chromatic modulation sensitivity of macaque ganglion cells and human observers. *J Opt Soc Am A*; 7(12):2223-36.

Lee, B.B., Martin, P.R., Valberg, A., & Kremers, J. (1993). Physiological mechanisms underlying psychophysical sensitivity to combined luminance and chromatic luminance modulation. *J Opt Soc Am A*; 10:1403-1412.

Lee, B.B. (1996). Receptive field structure in the primate retina. [Review]. *Vision Res*; 36:631-644.

Legge, G.E. (1978). Sustained and transient mechanisms in human vision: temporal and spatial properties. Vision Res; 18:69-81.

Leonova, A., Pokorny, J., & Smith, V.C. (2003). Spatial frequency processing in inferred PC- and MC-pathways. *Vision Res*; 43(20):2133-2139

Levi, D.M., Klein, S.A., & Aitsebaomo, A.P. (1985). Vernier acuity, crowding and cortical magnification. *Vision Res; 25*:963-977.

Levine, M.W., & McAnany, J.J. (2005). The relative capabilities of the upper and lower visual hemifields. *Vision Res; 45*(21):2820-2830.

Liu, T., Heeger, D. J., & Carrasco, M. (2006). Neural correlates of the visual vertical meridian asymmetry. *J Vis*; 6(11):12, 1294-1306.

Livingstone, M.S., & Hubel, D.H. (1988). Do the relative mapping densities of the magno- and parvocellular systems vary with eccentricity? *J Neurosci*; 8(11):4334-4339.

Lynch, J.J. 3rd., Silveira, L.C., Perry, V.H., & Merigan, W.H. (1992). Visual effects of damage to P ganglion cells in macaques. *Vis Neurosci*; 8:575-583.

MacLeod, D.I.A. & Boynton, R.M. (1979). Chromaticity Diagram Showing Cone Excitation by Stimuli of Equal Luminance. *J Opt Soc Am A;* 69:1183-1186.

Mackeben, M. (1999). Sustained focal attention and peripheral letter recognition. *Spatial Vision; 12*:51-72.

Maddess, T. & Henry, G.H. (1992). Nonlinear visual responses and visual deficits in ocular hypertensive and glaucoma subjects. *Clin Vis Sci*; 7:371-383.

Maddess, T., Goldberg, I., Wine, S., Dobinson, J., Welsh, A.H., & James, A.C. (1999). Testing for glaucoma with the spatial frequency doubling illusion. *Vision Res*; 39:4258-4273.

Maia-Lopes, S., Silva, E.D., Silva, M.F., Reis, A., Faria, P., & Castelo-Branco, M. (2008). Evidence of widespread retinal dysfunction in patients with stargardt disease and morphologically unaffected carrier relatives. *Invest Ophthalmol Vis Sci*; 49(3):1191-1199.

Marmor, M. F., Hood, D. C., Keating, D., Kondo, M., Seeliger, M. W., and Miyake, Y. (2003). Guidelines for basic multifocal electroretinography (mfERG). *Doc Ophthalmol;* 106:105-115.

Martínez-Belló, C., Chauhan, B.C., Nicolela, M.T., McCormick, T.A., & LeBlanc, R.P. (2000). Intraocular pressure and progression of glaucomatous visual field loss. *Am J Ophthalmol*; 129(3):302-308.

Marx, M., Bodis-Wollner, I., Bobak, P., Harnois, C., Mylin, L., & Yahr, M. (1986).Temporal frequency-dependent VEP changes in Parkinson's disease. *Vision Res*; 26:185-193.

Matsumoto C, Okuyama S, Iwagaki A, Otsuki T, Uyama K, Otori T. The influence of target blur on perimetric threshold values in automated light-sensitive perimetry and flicker perimetry. In: Wall M, Heijl A, editors. Perimetry Update 1996/97. Amsterdan: Kugler; 1997. p.191-200.

Matsumoto C. (1998). Automated flicker perimetry in glaucoma and retinal detachment patients. 6th International OCTOPUS Users´Visual Field Symposium Switzerland.

McAnany, J.J., & Levine, M.W. (2007). Magnocellular and parvocellular visual pathway contributions to visual field anisotropies. *Vision Res;* 47(17):2327-2336.

McKendrick, A.M., Anderson, A.J., Johnson, C.A., & Fortune, B. (2003). Appearance of the frequency doubling stimulus in normal subjects and patients with glaucoma. *Invest Ophthalmol Vis Sci*; 44:1111-1116.

Mendes, M., Silva, F., Simoes, L., Jorge, M., Saraiva, J., Castelo-Branco, M. (2005). Visual magnocellular and structure from motion perceptual deficits in a neurodevelopmental model of dorsal stream function. *Brain research. Cognitive brain research, 25*:788–798.

Merigan, W.H. (1989). Chromatic and achromatic vision of macaques: role of the P pathway. *J Neurosci*; 9(3):776-783.

Merigan, W.H., & Maunsell, J.H. (1990). Macaque vision after magnocellular lateral geniculate lesions. *Vis Neurosci*; 5:347-352.

Merigan, W. H., Byrne, C. E., & Maunsell, J. H. R. (1991a). Does primate motion perception depend on the magnocellular pathway? *J Neurosci*; 11:3422-3429.

Merigan, W. H., Katz, L. M., & Maunsell, J. H. R. (1991b). The effects of parvocellular lateral geniculate lesions on the acuity and contrast sensitivity of macaque monkeys. *J Neurosci*; 11:994-1001.

Merigan, W.H., & Maunsell, J.H.R. (1993). How parallel are the primate visual pathways? *Annual Review of Neuroscience*; 16:369-402.

Mestre, D., Blin, O., Serratrice, G., & Pailhous, J. (1990a). Human spatio-temporal contrast sensitivity: dopaminergic induced variations. *Eur J Pharmacol*; 183:1022-3.

Mestre, D., Blin, O., Serratrice, G., & Pailhous, J. (1990b). Spatiotemporal contrast sensitivity differs in normal aging and Parkinson's disease. *Neurology*; 40:1710-4.

Mestre, D., Blin, O., van den Brand, C.L., Azulay, J.P., & Serratrice, G. (1996). Effects of L-DOPA on spatiotemporal contrast sensitivity in Parkinson's disease. *Adv Neurol*; 69:503-511.

Miyake, Y., Shiroyama, N., Horiguchi, M., & Ota, I. (1989). Asymmetry of focal ERG in human macular region. *Invest Ophthalmol Vis Sci*; 30(8):1743-1749.

Miyake, Y. (1990). Macular oscillatory potentials in humans. Macular OPs. *Doc Ophthalmol*; 75(2):111-124.

Mollon, J.D. (1989). "Tho' she kneel'd in that place where they grew..." The uses and origins of primate colour vision. J Exp Biol; 146:21-38.

Mollon, J.D. (1991). In Cronly-Dillon,J.R. and Gregory,R.L. (eds), Vision and Visual Dysfunction. Macmillan Press, London, Vol. 2, pp. 306-319.

Mullen, K.T., & Kingdom, F.A. (2002). Differential distributions of red-green and blue-yellow cone opponency across the visual field. *Vis Neurosci*; 19:109-118.

Myerson, J., Manis, P.B., Miezin, F.M., & Allman, J.M. (1977). Magnification in striate cortex and retinal ganglion cell layer of owl monkey: A quantitative comparison. *Science*; *198*:855-857.

Nagatomo, A., Nao-i, N., Maruiwa, F., Arai, M., & Sawada, A. (1998). Multifocal electroretinograms in normal subjects. *Jpn J Ophthalmol*; 42(2):129-135.

Nakayama, K., & Mackeben, M. (1989). Sustained and transient components of focal visual attention. *Vision Res; 29*:1631-1646.

Nguyen-Legros, J. (1988). Functional neuroarchitecture of the retina: hypothesis on the dysfunction of retinal dopaminergic circuitry in Parkinson's disease. *Surg Radiol Anat*; 10:137-144.

Østerberg, G. (1935). Topography of the layer of rods and cones in the human retina. Acta Ophthalmol*; 13*:1.103.

Otto, H., & SCHADE, S.R., (1956). Optical and Photoelectric Analog of the Eye. *J Opt Soc Am;* 46:721-738

Packer, O., Hendrickson, A. E., & Curcio, C. A. (1989). Photoreceptor topography of the retina in the adult pigtail macaque (Macaca nemestrina). *J Comp Neurol; 288*:165-183.

Packer O, Williams D.R. Light, the retinal image, and photoreceptors. In: Shevell SK, editor. The science of color. 2nd edn. Oxford: Elsevier; 2003. Chapter: 2.

Paczka, J.A., Friedman, D.S., Quigley, H.A., Barron, Y., & Vitale, S. (2001). Diagnostic capabilities of frequency-doubling technology, scanning laser polarimetry, and nerve fibre layer photographs to distinguish glaucomatous damage. *Am J Ophthalmol*; 131:188-197.

Parkinson, J. (2002). An essay on the shaking palsy. 1817. *J. Neuropsychiatry Clin. Neurosci*. 14: 223-236.

Parks, S., Keating, D., Williamson, T.H., Evans, A.L., Elliot, A.T., & Jay J.L. (1996). Functional imaging of the retina using the multifocal electroretinograph: a control study. Br J Ophthalmol; 80:831-834.

Pearson, P., Swanson, W.H., & Fellman, R.L. (2001). Chromatic and achromatic defects in patients with progressing glaucoma. *Vision Res*; 41:1215-1227.

Perry, V.H., Oehler, R., & Cowey, A. (1984). Retinal ganglion cells that project to the dorsal lateral geniculate nucleus in the macaque monkey. *Neuroscience*; 12(4):1101-1123.

Perry, V.H., & Cowey, A. (1985). The ganglion cell and cone distribution in the monkey retina: Implications for central magnification factors. *Vision Res; 25*:1795-1810.

Pieri, V., Diederich, N.J., Raman, R., & Goetz, C.G. (2000). Decreased color discrimination and contrast sensitivity in Parkinson's disease. *J Neurol Sci*; 172:7-11.

Pokorny, J., Smith, V. C., & Lutze, M. (1987). Aging of the human lens. *Appl Opt*; 26:1437-1440.

Pokorny, J., & Smith, V.C. (1997). Psychophysical signatures associated with magnocellular and parvocellular pathway contrast gain. J Opt Soc Am A Opt Image Sci Vis; 14(9):2477-2486.

Polito, A., Del Borrello, M., Isola, M., Zemella, N., & Bandello, F. (2005). Repeatability and reproducibility of fast macular thickness mapping with Stratus optical coherence tomography. Archives of Ophthalmology; 123:1330-1337.

Porter, J., Queener, H., Lin, J., Thorn, K., & Awwal, A. editors (2006). *Adaptive Optics for Vision Science*, Wiley-Interscience.

Price, M.J., Feldman, R.G., Adelberg, D., & Kayne, H. (1992). Abnormalities in color vision and contrast sensitivity in Parkinson's disease. *Neurology*; 42:887-890.

Previc, F.H. (1990). Functional specialization in the lower and upper visual fields in humans: Its ecological origins and neurophysiological implications. *Behav Brain Sci; 13*:519-575.

Pugh, E. N. Vision: Physics and retinal physiology. (1988). In R. C. Atkinson (Ed.), *Stevens handbook of experimental psychology*. New York: Wiley.

Purpura, K., Kaplan, E., & Shapley, R.M. (1988). Background light and the contrast gain of primate P and M retinal ganglion cells. *Proc Natl Acad Sci USA*; 85:4534-4537.

Purpura, K., Trachina, D., Kaplan, E., & Shapley, R.M. (1990). Light adaptation in the primate retina: analysis of changes in the gain and dynamics of monkey retinal ganglion cells. *Vis Neurosci*; 4:75-93.

Purves, D., Augustine, G.J., Fitzpatrick, D., Hall, W.C., LaMantia A.-S., McNamara, J., Williams, S.M. (2004). *Neuroscience*. Sinauer Associates, Inc., MA. (3rd edition).

Quigley, H.A., Dunkelberger, G.R., & Green, W.R. (1988). Chronic human glaucoma causing selectively greater loss of large optic nerve fibers*. Ophthalmol*; 95:357-363.

Quigley, H.A., Sanchez, R.M., Dunkelburger, G.R., Henaut, N.L., & Baginski, T.A. (1987). Chronic glaucoma selectively damages large optic nerve fibers. *Invest Ophthalmol Vis Sci*; 28:913-918.

Rangaswamy, N. V., Hood, D. C., & Frishman, L. J. (2003). Regional variations in local contributions to the primate photopic flash ERG: Revealed using the slow-sequence mfERG. *Invest Ophthalmol Vis Sci*; 44:3233-3247.

Raskin, S.A., Borod, J.C., Wasserstein, J., Bodis-Wollner, I., Coscia, L., Yahr, M.D. (1990). Visuospatial orientation in Parkinson's disease. *Int J Neurosci*; 51:9-18.

Rijsdijk, J.P., Kroon, J.N., & van der Wilt, G.J. (1980). Contrast sensitivity as a function of position on the retina. *Vision Res;* 20:235-241.

Reeves, B.C, Hill, A.R., Aspinall, P.A. (1989). Normative data for the significance of change in error score of the Farnsworth Munsell 100 hue test. In DRUM B., VERRIEST G. eds: Colour vision deficiencies IX. Doc. Ophthalmol. Proc Ser. Kluwer, Acad publ., Dordrecht; 52:417-423.

Regan D, Maxner C. (1987). Orientation-selective visual loss in patients with Parkinson's disease. *Brain*; 110:415-32.

Regan, B.C., Reffin, J.P., & Mollon, J.D. (1994). Luminance noise and the rapid determination of discrimination ellipses in colour deficiency. *Vision Res*; 34:1279-1299.

Regan, B.C., Freudenthaler, N., Kolle, R, Mollon, J.D., & Paulus, W. (1998). Colour discrimination thresholds in Parkinson's disease: results obtained with a rapid computer-controlled colour vision test. *Vision Res*; 38:3427-3431.

Remky, A., Arend, O., & Hendricks, S. (2000). Short-wavelength automated perimetry and capillary density in early diabetic maculopathy. *Invest Ophthalmol Vis Sci*; 41(1):274-281

Risse, J.F. (1999). Exploration de la fonction visuelle : application au domaine sensoriel de l'œil normal et en pathologie, Editions Masson, Paris.

Robson, J. G. (1975). Receptive fields: Neural representation of the spatial and intensive attributes of the visual image. In E. C. Carterette & M. P. Friedman (Eds.), *Handbook of perception V: Seeing* (pp. 81-116). New York: Academic Press.

Rolls, E. T., and Cowey, A. (1970). Topography of the retina and striate cortex and its relationship to visual acuity in rhesus monkeys and squirrel monkeys. *Experimental Brain Research; 10*:298-310.

Roth A and Lanthony P. Vision des couleurs *in* Risse JF ed. Exploration de la Fonction Visuelle. Paris, Masson, 1999:129-151.

Rovamo, J., Virsu, V., and Nasanen, R. (1978). Cortical magnification factor predicts the photopic contrast sensitivity of peripheral vision. *Nature;* 271:54–56.

Rovamo, J., and Virsu, V. (1979). An estimation and application of the human cortical magnification factor. *Experimental Brain Research; 37*:495–510.

Rubin, N., Nakayama, K., and Shapley, R. (1996). Enhanced perception of illusory contours in the lower versus upper visual hemifields. *Science; 271*:651-653.

Sample, P.A., Bosworth, C.F., & Weinreb, R.N. (1997). Short-wavelength automated perimetry and motion automated perimetry in patients with glaucoma. *Arch Ophthalmol*; 115:1129-1133.

Sample, P.A., Taylor, J.D.N., Martinez, G., Lusky, M., & Weinreb, R.N. (1993). Shortwavelength color visual fields in glaucoma suspects at risk. *Am J Ophthalmol*; 115:225-233.

Schein, S.J. (1988). Anatomy of macaque fovea and spatial densities of neurons in foveal representation. *The Journal of Comparative Neurology*; *269*:479-505.

Schiller, P.H., & Colby, C.L. (1983). The responses of single cells in the lateral geniculate nucleus of the rhesus monkey to color and luminance contrast. *Vision Res*; 23(12):1631-1641.

Schiller, P. H., Logothetis, N. K., & Charles, E. R. (1990a). Functions of the colour-opponent and broad-band channels of the visual system. *Nature*; 343:68-70.

Schiller, P. H., Logothetis, N. K., & Charles, E. R. (1990b). Role of the color-opponent and broad-band channels in vision. *Vis Neurosci*; 5:321-346.

Schiller, P.H., Logothetis, N.K., & Charles, E.R. (1991). Parallel pathways in the visual system: their role in perception at isoluminance. *Neuropsychologia*; 29(6):433-441.

Sclar, G., Maunsell, J.H., Lennie, P. (1990). Coding of image contrast in central visual pathways of the macaque monkey. Vision Res; 30(1):1-10.

Seeliger M.W., Kretschmann U.H., Apfelstedt-Sylla E, Zrenner E. (1998). Implicit time topography of multifocal electroretinograms. Investigative Ophthalmology & Visual Science; 39 718-723.

Seiple W. & Holopigian K. (1996). Outer-retina locus of increased flicker sensitivity of the peripheral retina. *J Opt Soc Am A Opt Image Sci Vis*; 13(3):658-66.

Seiple, W., Holopigian, K., Szlyk, J. P., & Wu, C. (2004). Multidimensional visual field maps: relationships among local psychophysical and local electrophysiological measures. *J Rehabil Res Dev*; 41(3A), 359-372.

Sekuler, R. & Blake, R. (1994). *Perception*. (3rd edition), New York: McGraw Hill.

Shabana, N., Peres, V.C., Carkeet, A. & Chew, P.T. (2003). Motion perception in glaucoma patients. *Surv Ophthalmol*; 48:92-106.

Shapley R.M. & Victor J.D. (1980). The effect of contrast on the non-linear response of the Y-cell. *J Physiol*; 302: 535-547.

Shapley, R., Kaplan, E., & Soodak, R. (1981). Spatial summation and contrast sensitivity of X and Y cells in the lateral geniculate nucleus of the macaque. *Nature*; 292:543–545.

Shapley, R., & Perry, V.H. (1986). Cat and monkey retinal ganglion cells and their visual functional roles. *Trends in Neurosciences*; 9:229-235.

Shapley, R. (1990). Visual sensitivity and parallel retinocortical channels. *Annu Rev Psychol*; 41:635-658.

Shevell, SK. The science of color. 2nd edition. Oxford: Elsevier; 2003.

Shmuelof, L., & Zohary, E. (2005). Dissociation between ventral and dorsal fMRI activation during object and action recognition. Neuron; 47(3):457-470.

Siegel S and Castellan NJ. (1988). Nonparametric Statistics for the Behavioural Sciences, McGraw-Hill, New York.

Silva M.F., Guerreiro, M, Castelo-Branco M. (2004). Disadvantage of the superotemporal field in normal subjects as revealed by techniques that study the function of the magnocellular pathway. *Ophthalmic Res*; 36 S1:60.

Silva, M.F., Faria, P., Regateiro, F.S., Forjaz, V., Januario, C., Freire, A., & Castelo–Branco M. (2005). Independent patterns of damage within magno-, parvo- and koniocellular pathways in Parkinson's disease. *Brain*; *128*: 2260-2271.

Silva, M. F. Maia-Lopes, S., Mateus, C., Guerreiro, M., Sampaio, J., Faria, P., & Castelo-Branco M. (2008). Retinal and cortical patterns of spatial anisotropy in contrast sensitivity tasks. *Vision Res*; 48(1):127-135.

Silveira, L.C., Perry & V.H. (1991). The topography of magnocellular projecting ganglion cells (M-ganglion cells) in the primate retina. *Neuroscience*; 40:217-237.

Silveira L.C., Lee B.B., Yamada E.S., Kremers J., Hunt D.M., Martin P.R., & Gomes FL. (1999). Ganglion cells of a short-wavelength-sensitive cone pathway in New World monkeys: morphology and physiology. *Vis Neurosci*; 16:333-343.

Skrandies W, & Gottlob I. (1986). Alterations of visual contrast sensitivity in Parkinson's disease. *Hum Neurobiol*; 5: 255-9.

Skrandies, W., & Baier, M. (1986). The standing potential of the human eye reflects differences between upper and lower retinal areas. *Vision Res*; 26:577.

Skottun, BC. (2000). The magnocellular deficit theory of dyslexia: the evidence from contrast sensitivity. *Vision Res*; 40:111-127.

Skottun, B.C., & Skoyles, J.R. (2007). Contrast sensitivity and magnocellular functioning in schizophrenia*. Vision Res*; 47:2923-2933.

Smith, V. & Pokorny J. (1975). Spectral Sensitivity of the Foveal Cone Photopigments between 400 and 500 nm. *Vision Res;* 15:161-171.

Solomon, S.G., White, A.J., & Martin, P.R. (1999). Temporal contrast sensitivity in the lateral geniculate nucleus of a New World monkey, the marmoset Callithrix jacchus. *J Physiol*; 517:907-917.

Sommer, M.A., & Wurtz, R.H. (2004). What the brain stem tells the frontal cortex. II. Role of the SC-MD-FEF pathway in corollary discharge. *J Neurophysiol*; 91(3):1403-1423.

Spry, P. G., Furber, J. E., & Harrad, R. A. (2002). The effect of ocular dominance on visual field testing. *Optometry & Vision Science*; *79*(2):93-97.

Stiles, W. S. & Burch J. M. (1959). “NPL Colour-matching Investigation: Final Report (1958).” *Optica Acta;* 6:1-26.

Stockman, A. & Brainard, D.H. (2010). Color vision mechanisms. To appear in the OSA Handbook of Optics (3rd edition, M. Bass, ed). McGraw-Hill, New York, pp. 11.1-11.104.

Sutter, E.E. & Tran, D. (1992). The field topography of ERG components in man-I. The photopic luminance response. *Vis Res*; 32: 433-466.

Sutter E.E. (2001). Imaging visual function with the multifocal m-sequence technique. *Vision Res*; 41(10-11):1241-55.

Tagliati M., Bodis-Wollner I. & Yahr M.D. (1996). The pattern electroretinogram in Parkinson's disease reveals lack of retinal spatial tuning. *Electroencephalogr Clin Neurophysiol*; 100:1-11.

Tebartz van Elst L., Greenlee M.W., Foley J.M. & Lucking C.H. (1997). Contrast detection, discrimination and adaptation in patients with Parkinson's disease and multiple system atrophy. *Brain*; 120: 2219-28.

Thibos, L. N., Cheney, F. E., & Walsh, D. J. (1987). Retinal limits to the detection and resolution of gratings. *J Opt Soc Am A*; 4:1524-1529.

Tolhurst, D. J. (1975). Reaction times in the detection of gratings by human observers: a probabilistic mechanism. *Vision Res*; 15:1143-1149.

Trible, J.R., Schultz, R.O., Robinson, J.C., & Rothe, T.L. (2000) Accuracy of glaucoma detection with frequency-doubling perimetry. *Am J Ophthalmol*; 129:740-45.

Trick, G.L. (2003). Beyond visual acuity: new and complementary tests of visual function. *Neurol Clin*; 21(2):363-386.

Ungerleider, L.G., & Mishkin, M. (1982). Two cortical visual systems. In: Analysis of visual behavior, (Ingle DJ. Goodale MA, Mansfield RJW, eds), pp 549-586. Cambridge, MA: MIT Press.

Ungerleider, L.G, & Haxby, J.V. (1994). 'What' and 'where' in the human brain. *Curr Opin Neurobiol*; 4:157-165.

Van Essen, D.C., Newsome, W.T., & Maunsell, J.H.R. (1984). The visual field representation in striate cortex of the macaque monkey: Asymmetries, anisotropies, and individual variability. *Vision Res;* 24:429-448.

Van Essen, D.C., & DeYoe, E.A. (1995). Concurrent processing in the primate visual cortex. In M. Gazzaniga (Ed.), *The cognitive neurosciences* (pp. 383-400).

Virsu, V., & Rovamo, J. (1979). Visual resolution, contrast sensitivity, and the cortical magnification factor. *Experimental Brain Research;* 37:475-494.

Wall, M. (1991). High-pass resolution perimetry in optic neuritis. *Invest Ophthalmol Vis Sci*; 32(9):2525-2529.

Westcott, M.C., Fitzke, F.W., Crabb, D.P., & Hitchings, R.A. (1999). Characteristics of frequency-of-seeing curves for a motion stimulus in glaucoma eyes, glaucoma suspect eyes, and normal eyes. *Vision Res*; 39:631-639.

Weymouth, F.W. (1958). Visual sensory units and the minimal angle of resolution. Am J Ophthalmol*;* 46:102-113.

Wikler, K.C., & Rakic, P. (1990a). Distribution of photoreceptor subtypes in the retina of diurnal and nocturnal primates. J Neurosci*;* 10:3390-3401.

Wikler, K. C., Williams, R. W., and Rakic, P. (1990b). Photoreceptor mosaic: Number and distribution of rods and cones in the rhesus monkey retina. J Comp Neurol*;* 297:499-508.

Williams, D. R., and Coletta, N. J. (1987). Cone spacing and the visual resolution limit. J Opt Soc Am A*;* 4:514-1523.

Wright, W.D. (1928–1929). A Re-determination of the Trichromatic Coefficients of the Spectral Colours. *Transactions of the Optical Society;* 30:141-164.

Weinstein, A., Troscianko, T., & Calvert, J. (1997). Impaired visual search mechanisms in Parkinson's disease (PD): a psychophysical and event-related potentials study. *J Psychophysiol*; 11:33-47.

Werner, J.S., Peterzell, D.H., & Scheetz, A.J. (1990). Light, vision, and aging. [Review]. *Optom Vis Sci*; 67:214-29.

Willis, A., & Anderson, S.J. (2000). Effects of glaucoma and aging on photopic and scotopic motion perception. *Invest Ophthalmol Vis Sci*; 41:325-335.

Wilson, H.R., & Wilkinson, F. (1997). Evolving concepts of spatial nels in vision: From independence to nonlinear interactions. *Perception; 26*: 939-960.

Wu, S., & Sutter, E.E. (1995). A topographic study of oscillatory potentials in man. *Visual Neuroscience*; 12(6):1013-1025.

Wyszecki, G., & Stiles, W.S. (1982). Color science: Concepts and methods, quantitative data and formulae (2nd edition). New york: Wiley, 1982.

Xu, X., Ichida, J. M., Allison, J. D., Boyd, J. D., Bonds, A. B., & Casagrande, V. A. (2001). A comparison of koniocellular, magnocellular and parvocellular receptive field properties in the lateral geniculate nucleus of the owl monkey (Aotus trivirgatus). *Journal of Physiology;* 531:203-218.

Yamada, E.S., Marsha, D.W., Silveira L.C., & Casagrande, V.A. (1998). Morphology of P and M retinal ganglion cells of the bush baby. *Vision Res*; 38(21):3345-3352.

Yamada, E.S., Silveira, L.C., Perry, V.H., & Franco, E.C. (2001). M and P retinal ganglion cells of the owl monkey: morphology, size and photoreceptor convergence. *Vision Res*; 41(2): 119-131.

Yang, Y.X., Wood, N.W., & Latchman, D.S. (2009). Molecular basis of Parkinson's disease. *Neuroreport*; 20(2):150-156.